



# Durability of geo-polymer mortar with respect to alkali silica reaction

**Author:**

Habaragamu Arachchige, Dinesh Mahanama

**Publication Date:**

2018

**DOI:**

<https://doi.org/10.26190/unsworks/3806>

**License:**

<https://creativecommons.org/licenses/by-nc-nd/3.0/au/>

Link to license to see what you are allowed to do with this resource.

Downloaded from <http://hdl.handle.net/1959.4/63748> in <https://unsworks.unsw.edu.au> on 2024-05-02

**DURABILITY OF GEO-POLYMER MORTAR  
WITH RESPECT TO ALKALI SILICA  
REACTION**

**Dinesh Mahanama Habaragamu Arachchige**

A thesis in fulfilment of the requirements for the degree of  
Doctor of Philosophy



School of Civil and Environmental engineering

Faculty of Engineering

August 2018



## **ORIGINALITY STATEMENT**

“I hereby declare that this submission is my own work and to the best of my knowledge it contains no materials previously published or written by another person, or substantial proportions of material which have been accepted for the award of any other degree or diploma at UNSW or any other educational institution, except where due acknowledgement is made in the thesis. Any contribution made to the research by others, with whom I have worked at UNSW or elsewhere, is explicitly acknowledged in the thesis. I also declare that the intellectual content of this thesis is the product of my own work, except to the extent that assistance from others in the project's design and conception or in style, presentation and linguistic expression is acknowledged.”

Sign: .....

(Dinesh Mahanama Habaragamu Arachchige)

Date: .....

## **COPYRIGHT STATEMENT**

I hereby grant the University of New South Wales or its agents the right to archive and to make available my thesis or dissertation in whole or part in the University libraries in all forms of media, now or here after known, subject to the provisions of the Copyright Act 1968. I retain all proprietary rights, such as patent rights. I also retain the right to use in future works (such as articles or books) all or part of this thesis or dissertation.

I also authorise University Microfilms to use the 350 word abstract of my thesis in Dissertation Abstract International (this is applicable to doctoral theses only).

I have either used no substantial portions of copyright material in my thesis or I have obtained permission to use copyright material; where permission has not been granted, I have applied/will apply for a partial restriction of the digital copy of my thesis or dissertation.'

Signed .....

Date .....

## **AUTHENTICITY STATEMENT**

'I certify that the Library deposit digital copy is a direct equivalent of the final officially approved version of my thesis. No emendation of content has occurred and if there are any minor variations in formatting, they are the result of the conversion to digital format.'

Signed .....

Date .....

## INCLUSION OF PUBLICATIONS STATEMENT

UNSW is supportive of candidates publishing their research results during their candidature as detailed in the UNSW Thesis Examination Procedure.

**Publications can be used in their thesis in lieu of a Chapter if:**

- The student contributed greater than 50% of the content in the publication and is the “primary author”, ie. the student was responsible primarily for the planning, execution and preparation of the work for publication
- The student has approval to include the publication in their thesis in lieu of a Chapter from their supervisor and Postgraduate Coordinator.
- The publication is not subject to any obligations or contractual agreements with a third party that would constrain its inclusion in the thesis

Please indicate whether this thesis contains published material or not.

- This thesis contains no publications, either published or submitted for publication (if this box is checked, you may delete all the material on page 2)*
- Some of the work described in this thesis has been published and it has been documented in the relevant Chapters with acknowledgement (if this box is checked, you may delete all the material on page 2)*
- This thesis has publications (either published or submitted for publication) incorporated into it in lieu of a chapter and the details are presented below*

### CANDIDATE’S DECLARATION

I declare that:

- I have complied with the Thesis Examination Procedure
- where I have used a publication in lieu of a Chapter, the listed publication(s) below meet(s) the requirements to be included in the thesis.

Name	Signature	Date (dd/mm/yy)

### Postgraduate Coordinator’s Declaration (to be filled in where publications are used in lieu of Chapters)

I declare that:

- the information below is accurate
- where listed publication(s) have been used in lieu of Chapter(s), their use complies with the Thesis Examination Procedure
- the minimum requirements for the format of the thesis have been met.

PGC’s Name	PGC’s Signature	Date (dd/mm/yy)

### **Publications related to this study**

- D. Mahanama, P.De Silva, T. Kim, A. Castel, M.S.H. Khan 2018, ‘Evaluating the Effect of GGBFS in Alkali Silica Reaction in Geopolymer Mortar with Accelerated Mortar Bar Test’, *Journal of Materials in Civil Engineering (ASCE)*. (under review)
- T. KIM, D. H. Arachchige, Q. Nguyen, M. Khan, and A. Castel 2019, ‘The Effects of different cementitious binders on expansion induced by alkali silica reaction’, *RILEM Spring Convention and Sustainable Materials, Systems and Structures Conference, Rovinj, Croatia* . (under review)
- D. Mahanama 2018, ‘Durability of Geopolymer Mortar with respect to Alkali Silica Reaction’, *Postgraduate Research Symposium UNSW, Sydney, Australia*.
- D. Mahanama, P.De Silva, T. Kim, A. Castel 2018, ‘Use of Amorphous Silica Aggregate to Assess Alkali Silica Reaction in Geopolymer’ , *Journal of Materials in Civil Engineering (ASCE)*. (under preparation)- Related to Chapter 8
- D. Mahanama, P.De Silva, T. Kim, A. Castel 2018, ‘Effect of External Calcium in Deleterious Alkali Silica Reaction in Geopolymer’, *Journal of Materials in Civil Engineering (ASCE)*. (under preparation)- Related to Chapter 6

## ABSTRACT

Geopolymer is a potential alternative to OPC binder which is labelled as a less sustainable and less eco-friendly material despite being one of the highly consumable materials in the world. However, use of this technology has been hindered for decades due to some grey areas which need further clarifications. Alkali aggregate reaction (AAR) is one of the main concerns raised with respect to geopolymer binders as it uses a highly alkaline solution to activate. Even though fly ash based geopolymers have performed exceptionally even with highly reactive aggregates, many researchers were concerned on the use of GGBFS in geopolymer since high GGBFS contents seem to trigger the ASR. Since GGBFS also governs the early age properties of geopolymer concrete, optimisation of GGBFS in mix design is one of the key components in the commercial adaptation of geopolymer concrete. This research is focused on laying the platform to this by identifying the ASR mechanism in geopolymer binders and the specific role of GGBFS in it.

This study is based on the accelerated mortar bar test of mortar mixes cast with four aggregates representing nonreactive (basalt), natural reactive (culcairn), manufactured reactive (ferronickel slag) and amorphous (fused silica) aggregate categories. Three main geopolymer mixes with fly ash/GGBFS ratio 9, 4 and 1 along with the standard OPC mix (control test) were used to assess aggregates. It should be noted that all parameters except the fly ash/GGBFS ratio kept constant in the geopolymer mixes. Two subsidiary mixes with fly ash/GGBFS ration 9, and 1 was used with Culcairn aggregate to analyse the effect of mechanical properties on the expansion development. Mortar bars were exposed to 1M NaOH at 80 °C to accelerate the ASR. In addition, geopolymer mixes with Culcairn aggregate were exposed to 0.03M NaOH, 1M NaOH saturated with Ca(OH)<sub>2</sub> and water at 80 °C to assess the effect of curing solution on the

ASR expansion development. Prolonged testing time is incorporated in accelerated mortar bar test to identify any late expansions. Microstructural analysis (backscattered SEM-EDS analysis) was performed on each mix at 21 days and 150 days to identify the ASR gel formations. Si dissolution test was carried out on the reactive aggregate to assess their Si providing capability and identify the factors affecting it.

The experimental data articulate the low ASR potential of geopolymer mortar compared to OPC mortar. Furthermore, final expansions of geopolymer mortar bars suggest that ASR in geopolymer mortar increases with the increase in the GGBFS content in the mix design. In fact, based on this study, mixes with GGBFS content less than 61.5 kg/m<sup>3</sup> can be categorised as extremely low risk and can be used even with reactive aggregates. In addition, both expansion and microstructural analysis results emphasise the importance of Ca in deleterious ASR: first by facilitating the Si ion saturation and then entrapping the ASR gel to amplify the stress development. In fact, expansion results of mortar bars exposed to 1M NaOH saturated with Ca(OH)<sub>2</sub> illustrate that even an external Ca supply can induce ASR expansions in geopolymer mortar which alarmed on the use of Ca-rich aggregates in geopolymer binders. Experimental results of mortar bars exposed to 0.03M NaOH suggest that geopolymer do not encompass any additional risk of ASR due to the use of alkali activator. Thus, aggregates cleared for OPC can be used with geopolymer mortar as well. SEM-EDS analysis identified the formation of Al-rich ASR gel in geopolymer mortar bars. This study recommended analysing the expansiveness of Al rich ASR gel since theoretically, Al might reduce the swelling capacity of ASR gel.

This research also emphasises that the standard accelerated mortar bar test (AS 1141.60.1) needs to be modified before adopting it in geopolymer mortar. Geopolymer mortar bars typically consist of an initial time lag and thus requires a prolonged testing

time period to identify the ASR. This study further recommended to revise the existing expansion limits in standard accelerated mortar bar test before used with geopolymer by paying extra attention on its stress strain behaviour (quasi brittle behaviour).

## **ACKNOWLEDGEMENT**

First and foremost, I would like to express my sincere gratitude to my supervisor A/Prof. Arnaud Castel for his enthusiastic support, valuable suggestions, and continuous encouragement throughout this doctoral study. I would also like to acknowledge my co-supervisors Dr. Pre De Silva, and Prof. Vute Sirivivatnanon for all their continuous assistance and insightful guidance provided during my stay here.

I also extend my sincere thanks to Dr. Taehwan Kim for his assistance all the time and constructive comments. Further, I am grateful to Dr. Mohamad Khan, Amin Noushini, Hammad Anis Khan and Adrian Chan for their support for this study.

The financials support provided by the University Postgraduate Award (UPA) at UNSW to conduct this research study is gratefully appreciated.

I also wish to acknowledge the assistance made by the technical officers during my laboratory experiments in the University of New South Wales, Dr. Gautam Chattopadhyay, Paul Gwynne, William Terry, Anthony Macken, Simon Hager, Dorothy Yu and George Yang.

I extend my sincere thanks to all academic and administration staff in faculty of engineering and colleagues at University of New South Wales. Moreover, I am thankful to all my friends in Wollongong and Sydney for making my stay in Australia an enjoyable one.

I am profoundly indebted to my parents H.A. Mahanama and Hemanthi Gunawardena for everything they have done in my life, for all their sacrifice, encouragement and moral support. I am thankful to my brother Janaka Mahanama, my sister Hasini Mahanama and mother-in-law Champa Kariyawasam who have given their time, enjoyment, support and encouragement during this course.

Last but not least, I would like to extend my sincere thanks to my loving wife Chamindi Jayasuriya for her continual love, encouragement and care thorough out this journey and my little daughter Sandasi Mahanama for her beautiful smile all the time.

# TABLE OF CONTENTS

<b>CHAPTER 1 :Introduction</b>	<b>1</b>
1.1 Background	1
1.2 Aim and Objectives	3
1.3 Scope of study	3
1.4 Research significance	5
1.5 Thesis Outline	5
<b>CHAPTER 2 :Literature Review</b>	<b>8</b>
2.1 Overview	8
2.2 Geopolymer technology	9
2.2.1 History	9
2.2.2 Geopolymer Chemistry	10
2.2.3 Geopolymerization mechanism	14
2.2.4 Constituents of Geopolymer binder	16
2.2.5 Properties of geopolymer binder	21
2.2.6 Socio-economic and environmental factor	25
2.2.7 Challenges of geopolymer	26
2.3 Alkali Aggregate Reaction (AAR)	27
2.3.1 Introduction	27
2.3.2 Alkali-carbonate reaction (ACR)	28
2.3.3 Alkali silica reaction (ASR)	28
2.3.4 Factors affecting AAR	30
2.3.5 Identification of AAR	40
2.4 Alkali aggregate reaction in geopolymer	47
2.4.1 Effect of slag content	49
2.4.2 Effect of activator	49
2.4.3 Testing methods	50



<b>CHAPTER 5 :Alkali aggregate reaction in natural nonreactive aggregates</b>	<b>103</b>
5.1 Overview	103
5.2 Result and analysis	104
5.2.1 Expansion test	104
5.2.2 Compressive strength variation	107
5.2.3 Scanning Electron Microscope (SEM) Analysis	108
5.2.4 Mortar bar images	116
5.3 Discussion	117
<b>CHAPTER 6 :Alkali silica reaction in natural reactive aggregate</b>	<b>123</b>
6.1 Overview	123
6.2 Result and analysis	124
6.2.1 Effect of GGBFS content	124
6.2.2 Effect of mix design	140
6.2.3 Effect of curing solution	153
6.3 Discussion	165
6.3.1 Alkali silica reaction mechanism in geopolymer mortar	165
6.3.2 Effect GGBFS content	167
6.3.3 Effect of mix design	170
6.3.4 Effect of curing conditions	170
6.3.5 Role of Aluminium	171
6.3.6 Validation of standard expansion test methods	172
<b>CHAPTER 7 :Alkali aggregate reaction in manufactured reactive aggregate</b>	<b>174</b>
7.1 Overview	174
7.2 Result and analysis	176
7.2.1 Expansion test	176
7.2.2 Compressive strength variation	178
7.2.3 Scanning Electron Microscope (SEM) Analysis	180
7.2.4 Mortar bar images	190

7.3	Discussion	191
<b>CHAPTER 8 :Alkali aggregate reaction in fused silica</b>		<b>199</b>
8.1	Overview	199
8.2	Result and analysis	200
8.2.1	Expansion test	200
8.2.2	Compressive strength variation	204
8.2.3	Scanning Electron Microscope (SEM) Analysis	205
8.2.4	Mortar bar images	215
8.3	Discussion	216
<b>CHAPTER 9 :Conclusions and Recommendations</b>		<b>222</b>
9.1	General	222
9.2	Chemical performance of reactive aggregates exposed to an alkali solution	222
9.3	Alkali aggregate reaction in natural non-reactive aggregate	223
9.4	Alkali aggregate reaction in natural reactive aggregate	<b>Error! Bookmark not defined.</b>
9.5	Alkali aggregate reaction in manufactured reactive aggregate	<b>Error! Bookmark not defined.</b>
9.6	Alkali aggregate reaction in amorphous silica	<b>Error! Bookmark not defined.</b>
9.7	Recommendations for future study	228
<b>References</b>		<b>231</b>

## LIST OF FIGURES

Figure 2-1: Classification of different alkali activated materials. Darker shadings correspond to higher alkali concentrations .....	10
Figure 2-2 : Poly(sialate) network in geopolymer binder $K^+$ can be any monovalent cation .....	11
Figure 2-3 : Terminology of poly-sialate .....	13
Figure 2-4 : Mathematical model for alkali activation of low calcium aluminosilicate source materials.....	15
Figure 2-5 : Pessimism behaviour of aggregate (Hobbs 1988) .....	32
Figure 2-6 : Graphical representation of ASR gel formation mechanism (after Hou et al. (2004), Kim, Taehwan and Olek, Jan (2014) and Kim, Taehwan and Olek, Jan (2014)) .....	36
Figure 2-7 : Reaction rim theory (after Ichikawa and Miura (2007)) .....	37
Figure 2-8 : ASR gel expansion mechanism.....	37
Figure 2-9 : Map cracking due to alkali silica reaction identified in causeway bridge in Perth (Australia 2015).....	45
Figure 2-10 : Surface pop outs due to alkali aggregate reaction (Thomas et al. 2011) ..	46
Figure 2-11 : Differential movement of parapet walls in a bridge due to AAR (Thomas et al. 2011).....	47
Figure 3-1 : Particle size distribution of GGBFS and Fly ash .....	53
Figure 3-2 : SEM image of fly ash.....	54
Figure 3-3 : SEM image of GGBFS.....	55
Figure 3-4 : SEM image of OPC.....	56

Figure 3-5 : TAS Classification for volcanic rock (adapted from ( <a href="http://www.sandatlas.org">http://www.sandatlas.org</a> )) .....	59
Figure 3-6 : Basalt aggregate prepared for a mix.....	60
Figure 3-7 : SEM image of crushed basalt aggregates.....	60
Figure 3-8 : XRD analysis result of basalt aggregate .....	61
Figure 3-9 : Culcairn aggregate prepared for a mix.....	63
Figure 3-10 : SEM image of crushed culcairn aggregates .....	63
Figure 3-11 : XRD analysis result of culcairn aggregate.....	64
Figure 3-12 : Ferronickel slag aggregate prepared for a mix.....	66
Figure 3-13 : SEM image of crushed ferronickel slag aggregates .....	66
Figure 3-14 : XRD analysis result of ferronickel aggregate .....	67
Figure 3-15 : Fused silica slag aggregate prepared for a mix .....	69
Figure 3-16 : SEM image of crushed fused silica.....	69
Figure 3-17 : XRD analysis result of fused silica .....	70
Figure 3-18 : Summary of testing procedure .....	71
Figure 3-19 : Jaw crusher and sieve shaker used to prepare aggregate .....	73
Figure 3-20 : Crack development in mortar bars during the thermal curing .....	74
Figure 3-21 : Moulds ready for casting.....	74
Figure 3-22 : Mould set up of mortar bars .....	74
Figure 3-23 : Summary of mortar mixes implemented in the study .....	75
Figure 3-24: Materials prepared for mixing.....	77
Figure 3-25 : Compacting the specimens with a vibration table.....	78
Figure 3-26 : Measuring the length variation with a dial gauge .....	80
Figure 3-27 : Mortar bars kept in 1M NaOH solution .....	81
Figure 3-28 : SEM 3400 equipment used for the analysis.....	83

Figure 3-29 : Large cracks with no gel formations .....	84
Figure 3-30 : Gel formation at the aggregate binder interface.....	84
Figure 4-1 : Aggregates (0.6mm-0.3mm) prepared for testing.....	88
Figure 4-2 : Si dissolution of aggregates over the time. (a) immersed in 1M NaOH solution. (b) immersed in 0.03M NaOH solution. (c) immersed in 0.003M NaOH solution. (d) immersed in 0.0003M NaOH solution .....	93
Figure 4-3 : Si dissolution of aggregates with base solution alkalinity (a) Culcairn aggregate (b) Ferronickel slag aggregate (c) Fused silica.....	96
Figure 4-4 : Si dissolution of Culcairn aggregate with time (a) 1M NaOH solution (b) 0.03M NaOH solution (c) 0.003M NaOH solution (d) 0.0003M NaOH solution.....	98
Figure 4-5 : Formation of whitish products in the test set up; (a) Culcairn in 1M NaOH solution (b) Ferronickel slag aggregate in 1M NaOH solution (c) Fused silica in 1M NaOH solution .....	100
Figure 5-1 : Expansion characteristics of mix 1-4 over 150 days when exposed to accelerated curing conditions.....	105
Figure 5-2 : Compressive strength variation of mix 1-4 over 29 days of casting.....	107
Figure 5-3 : Alkali silica gel identified in the aggregate of mix 1 at 21 days.....	109
Figure 5-4 : Alkali silica gel identified in the aggregate of mix 1 at 150 days.....	109
Figure 5-5 : Alkali silica gel identified in the aggregate of mix 2 at 150 days.....	110
Figure 5-6 : Alkali silica gel identified in the aggregate of mix 3 at 150 days.....	110
Figure 5-7 : Alkali silica gel identified in the aggregate of mix 4 at 150 days.....	110
Figure 5-8 : ASR gel composition interpreted in a ternary diagram.....	111
Figure 5-9 : Micro crack propagation in mix 1-4; (a) SEM image of mix 1 at 21 days, (b) SEM image of mix 1 at 150 days, (c) SEM image of mix 2 at 21 days, (d) SEM image of mix 2 at 150 days, (e) SEM image of mix 3 at 21 days, (f) SEM image of mix 3 at	

150 days, (g) SEM image of mix 4 at 21 days, (h) SEM image of mix 4 at 150 days, .....	114
Figure 5-10 : SEM/EDS line profile of new product form inside the cracks of aggregates in mix 4 at 150 days .....	115
Figure 5-11 : Mortar bar images of mix 1-4 after the test (150 days); (a) Mix 1 at 150 days, (b) Mix 2 at 150 days, (c) Mix 3 at 150 days, (d) Mix 4 at 150 days .....	116
Figure 5-12 : surface holes identified in mix 2 .....	116
Figure 6-1 : Expansion characteristics of mix 1-4 over 150 days when exposed to accelerated curing conditions .....	125
Figure 6-2 : Compressive strength variation of mix 1-4 over 29 days of casting .....	128
Figure 6-3 : ASR cracks identified in different locations of Mix 4 at 150 days .....	130
Figure 6-4 : ASR gel identified inside aggregate of Mix 1 at 21 days .....	130
Figure 6-5 : ASR gel identified inside aggregate of Mix 1 at 150 days .....	131
Figure 6-6 : ASR gel identified inside aggregate of Mix 2 at 150 days .....	131
Figure 6-7 : ASR gel identified inside aggregate of Mix 3 at 21 days .....	131
Figure 6-8 : ASR gel identified inside aggregate of Mix 3 at 150 days .....	132
Figure 6-9 : ASR gel identified inside aggregate of Mix 4 at 21 days .....	132
Figure 6-10 : ASR gel identified inside aggregate of Mix 4 at 150 days .....	132
Figure 6-11 : ASR gel identified in the aggregate binder interface of Mix 4 at 150 days .....	133
Figure 6-12 : ASR gel identified inside the binder of Mix 4 at 150 days .....	133
Figure 6-13 : ASR gel composition interpreted in a ternary diagram .....	135
Figure 6-14 : Variation in Na+K/Si vs. Ca/Si (atomic ratio) of ASR gels at 21 days and 150 days from Mix 1-4; shaded area is the alkali silica gel compositions developed base	

on Thaulow et al. (1996), Leemann et al. (2016), Leemann and Lura (2013) and Leemann and Merz (2013).....	136
Figure 6-15 : Micro crack propagation in mix 1-4; (a) SEM image of mix 1 at 21 days, (b) SEM image of mix 1 at 150 days (c) SEM image of mix 2 at 21 days, (d) SEM image of mix 2 at 150 days, (e) SEM image of mix 3 at 21 days, (f) SEM image of mix 3 at 150 days, (g) SEM image of mix 4 at 21 days, (h) SEM image of mix 4 at 150 days, .....	139
Figure 6-16 : Mortar bar images of mix 1-4 after the test (150 days); (a) Mix 1 at 150 days, (b) Mix 2 at 150 days, (c) Mix 3 at 150 days, (d) Mix 4 at 150 days.....	140
Figure 6-17 : Expansion behaviour of main mixes and subsidiary mixes when exposed to accelerated curing conditions.....	142
Figure 6-18 : Compressive strength variation of mixes over 29 days after casting.....	144
Figure 6-19 : ASR gel identified inside aggregate of mix 2a at 21 days .....	146
Figure 6-20 : ASR gel identified inside aggregate of mix 2a at 150 days .....	146
Figure 6-21 : ASR gel identified inside aggregate of mix 4a at 21 days .....	147
Figure 6-22 : ASR gel identified inside aggregate of mix 4a at 150 days .....	147
Figure 6-23 : ASR gel composition interpreted in a ternary diagram.....	149
Figure 6-24 : Micro crack propagation of mixes over the time; (a) SEM image of mix 2 at 21 days, (b) SEM image of mix 2 at 150 days (c) SEM image of mix 2a at 21 days, (d) SEM image of mix 2a at 150 days, (e) SEM image of mix 4 at 21 days, (f) SEM image of mix 4 at 150 days, (g) SEM image of mix 4a at 21 days, (h) SEM image of mix 4a at 150 days, .....	151
Figure 6-25 : Mortar bar images of main mixes and their subsidiary mixes; (a) Mix 2 at 150 days, (b) Mix 2a at 150 days, (c) Mix 4 at 150 days, (d) Mix 4a at 150 days .....	153

Figure 6-26 : Expansion characteristics of Mix 2-4 over 150 days when exposed to different curing conditions .....	154
Figure 6-27 : the 29-day compressive strength of Mix 2-4 exposed to different curing conditions .....	157
Figure 6-28 : ASR gel identified inside aggregate of Mix 2 exposed to curing condition III for 150 days.....	158
Figure 6-29 : ASR gel identified at aggregate binder interface of Mix 2 exposed to curing condition III for 150 days.....	159
Figure 6-30 : ASR gel identified inside aggregate of Mix 3 exposed to curing condition III for 150 days.....	159
Figure 6-31 : ASR gel identified at aggregate binder interface of Mix 3 exposed to curing condition III for 150 days.....	159
Figure 6-32 : ASR gel identified at aggregate binder interface of Mix 4 exposed to curing condition III for 150 days.....	160
Figure 6-33 : Micro crack propagation of Mix 2-4 at 150 days exposed to Curing condition I (1M NaOH at 80 °C) and Curing condition II (0.003M NaOH at 80 °C).....	162
Figure 6-34 : Micro crack propagation of Mix 2-4 at 150 days exposed to Curing condition III (1M NaOH saturated with Ca(OH) <sub>2</sub> at 80 °C) and Curing condition IV (Water at 80 °C) .....	163
Figure 6-35 : Mortar bar images of mix 1-4 after the test (150 days); (a) Mix 1 at 150 days, (b) Mix 2 at 150 days, (c) Mix 3 at 150 days, (d) Mix 4 at 150 days .....	165
Figure 6-36 : Alkali silica reaction mechanism in geopolymer mortar ( .....	166
Figure 7-1 : Expansion characteristics of mix 1-4 over 150 days when exposed to accelerated curing conditions .....	177
Figure 7-2 : Compressive strength variation of mix 1-4 over 29 days after casting.....	179

Figure 7-3 : ASR cracks identified in different locations of Mix 3 at 150 days .....	181
Figure 7-4 : ASR gel identified inside aggregate of mix 1 at 21 days .....	181
Figure 7-5 : ASR gel identified inside aggregate of mix 1 at 150 days .....	182
Figure 7-6 : ASR gel identified inside aggregate of mix 2 at 21 days .....	182
Figure 7-7 : ASR gel identified inside aggregate of mix 2 at 150 days .....	182
Figure 7-8 : ASR gel identified inside aggregate of mix 3 at 21 days .....	183
Figure 7-9 : ASR gel identified inside aggregate of mix 3 at 150 days .....	183
Figure 7-10 : ASR gel identified inside aggregate of mix 4 at 21 days .....	183
Figure 7-11 : ASR gel identified inside aggregate of mix 4 at 150 days .....	184
Figure 7-12 : ASR gel identified in aggregate binder interface of Mix 3 at 150 days..	184
Figure 7-13 : ASR gel identified inside the binder of Mix 3 at 150 days .....	184
Figure 7-14 : ASR gel composition interpreted in a ternary diagram .....	186
Figure 7-15 : Variation in Na+K/Si vs. Ca/Si (atomic ratio) of ASR gels at 21 days and 150 days from Mix 1-4; shaded area is the alkali silica gel compositions developed base on Thaulow et al. (1996), Leemann et al. (2016), Leemann and Lura (2013) and Leemann and Merz (2013) .....	187
Figure 7-16 : Micro crack propagation in mix 1-4; (a) SEM image of mix 1 at 21 days, (b) SEM image of mix 1 at 150 days (c) SEM image of mix 2 at 21 days, (d) SEM image of mix 2 at 150 days, (e) SEM image of mix 3 at 21 days, (f) SEM image of mix 3 at 150 days, (g) SEM image of mix 4 at 21 days, (h) SEM image of mix 4 at 150 days, .....	189
Figure 7-17 : Mortar bar images of mix 1-4 after the test (150 days); (a) Mix 1 at 150 days, (b) Mix 2 at 150 days, (c) Mix 3 at 150 days, (d) Mix 4 at 150 days .....	191
Figure 8-1 : Expansion characteristics of mix 1-4 over 150 days when exposed to accelerated curing conditions .....	202

Figure 8-2 : Compressive strength variation of mix 1-4 over 29 days after casting .....	205
Figure 8-3 : ASR cracks identified at different locations of Mix 3 at 150 days .....	206
Figure 8-4 : ASR gel identified inside aggregate of mix 1 at 21 days .....	206
Figure 8-5 : ASR gel identified inside aggregate of mix 2 at 21 days .....	207
Figure 8-6 : ASR gel identified inside aggregate of mix 2 at 150 days .....	207
Figure 8-7 : ASR gel identified inside aggregate of mix 3 at 21 days .....	207
Figure 8-8 : ASR gel identified inside aggregate of mix 3 at 150 days .....	208
Figure 8-9 : ASR gel identified inside aggregate of mix 4 at 21 days .....	208
Figure 8-10 : ASR gel identified inside aggregate of mix 4 at 150 days .....	208
Figure 8-11 : ASR gel identified in aggregate mortar interface of Mix 3 at 150 days .	209
Figure 8-12 : ASR gel identified inside mortar of Mix 3 at 150 days .....	209
Figure 8-13 : Variation in Na+K/Si vs. Ca/Si (atomic ratio) of ASR gels at 21 days and 150 days from Mix 1-4; shaded area is the alkali silica gel compositions developed base on Thaulow et al. (1996), Leemann et al. (2016), Leemann and Lura (2013) and Leemann and Merz (2013).....	210
Figure 8-14 : ASR gel composition interpreted in a ternary diagram.....	211
Figure 8-15 : Circular carves identified in Mix 3 at 150 days .....	213
Figure 8-16 : Micro crack propagation in mix 1-4; (a) SEM image of mix 1 at 21 days, (c) SEM image of mix 2 at 21 days, (d) SEM image of mix 2 at 150 days, (e) SEM image of mix 3 at 21 days, (f) SEM image of mix 3 at 150 days, (g) SEM image of mix 4 at 21 days, (h) SEM image of mix 4 at 150 days, .....	214
Figure 8-17 : Mortar bar images of mix 1-4 after the test completion; (a) Mix 1 at 21 days, (b) Mix 2 at 150 days, (c) Mix 3 at 150 days, (d) Mix 4 at 150 days .....	215
Figure 9-1: Alkali silica reaction mechanism in geopolymer mortar .....	224



## LIST OF TABLES

Table 2-1 : Applications of geopolymer materials based on the Si/Al ratio .....	12
Table 2-2: Chemical composition of fly ash .....	18
Table 2-3: Chemical composition of GGBFS (Li et al. 2010).....	19
Table 3-1 : Chemical composition of cementitious materials based on XRF analysis ...	54
Table 3-2 : Chemical composition of sodium silicate.....	57
Table 3-3 : Water absorption and apparent density of aggregates .....	58
Table 3-4 : XRF analysis results of aggregates.....	58
Table 3-5 : Grading requirement as specified in AS 1141.60.1.....	72
Table 3-6 : Mix design details.....	76
Table 3-7 : Sample preparation techniques for SEM analysis .....	82
Table 4-1 : Preparation of NaOH solutions .....	88
Table 4-2 : Operational parameters adopted for the ICP analysis .....	90
Table 4-3 : Pre-treatment acquired in each solution .....	91
Table 4-4 : Analytes and their respective wavelengths targeted during the analysis.....	91
Table 4-5 : Summary of final outcomes.....	99
Table 5-1 : Average expansion of mortar bars with basalt at 10, 21 and 150 days .....	104
Table 5-2 : Summary of SEM /EDS analysis on ASR gel located in mix 1-4.....	109
Table 5-3 : Average chemical composition of the compound .....	115
Table 6-1 : Average expansion of mortar bars at 10, 21 and 150 days.....	126
Table 6-2 : Summary of SEM /EDS analysis on ASR gel located in Mix 1-4 .....	134
Table 6-3 : Average expansion of mortar bars at 10, 21 and 150 days.....	143
Table 6-4 : Summary of SEM /EDS analysis on ASR gel in geopolymer mixes .....	147

Table 6-5 : Average expansion of mortar bars at 10, 21, 29 and 150 days.....	155
Table 6-6 : Summary of SEM /EDS analysis on ASR gel located in mix 2-4 exposed to curing condition III for 150 days .....	160
Table 7-1 : Average expansion of mortar bars at 10, 21 and 150 days.....	177
Table 7-2 : Summary of SEM /EDS analysis on ASR gel located in mix 1-4.....	185
Table 8-1 : Average expansion of mortar bars at 10, 21, 100 and 150 days.....	201
Table 8-2 : Summary of SEM /EDS analysis of ASR gel located inside aggregates of mix 1-4 .....	210

## LIST OF NOTATIONS

AAM	:	Alkali Activated Material
AAR	:	Alkali aggregate reaction
ACR	:	Alkali Carbonate Reaction
AMBT	:	Accelerate Mortar Bar Test
ASR	:	Alkali Silica Reaction
CASH	:	Calcium Aluminium Silicate Hydrate
CPT	:	Concrete Prism Test
CSH	:	Calcium Silicate Hydrate
EDS	:	Energy Dispersive Spectroscopy
FA	:	Fly Ash
GGBFS	:	Ground Granulated Blast Furnace Slag
GPC	:	Geopolymer Cement
ICP	:	Inductively Coupled Plasma
MK	:	Meta Kaolin
NASH	:	Sodium Aluminium Silica Hydrates
OPC	:	Ordinary Portland cement
SCM	:	Supplementary Cementitious materials
SEM	:	Scanning Electron Microscope
SSD	:	Saturated Surface Dry
TAS	:	Total Alkali Silica
TEM	:	Transmission electron microscope
XRD	:	X-ray Powder Diffraction
XRF	:	X-ray Fluorescence

# CHAPTER 1 : Introduction

---

## 1.1 Background

Concrete is the most widely used construction material in the world. In fact, it is estimated that the annual concrete consumption is second only to the annual water consumption (Neves 2016). Thus, being the main constituent of concrete, Ordinary Portland cement (OPC) also ranked among the highly consumed materials in the world reaching its billion tonnes in 2016 (CEMBUREAU 2016; Nath 2014). However, high carbon footprint and high embodied energy associated with OPC has initiated a broad discussion on an adaptation of sustainable and eco-friendly alternatives to Portland cement over the past few decades.

Utilization of industrial by-products as supplementary cementitious materials (SCM) in OPC concrete to enhance its properties and reduce the environmental impact have been well established for decades (Malhotra 2002). In alkali-activated cement, OPC is fully replaced by aluminosilicate source with alkali source as the activator. Even though the alkali activation technology was introduced back in 1908 by Kuehl, it got greater attention in the late 1970s when Davidovits discovered the geopolymer binders, more stable subcategory of alkali-activated materials (AAM) (Davidovits 2008; Provis 2014).

Geopolymer is an alkali silicon-oxo-aluminate network formed when aluminosilicate materials such as fly ash (FA), ground granulated blast furnace slag (GGBFS), metakaolin (MK) react with the alkali reagents (Davidovits 2008). Mechanical properties, bond characteristics and workability of concrete made out of geopolymers have been found similar to those of the OPC based concrete (Aldred & Day 2012; Castel

& Foster 2015; Duxson et al. 2007; Fernandez-Jimenez et al. 2006; Lloyd & Rangan 2010; Sofi et al. 2007a). The environmental and socioeconomic factors of geopolymer concrete have been also well reviewed during the last few decades making its path even clearer to become a promising alternative to Portland cement (Aldred & Day 2012; Davidovits 1994; Hardjito, Djwantoro et al. 2004; Van Deventer et al. 2007). Moreover, many researchers suggest that geopolymer concrete may perform satisfactorily against most of the durability issues identified for OPC concrete (Aldred & Day 2012; Law et al. 2015; Singh et al. 2015; Van Deventer et al. 2007).

Alkali aggregate reaction (AAR) is a long-term durability issue in concrete that occurs due to the formation of the hydroscopic gel as a result of a chemical reaction between reactive phases of aggregates and alkalis from cement paste (Hobbs 1988; Glasser and Kataoka, 1981). The theoretical risk of AAR is higher in geopolymer concrete compared to OPC concrete due to the high alkali content in the activator. However, the published works on AAR in alkali-activated concrete reveal that the effect of AAR also depends on the aluminosilicate source. (Bakharev et al. 2001a; Fadhil Nuruddin & Razak 2014; Krivenko et al. 2014; Kupwade-Patil & Allouche 2012; Shi, C et al. 2015; Shi, Z et al. 2015). Most of the researchers (Fadhil Nuruddin & Razak 2014; García-Lodeiro et al. 2007; Kupwade-Patil & Allouche 2012) who worked with low calcium aluminosilicate sources (low calcium fly ash and metakaolin) concluded that the potential risk of alkali silica reaction (ASR) is very low in those systems. On the other hand, alkali-activated binders with high calcium content (high calcium fly ash and GGBFS) have shown significant expansions in ASR testing (Bakharev et al. 2001a; Shi, Z et al. 2015). Furthermore, studies of Fernández-Jiménez and Puertas (2002) reported that alkali activated mortar might show delayed expansion which urged some modifications in current ASR testing protocols.

## **1.2 Aim and Objectives**

This research aims to assess the risk of alkali aggregate reaction in geopolymer concrete prepared using fly ash and GGBFS as aluminosilicate source materials. The following objectives were defined in order to achieve the main goal.

1. Study the chemistry and mechanisms of AAR in geopolymer mortars
2. Investigate the role of GGBFS in AAR in geopolymer mortars
3. Study the AAR of geopolymer mortar using natural and manufactured aggregates
4. Modify the existing test protocols (accelerated mortar bar test) to suit for geopolymer mortar.

## **1.3 Scope of study**

This study mainly will involve two tests: chemical test and accelerated mortar bar test (Australia 2014, 2015). For the chemical test, three reactive aggregates will be immersed in NaOH solutions with different concentrations for 100 days and ions concentration of the solutions be monitored periodically by inductively coupled plasma (ICP) analysis to determine the silica dissolution capability of aggregates.

Expansion test developed based on the accelerated mortar bar test (AMBT) was adapted in this study to compare the degree of ASR in different scenarios which were further discussed in Section 3. Even though it is widely accepted that the severe exposure conditions in accelerated mortar bar test might over predict the reactivity, it should be noted that the prime focus of this study is not to evaluate the reactivity but to compare the effect of different parameters on alkali silica reaction in geopolymer mortar in order to identify the ASR mechanism. In fact, short testing period in AMBT compared to concrete prism test (CPT) would allow to cover significant number of parameters even

with extended testing time which would be an additional advantage in achieving the main goal.

For the accelerated mortar bar test, 25x25x285 mortar bars were cast and tested for 150 days. Ground granulated blast furnace slag (GGBFS) from Blue Circle Southern Cement Australia and low calcium (Class F) fly ash from the Eraring power plant in New South Wales, Australia was used as the aluminosilicate sources in this study. A mix of sodium silicate ( $\text{Na}_2\text{SiO}_3$ ) solution and sodium hydroxide (NaOH) solution was used as the alkaline activator. Four aggregates with different chemical and phase compositions were used in the study. Basalt in this study is a natural aggregate considered non-reactive based on its field records and the accelerated mortar test results. Culcairn (aggregate named after the quarry) is a reactive natural aggregate based on the accelerated mortar bar test results. Ferronickel slag aggregate is a by-product of nickel manufacturing in SLN production plant in New Caledonia. The initial testing showed that ferronickel slag aggregate contains highly reactive amorphous silica which placed it among the reactive aggregate category. Fused silica is a highly reactive pure amorphous silica which is theoretically the most reactive aggregate type available for testing.

Six mix designs including three main geopolymer mixes with fly ash to GGBFS weight ratio 9, 4 and 1, two subsidiary mixes with fly ash to GGBFS ratio 9 and 1 and an OPC mix based on the mix design details in AS 1141.60.1 were used during this study. In main geopolymer mixes, all the ratios except aluminosilicate source ratio were kept constant while deviator mixes were developed targeting lower strengths but with same fly ash/ GGBFS content as in main geopolymer mixes.

For accelerate mortar bar test (AMBT), two curing solutions (1M NaOH solution and 0.003M NaOH solution) were used in the study. The length changes in the mortar bars were measured periodically, and representative samples were extracted for SEM-EDS

analysis at 21 days and 150 days. Compressive strength variation over the initial 28 days was measured as well by testing mortar cubes.

## **1.4 Research significance**

Geopolymer concrete has emerged over the last few decades to become a sustainable, eco-friendly alternative to ordinary Portland cement. Even though it exhibits notable benefits with respect to mechanical properties, environmental and socioeconomic factors doubt arise regarding its durability performance including alkali aggregate reaction.

This work aims to identify the chemistry and the reaction mechanism of alkali aggregate reaction in geopolymer systems. Furthermore, it is anticipated that the outcome of this study would help in the development of geopolymer concrete mixes that allow utilising the aggregates, otherwise previously abandoned in OPC based concrete production due to their alkali reactive nature. This is especially beneficial for some manufactured aggregates as it clears up another way to deploy the industrial by-products effectively.

On the other hand, this study also proposes some major modifications to the existing accelerated mortar bar test (AS 141.60.1) to be used for geopolymer concrete. Establishing guidelines and specifications are the main barriers to the adoption of geopolymer concrete in the construction industry. Thus, the knowledge gained from this research is expected to promote the use of geopolymer concrete in the industry.

## **1.5 Thesis Outline**

The thesis consists of nine chapters as outlined below:

Chapter 1 contains a brief background study, research objectives, scope of the research and research significance.

Chapter 2 provides a comprehensive review of the current state of the research. It commences with a brief investigation of the general chemistry and properties of geopolymer binders and recent development in the understanding of alkali aggregate reaction. Existing studies on alkali aggregate reaction in geopolymer binders and the test methodologies currently used to identify alkali aggregate reaction in concrete are extensively reviewed with respect to available literature and case studies.

Chapter 3 describes the relevant details of materials, sample preparation, mix designs used in this study, instrumentation and data acquisition and details of the experimental procedure adopted.

Chapter 4 presents the experimental results of the Si dissolution test performed on reactive aggregates.

Chapter 5 presents the experimental results relating to the assessment of alkali aggregate reaction in geopolymer mortar with Basalt aggregates which considered nonreactive in OPC based concrete.

Chapter 6 presents the experimental analysis related to alkali aggregate reaction geopolymer mortar with Culcairn aggregates which considered reactive in OPC mortar. The effect of different curing conditions and different geopolymer mix designs (variation in mechanical properties) over alkali aggregate reaction are also analysed.

Chapter 7 presents the experimental study on alkali aggregate reaction in geopolymer mortar with manufactured reactive aggregates (Ferronickel slag aggregates).

Chapter 8 presents the performance of geopolymer mortars with highly reactive pure amorphous silica (fused silica) with respect to the alkali aggregate reaction.

Chapter 9 contains the conclusion and the recommendations for future works.

## **CHAPTER 2 : Literature Review**

---

### **2.1 Overview**

Concrete is the most consumed man-made material and second most consumed product by human beings after water (Neves 2016; Penttala 1997). Thus, being the main constituent for concrete, cement production also increases significantly over the past few decades reaching 4.65 billion tonnes in 2016 according to the annual activity report of CEMBUREAU (CEMBUREAU 2016). Furthermore, Hasanbeigi et al. (2012) reported that the production of one metric ton of cement might result in 0.73-0.99 tonnes of carbon dioxide release to the atmosphere. The carbon dioxide emission from the cement industry accounts for approximately 5-8 % of the total greenhouse gas emissions by human activities (Mikulčić et al. 2016; Summerbell et al. 2016). Since greenhouse gases are directly responsible for the global warming, it is clear that the ordinary Portland cement (OPC) concrete plays a significant role in the global environmental crisis. Cement also has a high embodied energy which categorised it among the non-sustainable construction material group after aluminium and steel (Hardjito 2005; Tennakoon 2016). Furthermore, premature deterioration in Portland cement structures, especially in severe environmental conditions, has become a serious issue over the last couple of decades as approximately 20-25% of annual cement production is used for the renovation of existing structures (Palomo et al. 2014; Song 2007). Durability issues along with the environmental and sustainable issues associated with the Portland cement led researchers to develop alternative solutions in the last few decades.

## **2.2 Geopolymer technology**

### **2.2.1 History**

The term, “Geopolymer” was first introduced by Davidovits in 1979 to describe the inorganic binder group with three-dimensional polymeric structure (Davidovits 1991; Song 2007). van Deventer et al. (2010) suggested that geopolymer is a subcategory of alkali-activated materials (see Figure 2-1) based on their chemical structures.

Alkali-activated materials (AAM) were first formally introduced by Kuehl in 1908 (Kuehl 1908; Provis 2014). But it only got proper attention when Purdon develops the first alkali-activated binder using blast furnace slag and sodium hydroxide (Provis 2014). However, its commercial value risen with the works of Glukhovsky who developed a binder called “soil cement” which was successfully used in construction works by Glukhovsky Institute in Kiev, Ukraine (Provis 2014; Shi et al. 2006; van Deventer et al. 2010). Geopolymer came to the picture in the late 1970s but took another two decades to stabilise its platform before having a boom in late 1990s in the research arena (Nath 2014; Palomo et al. 2014).

Even though the recent history of alkali-activated materials starts after Kuehl, many believe that Egyptians and Romans used it as a construction material in their structures (Li et al. 2004; van Deventer et al. 2010). In fact, it is reported that Glukhovsky studied the binders used in Egyptian and Roman civilisations before developing the soil cement in the 1950s (van Deventer et al. 2010).

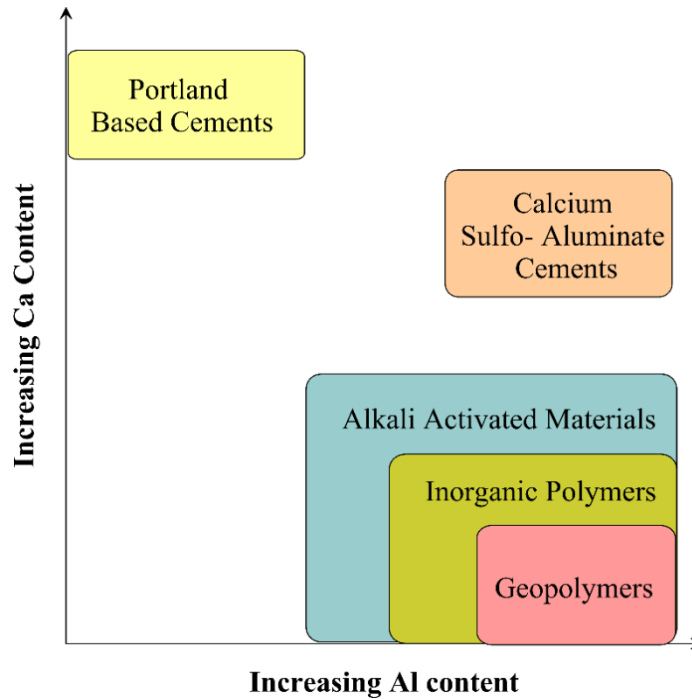


Figure 2-1: Classification of different alkali activated materials.

Darker shadings correspond to higher alkali concentrations

Adopted from van Deventer et al. (2010)

### 2.2.2 Geopolymer Chemistry

Alkali-activated materials (AAM) are inorganic polymers result from the reaction between aluminosilicate and alkali sources (Nath 2014; van Deventer et al. 2010). However, if the final product has a highly coordinated three-dimensional structure, then it can be further categorised as geopolymer binders (Nath 2014; van Deventer et al. 2010). The primary building unit in geopolymer network is sialate (Alkali - Si - O - Al) which gives the name poly(sialate) to the geopolymer binder structure (Davidovits 1994; Nath 2014).

In poly(sialate) structures, four-fold aluminium ions ( $Al^{3+}$ ) and Si ions ( $Si^{4+}$ ) linked via oxygen ions to form a network as shown in Figure 2-2. The negative charge of the aluminium ions shall be neutralized by the cations ( $Na^+$ ,  $K^+$ ,  $Ca^{2+}$  etc.) (Abdullah et al. 2011; Davidovits 1994).

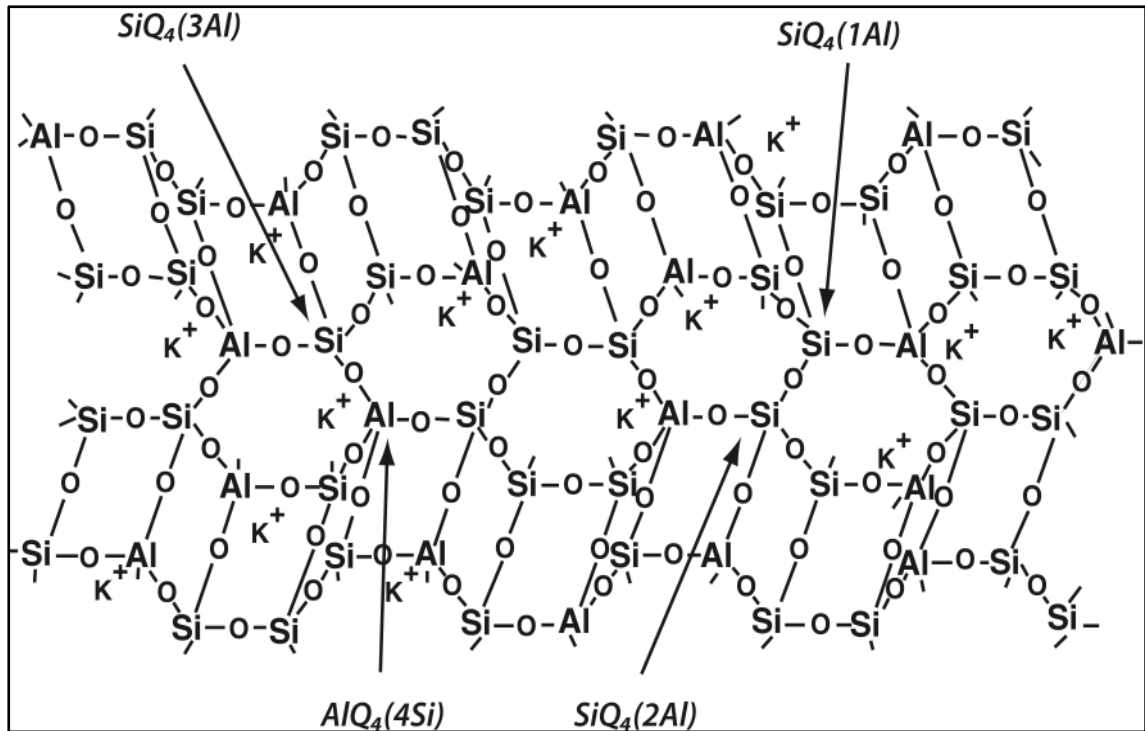


Figure 2-2 : Poly(sialate) network in geopolymer binder  $K^+$  can be any monovalent cation  
Adapted from Davidovits (1994)

Davidovits (1994) also suggested an empirical formula for poly(sialate).

$$M_n [-(SiO_2)_z - AlO_2]_n w H_2O \quad \text{Eq. 2-1}$$

Where M is any cation ( $Na^+$ ,  $K^+$ ,  $Ca^{2+}$ , etc.)

$z = 1, 2, 3$  or higher

$n$  is the degree of condensation

Based on the  $z$  (Si/Al ratio), Davidovits (2008) has further categorised the poly(sialate) into four subgroups as shown below and each subgroup consists of their properties. Thus, the functionality and the use of each subgroup is different as shown in Table 2-1.

Sialate  $z=1$  (Si/Al = 1)

The primary building unit is (-Si-O-Al-O-) and can be formulated as a chain or ring-like structures as shown in Figure 2-3. This can be the product of poly-condensation of ortho-sialate  $(OH)_3 - Si - O - Al - (OH)_3$ .

Sialate-siloxo  $z=2$  ( $Si/Al = 2$ )

The primary building unit is  $(- Si - O - Al - O - Si - O -)$ . This can be the product of condensation reaction between orthosilicate and ortho-silicic acid ( $Si(OH)_4$ ). There can be two types of isomorphs, linear and cycle.

Sialate-disiloxo  $z=3$  ( $Si/Al = 3$ )

The primary building unit is  $(- Si - O - Al - O - Si - O - Si - O -)$ . This can be the product of condensation reaction between orthosilicate and two ortho-silicic acids ( $Si(OH)_4$ ). Thus, the sialate unit may be located at the beginning, middle or end of the sequence. There can be three types of isomorphs, linear, branched and cycles as shown in Figure 2-3 : Terminology of poly-sialate.

Sialate link  $z > 3$  ( $Si/Al > 3$ )

These are the poly(sialate), poly(silaxonate) or poly(silanol) chains bridged with Aluminium link  $(-O - Al - O-)$  as shown in Figure 2-3.

Table 2-1 : Applications of geopolymer materials based on the Si/Al ratio

Adapted from Hardjito (2005)

Si/Al (z)	Applications
1	Bricks, ceramics, fire protection
2	Concrete, low CO <sub>2</sub> cement, radioactive and toxic waste encapsulation
3	Fibreglass composites, heat resistance composites, foundry equipment
>3	Sealants
20<Si/Al<35	Heat resistance and fire resistance fibre

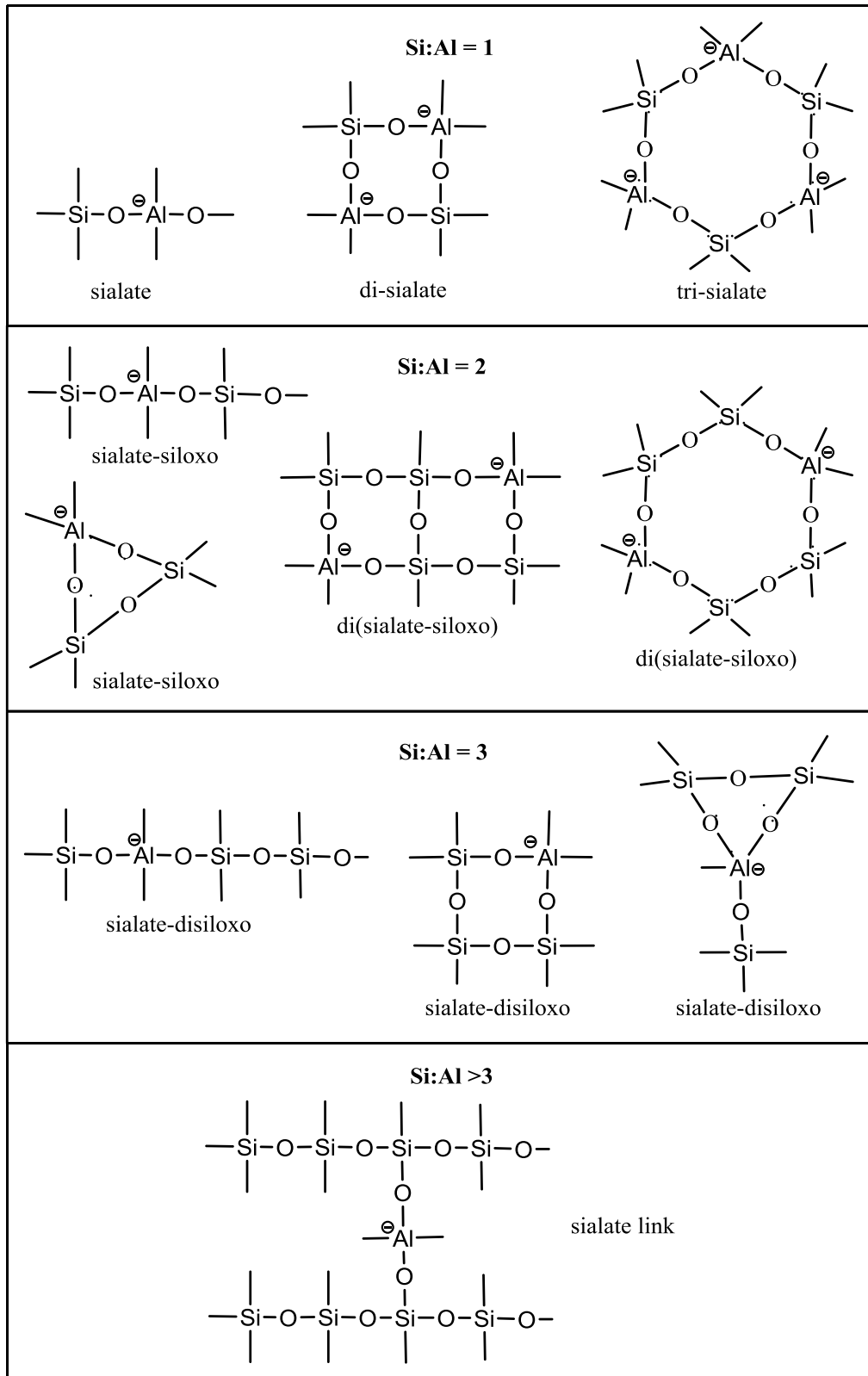


Figure 2-3 : Terminology of poly-sialate

⊖ Represent the negative charge of Aluminium ion

Adapted from Davidovits (2008)

### 2.2.3 Geopolymerization mechanism

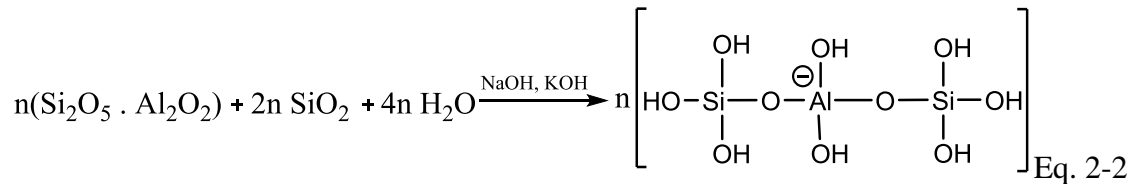
In simple terms, Geopolymerization is the reaction between aluminosilicate source and alkali source which may result in a polymeric compound. However, the properties of the final product largely depend on the reaction mechanism and the source materials. Thus, it is essential to control the geopolymerization process in order to achieve the desired output (Provis 2014).

Glukhovskiy has developed the initial concept which was extended and refined by many others (Duxson et al. 2007). However, it is possible to identify three distinct processes in most of those models (Nath 2014; Provis 2014);

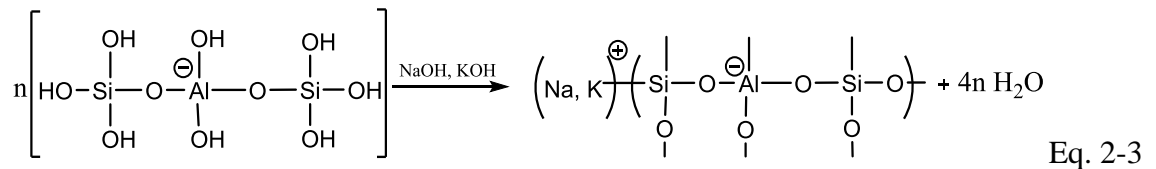
1. Dissolution of Si and Al from the source materials
2. Rearrangement and condensation of precursor ions to monomers
3. Polycondensation of monomers

Chemical interpretation of the above processes as follows (Davidovits 1994; Nath 2014);

Dissolution and formation of monomers (see Eq. 2-2 and Eq. 2-3)



Polycondensation of monomers



However, the above two processes can overlap each other and occur almost simultaneously. Therefore, it is extremely difficult to isolate and study each of them separately (Palomo et al. 1999).

Van Deventer et al. (2007) proposed a mathematical model for the alkali activation (Figure 2-4) process of low calcium aluminosilicate source materials.

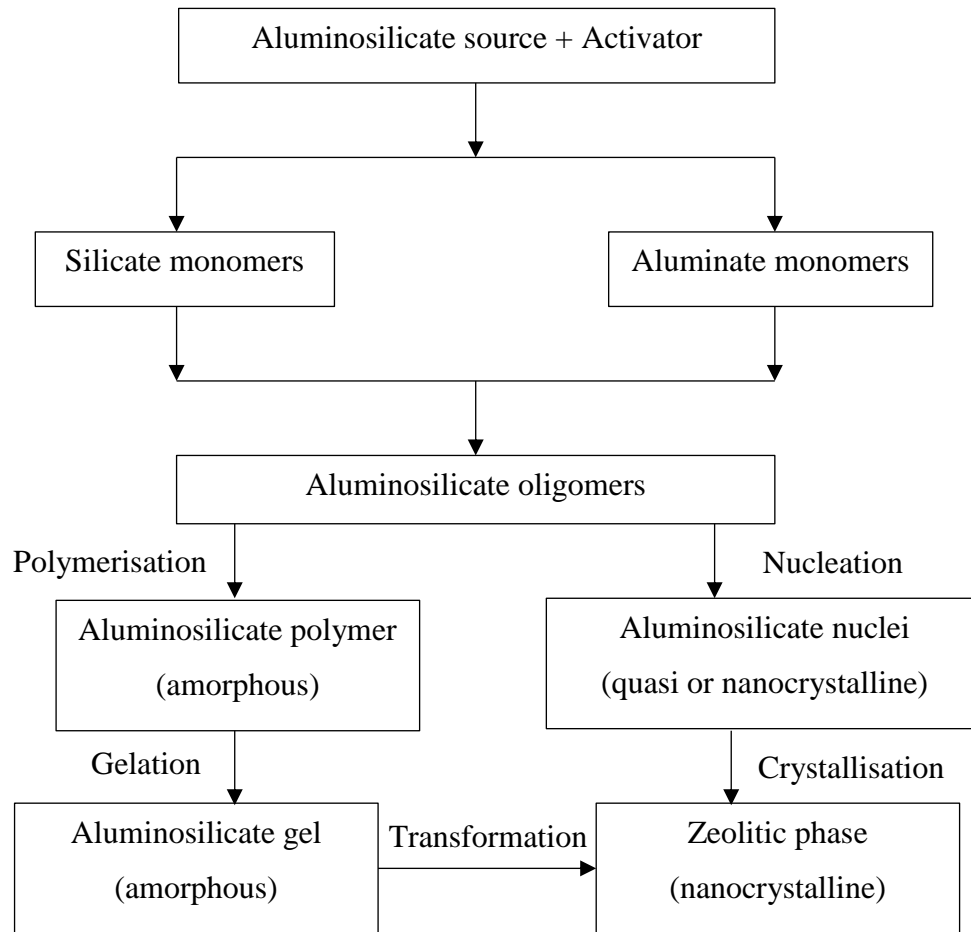


Figure 2-4 : Mathematical model for alkali activation of low calcium aluminosilicate source materials

Adapted from Van Deventer et al. (2007)

#### 2.2.4 Constituents of Geopolymer binder

##### Aluminosilicate source

Theoretically, any material that can supply aluminium and silica under high alkalinity environment can be used as an aluminosilicate source in geopolymer reaction (Nath 2014). However, many researchers claimed that the properties of aluminosilicate sources such as chemical content, particle size distribution, amorphous content, etc. have a direct influence on the properties on geopolymer products (Fifinatasha et al. 2013; Provis 2014; Van Jaarsveld et al. 2003). Thus, Provis (2014) stated that the alkali activation is a solution mediated process, which needs proper understanding and guidance in mix design stage to achieve the desired properties in geopolymer binders.

There are various aluminosilicate sources identified as potential feedstocks in geopolymer production which include but not restricted to industrial by products such as fly ash (Class C and F), GGBFS (Ground Granulated Blast Furnace Slag) and naturally occurring materials such as metakaolin, feldspar, mine tailings etc. (Hardjito 2005). Gourley (2003) stated that metakaolin is preferred over others due to its high dissolution rate and easier control on the Si/Al ratio. However, the use of metakaolin in geopolymer production is restricted by its expensiveness and the high energy consumption (Hardjito 2005). Thus, many researchers have tried to use industrial by-products such as fly ash and GGBFS in geopolymer production as they have very low energy footprint and eventually reduces the waste dump through recycling (Al Bakri et al. 2013; Hardjito 2005; Tennakoon 2016).

## **Fly ash**

Fly ash is the main by-product of the coal power plants. It is estimated that the current global annual fly ash production is approximately 500 million tonnes with approximately 40% utilisation (Soh et al. 2017). There are two types of fly ash, Class F and Class C based on its chemical composition (Ca content) as shown in Table 2-2 (ASTM-C618-17 2017; Christy & Tensing 2011). Diaz et al. (2010) stated that fly ash with higher glass phase and finer particle size might increase the geopolymerization reaction and thus the mechanical properties of the final product such as compressive strength. Furthermore, Fernández-Jiménez and Palomo (2003) reported that in order to achieve optimal binding properties in alkali activation fly ash should have the following characteristic:

- Percentage of unburned particles < 5%
- $\text{Fe}_2\text{O}_3$  content  $\leq 10\%$
- CaO content  $\leq 10\%$
- Reactive silica content 40-50%
- 80-90% fraction of particles lower than 45  $\mu\text{m}$
- Vitreous phase should be >50%
- $[\text{SiO}_2]_{\text{reactive}}/[\text{Al}_2\text{O}_3]_{\text{reactive}} > 1.5$

Many researchers who worked on the durability of geopolymer binder concluded that typically geopolymer with class F fly ash is more durable compared to class C fly ash (Bakharev 2005; Duxson & Provis 2008; Temuujin et al. 2013). Thus, despite having a lower early strength development, most of the researchers preferred class F fly ash as aluminosilicate source over class C fly ash in geopolymer binders (Nath 2014; Tennakoon 2016). Furthermore, class C fly ash is limited to few countries which further reduces its value as an aluminosilicate source material (Tennakoon 2016).

Table 2-2: Chemical composition of fly ash

Chemical component	Class F (wt. %)	Class C (wt.%)
SiO <sub>2</sub>	20-60	15-45
Al <sub>2</sub> O <sub>3</sub>	5-35	20-25
Fe <sub>2</sub> O <sub>3</sub>	6-24	4-15
CaO	1-12	15-40
MgO	0-5	3-10
K <sub>2</sub> O	0-3	0-4
Na <sub>2</sub> O	0-4	0-6
SO <sub>3</sub>	0-4	0-10
TiO <sub>2</sub>	1-2	<1
LOI	0-15	0-5

**Ground granulated blast furnace slag (GGBFS):**

Slag is the main by-product of the iron and steel industry which used as a blending material in geopolymer production (Li et al. 2010). The global annual GGBFS production in 2015 is estimated to be 300-360 million tonnes (Gijbels et al. 2017). Granulated blast furnace slag is a glassy coarse material (unprocessed particle size is greater than 4.5mm) which contains gehlenite ( $2\text{CaO} \cdot \text{Al}_2\text{O}_3 \cdot \text{SiO}_2$ ), akermanite ( $2\text{CaO} \cdot \text{MgO} \cdot 2\text{SiO}_2$ ) and calcium silicate glass (Kumar et al. 2010; Tennakoon 2016). Table 2-3 contains the typical chemical composition of slag (Li et al. 2010). Duxson and Provis (2008) stated that the reactivity of GGBFS depends on the free Ca free Si molar ratio, which typically lies in between 1.3-1.5 for slag. Due to the presence of significant amount of free calcium in GGBFS, calcium silicate hydrate (CSH) and calcium aluminosilicate hydrate (CASH) also form in the geopolymer system along with sodium aluminosilicate hydrate (NASH) during the alkali activation reaction (Kumar et al. 2010; Puertas et al. 2000). Formation of CSH in geopolymer system may improve the initial setting time and result in early

strength gain (Kumar et al. 2010; Yip et al. 2008). However, Puertas et al. (2000) further stated that CSH in alkali-activated system has lower calcium content compared to the CSH in OPC binders.

Table 2-3: Chemical composition of GGBFS (Li et al. 2010)

Chemical component	wt. %
SiO <sub>2</sub>	31-38
CaO	38-44
Al <sub>2</sub> O <sub>3</sub>	9-13
MgO	7-12

#### 2.2.4.1 Alkali activator

Combinations of sodium hydroxide (NaOH) and sodium silicate (Na<sub>2</sub>SiO<sub>3</sub>) or potassium hydroxide (KOH) and potassium silicate (K<sub>2</sub>SiO<sub>3</sub>) is the most common and effective alkali activator solutions used for geopolymerization (Davidovits 2008; Lee & Van Deventer 2007; Xu & Van Deventer 2002). However, due to the expensiveness of the potassium salts, most researches used sodium based solutions as the activator (Tennakoon 2016).

Palomo et al. (1999) reported that the reaction rate is higher when alkali activator contains soluble silicates. However high sodium silicate concentrations may inhibit the polycondensation reaction as the excessive Si ions ( $\text{SiO}_2/\text{M}_2\text{O} > 2$ ; M is Na<sup>+</sup> or K<sup>+</sup>) in the system may restrict the Al ion contribution to the polymeric reaction (Sindhunata et al. 2006). The initial ion dissolution rate in geopolymer depends on the hydroxyl ion concentration (OH<sup>-</sup>) in the system (Antonić et al. 1994). In fact, it is established that when the hydroxyl ion concentration is higher, most of the silicates present in aggregates dissolved in the solution minimising the effect of the internal bond structure of aggregates

in Si dissolution (Álvarez-Ayuso et al. 2008; Davidovits 2008). van Jaarsveld and Van Deventer (1999) who worked on different types of alkali hydroxides concluded that the type of cation has influence throughout the geopolymerization process since they experienced different Si/Al ratios when used different cations. Moreover, earlier studies by McCormick and Bell (1989) revealed that size of cations affect the rate of zeolite nucleation which is in line with the theoretical aspect of larger cations may increase the extent of condensation in geopolymerization process (van Jaarsveld & Van Deventer 1999). Thus, van Jaarsveld and Van Deventer (1999) concluded that larger cation (potassium) might result in higher compressive strengths but also the low crystallinity of those structures makes them vulnerable to acid attacks.

The current practice in activator preparation is to let them settle for 24 hours after mixing alkali hydroxide and the alkali silicate solutions (Tennakoon 2016). However, since industry prefers to work with dry powder rather than solutions, it is necessary to implement a method to incorporate solid activator before initiating the large-scale geopolymer production (Tennakoon 2016).

#### **2.2.4.2 Water**

Even though water is not a main reactant in geopolymerization, it plays a vital role by altering the properties of the geopolymer mix. Experimental results of Panias et al. (2007) suggested a decrease in compressive strength when the solid to liquid ratio is greater than 2.05 g/ml. Furthermore, when the water content is low, casting defects due to the low workability of the mix may also result in low compressive strengths (Panias et al. 2007). Zuhua et al. (2009) has identified three roles of water in geopolymerization

1. Facilitate the ion transportation
2. Contribution to the hydrolysis
3. Polycondensation by releasing the water

Fang and Kayali (2013) stated that about 10.74% of added water is non-evaporable even at very high temperatures. Zuhua et al. (2009) further added that this water does not create any drying shrinkage but helps to sustain the long-term strength in geopolymer binders. On the other hand, Diaz and Allouche (2010) illustrated the importance of water by showing that high alkalinity in activator may induce pores in hardened concrete which eventually weaken the geopolymer binder.

## **2.2.5 Properties of geopolymer binder**

Properties of geopolymer concrete depend on several factors including; aluminosilicate source material type and content, alkali activator type and content, water content, curing condition, mixing parameters, etc. (Tennakoon 2016).

### **2.2.5.1 Properties of fresh binder**

Geopolymer is a cohesive binder with a high viscosity which significantly decreases its workability properties (Hardjito & Rangan 2005). Most of the accelerators, retarders and superplasticisers used in Portland cement mixes are not effective in geopolymer binders (Puertas et al. 2014). In fact, some researchers stated that the use of admixtures might result in loss of mechanical properties in geopolymer binder (Chindaprasirt et al. 2007; Hardjito, Djwantoro et al. 2004). Chindaprasirt et al. (2007) concluded that an increase in water content could improve the workability of the geopolymer mix to a certain extent without a significant effect on its structural properties. The setting time of geopolymer binder can be controlled by altering the fly ash to GGBFS ratio in the mix design (Tennakoon 2016). This phenomenon was successfully implemented by Deb et al. (2014) in developing an ambient cured geopolymer concrete. Thus, it is clear that geopolymer binder properties can be controlled effectively by adjusting the mix proportions rather than introducing admixtures.

### **2.2.5.2 Properties of hardened binder**

#### **Compressive and tensile strength**

Diaz and Allouche (2010) concluded that fly ash based geopolymer could achieve similar or slightly higher compressive strength compared to OPC concrete. Moreover, the works of Hardjito, Djwantoro et al. (2004) illustrated that the inclusion of calcined phases into the geopolymer binder increases the final compressive strength significantly. In fact, geopolymer concrete can gain 70% of its characteristic strength within the first few hours of hardening (Davidovits 2002; Li et al. 2004). Hardjito, D et al. (2004) stated that curing time and temperature have a significant influence on the strength development of geopolymer concrete. However, Van Jaarsveld et al. (2002) found that exposing geopolymer to high temperatures for too long may result in a reduction of the compressive strength. As discussed above in section 2.2.4.2, water also has a pessimum effect on the structural properties.

Geopolymer concrete also has a superior flexural and tensile splitting strength compared to that of OPC concrete (Ryu et al. 2013; Sarker 2011; Sofi et al. 2007b). Sarker (2011) experimentally showed that the bond characteristic of geopolymer concrete is better than that of OPC. Furthermore, Davidovits (2008) stated that the structural behaviour of reinforced geopolymer concrete structures was more or less similar to the reinforced OPC concrete structures. In fact, the experimental failure loads were almost similar to the calculated failure loads based on AS 3600 and ACI 318-02 which implies that the existing design codes can be successfully implemented to the structural designs of geopolymer concrete for ultimate capacity (Davidovits 2008).

### **Stress-strain characteristics**

Stress-strain behaviour of concrete is very important in determining the serviceability properties of the structure (Tennakoon 2016). The elastic modulus of geopolymer concrete is said to be lower than that of OPC concrete (Hardjito & Rangan 2005; Noushini et al. 2016). In fact, Fernandez-Jimenez et al. (2006) and Sofi et al. (2007b) claimed that the elastic modulus of geopolymer is less than the predicted values based on standards. However experimental works of Hardjito and Rangan (2005) concluded that the poisons ratio of both geopolymer and OPC falling to a similar range.

### **Shrinkage**

There are different types of shrinkages in concrete: drying shrinkage, autogenous shrinkage, plastic shrinkage, chemical shrinkage, thermal shrinkage and carbonation shrinkage (Šahinagić-Isović et al. 2012). Drying shrinkage in geopolymer concrete may be affected by several factors: absence of appropriate curing (Provis et al. 2014), high water content (Kukko & Mannonen 1982; Provis et al. 2014) and activator properties (Douglas et al. 1992; Neto et al. 2008; Zheng 2009). Drying shrinkage of heat cured geopolymer is lower than that of OPC (Davidovits 2008; Wallah & Rangan 2006). However, Davidovits (2008) reported that drying shrinkage of ambient cured geopolymer is even higher than that of OPC.

#### **2.2.5.3 Durability**

This section includes a brief analysis of the performance of geopolymer over conventional durability issues in OPC structures. However, alkali aggregate reaction (AAR) in geopolymer concrete is not discussed here as it needed a broader discussion and thus a separate section.

## **Sulphate attack**

Formation of expansive compounds like gypsum ( $\text{CaSO}_4 \cdot \text{H}_2\text{O}$ ), ettringite ( $\text{CaO} \cdot \text{Al}_2\text{O}_3 \cdot 3\text{CaSO}_3 \cdot 32\text{H}_2\text{O}$ ), thaumasite ( $\text{Ca}_3\text{Si}(\text{OH})_6\text{CO}_3\text{SO}_4 \cdot 12\text{H}_2\text{O}$ ) etc. due to the reaction between sulphate ions and cement is commonly known as the sulphate attack (Tennakoon 2016). Apart from the internal pressure generated from the expansive products, sulphate attack also deteriorates the paste as it consumes calcium and silica ions (Neville 2011).

Many researchers concluded that sulphate resistance of geopolymer binder is higher than that of OPC due to its C/N-A-S-H structure (Bakharev et al. 2002; Dung et al. 2014; Wallah et al. 2005). However, works of Bakharev et al. (2002) showed that alkali-activated materials are susceptible to sulphate attack due to magnesium-based solutions ( $\text{MgSO}_4$ ) rather than sodium based solutions ( $\text{Na}_2\text{SO}_4$ ). Ismail et al. (2013) further added that magnesium (Mg) ions in the system attacks the CSH and C/N-A-S-H phases in the binder which might change the microstructure of the binder along with its mechanical properties.

## **Carbonation**

Steel corrosion in concrete can start when the concrete pH reduced below 9. The main reason for the pH reduction is the carbon dioxide penetration into the concrete through the permeable voids which is known as the carbonation (Tennakoon 2016). Carbonation of alkali-activated systems has created a dispute among the researchers (Bakharev et al. 2001b; Bernal et al. 2012; Davidovits 2008; Law et al. 2015). However, many agree that calcium in the system has a significant effect on the pH drop as it enforces the formation of  $\text{CaCO}_3$  in the system which leads to a lower pH (pH 8-9) over the typical  $\text{Na}_2\text{CO}_3$  or  $\text{K}_2\text{CO}_3$  formations (pH 10-10.5) (Badar et al. 2014; Davidovits 2008).

## **Chloride ingress**

Steel corrosion due to the electrochemical reaction between the chloride ions ( $\text{Cl}^-$ ) and ferrous or ferric ions ( $\text{Fe}^{2+}$  or  $\text{Fe}^{3+}$ ) from reinforcement has become one of the biggest durability issues in reinforced concrete (Neville 1995).

Most of the researchers who worked on chloride attack in geopolymer concrete claimed that corrosion resistance of steel in geopolymer concrete is similar or higher compared to the OPC (Ganesan et al. 2015; Ma et al. 2016; Miranda et al. 2005; Monticelli et al. 2016; Reddy et al. 2012). Works of Ma et al. (2016) concluded that slag based geopolymer has a lower chloride ion diffusion rate compared to OPC while Ganesan et al. (2015) reported of similar diffusion rates in fly ash based geopolymer and OPC. Thus, it can be concluded that the chloride diffusion rate depends on the microstructure of the geopolymer binder. Reddy et al. (2012) studied the performances of low calcium fly ash geopolymer concrete subjected to the aggressive marine environment and concluded that time to generate cracks in geopolymer was higher compared to OPC. Monticelli et al. (2016) found a surface layer consisting of akaganeite of the reinforced bars of geopolymer concrete which might result in non-uniform corrosion even though geopolymer has a better resistance over chloride attack. Furthermore, Kriven et al. (2007) successfully reduced the steel corrosion using a metakaolin based geopolymer coating on steel bars.

### **2.2.6 Socio-economic and environmental factor**

As discussed above in section 2.2.5, generally geopolymer binders are associated with superior intrinsic properties compared to OPC. However, it is the socio-economic and environmental benefits that make geopolymer a better alternative to OPC.

Use of by-products as one of the main constituents of geopolymer concrete reduces the cost of production by a considerable margin. In fact, Duxson et al. (2007)

stated that the cost of geopolymer is lower than OPC by a factor of 10-30% even with the high cost of activator. On the other hand, using by-products in large scale make it a perfect recycling method for industries like coal power (fly ash), steel (slag), mining (mine tailings) etc. (Davidovits 2008). Geopolymer also consists of low carbon footprint and embedded energy compared to OPC which would classify it as a sustainable, eco-friendly building material over OPC (Neves 2016). Furthermore, superior durability qualities in geopolymer as discussed in section 2.2.5.3 may yield economic benefits in long-term as it increases the lifespan of the structure and thus reduces the service cost.

Chemical structure of geopolymer binders expands its usage further as it can be successfully used in toxic waste management to trap larger cations ions without having any leaching problem (Davidovits 2008). Moreover, high initial strength gain in geopolymer is beneficial in the precast industry (Lloyd & Rangan 2010).

### **2.2.7 Challenges of geopolymer**

Even though geopolymer can show superior intrinsic properties and associates with lots of socioeconomic advantages and environmental benefits, there are some limitations and challenges to be addressed before it can successfully replace the OPC. The main reason for the delay in the adoption of geopolymer is the lack of information such as long-term behaviour, standards, specifications and regulations (Nath 2014).

Apart from the above, there are some other minor concerns that require attention. Controlling the geopolymer binder chemistry is difficult as by-products may contain some undesirable substances such as toxic and heavy metal ions (Álvarez-Ayuso et al. 2008). Lloyd et al. (2010) reported that alkali cations might leach out from the polymeric network when in contact with water which might affect the performance of geopolymer.

Commercial scale production of geopolymer concrete also limited by the use of liquid state activator which might lead to health and safety risks while preparing,

transporting and handling the mixes (Davidovits 2008; Nath 2014). Moreover, the need of thermal treatment to achieve better characteristic might limit geopolymer operation to precast production (Lloyd & Rangan 2010) along with the lack of control over fresh concrete properties due to the unavailability of admixtures (Nath 2014).

## **2.3 Alkali Aggregate Reaction (AAR)**

### **2.3.1 Introduction**

Thomas Stanton, an engineer in California State Division of Highways, reported a new durability issue of concrete in 1940 based on the cracks and blotches fringed with a white efflorescence spotted in mortar cylinders. He further described this as a result of the reaction between alkali in cement and certain types of aggregates (Hobbs 1988). This phenomenon has attracted lots of attention at that time as it explains the mysterious cracks observed in some of the critical structures like dams, bridges, retaining structures, etc. (Australia 2015). Thus, US Bureau of Reclamation placed an upper limit of 0.60% (by mass) on the alkali content in cement used in the major construction projects based on Stanton's works (Hobbs 1988). However, most of the structures identified with the alkali aggregate reaction have managed to serve their service life satisfactorily under precautionary measures and regular inspections (Curtis, 2000; Hobbs 1988). HB79 tabularized the reported cases in Australia up until 2006 which includes major structures like dams, bridges, water tanks, etc. (Australia 2015).

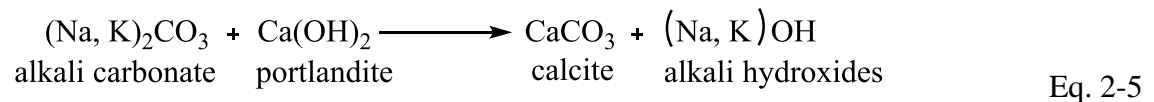
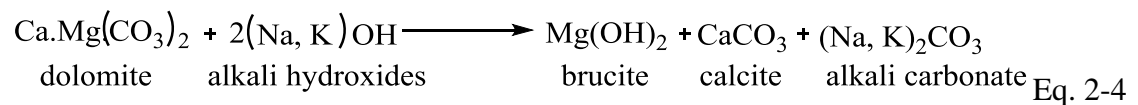
Formation of the hygroscopic gel due to the chemical reaction between alkali hydroxides and reactive phases of the aggregate is termed as the alkali aggregate reaction. Even though the alkali aggregate gel itself is not expansive, hydraulic reaction with water (or moisture) may result in swelling of the gel which can induce high internal pressures

and thus, results in severe distresses in structures (Fernandes & Broekmans 2013; Hobbs 1988). There are two main types of deleterious alkali aggregate reactions;

1. Alkali-carbonate reaction
2. Alkali silica reaction

### 2.3.2 Alkali-carbonate reaction (ACR)

When aggregates containing dolomitic limestones are exposed to alkali hydroxides, de-dolomization (see Eq. 4) takes place. The resulting products of this reaction consist of brucite ( $Mg(OH)_2$ ) which have hygroscopic properties (Australia 2015; Fournier & Bérubé 2000). Furthermore, Fournier and Bérubé (2000) showed that alkali carbonate reaction might proceed indefinitely when the system contains a significant amount of portlandite (see Eq. 5)



However, there are very few cases of ACR affected structures reported all around the world (Fournier & Bérubé 2000) and non-reported in Australia (Australia 2015).

### 2.3.3 Alkali silica reaction (ASR)

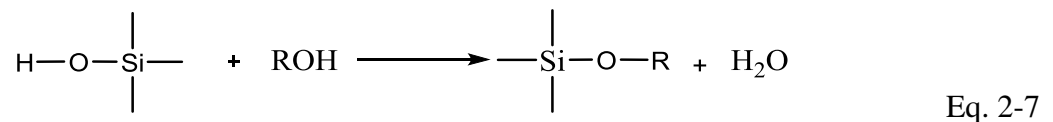
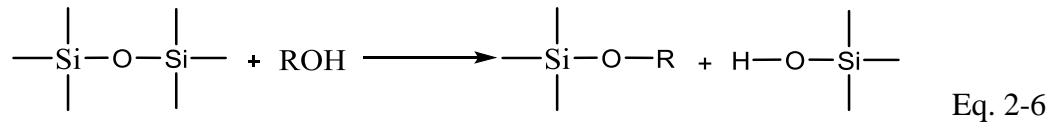
Formation of the hygroscopic gel due to the chemical reaction between silica or silicate ions from aggregate and alkali hydroxides in the paste is termed as alkali silica reaction. Even though initially, the alkali silicate reaction was categorised separately, HB 79 described it as a slow or late type of ASR (Australia 2015; Fournier & Bérubé 2000). Furthermore, Fournier and Bérubé (2000) classified the ASR into two major categories based on the silica form incorporated. The first category included rocks with poorly crystalline or metastable silica minerals such as opal, tridymite, cristobalite, volcanic

glasses, etc. Concrete with even a very small amount of these aggregates (as low as 1-2%) may suffer from severe distresses within few years after construction if all the other essential components for ASR exist (Fournier & Bérubé 2000). The second category includes the aggregates with micro to cryptocrystalline quartz or any other micro granular quartz. The second category incorporated with the slow or delayed reaction which can extend even up to 25 years after construction (Fournier & Bérubé 2000).

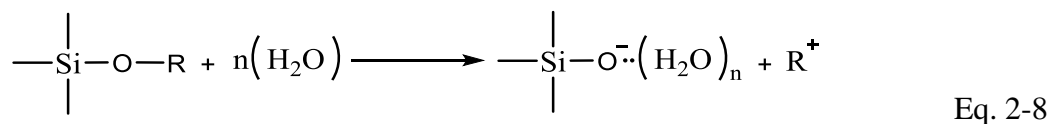
### 2.3.3.1 Reaction mechanism

Even though there are slight variations, most of the proposed reaction mechanisms consist of two main processes (Garcia-Diaz et al. 2006; Ichikawa & Miura 2007; Pan et al. 2012; Rajabipour et al. 2015; Stokes 2011).

Step 1- Dissolution of silica and formation of alkali silicates



Step 2- Hydration



R – Na or K

n – hydration number

Hydroxyl ions in the system initiate the reaction by attacking the siloxane network of the aggregate which results in the formation of alkali silicates and silicic acid

(see Eq. 2-6). Silicic acid further reacts with the hydroxyl ions in the system to form alkali silicate and H<sub>2</sub>O (see Eq. 2-7). Alkali silicates formed in Eq. 6 and Eq. 7 are amorphous and have hygroscopic properties as shown in Eq. 2-8 (Ichikawa & Miura 2007; Pan et al. 2012).

### **2.3.3.2 Expansion mechanism**

Even with the hygroscopic properties of ASR gel, many researchers confused by the internal stresses developed due to the formation of the low viscosity ASR gel (Pan et al. 2012; Struble & Diamond 1981). Thus, over the years, many attempts have been made to develop a mechanism that can explain the experimental results (Pan et al. 2012). Theory of osmotic pressure (Glasser 1979), theory of gel dispersion (Garcia-Diaz et al. 2006), theory of gel crystallization pressure (Garcia-Diaz et al. 2006), theory of ion diffusion (Chatterji et al. 1986), theory of electrical double layer (Prezzi et al. 1997), reaction rim theory (Ichikawa & Miura 2007) etc. are some of the proposed mechanism to explain the pressure development due to ASR. However, among all, the reaction rim theory gained more attention as it can be used to explain most of the ASR related issues (see section 2.3.4.4.)

### **2.3.4 Factors affecting AAR**

Based on the above mechanisms, there are three main factors essential for deleterious alkali aggregate reaction;

1. Reactive aggregate
2. Free alkali (Na<sup>+</sup> and K<sup>+</sup>) and OH<sup>-</sup> content
3. Moisture movement

Apart from the above three, there are many other factors which have a significant influence on the deleterious alkali aggregate reaction which includes; the presence of

calcium, the presence of aluminium, material properties of the paste, exposure conditions, etc.(Hobbs 1988)

#### **2.3.4.1 Effect of aggregates**

As described above in section 2.3.2 and 2.3.3, it is clear that aggregate type governed the type and degree of reaction occurring in the system. In fact, the reactivity of aggregate increases with the degree of microstructural disorder in the aggregates. Amorphous SiO<sub>2</sub> (ex: Opal) is the most reactive followed by meta-stable crystals (ex: cristobalite and tridymite), microcrystalline silica and other crystalline silica with lattice defects (Hobbs 1988; Rajabipour et al. 2015). Thus, Swamy (2002) suggested that ASR potential of aggregate depends on its mineral composition rather than the rock type.

Studies of Standon (1940), Poyet et al. (2007) and Multon et al. (2008) confirmed that reactive aggregate size has a pessimum behaviour on the expansion magnitude and the optimum aggregate fraction depends on the aggregate type. However, the mechanism behind the above behaviour is yet to understand (Rajabipour et al. 2015). Research works of Sanchez et al. (2016) revealed that even though the damage rating index (DRI) is unaffected by the reactive aggregate size, crack propagation inside the mortar become more sparsely distributed with the fine reactive aggregates.

Hobbs (1988) reported that reactive mineral content also follows a pessimum behaviour as shown in Figure 2-5. Mechanism of the pessimum behaviour of reactive content is explained by the equilibrium between reactive silica and alkali content in the system (Hobbs 1988; Ichikawa, 2009). In fact, it is clear that expansion can become zero when the reactive content exceeds the threshold limit of the system (see Figure 2-5). It is possible to deduce the pessimum ratio of reactive silica content to equivalent Na<sub>2</sub>O content which depends on the type of reactive aggregate. For opaline silica, this ratio is observed as approximately 6 (Hobbs 1988; Rajabipour et al. 2015).

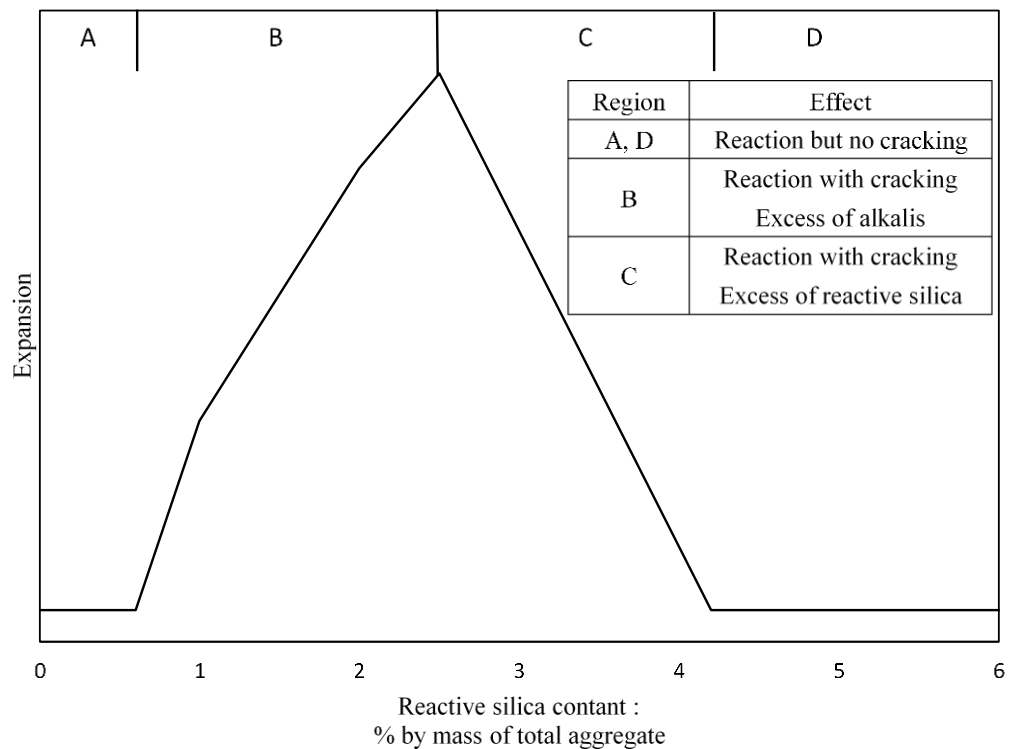


Figure 2-5 : Pessim behaviour of aggregate (Hobbs 1988)

#### 2.3.4.2 Effect of free alkali content

The reaction mechanisms in sections 2.3.2 and 2.3.3 both revealed that alkali has a significant role in alkali aggregate reaction. Apart from alkalis (Na and K), calcium (Ca) also contributed to the reaction significantly resulting in calcium silicate products due to the very high calcium content in OPC systems. Even though calcium based gel products are important to have a deleterious alkali aggregate reaction in OPC systems (described in section 2.3.4.4), many researches point out that its swelling capacity is lower compared to alkali based gel thus, creating negligible problems individually (Kim, Taehwan & Olek, Jan 2014; Struble & Diamond 1981; Wang & Gillott 1991).

Being an alkali, lithium (Li) is also expected to cause deleterious ASR expansions just like sodium and potassium. But instead, it is proven that it has an adverse effect on ASR and successfully used to mitigate ASR in concrete since it was first reported by McCoy and Caldwell (1951) in 1951. However, the exact ASR prevention mechanism of

Li salt is not completely comprehended (Islam and Ghafoori, 2016, Zapała-Sławeta and Owsiak, 2016, Kawamura and Fuwa, 2003). Studies showed that the amount of Li needed to inhibit the ASR related distress in concrete is a function of sodium equivalent ( $\text{Na}_2\text{O}_{\text{eq}}$ ) of the system (Islam and Ghafoori, 2016). In fact, few studies suggest that the reactivity of the aggregate also have an impact on the amount of Li needed to dismantle the ASR effect (Zapała-Sławeta and Owsiak, 2016). However, some researchers have suggested that Li has a pessimism behaviour towards ASR concrete creating more problems when used excessively (Kawamura and Fuwa, 2003, Zapała-Sławeta and Owsiak, 2016).

Besides being a major constituent, alkali also has a secondary role in alkali aggregate reaction, maintaining a high pH in pore solution (Rajabipour et al. 2015). Since pH is a measure of hydroxyl ion concentration, based on Eq. 2-2, Eq. 2-3, Eq. 2-4, Eq. 2-6 and Eq. 2-7 reaction rate increases with pore solution pH.

All the alkali sources can be categorised into two subgroups;

1. Internal alkali sources

If the alkalis supplied by the constituent of the concrete, then those constituents are categorised as internal alkali sources. Internal alkali sources include cement, SCM, aggregates, water, activator, admixtures, etc. If the main alkali source is internal, it is hard to control the reaction once it occurred. Thus, controlling the alkali content at the designing stage is the most desirable method to mitigate AAR (Australia 2015; Farny & Kosmatka 1997; Rajabipour et al. 2015).

2. External alkali sources

If the alkalis supplied from the outside environment such as de-icing agents, sea water, waste water, ground water etc. then those sources are categorised under the external alkali sources. The best way to control the

alkali aggregate reaction in these types of situations is to cut off the alkali sources (Farny & Kosmatka 1997; Rajabipour et al. 2015). Grattan-Bellew (1992) pointed out that high permeability and crack propagation in structures may further increase the alkali aggregate reaction as it increases the ion transportation capability of the medium.

#### **2.3.4.3 Moisture movement**

ASR gel is hygroscopic and thus able to swell by chemically dwelling some water molecules. Thus, in order to develop the internal stress due to AAR, water is also an essential ingredient (Australia 2015; Fournier & Bérubé 2000; Rajabipour et al. 2015). In fact, Stark (1991) reported that in order to have the significant expansion, the internal relative humidity should be greater than 80%. Multon and Toutlemonde (2010) reported that the gelation part of the AAR (see Eq. 2-2 to Eq. 2-7) might occur even at lower humidity levels, even though the swelling phase required a humid environment. However, many researchers reported that ASR gel properties might change significantly resulting in lower swelling properties if exposed to low humidity environment (Fournier & Bérubé 2000; Rajabipour et al. 2015; Struble & Diamond 1981).

#### **2.3.4.4 Role of calcium**

The exact role of calcium in deleterious alkali aggregate reaction is not yet defined. Studies of Struble and Diamond (1981) revealed that calcium rich gel (calcium silicate gel) is highly viscous compared to ASR gel and able to maintain its form even at pressures where typical alkali silicates liquefy. However, they further proved that expansive properties of calcium based gel is lower than that of sodium based gel which signifies that the formation of calcium based gel may reduce the expansiveness (Struble & Diamond

1981). But the experimental studies of Ichikawa and Miura (2007), Wang and Gillott (1991), Hou et al. (2004) and Thomas (1998) highlighted the importance of calcium in deleterious alkali aggregate reaction. Thus, it is possible to conclude that even though calcium reduces the expansiveness of the gel, it increases the effective internal pressure development. Different researchers developed a different hypothesis to explain this phenomenon as described below.

### **Importance of calcium in ASR gel formation**

The effect of calcium in ASR gel formation was well documented by many researchers including Hou et al. (2005), Hou et al. (2004), Leemann et al. (2011), Kim, Taehwan and Olek, Jan (2014) and Kim, Taehwan and Olek, Jan (2014). They suggested that dissolved silica (from the aggregates) first react with the available calcium to form CSH because CSH has lower saturation energy compared to ASR gel. Thereafter, highly dense CSH acts as a rigid barrier to isolate certain areas in the aggregates, allowing silica ions concentration to increase and reach the saturation point of ASR gel. Figure 2-6 is the graphical representation of the ASR mechanism described above.

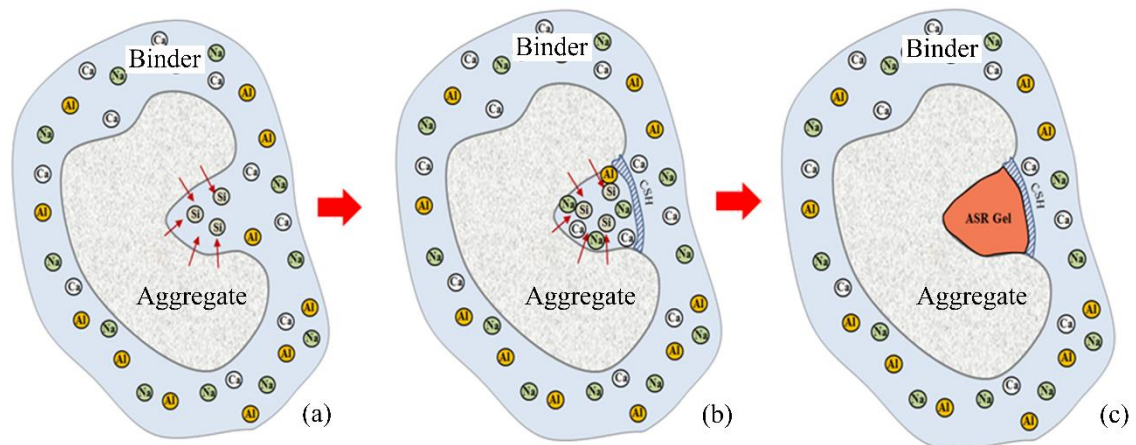


Figure 2-6 : Graphical representation of ASR gel formation mechanism; (a) Si dissolution; (b) Formation of CSH barrier; (c) Formation of ASR gel (after Hou et al. (2004), Kim, Taehwan and Olek, Jan (2014) and Kim, Taehwan and Olek, Jan (2014))

### **Importance of calcium in the expansive mechanism (Reaction rim theory)**

As explained in section 2.3.3.2, many theories have been introduced to explain the expansion mechanism of the alkali aggregate reaction. However, the reaction rim theory gained more attention among them as it fit to most of the experimental and field observations regarding AAR. The reaction rim theory is based on the formation of a semipermeable layer to entrap alkali silica gel inside while allowing ions to pass through the layer (Ichikawa 2009; Ichikawa & Miura 2007). Ichikawa (2009) further explained that it is the calcium silica hydrates that act as a semipermeable layer to entrap alkali silica gel. Alkali silica gel chemically couples with water particles in the system and swells, exerting internal stresses on aggregate and paste (Ichikawa 2009). Figure 2-7 is a simple graphical representation of reaction rim theory (Ichikawa 2009).

This theory also perfectly aligns with the above gel formation mechanism as both rely on the formation of calcium-based gel. Thus, reaction rim theory can be combined

with the above mentioned gel formation mechanism to explain the expansion mechanism (see Figure 2-8)

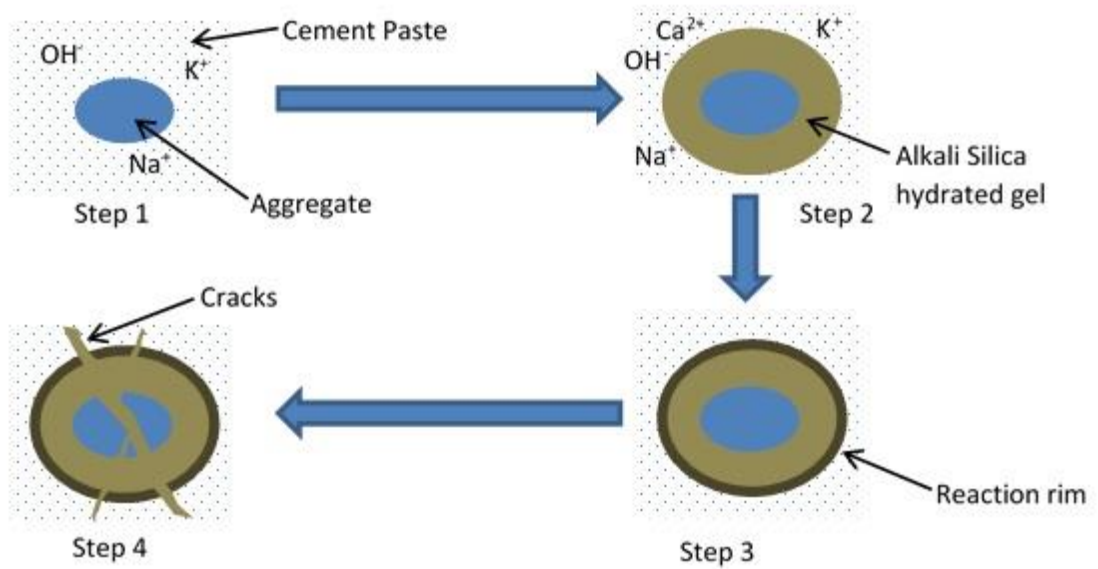


Figure 2-7 : Reaction rim theory (after Ichikawa and Miura (2007))

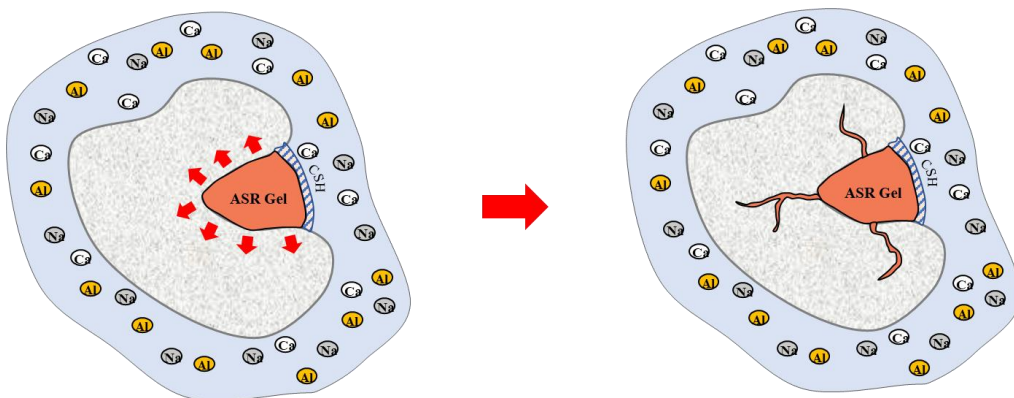


Figure 2-8 : ASR gel expansion mechanism

### Secondary role of calcium

Apart from directly contributing to the main mechanisms as described above, calcium also has a secondary role in alkali aggregate reaction (Wang & Gillott 1991).

- Calcium can replace the occupied alkalis in the system which eventually increases the free alkali content.
- Calcium hydroxides in the system act as a buffer to maintain the high pH in the system which eventually maintain the Si dissolution rate (see Eq. 2-3 and Eq. 2-4).

#### **2.3.4.5 Role of aluminium**

Even though the exact role of aluminium (Al) in ASR is not clear, there are solid evidences that the soluble aluminium may significantly lower the risk of ASR (Rajabipour et al. 2015). Research works of Aquino et al. (2001) pointed out that aluminium rich SCM (metakaolin, fly ash, etc.) are more effective in mitigating ASR compared to silica rich SCM (silica fume). Furthermore, Warner (2012) and Schwing (2010) demonstrated that fly ash with high alumina content ( $\text{Al}_2\text{O}_3 > 20\%$ ) controls the ASR more effectively compared to fly ash with low alumina content ( $\text{Al}_2\text{O}_3 < 20\%$ ). Shafaatian (2012) used  $\text{Al}(\text{OH})_3$  to reduce the expansion caused by ASR in concrete mortar bars which also aligns with the above studies. Rajabipour et al. (2015) have summarised the possible actions of aluminium in reducing ASR.

- Reduce silica dissolution rate from the aggregates
- Reduce the pH and thus the alkali content by the formation of CASH over CSH
- Reduce free calcium content by formation of calcium aluminate phases
- Reduce the swelling properties of ASR gel
- Reduce the permeability of concrete

Chappex and Scrivener (2012) highlighted that the aluminium ions in the pore solutions might limit the Si ion dissolution rate from the aggregates. There are several hypotheses to explain their observations;

- Aluminium ions react with silica ions and form an aluminosilicate layer on top of the aggregate which stops the hydroxyl ion attack and thus the Si dissolution (Sang et al. 1994).
- Aluminium ions react with hydroxyl ions to form  $\text{Al}(\text{OH})^-$  which adsorb on the aggregate surfaces and repel hydroxyl ions away and thus retard the silica dissolution process (Bickmore et al. 2006).

Many researchers showed that aluminium ions would interact with CSH to form CASH (Rajabipour et al. 2015) while studies of Hong and Glasser (2002) suggest that CASH has a better alkali bonding capacity compared to CSH. However, swelling properties of aluminium rich ASR gel is not studied extensively yet but need more attention in the near future as many have identified such gel formations especially in geopolymer systems (García-Lodeiro et al. 2007).

#### **2.3.4.6 Effect of exposure conditions**

As many of the other chemical reactions, alkali aggregate reaction is also sensitive to the exposure conditions. There are three main exposure conditions (HB79, 2015);

1. Moisture movement/ Humidity
2. Temperature
3. Pressure

Effect of the moisture movement has been discussed separately in Chapter 2.3.4.3 as it is one of the major factors in AAR. Effect due to pressure variation is insignificant in most of the cases because structures are mostly exposed to atmospheric pressure.

Temperature exhibits a positive relationship with the reaction kinetic of AAR (Comi et al., 2012, Chatterji and Christensen, 1990). AAR is a slow reaction which typically takes 5-10 years to manifest symptoms in field conditions (HB79, 2015). However, in colder environments, concrete with moderately-reactive aggregates may take

15-20 years to show up the symptoms whereas concrete with highly reactive aggregates may exhibit severe distresses in less than 2 years under hot, humid conditions (HB79, 2015).

#### **2.3.4.7 Effect of material properties of binder and external loading**

Even though material properties do not affect the chemical reaction directly, it may have certain influence on the distress development in mortar. Based on the stress strain relationship of the materials it is obvious that young modulus, have an impact on the expansion development of the mortar (Hobbs, 1988). Use of air entrapment is one of the precautionous actions taken to restrict ASR distresses. It is believed that the ASR gel formed may dispersed into these voids without applying any distress on the mortar (Jensen et al., 1984).

Many researchers have claimed that the restraints in actual structural elements may decrease the respective ASR expansion (Multon and Toutlemonde, 2006, Jones and Clark, 1996). In fact, there are three kinds of restraints; external loads; reinforcement and adjacent elements which restrict the movements (Jones and Clark, 1996). Giorla (2013) showed that the compressive stresses may reduce the expansion development along the corresponding direction. However, it should be noted that except the reduction of expansion due to reinforcement, other two restraints may increase the internal stresses causing higher crack formations. Effect of reinforcement on the expansion development is also studied by many researchers (Multon and Toutlemonde, 2006, Hobbs, 1988).

#### **2.3.5 Identification of AAR**

AAR identification mainly consists of two stages;

1. Laboratory identification
2. Field identification

### **2.3.5.1 Laboratory identification**

Alkali aggregate reaction usually takes a long time to show the initial symptoms. However, once initiated, it is very hard to mitigate or even control the reaction in the field structures (HB79, 2015; Hobbs 1988). Thus, the normal practice is to identify the probable alkali aggregate reaction in the design stage and take appropriate mitigatory actions (Australia 2015). There are few established laboratory testing methods

#### **Petrographic analysis**

Identification of potentially reactive mineral phases in aggregate based on the microscopic images is called as petrographic analysis (Farny & Kosmatka 1997; Hobbs 1988). There are two types of petrographic analysis based on the specimen preparation (Ahmed and Vander Voort, 2000);

1. Analysis of bulk specimens – surface polished thick samples were examined with a reflected light microscope.
2. Analysis of thin sections – polished thin specimens (thickness < 30 $\mu$ m) were examined with transmitted polarized light microscope.

Analysis of bulk specimens is frequently used to identify the ASR concrete (Rivard et al., 2002, Sanchez et al., 2016). However, petrographic analysis does not encompass any quantitative data which significantly limits its use (Hobbs, 1988, Farny and Kosmatka, 1997). But many researchers adapted petrographic analysis along with a quantitative technique such as infrared spectroscopy, X-ray diffraction, Raman spectroscopy, damage rating index (DRI) etc. (Farny and Kosmatka, 1997, Rivard et al., 2002, Sanchez et al., 2016)

The main benefit of the petrographic analysis is that it requires significantly less time compared to most of the other test methods while engaging with high accuracy. However, it also has few disadvantages such as the need of highly skilled manpower,

need of high-tech equipment, etc. which may result in larger overheads (Farny & Kosmatka 1997).

#### Damage rating index (DRI)

DRI was introduced by Grattan-Bellew and his team as a semi-quantitative tool to use along with petrographic analysis in identifying ASR in early 90's (Sanchez et al., 2016). Since then it has become one of the frequently used semi-quantitative tool accompanied with petrographic analysis due to its simplicity with respect to methodology and technology (Ahmed and Vander Voort, 2000). In DRI, 1cm<sup>2</sup> grid was drawn on the targeted surface and count the damage features of ASR in each grid. Then, number of counts corresponding to each damage feature was multiplied by the weighing factor to balance the relative importance of each feature towards ASR and take the normalized value for 100 cm<sup>2</sup> as DRI in the sample. It should be noted that, ideally at least 200 cm<sup>2</sup> surface should be analysed to calculate the DRI (Rivard et al., 2002, Sanchez et al., 2016).

#### **Chemical test**

A chemical test is a quick and easy test to identify probable alkali silica reaction (ASR) based on the ion dissolution rate from the aggregate (Hobbs 1988). Crushed aggregates were exposed to 1M NaOH solution at 80 °C for 24 hours before measuring the dissolve silica content and the reduction in alkalinity by titration with acid. The final categorisation is based on a standard curve developed experimentally (ASTM-C289-07 2007). However, many researchers have questioned the accuracy of the final outcome of this test (Farny & Kosmatka 1997; Hobbs 1988). Moreover, the use of this test is limited to siliceous aggregate as it analyses the Si dissolution rate of the aggregate (Farny & Kosmatka 1997).

### **Accelerated mortar bar test (AMBT)**

Accelerated mortar bar test is the most widely used laboratory test method to identify deleterious alkali aggregate reaction in concrete (Shon et al. 2002). Rapid assessment process and simplicity along with the reasonably accurate outcomes makes it more versatile compared to other testing methods (Australia 2015). In AMBT, 25mm\*25mm\*285mm mortar bars are cast using general purpose cement (GPC) and crushed aggregates while maintaining the mix ratios specified in the standard (AS 1141.60.1). Then, the length change in those mortar bars over 21 days is measured while exposing them to 1M NaOH solution at 80 °C (Australia 2014).

AMBT incorporates several approaches to accelerate the alkali aggregate reaction (Australia 2014);

- Using crushed aggregates – increase the surface area (increase the Si dissolution rate)
- Elevate the temperature to 80 °C – increase the reaction rate.
- Immerse in 1M NaOH solution – Supply Na<sup>+</sup> ions
  - Maintain good moisture movement
  - Elevate the internal pH

However, due to the severeness of the test conditions, some of the aggregates with good field records have also shown excessive expansions with this test (Australia 2015). On the other hand, the mix design of standard AMBT (as in AS 1141.60.1) is kept constant to simplify the outcome which limited its capability to the categorisation of aggregates (Australia 2014). Thus, HB 79 is recommending standard AMBT as a screening test which means, if the aggregates failed this test more reliable long-term test

(concrete prism test) should be used to confirm the reactivity (Australia 2015; Farny & Kosmatka 1997).

### **Concrete prism test (CPT)**

Concrete prism test was originally developed in Canada to evaluate the potential alkali carbonate reaction (ACR) (Australia 2015). It is recognised as the most reliable laboratory testing methodology to identify alkali aggregate reaction in concrete (Australia 2015). Even though the testing conditions are much milder than the accelerated mortar bar test, it takes at least a year to have a definite outcome (AS1141.60.2 2014). Thus, CPT is mainly recommended, if the time is not critical or as a confirmation test to AMBT (Australia 2015).

#### **2.3.5.2 Field Inspection**

Field performance records are the most reliable source to identify the alkali aggregate reactivity of concrete (Australia 2015; Farny & Kosmatka 1997). However, before evaluating aggregates based on performance history, the effect of the following parameters should be taken into account (Farny & Kosmatka 1997)

- Cement content of the concrete, alkali content in cement and water cement ratio of the concrete are similar or less than that of the proposed mix design.
- Targeted field concrete is old enough (at least 15 years old)
- Anticipated exposure conditions are similar or less severe compared to the existing conditions
- Effect of SCMs in the existing structure and the proposed structure

Diagnosis of alkali aggregate reaction in the field based on the visual symptoms is a difficult task as most of the symptoms are common to other durability issues. Thus, it is

recommended to follow up the visual inspection with laboratory testing and risk assessment to evaluate ASR progression (Farny & Kosmatka 1997; Thomas et al. 2011).

### **Surface Crack propagation**

Randomly oriented crack propagation in the surface which is called as map cracking (also called as alligator cracking or pattern cracking) is the typical crack pattern associated with ASR (Thomas et al. 2011). Figure 2-9 is a classic example for map cracking due to ASR found in a causeway bridge in Perth, Western Australia (Australia 2015). Even though theoretically, map cracking shall spread evenly over all the directions of the concrete structure, there may be directional orientated cracks due to internal confinement from reinforcement provided or external confinements by restrained provided such as adjacent structures or the ground (Thomas et al. 2011). It should be noted that, there can be crack propagations due to the weather and exposure conditions in field structures and thus, requires expertise knowledge on ASR to diagnose ASR in field conditions.



Figure 2-9 : Map cracking due to alkali silica reaction identified in causeway bridge in Perth (Australia 2015)

### **Gel exudation**

Cracks enclosed by broad brownish zone as in Figure 2-9 is a typical sign of ASR in a structure (Australia 2015; Thomas et al. 2011). However, efflorescence due to the transmission of water and salt is often misidentified as AAR exudate. Thus, it is recommended to carry out a petrographic analysis on the gel exudates to confirm the AAR (Australia 2015).

### **Surface pop outs**

Despite being rare, it is possible to observe a surface deterioration due to detachment of small pieces of the surface layer of mortar in extreme cases of AAR as shown in Figure 2-10 (Thomas et al. 2011). This is due to the formation of highly expansive gel products closed to the surface due to alkali aggregate reaction (Australia 2015). Freeze-thaw actions along with the presence of certain aggregate types may worsen this effect (Thomas et al. 2011).



Figure 2-10 : Surface pop outs due to alkali aggregate reaction (Thomas et al. 2011)

## **Deformations and displacements**

Severe AAR is always accompanied by excessive expansions which may cause significant deformations in the affected as well as the surrounded structures. Closure of expansion joints, exudations of joint fillers, relative displacement to adjacent sections, twisting and warping of the structural members, the structural crushing of concrete etc. are the typical symptoms of excessive stress development due to AAR gel formation. Furthermore, the mechanical equipment attached to the affected structure may also be malfunction due to alignment issues caused by deformations (Australia 2015). Figure 2-11 is the differential movement of parapet walls in a bridge due to AAR (Thomas et al. 2011).



Figure 2-11 : Differential movement of parapet walls in a bridge due to AAR (Thomas et al. 2011)

## **2.4 Alkali aggregate reaction in geopolymer**

Theoretically, geopolymer concrete is associated with higher risk of alkali aggregate reaction compared to OPC due to the use of alkali solution as an activator (Bakharev et al. 2001a). However, among the limited amount of research works available,

most studies suggest that the actual risk AAR in alkali activated materials is lower than that of OPC (Shi, C et al. 2015). Even though most of the existing studies targeted on the performance of geopolymer over alkali silica reaction, research works of Gifford and Gillott (1996) illustrated that alkali activated systems are more susceptible to alkali carbonate reaction over alkali silica reaction.

Alkali aggregate reaction in slag based alkali activated materials has created a dispute among researchers as some claimed that the risk of AAR is even higher compared to OPC (Bakharev et al. 2001a; Puertas et al. 2009). However, the alkali aggregate resistance of fly ash based geopolymer is experimentally proven by several researchers using different test methodologies and constituent (García-Lodeiro et al. 2007; Kupwade-Patil & Allouche 2012; Lu et al. 2013; Shi, C et al. 2015).

The following points are brought up to describe the alkali aggregate resistance of geopolymer concrete by different researchers;

- Majority of the alkali ions are preoccupied in the geopolymer network thus free alkali ions available for the AAR is quite lower than initial alkali ion content (Fernández-Jiménez & Puertas 2002)
- Strong and dense bond network formed in the vicinity of the aggregates decreases the hydroxyl ion attack and hence the Si dissolution (Krivenko et al. 2014).
- High early alkalinity (high pH) of the mixture enforces most of the reactive silica to dissolve even before the final setting time which will reduce the reactive Si ion content for AAR (Shi, C et al. 2015)
- High early strength gain increases the resistivity of the binder to internal stresses developed due to AAR (Shi, C et al. 2015)

- Low calcium content reduces the reaction rate and the expansiveness of the AAR as described in section 2.3.4.4 (Fernández-Jiménez & Puertas 2002; Kupwade-Patil & Allouche 2011; Kupwade-Patil & Allouche 2012; Pouhet & Cyr 2015)
- High aluminium content in the system retards the AAR as described in section 2.3.4.5 (Krivenko et al. 2014)
- Low pore solution pH decreases the Si ion dissolution rate (Pouhet & Cyr 2015; Shi et al. 2017; Shi, Z et al. 2015)

#### **2.4.1 Effect of slag content**

Effect of slag content in alkali activated materials over the alkali aggregate reaction is under the light as some researchers reported excessive expansions in slag based alkali activated materials (Bakharev et al. 2001a; Puertas et al. 2009; Shi et al. 2017). Most of the researchers claimed that slag act as the main calcium source in the absence of OPC (portlandite) to boost the alkali aggregate reaction as described in section 2.3.4.4 (García-Lodeiro et al. 2007; Kupwade-Patil & Allouche 2011; Pouhet & Cyr 2015; Shi, C et al. 2015; Shi, Z et al. 2015). Since slag is an important constituent in the mix design which enhances the setting properties and initial mechanical properties, slag content optimization is necessary to achieve better mix design (Tennakoon 2016).

#### **2.4.2 Effect of activator**

Activator is the main supplier of alkali in geopolymer mix. Thus, activator type and the concentration are playing a vital role in the risk of alkali aggregate reaction in alkali activated materials (Shi, C et al. 2015; Tänzer et al. 2017; Williamson & Juenger 2016; You-zhi et al. 2002). In fact, research studies of You-zhi et al. (2002) concluded that water glass ( $\text{Na}_2\text{SiO}_3$ ) has the maximum effect on AAR followed up by  $\text{Na}_2\text{CO}_3$ ,

Na<sub>2</sub>SO<sub>4</sub> and NaOH respectively. Furthermore, many researchers have noticed a pessimum behaviour of silicate modulus (Al-Otaibi 2008; Shi, C et al. 2015) and also the alkali content over AAR expansion (Shi, C et al. 2015; Shi et al. 2017) which emphasized the importance of optimization of activator content to achieve better mix design.

### **2.4.3 Testing methods**

Accelerated mortar bar test (AMBT) and concrete prism test (CPT) are the two most common testing mechanisms used to investigate alkali aggregate reaction in alkali activated materials (Shi, C et al. 2015). However, Fernández-Jiménez and Puertas (2002) concluded that the short testing time stipulated in accelerate mortar bar test is not enough to identify the alkali aggregate reaction as alkali activated materials prone to show later expansions. Experimental studies of Bakharev et al. (2001a) and Al-Otaibi (2008) align with the above suggestion as they concluded that high strength gain of slag based alkali activated concrete might temporary inhibit the AAR. Thus, many researchers recommended long term test like concrete prism test to investigate the alkali aggregate reactivity of alkali activated materials (Shi, C et al. 2015).

## **2.5 Summary**

Geopolymer is considered as a potential substitute to OPC. However, there are many grey areas which need attention before geopolymer concrete adoption by the industry

Alkali aggregate reaction is a chemical reaction that can induce severe distresses inside the mortar. Despite being identified in early 1940s, the exact mechanism of AAR is not completely comprehended which makes it even harder to control. AAR typically takes 5-10 years to show the initial symptoms and once initiated it is extremely hard to

mitigate or even control the reaction. Thus, identification of potential reactive aggregates through laboratory testing is crucial to minimize ASR related issues.

Geopolymer possess extremely high theoretical risk of AAR due to the use of high alkaline activator. However, existing studies showed that the actual risk of AAR is much lower in GPC with no slags compared to OPC. The effect of slag on AAR in geopolymer concrete requires clarification. In addition, studies showed that existing test methods require modifications to be used for the assessment of AAR in geopolymer concrete.

## CHAPTER 3 : Materials and Methodology

---

### 3.1 Overview

This chapter contains the details of the materials and the experimental methodology acquired in this study. Being a slow reaction in natural conditions, alkali aggregate reaction requires to be accelerated in laboratory scale testings to have observable outcomes within a short time frame. Therefore, accelerated mortar bar test based on the AS 1141.60.1 was adopted in this study.

A mixture of GGBFS and low calcium fly ash is used as the main aluminosilicate source whereas a mixture of NaOH and sodium silicate ( $\text{Na}_2\text{SiO}_3$ ) solutions are used as the activator solution in the geopolymer mixes. All the mix design parameters except the GGBFS to fly ash ratio (by weight) were kept constant in the geopolymer mixes and standard accelerated mortar bar test based on AS 1141.60.1 was used as the control test set up. Four aggregate types were used representing, Australian natural reactive aggregates (culcairn), Australian natural non-reactive aggregates (basalt), manufactured reactive aggregates (ferronickel slag) and amorphous silica source (fused silica). Representative mortar cubes were cast and tested in accordance with AS 1012.8.3 along with the mortar bars to assess the strength development during the initial 28 days. Dissolution potentials of aggregates were also tested by exposing them to NaOH solutions with different concentrations which simulate the pH of geopolymer mortar pore solutions.

Scanning electron microscopes (SEM) images along with energy dispersive spectroscopy (EDS) were used to identify the evolution of ASR gels and their composition over the testing period.

## 3.2 Test Materials

### 3.2.1 Cementitious materials

#### 3.2.1.1 Fly ash

Fly ash used in this study was generated in Eraring power plant in NSW and supplied by Boral Australia as a supplementary cementitious material to be used for construction purposes (in compliance with AS 3582.1). Figure 3-1 shows the particle size distribution of the aluminosilicate sources (fly ash and GGBFS) obtained via laser diffraction technique by using a Malvern Mastersizer 2000 instrument. Figure 3-1 clearly shows that 90% of the fly ash particles are passing through the 45  $\mu\text{m}$  sieve which is in acceptance with the limits provided in AS 3582.1 (Australia 2016a).

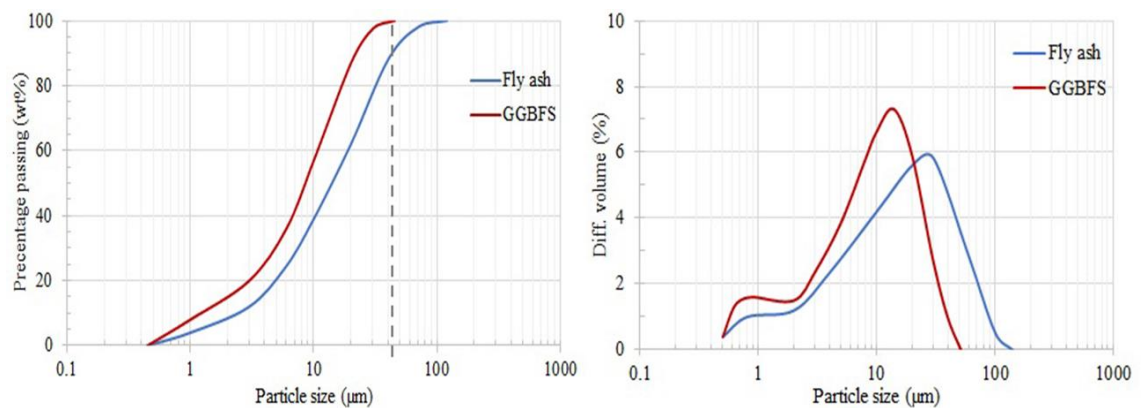


Figure 3-1 : Particle size distribution of GGBFS and Fly ash

Table 3-1 shows the chemical compositions of the cementitious materials obtained from the XRF analysis. Fly ash used in this study complies with the Australian standards and may categorise as Class F fly ash (low calcium fly ash) based on ASTM standards (ASTM-C618-17 2017; Australia 2016a).

Table 3-1 : Chemical composition of cementitious materials based on XRF analysis

	Fly Ash (wt%)	GGBFS (wt%)	OPC (wt%)
Silicon dioxide (SiO <sub>2</sub> )	61.000	33.799	19.539
Aluminium oxide (Al <sub>2</sub> O <sub>3</sub> )	26.045	13.688	4.725
Iron oxide (Fe <sub>2</sub> O <sub>3</sub> )	3.493	0.322	3.038
Calcium oxide (CaO)	2.137	42.049	63.798
Magnesium oxide (MgO)	0.477	5.511	1.175
Sodium oxide (Na <sub>2</sub> O)	0.498	0.331	0.350
Potassium oxide (K <sub>2</sub> O)	1.251	0.278	0.525
Titanium dioxide (TiO <sub>2</sub> )	1.012	1.2	0.285
Sulphur trioxide (SO <sub>3</sub> )	0.067	0.835	2.096
Loss on ignition	2.76	0.36	3.79
Specific gravity	2.1	2.8	3.1

Figure 3-2 shows a SEM image of fly ash obtained using a SEM 3400I equipment with 1000 magnification. This clearly indicates the existence of spherical shape particles in fly ash.

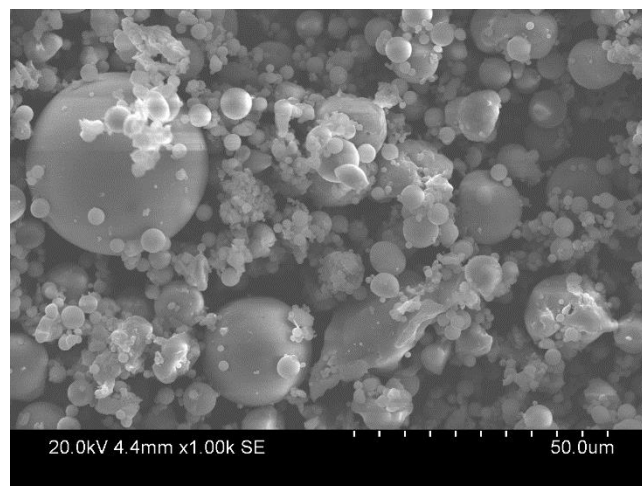


Figure 3-2 : SEM image of fly ash

### 3.2.1.2 Ground Granulated Blast Furnace Slag (GGBFS)

GGBFS used in this research complied with AS 3582.2 and was supplied by Blue Circle Southern Cement Australia. Figure 3-1 contains the particle size distribution of the GGBFS obtained via laser diffraction technique by using a Malvern Mastersizer 2000 instrument. Slag particles were exposed to rapid quenching process during manufacturing resulting in a glassy granular shape particles which can be clearly identified in the SEM images as shown in Figure 3-3 (Australia 2016b).

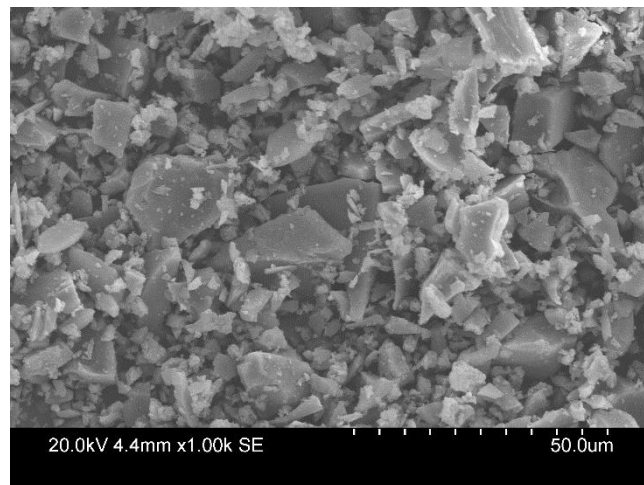


Figure 3-3 : SEM image of GGBFS

Based on the XRF analysis results presents in Table 3-1 : Chemical composition of cementitious materials based on XRF analysis, it is obvious that GGBFS is acting as the main calcium source in geopolymer binders. Thus, many researchers believed that the risk of alkali aggregate reaction increases with the GGBFS content (García-Lodeiro et al. 2007; Kupwade-Patil & Allouche 2011; Shi, C et al. 2015). Hence, in this research, the effect of GGBFS on alkali aggregate reaction was assessed by changing the GGBFS to fly ash ratio while keeping all the other parameters constant as discussed in section 3.3.1.3.

### 3.2.1.3 Ordinary Portland Cement (OPC)

General purpose cement distributed by Cement Australia was used in the study to cast the control specimens in accordance with AS 1141.60.1. Figure 3-4 shows a SEM image of OPC particles obtained with a 1000 magnification.

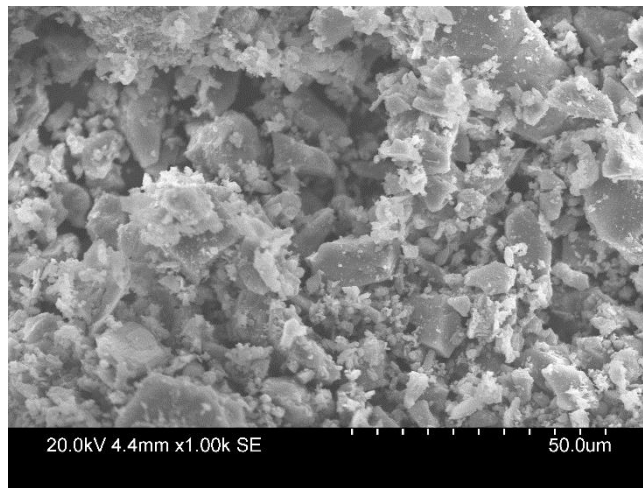


Figure 3-4 : SEM image of OPC

### 3.2.2 Activator

The activator used in this study consists of two parts; concentrated sodium hydroxide solution (12M NaOH) and water glass ( $\text{Na}_2\text{SiO}_3$ ). Sodium hydroxide solution was prepared in the laboratory by mixing technical grade sodium hydroxide pellets (98% purity) obtained from Ajax Finechem in Sydney tap water. For a single batch (4.2l of mortar) 141.2g of NaOH pallets had to be mixed with 227.9g water to prepare the required 12M NaOH solution. Sodium silicate solution with silica modulus 2.0 ( $M_s = \text{SiO}_2/\text{Na}_2\text{O}$ )

was purchased from PQ Australia to be used in the activator. Table 3-2 shows the chemical composition of the sodium silicate solution.

Table 3-2 : Chemical composition of sodium silicate

Chemical component	Na <sub>2</sub> O	SiO <sub>2</sub>	H <sub>2</sub> O
Mass proportion	14.7%	29.4%	55.9%

### 3.2.2.1 Preparation of activator

The activator used in this study was prepared 6 hours prior to mixing and stored in elevated temperature at 50 °C. This was to allow the possible reaction to complete in between the two components; 12M NaOH and Na<sub>2</sub>SiO<sub>3</sub> before used in the mix. The weight ratio of Na<sub>2</sub>SiO<sub>3</sub> to 12M NaOH solution was kept constant at 2.5 in all the mix designs. Activator was properly mixed just after adding the two components (NaOH and Na<sub>2</sub>SiO<sub>3</sub>) and just before batching to maintain the homogeneity.

### 3.2.3 Aggregate

Four aggregates representing the four different categories have been used in this study.

1. Natural non-reactive aggregate – Basalt
2. Natural reactive aggregate – Culcairn
3. Manufactured reactive aggregate – Ferronickel slag
4. Highly reactive (amorphous) aggregate – Fused silica

Table 3-3 shows the water absorption and apparent densities of aggregates which were implemented in the mix design calculations. Table 3-4 contains the chemical compositions of aggregates based on the XRF analysis results.

Table 3-3 : Water absorption and apparent density of aggregates

Aggregate type	Water absorption (%)	Apparent density (kg/m <sup>3</sup> )
Basalt	1.57	2895
Culcairn	1.05	2725
Ferronickel	0.68	2986
Fused silica	0.08	2258

Table 3-4 : XRF analysis results of aggregates

	Basalt (wt%)	Culcairn (wt%)	Ferronickel slag (wt%)	Fused silica (wt%)
Silicon dioxide (SiO <sub>2</sub> )	53.12	63.10	53.41	98.25
Calcium oxide (CaO)	6.35	4.76	0.22	-
Aluminium oxide (Al <sub>2</sub> O <sub>3</sub> )	16.58	15.66	2.52	-
Magnesium oxide (MgO)	3.10	2.10	32.08	-
Iron(III) oxide (Fe <sub>2</sub> O <sub>3</sub> )	7.97	5.55	10.69	-
Titanium oxide (TiO <sub>2</sub> )	0.98	0.80	0.06	-
Sodium oxide (Na <sub>2</sub> O)	4.34	3.35	0.09	-
Potassium oxide (K <sub>2</sub> O)	4.10	2.84	0.03	-
Loss of Ignition (LOI)	2.55	1.18	0.00	1.80

Figure 3-5 is the TAS (Total Alkali Silica) diagram developed to classify the igneous rocks by Le Maitre et al. (2005) based on their chemical compositions. TAS diagram (Figure 3-5) along with the XRF results in Table 3-4 is used to determine the mineralogy of natural rocks used in this study (refer section 3.2.3.1 and 3.2.3.2)

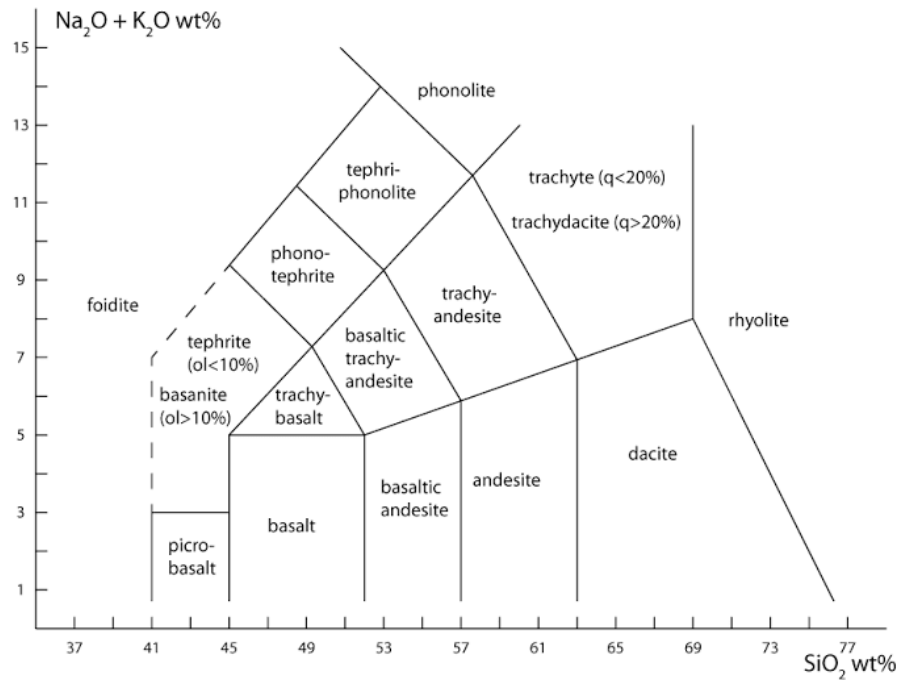


Figure 3-5 : TAS Classification for volcanic rock (adapted from <http://www.sandatlas.org>)

### 3.2.3.1 Basalt aggregate

Basalt is the mainstream quarried aggregate supplied by Boral Australia for the structural applications. Thus, it is selected as the natural non-reactive aggregate for the control tests.

Basalt is an igneous type rock formed due to rapid cooling of basaltic lava exposed near the surface. In fact, it is the most common rock type in the earth crust. Anorthite (calcic plagioclase) and augite (pyroxene) are the two most essential minerals in basalt along with quartz, olivine and feldspathoid ([www.mindat.org](http://www.mindat.org)). XRD analysis of basalt sample confirms the presence of anorthite, augite and quartz along with andesine (see Figure 3-8). XRF analysis on the aggregate sample (see Table 3-4) reveals that it belongs to the basaltic-trachyandesite section of the TAS diagram of igneous rocks. Thus, basalt used in this study may contain andesine along with other basic basalt minerals which are

classified as an alkali reactive mineral (Diamond 1976; [www.mindat.org](http://www.mindat.org)). Hence, basalt aggregate might also incorporate with some alkali aggregate reactivity. It should be noted that the amorphous and poorly crystalline phases could not be identified with XRD technology and thus there is still a possibility to have alkali silica reactive components in basalt to a certain degree. Figure 3-6 shows a sample of crushed aggregate prepared for the test. SEM analysis (see Figure 3-7) exhibits that basalt consists of angular particles with a rough surface.



Figure 3-6 : Basalt aggregate prepared for a mix

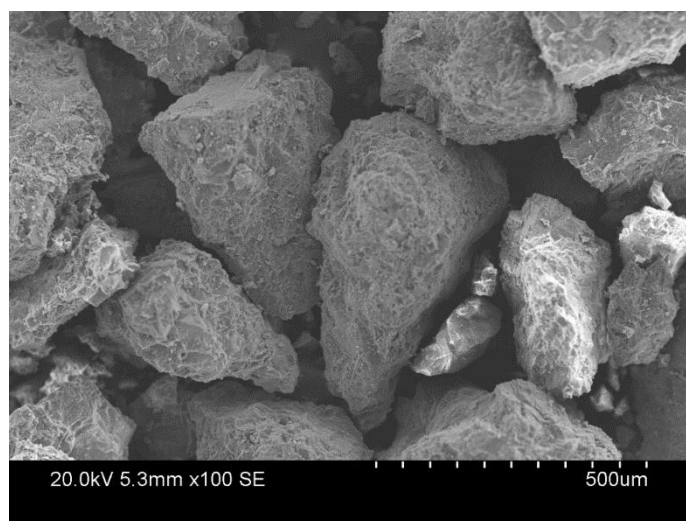


Figure 3-7 : SEM image of crushed basalt aggregate

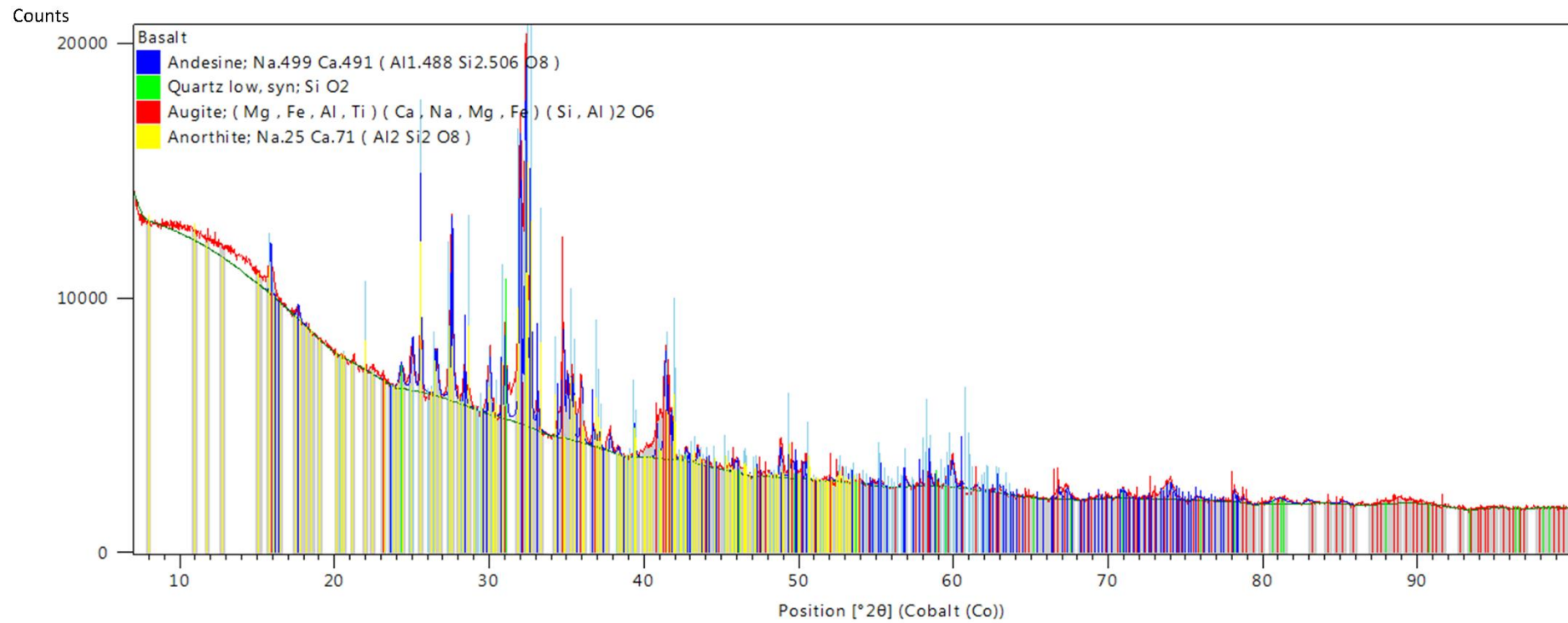


Figure 3-8 : XRD analysis result of basalt aggregate

### 3.2.3.2 Culcairn aggregate

Culcairn aggregate is supplied by Boral Australia from their quarry in Culcairn, NSW. The field records have proven the alkali aggregate reactivity of culcairn aggregate, and thus, it is used in this study to represent the natural reactive aggregate category.

XRF analysis in Table 3-4 shows that the chemical composition of culcairn aggregate consists of 63.1% of SiO<sub>2</sub> and 6.19% of total alkalis (Na<sub>2</sub>O +K<sub>2</sub>O). Thus, based on the TAS diagram (see Figure 3-5), the rock type of culcairn is dacite with properties closed to andesite. Dacite is an extrusive volcanic rock which consists of feldspar minerals rich in alkalis, albite-anorthite minerals and quartz. However, the presence of minerals like hornblende, amphiboles, augite, etc. are also possible in these rocks ([www.mindat.org](http://www.mindat.org)). XRD analysis results (see Figure 3-11) of culcairn aggregate shows traces of quartz, feldspar and anorthite. Feldspar minerals rich in alkalis (specially andesine) is classified as a reactive alkali mineral which is responsible for the alkali aggregate reactivity of culcairn aggregate along with microcrystalline quartz (Diamond 1976). However, it should to be noted that there can be amorphous and poorly crystalline phases in Culcairn aggregate which would not be identified with XRD but contribute to the alkali silica reactivity. Figure 3-9 shows a sample of crushed aggregate prepared for the test. SEM analysis (see Figure 3-10) exhibits flaky angular particles with rough surfaces in Culcairn aggregate.



Figure 3-9 : Culcairn aggregate prepared for a mix

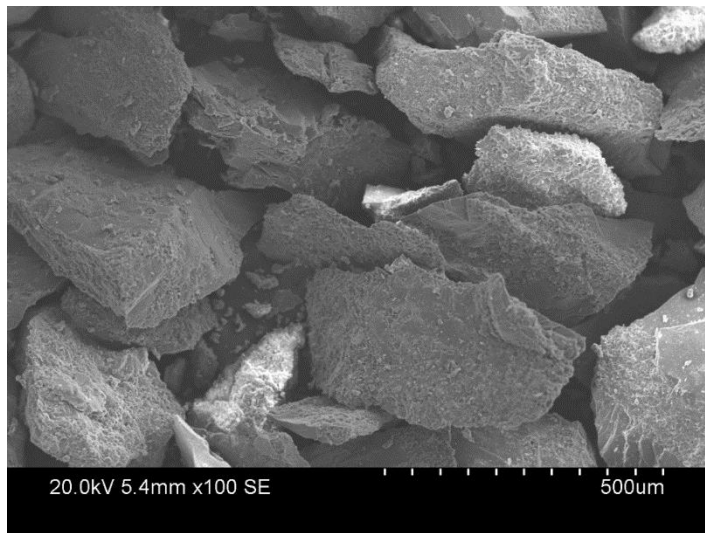


Figure 3-10 : SEM image of crushed culcairn aggregate

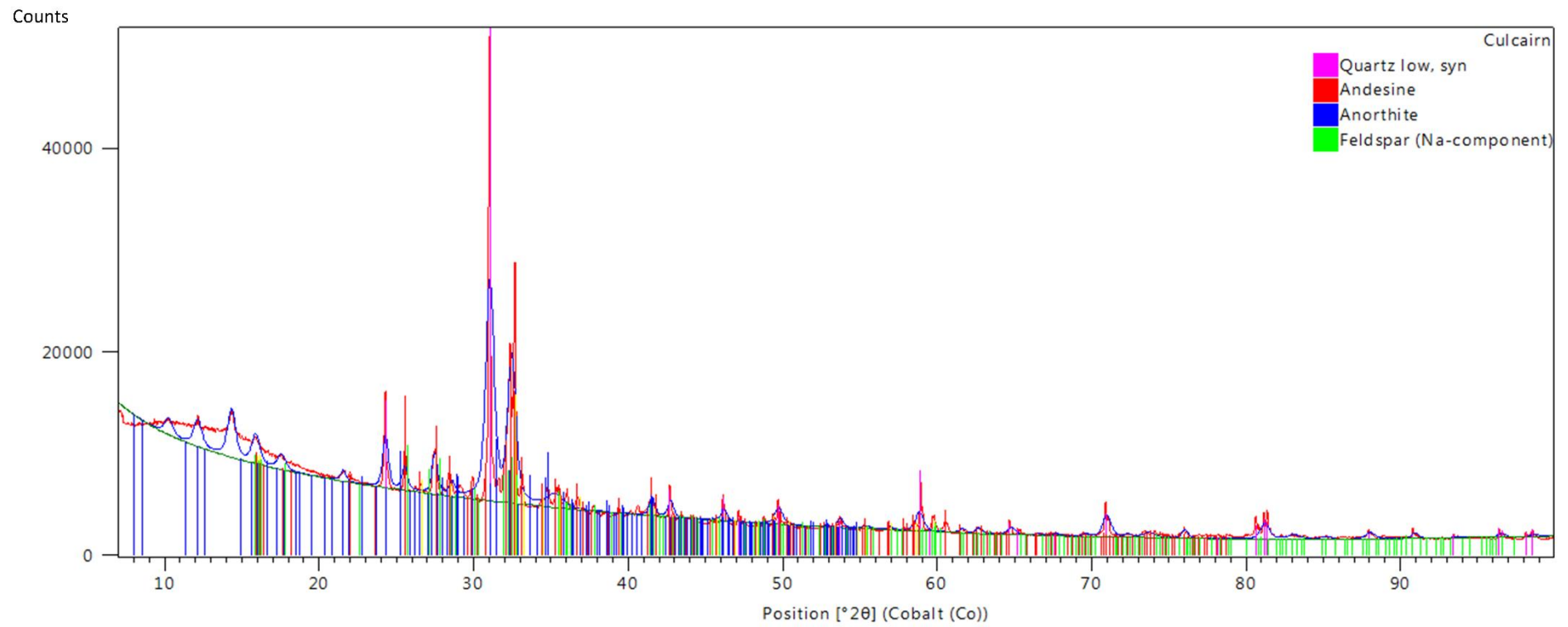


Figure 3-11 : XRD analysis result of culcairn aggregate

### 3.2.3.3 Ferronickel slag aggregate

Ferronickel slag aggregate is a by-product of nickel ore refining process. Le Nickel SLN has supplied the ferronickel slag aggregate (Le SAND) which is manufactured from their nickel refining plant in New Caledonia. Previous studies on ferronickel aggregate exposed its alkali aggregate reactivity when used in OPC based binders (Choi & Choi 2015; Saha & Sarker 2016). However, the partial replacement of natural fine aggregates with ferronickel slag sand did not lead to any ASR in fly ash based blended systems (Saha & Sarker 2017).

XRF analysis indicates that the main chemical constituents of ferronickel slag aggregate are Si ( $\text{SiO}_2 = 53.41\%$ ), Mg ( $\text{MgO} = 32.08\%$ ) and Fe ( $\text{Fe}_2\text{O}_3 = 10.69\%$ ). Formation of brucite ( $\text{Mg}(\text{OH})_2$ ) in the system may cause expansions due to alkali-carbonate reaction (ACR) as brucite can swell in the presence of water (Fournier & Bérubé 2000; HB79 2015). However, XRD analysis indicates that Mg presence in the form of forsterite and enstatite which can limit the brucite formation in the system (Choi & Choi 2015; Pokrovsky & Schott 2000). Thus, the reactivity of the ferronickel aggregate depends on the availability of amorphous silica which may form during the rapid cooling process and won't show up any spikes due to its amorphous form (Choi & Choi 2015). Figure 3-12 shows a sample of crushed aggregate prepared for the test. SEM analysis (see Figure 3-13) exhibits that ferronickel slag aggregate generally consists of sharp-edged particles with a smooth surface. However, as visible in SEM image (Figure 3-13) there are spherically shaped silica particles among other aggregates which might be responsible for the reactivity of the ferronickel slag,



Figure 3-12 : Ferronickel slag aggregate prepared for a mix

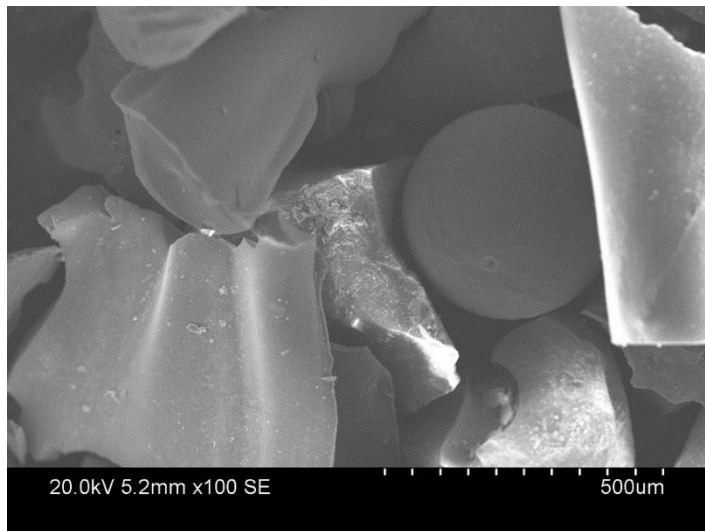


Figure 3-13 : SEM image of crushed ferronickel slag aggregate

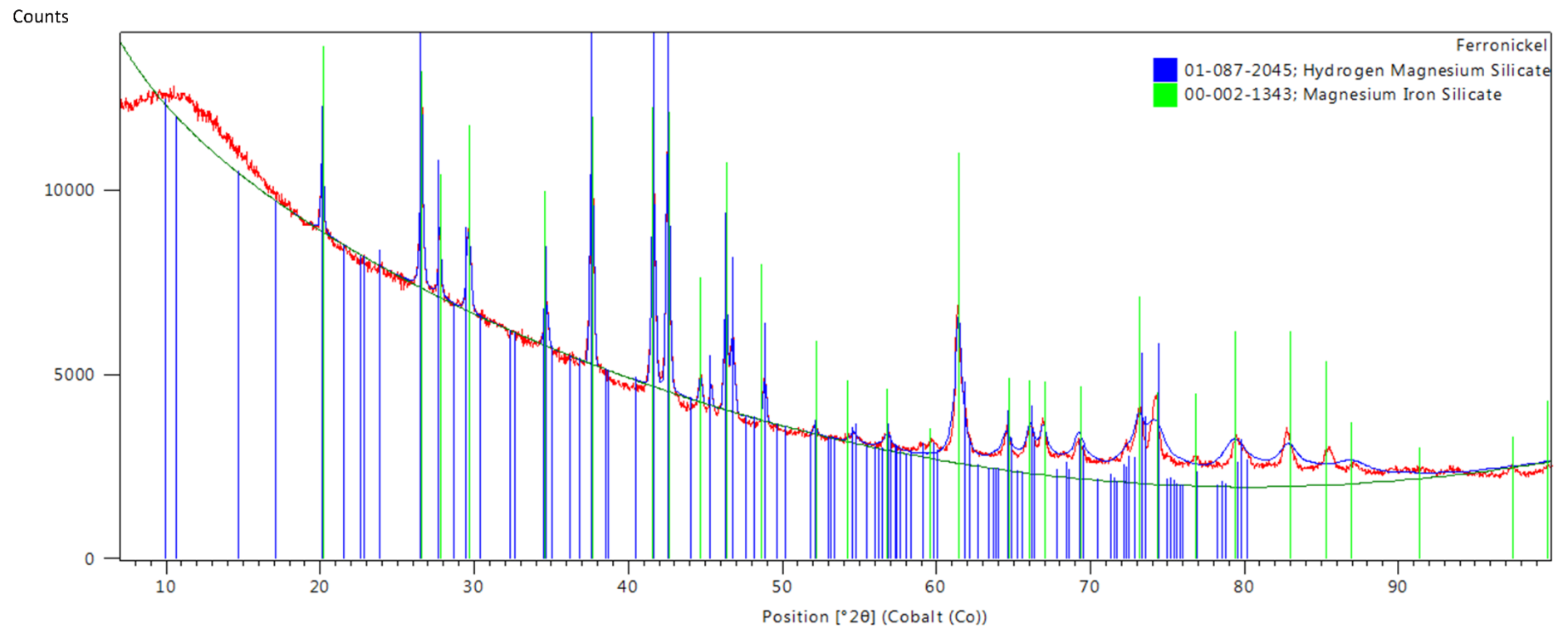


Figure 3-14 : XRD analysis result of ferronickel aggregate

#### **3.2.3.4 Fused silica**

Fused silica is a glassy material mostly composed of amorphous silica. For this study, fused silica was supplied by Sila Australia. Fused silica is considered a highly reactive material as it can supply more silica to the system due to its amorphous nature (Diamond, 1976; Hobbs 1988). Furthermore, the high purity of this aggregate also restrains the formation of other products along with the ASR gel.

XRF analysis confirmed the purity of the fused silica as SiO<sub>2</sub> content occupies 98.25% of the total (see Table 3-4). There are no major spikes visible in the XRD analysis results (see Figure 3-17) which confirms the amorphous nature of Fused silica. It should be noted that the peak visible in Figure 3-17 is most probably due to an impurity present in the sample. Therefore, it is expected to have significantly higher expansions in mortar bars cast with Fused silica compared to other aggregates because of its potential to release Si ions. Figure 3-15 shows a sample of crushed aggregate prepared for the test. SEM analysis (see Figure 3-16) reveals the presence of angular shaped glassy particles in fused silica.



Figure 3-15 : Fused silica slag aggregate prepared for a mix

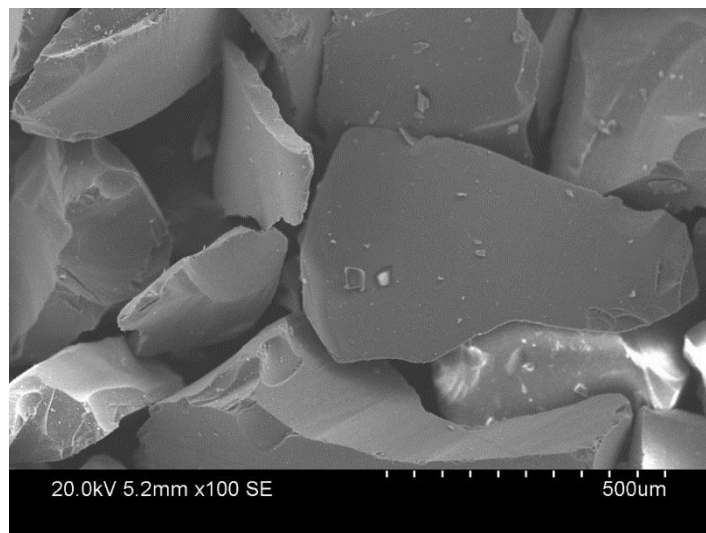


Figure 3-16 : SEM image of crushed fused silica

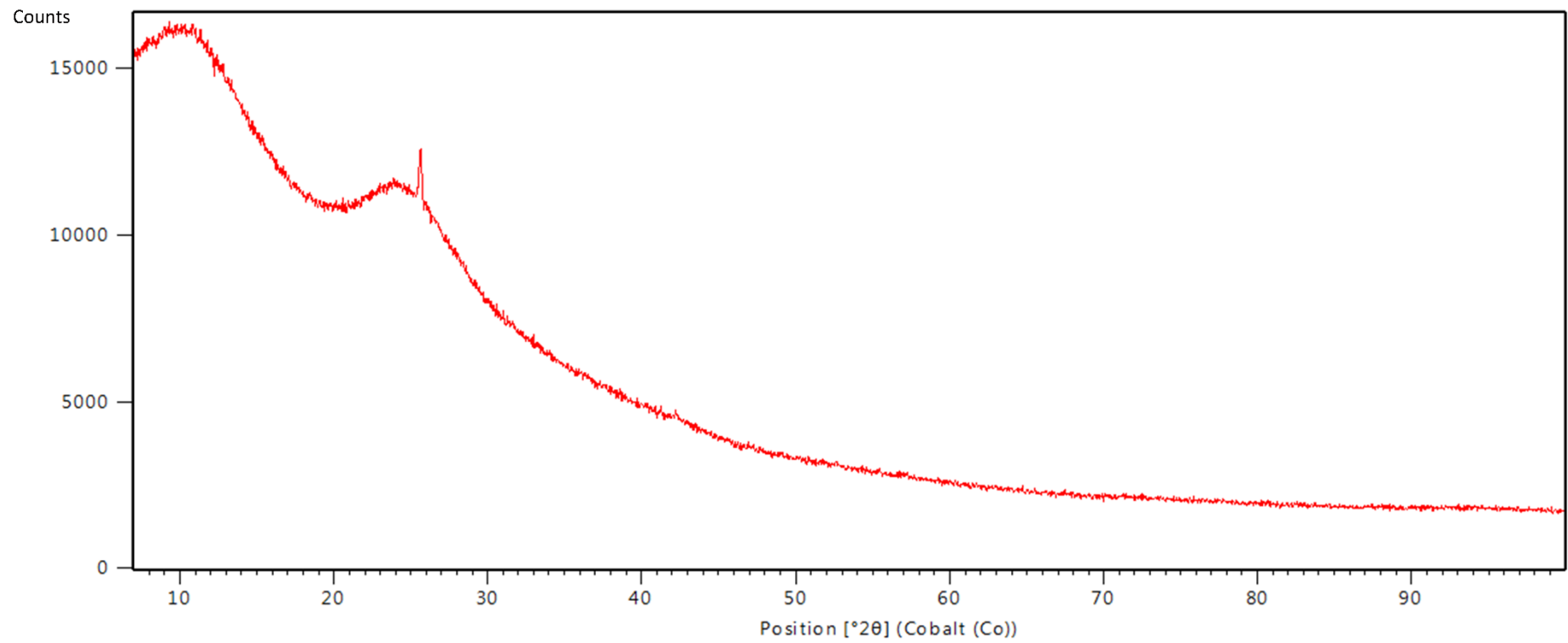


Figure 3-17 : XRD analysis result of fused silica

### 3.3 Test methodology

#### 3.3.1 Accelerated mortar bar test

Accelerated mortar bar test is the main testing method used in this study. The testing procedure was developed based on the standard accelerated mortar bar test specified in AS 1141.60.1 (AS1141.60.1 2014). However, changes were applied for the geopolymer mortar mixes to further assess the suitability of the existing test. Compressive strength variation of the mortar over 28 days was measured by crushing mortar cubes at specific time intervals as described in AS 1012.8.3. Figure 3-18 briefly summarised the testing procedure adapted during this study.

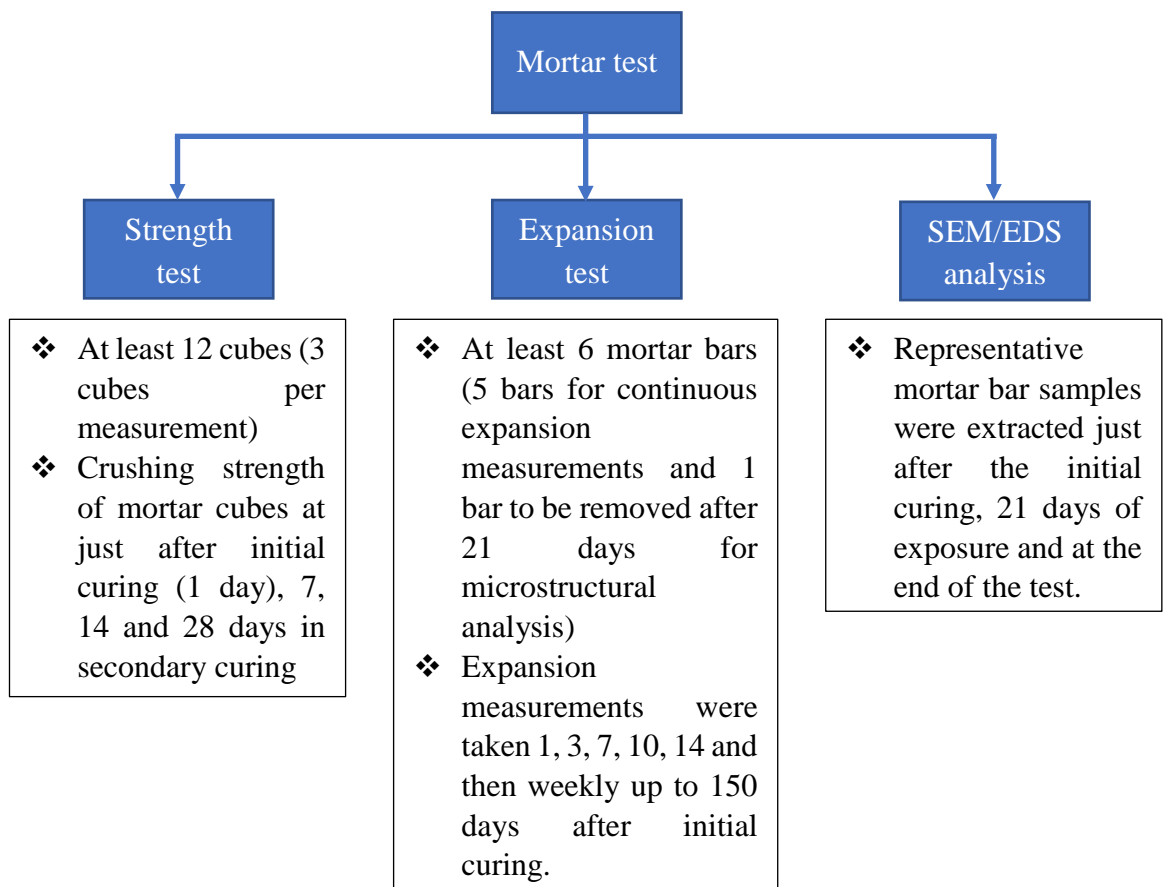


Figure 3-18 : Summary of testing procedure

### 3.3.1.1 Preparation of materials

Cementitious materials:

All the cementitious materials have been weighted and sealed 24 hours prior to the mixing.

Activator:

Activator has been prepared at least 6 hours prior to the mixing and stored at 50<sup>0</sup>C.

Aggregate:

All the aggregate except fused silica were crushed using a jaw crusher (see Figure 3-19) and then sieved using a sieve shaker (see Figure 3-19) to meet the gradation specified in AS 1141.60.1 (see Table 3-5). Then, the prepared aggregate were rinsed with tap water to remove any dust particles before being oven dried at 100 <sup>0</sup>C for 24 hours. 24 hours prior to batching, dry aggregate were mixed with water to attain saturated surface dry condition and sealed it in a plastic bag to avoid any water evaporation. Water needed to achieve the saturated surface dry condition was calculated from the water absorption percentages presents in Table 3-3.

Table 3-5 : Grading requirement as specified in AS 1141.60.1

Sieve size (mm)		% by mass
Passing	Retained on	
4.75	2.36	10
2.36	1.18	25
1.18	0.6	25
0.6	0.3	25
0.3	0.15	15



Figure 3-19 : Jaw crusher and sieve shaker used to prepare aggregate

### 3.3.1.2 Preparation of moulds

Preparation of moulds is a very important part of the mortar bar casting process. Generally, geopolymer mortar is more cohesive material than OPC mortar which allows it to have strong bonding with other materials (Deb et al. 2014). Even though it is a positive effect leading to high bond capacity with reinforcing bars, it has a negative impact while demoulding the specimens. Due to the small cross sections (25mm x 25mm), mortar bars tend to crack even before the demoulding (see Figure 3-19) due to the stresses generated during the heat treatment process. Thus, along with some modifications in curing methodology which will be discussed later in section 3.3.1.3, moulds were coated with two demoulding agents; first with a typical oil-based mould releasing agent used for OPC mortar and then water-based mould releasing agent developed for geopolymer mortars (Figure 3-20).

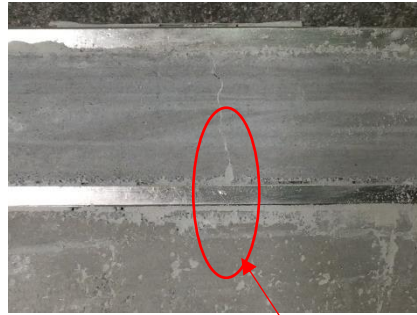


Figure 3-20 : Crack development in mortar during the thermal curing



Figure 3-21 : Moulds ready for casting

Placing the gauge studs also needs special attention as the gauge length has to be maintained at  $250 \pm 0.2$  mm to maximise the accuracy of readings (see Figure 3-22).

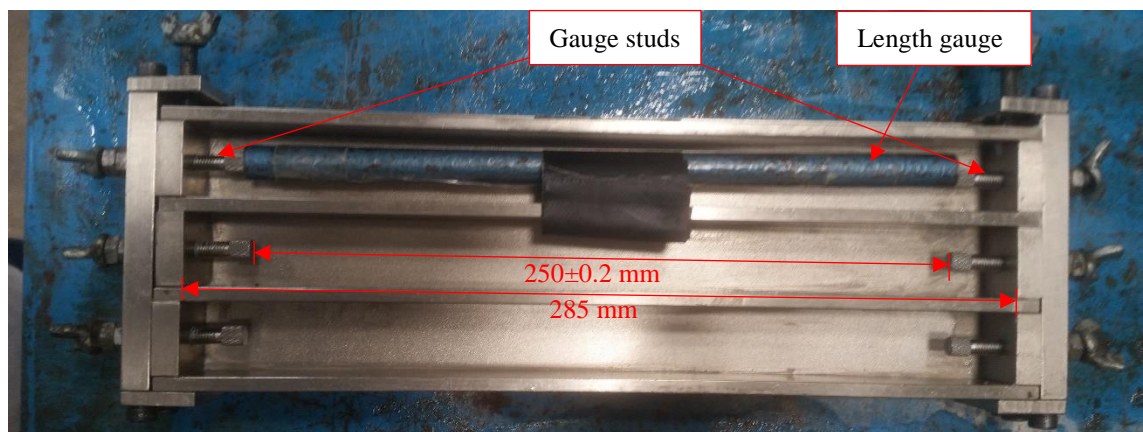
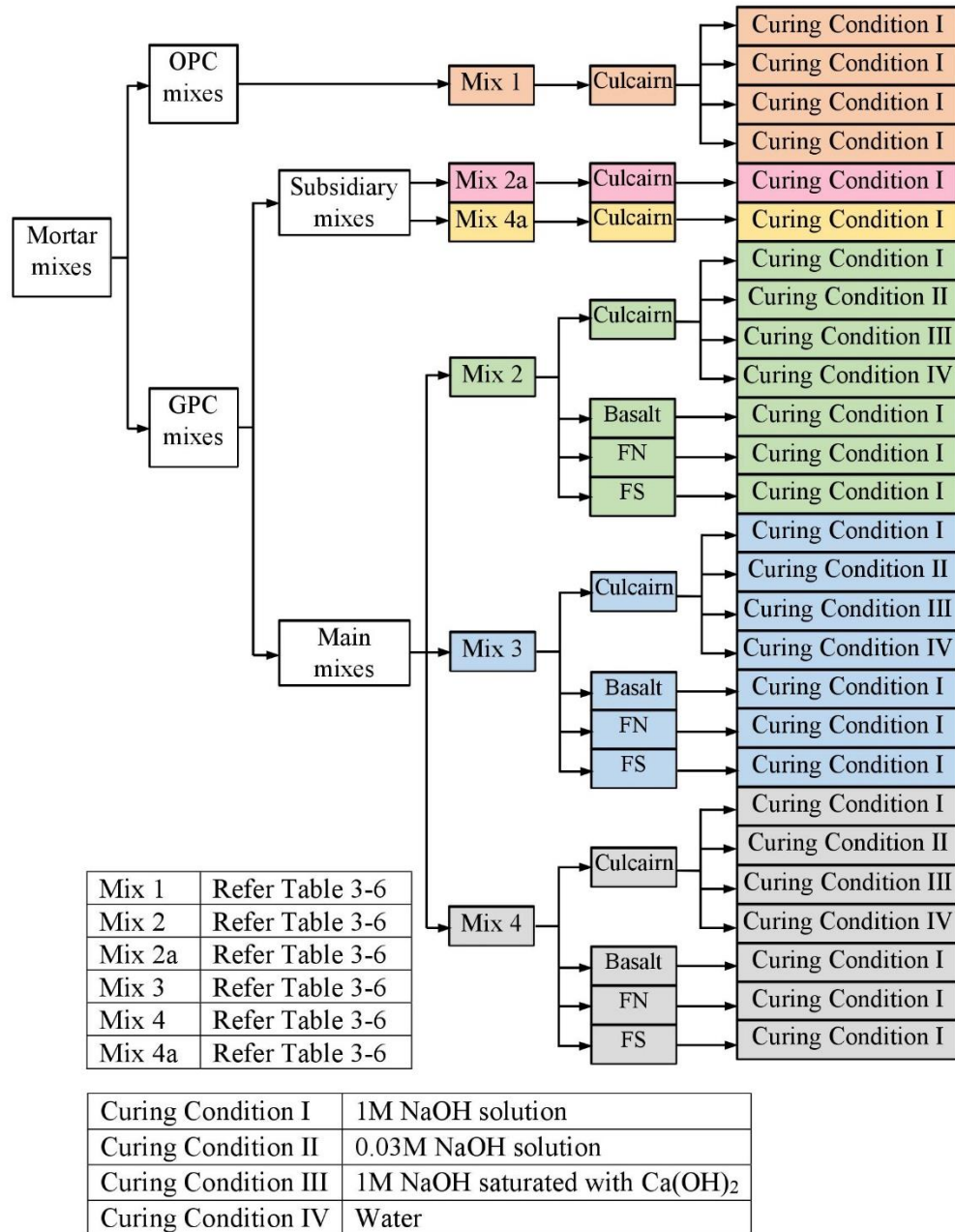


Figure 3-22 : Mould set up of mortar bars

### 3.3.1.3 Mortar preparation



Culcairn	Natural reactive aggregates from Culcairn quarry refer section 3.2.3.2
Basalt	Non-reactive aggregates from Boral Australia refer section 3.2.3.1
FN	Ferronickel - Manufactured reactive aggregates refer section 3.2.3.3
FS	Fused Silica - Amorphous aggregate refer section 3.2.3.4

Figure 3-23 : Summary of mortar mixes implemented in the study

Figure 3-23 summarizes the mortar bar test setup implemented during this study. 6 mortar mixes; 3 main geopolymer mixes with fly ash to GGBFS ratio 9 (Mix 2), 4 (Mix 3) and 1 (Mix 4), two subsidiary mixes with fly ash to slag ratio 9 (Mix 2a) and 1 (Mix 4a) and standard OPC mix (Mix 1) as in AS 1141.60.1 were considered as shown in Figure 3-23. Mix design details are summarized in

	Mix 1	Mix 2	Mix 2a	Mix 3	Mix 4	Mix 4a
Ratios (by weight)						
Water/cement	0.47	0.36	0.50	0.36	0.36	0.50
Activator/cement	-	0.50	0.33	0.50	0.50	0.33
Aggregate/cement	2.25	2.00	2.75	2.00	2.00	2.75
NaOH/Na <sub>2</sub> SiO <sub>3</sub>	-	0.40	0.16	0.40	0.40	0.16
Fly ash/GGBFS	-	9.00	9.00	4.00	1.00	1.00
Binder (kg/m <sup>3</sup> )						
OPC	580.6	0.00	0.00	0.00	0.00	0.00
Fly ash	0.00	553.6	447.4	492.1	307.6	248.6
Slag	0.00	61.5	49.7	123.0	307.6	248.6
Water and Activator (kg/m <sup>3</sup> )						
NaOH	0.00	87.9	22.2	87.9	87.9	22.2
Na <sub>2</sub> SiO <sub>3</sub>	0.00	219.7	143.5	219.7	219.7	143.5
Aggregate	1306.5	1230.3	1367.2	1230.3	1230.3	1367.2
Free water	272.9	47.0	155.0	47.0	47.0	155.0

Table 3-6 : Mix design details

	Mix 1	Mix 2	Mix 2a	Mix 3	Mix 4	Mix 4a
Ratios (by weight)						
Water/cement	0.47	0.36	0.50	0.36	0.36	0.50
Activator/cement	-	0.50	0.33	0.50	0.50	0.33
Aggregate/cement	2.25	2.00	2.75	2.00	2.00	2.75
NaOH/Na <sub>2</sub> SiO <sub>3</sub>	-	0.40	0.16	0.40	0.40	0.16
Fly ash/GGBFS	-	9.00	9.00	4.00	1.00	1.00

Binder (kg/m <sup>3</sup> )						
OPC	580.6	0.00	0.00	0.00	0.00	0.00
Fly ash	0.00	553.6	447.4	492.1	307.6	248.6
Slag	0.00	61.5	49.7	123.0	307.6	248.6
Water and Activator (kg/m <sup>3</sup> )						
NaOH	0.00	87.9	22.2	87.9	87.9	22.2
Na <sub>2</sub> SiO <sub>3</sub>	0.00	219.7	143.5	219.7	219.7	143.5
Aggregate	1306.5	1230.3	1367.2	1230.3	1230.3	1367.2
Free water	272.9	47.0	155.0	47.0	47.0	155.0

Mix 1-4 are used for all aggregates while subsidiary mixes (Mix 2a and 4a) used only with culcairn aggregate. The main purpose of those mixes is to assess the degree of ASR when the initial mortar strength is lower while keeping the same fly ash to GGBFS ratio. All the mixes except mix 1 were developed based on the experimental data available from previous studies at UNSW.

For each mix, 9 prismatic mortar bars (25mm x 25mm x 285mm) and 16 (50mm x 50mm x 50mm) cubes were cast.

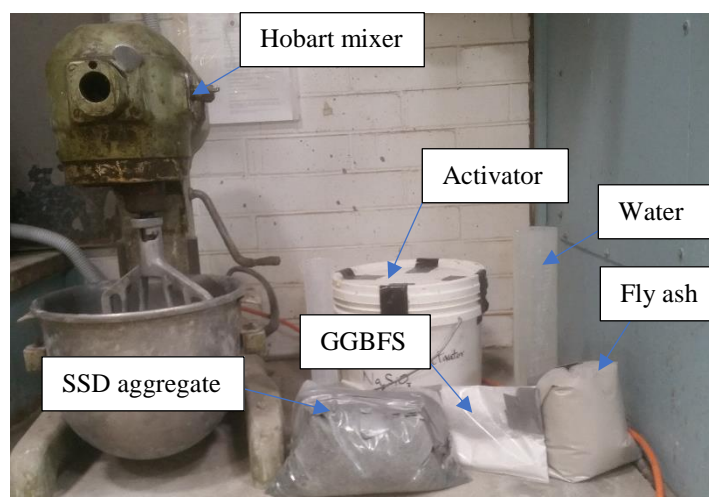


Figure 3-24: Materials prepared for mixing

### **Mixing of mortar**

Many researchers claimed that the mixing time and the method have a considerable impact on the properties of geopolymer binders (Davidovits 2011). Thus, the same mixing procedure was used in all the mixes to minimise the degree of error.

- a. Add SSD (saturated surface dry) aggregate to the bowl of a Hobart mixer and start the mixing at slow speed.
- b. Add fly ash over a 30 s period while mixing at slow speed
- c. Mix another 30 s and then add GGBFS to the bowl over a 30 s period while mixing at slow speed.
- d. Mix another 30 s and add activator and remaining water to the mix over a 30 s period while mixing at slow speed.
- e. Continue the mixing for another 60 s at slow speed
- f. Change the mixer to medium speed and mix the mortar for 30 s
- g. Stop the mixer and let the mortar stand for 60 s. During the initial 15 s quickly scrape down any mortar collected on the sides of the bowl.
- h. Finish mixing with 60 s mixing at medium speed.

### **Moulding of mortar**

- a. Moulds were filled with two approximately equal layers. Each layer was compacted using a vibration table for 15 s (see Figure 3-23)
- b. After compacting cut off the mortar flush and smooth the surface with a shovel. All the moulds shall be finished within 5 mins after finishing the mixing.
- c. Then place the moulds in a plastic bag and seal it to avoid any water evaporation during the initial curing period.



Figure 3-25 : Compacting the specimens with a vibration table

### Curing of specimens

As shown in Figure 3-20, initially, cracks can occur during the heat treatment process. Therefore, in order to prevent cracking, two curing periods were incorporated during the testing.

- a. Initial curing period started soon after finishing the moulding. The sealed mortar bars were placed in the temperature-controlled room at 25 °C for 16 hours. This allows mortar bars to develop enough strength before demoulding without causing any cracks.
- b. Initial curing period is followed by the demoulding process where all specimens were demoulded within 2 hours after finishing the initial curing phase.
- c. After demoulding, all mortar specimens were stored in airtight containers layered with wet cloths and exposed to the secondary curing condition; in an oven at 80 °C for 6 hours. The humidified environment developed inside the container helps to minimise the effect of drying during the secondary curing.

## Periodical reading

- a. Just after the secondary curing process, zero reading of the mortar bars were taken (see Figure 3-24). This reading should be done quickly (10 s per bar) to avoid any unnecessary errors due to variation in thermal contraction.
- b. 6 mortar bars and 12 cubes were placed in the curing solutions (see Figure 3-25). Four different curing solutions were used in this study,
  1. Curing condition I - 1M NaOH solution
  2. Curing condition II - 0.003M NaOH solution
  3. Curing condition III – 1M NaOH saturated with  $\text{Ca}(\text{OH})_2$
  4. Curing condition IV - Water

The solution to solid ratio in the container was kept constant at 4.2 in order to maintain the pH of mortar bars as constant as possible over the time. It should be noted that all the mortar bars were exposed to 80 °C temperature throughout the testing period.

- c. Readings were taken at 1 day, 3 days, 7 days, 10 days, 14 days and then weekly up until 150 days after the zero reading or excessive expansion occurs.
- d. Cubes were tested after the zero reading, 7 days, 21 days and 28 days after the secondary curing period. It should be noted that all cubes were dried before the crushing.
- e. Representative mortar bars were sampled just after heat curing, 21 days after heat curing and at the end of the test (150 days) for the microstructural analysis.

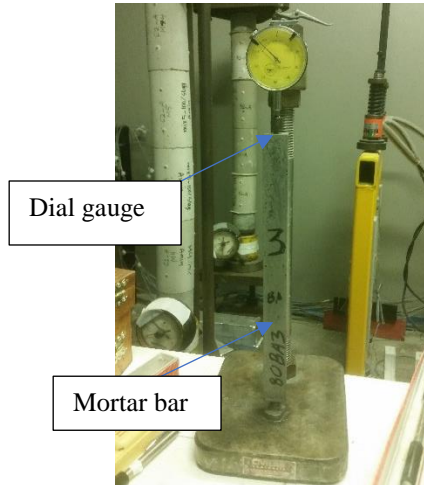


Figure 3-26 : Measuring the length variation with a dial gauge



Figure 3-27 : Mortar bars kept in 1M NaOH solution

### 3.3.2 SEM Analysis

Scanning electron microscope (SEM) analysis was carried out on the mortar bar samples extracted at 21 days and 150 days after secondary curing to identify any ASR gel formations. Energy dispersive X-ray spectroscopy (EDS) with a backscatter electron detector was incorporated into SEM analysis to further investigate the ASR gel formations and identify their chemical composition.

Mortar bar samples need to be prepared carefully for the SEM analysis as the final outcome vastly depends on the sample preparation process.

- a. First, roughly 20 mm thick section was cut from the mortar bar with a high-speed diamond saw and dried at 50 °C for 24 hrs.
- b. Then the top surface of the cut section was removed using a Struers minitom diamond saw operating at very low speed (150 rpm) with paraffin oil as the cooling agent. Samples were cleaned in an ultrasonic ethanol bath for 10 mins and dried at 50 °C for at least 24 hours.
- c. The grinding process consists of manual polishing the targeted surface starting with 320 grit (46µm) silicon carbide sheets and followed it with 800 grit (22µm), 1200 grit (15µm), 2000 grit (10µm) and 4000 grit (5µm) to achieve a smooth surface. The sample was ultrasonically cleaned in an ethanol bath for 5 mins and then dried with hot air flow for 5 minutes after each grinding step.
- d. After the polishing process, the specimens were placed in an oven at 50 °C for at least 24 hours.
- e. The appropriate coating was applied based on the analysis type required (see Table 3-7)

Table 3-7 : Sample preparation techniques for SEM analysis

Analysis type	Specification	Coating type	Coating equipment
SEM only	Clear images with high magnifications But chemical compositions not available	Gold coating	Emitech K550x Gold Sputter Coater

SEM/EDS	Image analysis with chemical compositions	Carbon coating	Hitachi Zone SEM
---------	---	----------------	------------------

SEM/EDS analysis was carried out using a Hitachi S3400 equipment located in Mark Wainwright Analytical Centre in UNSW (see Figure 3-26) to identify the ASR gel formation. It should be noted that backscattered electron (BSE) technology is used in EDS analysis to have more accurate results.

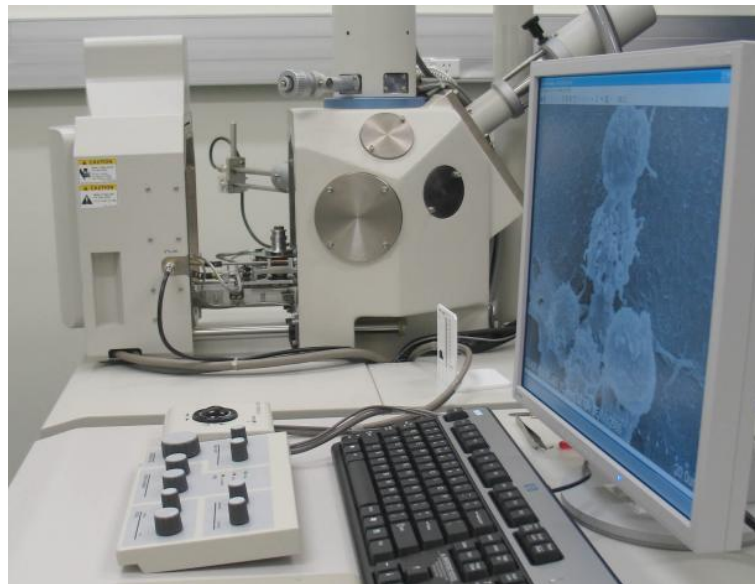


Figure 3-28 : SEM 3400 equipment used for the analysis

### 3.3.2.1 Water in sample preparation

Initially, water was used as the main lubricant in the sample preparation process (in both cutting and grinding processes). However, while performing SEM analysis, it was difficult to identify any gels even in mortar bars with considerable expansion despite having significant crack formations (see Figure 3-27). Therefore, it was decided to avoid water in both sample preparation processes; cutting and grinding. Paraffin oil was used

as the cooling agent in the low-speed cutter, and the water-based wet grinding process was replaced by a dry grinding process using the same sand papers. By adopting these two changes, it was possible to generate SEM images which clearly showed gel formations (see Figure 3-28).

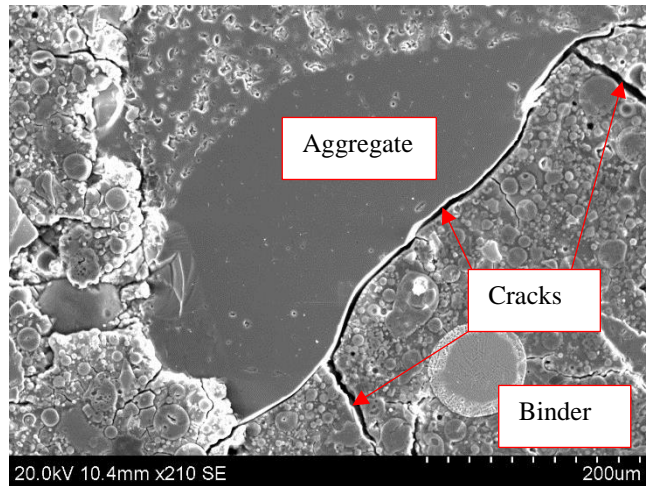


Figure 3-29 : Large cracks with no gel formations

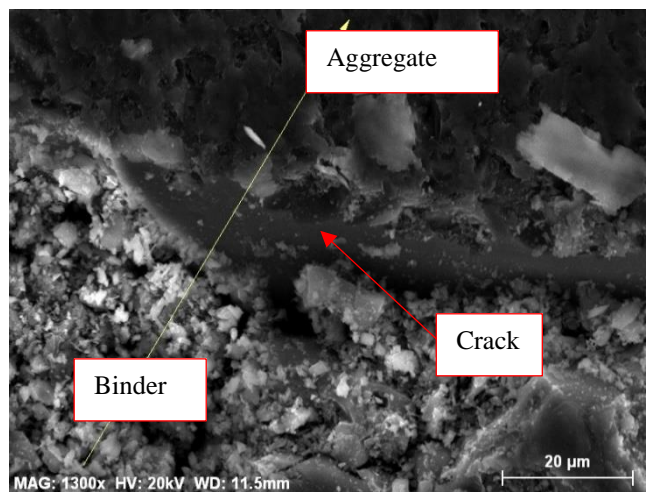


Figure 3-30 : Gel formation at the aggregate binder interface



# **CHAPTER 4 : Chemical performance of reactive aggregate exposed to an alkali solution**

---

## **4.1 Introduction**

Alkali silica reaction (ASR) initiates - by the aggregate Si ion dissolution as shown in Eq. 2-6 and Eq. 2-7 in section 2.3.3.1 which indicates that the extent of Si supply from aggregate directly governs the degree of ASR of the system. There are a lot of factors affecting the Si ion dissolution including phase and chemical composition of aggregate, the alkalinity of the solution ( $\text{OH}^-$  concentration), the exposed surface area of aggregate (particle size), physical properties such as temperature and pressure, etc. (Chan 1989; Niibori et al. 2000). However, phase and chemical composition of aggregate is the most important property among all as it solely depends on the origin of aggregate. Due to the slowness of the reaction, the quickest way to assess ASR risk is by assessing Si providing capability of aggregate which is adopted in many existing tests such as accelerated mortar bar test (AS 1141.60.1), chemical test (ASTM C289) etc. Nevertheless, all of these aggregate testing methods are only recommended as screening tests and required further investigations such as concrete prism test (AS 1141.60.2) to confirm their reactivity (HB79 2015; Hobbs 1988).

### **4.1.1 Aggregate type**

Dissolution characteristic of aggregates vastly depends on its chemical and phase composition which is governed by the origin of aggregate (Chan 1989). Si is the most common element present in aggregates after oxygen and, quartz is the most prevalent form of silica present in aggregates (Chan 1989; Tiecher et al. 2017). However, the presence of strong internal bonds in perfectly formed quartz crystalline structure reduces

Si dissolution significantly. Thus, most of the siliceous aggregates present in earth crust are innocuous (Tiecher et al. 2017). However, defects in the crystalline structure of quartz may make it vulnerable to hydroxyl ion attack which leads to Si ion dissolution, the initial reaction of ASR. Thus, alkali silica reactivity of siliceous aggregates increases with the degree of imperfection in their internal bond structures. In other words, the degree of amorphous nature of the silica phases of the aggregate is directly linked to their reactivity hence the dissolution of Si – the more amorphous the phase is more reactivity can be expected. (Hobbs 1988; Tiecher et al. 2017).

#### **4.1.2 The alkalinity of the solution**

Alkalinity (depicted by pH) of the exposed solution is another governing factor of the Si dissolution rate. Based on the Eq. 2-6, 2-7 and 2-8 in section 2.3.3.1 it is clear that hydroxyl ions ( $\text{OH}^-$ ) have a major role in Si dissolution process.

The behaviour of aggregates in different pH environments is an important factor in geopolymer binders since aggregate in geopolymer are exposed to a significant pH change (usually a reduction in pH) during the initial curing period as shown by Dang et al. (2016) compared to an almost constant pH in OPC (~13.0). The use of high concentration NaOH solution as the activator results in high initial pH (13.5~14.0), but with the geopolymerization process, the internal pH may drop below 11.0 within initial 24 hours (Dang et al. 2016; Patankar et al. 2014). Thus, high initial pH followed by comparatively low pH might be able to control the Si dissolution and limit ASR in geopolymer systems (Pouhet & Cyr 2015).

### **4.1.3 Particle size**

Particle size distribution of aggregate has a significant impact on Si dissolution rate since it correlates to the surface area of aggregate. It is obvious that for a similar weight of aggregate, smaller particles may entail with higher surface area compared to the larger particles. Since the reaction rate has a positive relationship with the effective surface area, the particle size has an inverse correlation with Si dissolution rate.

### **4.1.4 Temperature and pressure**

As with most chemical reactions, Si dissolution process is also accelerated with the increase in temperature and pressure of the reaction system (Chan 1989). Since the incorporation of higher pressure is practically difficult, an elevated temperature is used to accelerate the Si dissolution reaction in aggregate.

## **4.2 Test Methodology**

A simple dissolution test performed directly on aggregate to assess the effect of the following three factors.

1. Aggregate type
2. Alkalinity of the solution
3. Particle size

### **4.2.1 Preparation of aggregate**

Three reactive aggregates, Culcairn (see section 3.2.3.2), ferronickel slag aggregate (see section 3.2.3.3) and fused silica (see section 3.2.3.4) were used for this test.

All aggregate were crushed separately using a jaw crusher and then sieved using a sieve shaker to meet the required size fraction: 0.3mm-0.6mm. However, in order to assess the effect of aggregate size over Si dissolution capability, another size fraction

(8mm-9.5mm) was used along with the standard aggregate size. After sieving, all aggregates were thoroughly rinsed with distilled water to remove all dust particles and then dried in the oven at 100 °C for at least 24 hours to dry them. Finally, 15.0g of aggregate was sampled to be tested in different NaOH solutions as illustrated in Table 4-1.



Figure 4-1 : Aggregates (0.6mm-0.3mm) prepared for testing

#### 4.2.2 Preparation of solution

Sodium hydroxide was used as the base solution in all test setups. Table 4-1 shows the method adopted to prepare the NaOH solutions. 1M NaOH supplied by Sigma-Aldrich, Australia was used in this study.

Table 4-1 : Preparation of NaOH solutions

Concentration	pH	Directions for preparation	Volume
1 M	14	Directly use the 1M NaOH	2.25 l
0.03M	12.5	30ml from the 1M NaOH solution mixed with distilled water to achieve a total volume of 1000ml	2.25 l
0.003M	11.5	100ml from the 0.03M NaOH solution mixed with distilled water to achieve a total volume of 1000ml	2.25 l
0.0003M	10.5	10ml from the 0.003M NaOH solution mixed with distilled water to achieve a total volume of 1000ml	2.00 l

### **4.2.3 Preparation of test samples**

All three aggregates were used to assess the effect of aggregate type and alkalinity of the solution over the Si dissolution rate. Each aggregate type has a different phase and chemical composition based on their origin as described in section 3.2.3. Four sets of aggregate from each aggregate type (total of 12 sets) were prepared as described above in section 4.2.1. NaOH solutions were prepared as described above in section 4.2.2. Each aggregate set (15.0 g) was placed in a 500 ml borosilicate bottle, and then 450 ml of NaOH solution was added. Four solutions (1M, 0.03M, 0.003M and 0.0003M) were used for each aggregate type which sums up altogether 12 testing bottles for the whole testing program.

In order to assess the effect of aggregate size, another set of the test sample was prepared with Culcairn aggregate. In this new setup, all the testing conditions were kept unchanged except the size fraction of the aggregate which was changed to 8.0mm-9.5mm.

The test specimens were kept in an elevated temperature at 75 °C during the testing period (100 days) to accelerate the ion dissolution reaction.

### **4.2.4 Sample extraction**

A representative solution sample of 5ml was extracted from each bottle at 1, 3, 7, 21, 35, 49, 77 and 100 days to measure the ion concentrations by ICP analysis. The total volume of solution in the bottles was kept constant by replacing solutions with a similar amount (5 ml) of respective NaOH solution after each extraction.

#### 4.2.5 Inductively Coupled Plasma (ICP) analysis

ICP analysis was performed on extracted solutions to determine the ion content using a Perkin Elmer OPTIMA 7300 ICPOES equipment located in Mark Wainwright Analytical Centre (MWAC), UNSW. Table 4-2 illustrates all the operational parameter used during the ICP-OES analysis. ICP analysis was performed on at least three replicates for each sample, and the average was taken as the final ion content.

All the samples were diluted with 2% HNO<sub>3</sub> as shown in Table 4-3, in order to maintain the concentration of analytes within the linear calibration range of the equipment. Table 4-4 contains the set of analytes targeted during this study and their respective wavelengths.

Table 4-2 : Operational parameters adopted for the ICP analysis

RF Power	1300 watts
Plasma Gas Flow	15 L/min
Auxiliary Gas Flow	0.5 L/min
Nebulizer Gas Flow	0.70 L/min
Sample Introduction System	Burgener PEEK Mira Mist nebuliser with the cyclonic spray chamber
Pump rate	0.5 mL/min
Viewing height	15mm above load coil
View mode	Axial mode for trace elements. Radial mode for Na.

Table 4-3 : Pre-treatment acquired in each solution

NaOH concentration	Pre-treatment
1M	100 times with 2% HNO <sub>3</sub>
0.03M	10 times with 2% HNO <sub>3</sub>
0.003M	No dilution
0.0003M	No dilution

Table 4-4 : Analytes and their respective wavelengths targeted during the analysis

Analyte	Wavelength (nm) Monitored
Al	396.153
Ca	317.933
Fe	238.204
K	766.49
Mg	285.213
Na	589.592
Si	251.611
Y (Internal Standard)	371.029

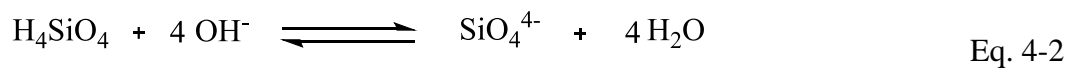
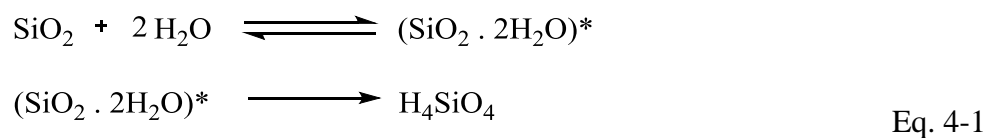
## 4.3 Results and Discussion

### 4.3.1 Aggregate type

Figure 4-2 show the variation in Si concentration of the four different base solutions (1M, 0.03M, 0.003M and 0.0003M) yielding three reactive aggregates. It should be noted that the graphs in Figure 4-2 featured with different scales for Y-axis (Si concentration) in order to make the variations more observable. All four graphs in Figure 4-2 follows a similar pattern, increment in Si concentration with retarding growth followed up by approximately constant phase. It can be noted that the magnitude of the

final Si concentration and the time to reach the stabilisation phase depend on the base solution alkalinity in each aggregate type.

The dissolution of SiO<sub>2</sub> in alkaline environments is shown in chemical equations 4-1 and 4-2. (Crundwell 2017; Schwartzentruber et al. 1987). It is obvious that, based on Eq. 4-1 and 4-2, higher hydroxyl ion concentration may result in higher Si dissolution. This has been observed in the dissolution tests (see Figure 4-1). In addition, at lower hydroxyl ion concentrations, Eq. 4-1; formation of silicic acid becomes the dominant reaction in Si dissolution kinetics which only occurred at the vicinity of the aggregate. Thus, Si dissolution in base solutions with low hydroxyl ion concentrations ends prematurely when the aggregate surfaces were covered with the silicic acids (Mitsyuk 1984; Schwartzentruber et al. 1987). Hence, higher Si concentration and larger time to achieve the stabilisation can be observed in solutions with higher hydroxyl ion contents (higher pH) compare to lower pH solutions.



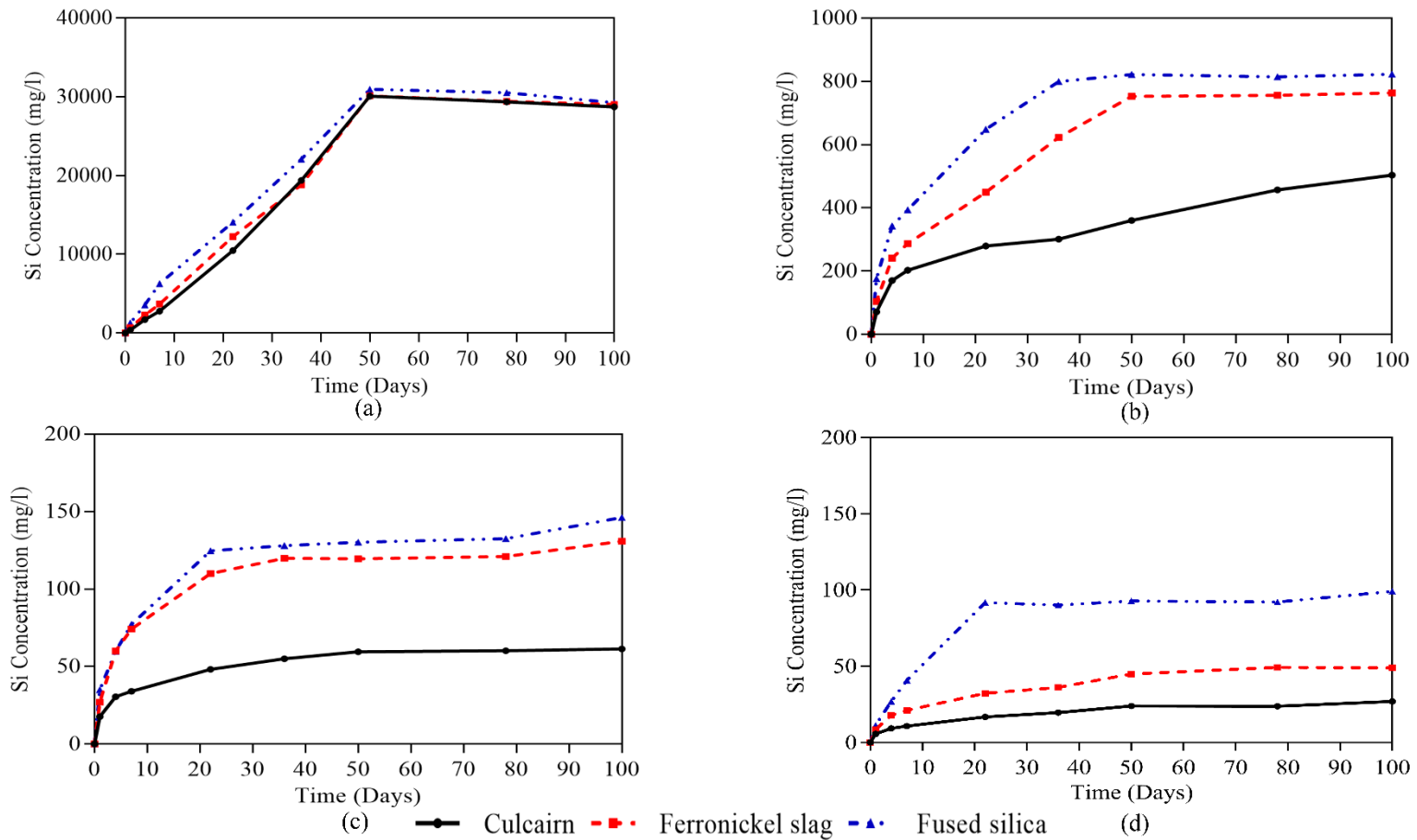


Figure 4-2 : Si dissolution of aggregates over the time. (a) immersed in 1M NaOH solution. (b) immersed in 0.03M NaOH solution. (c) immersed in 0.003M NaOH solution. (d) immersed in 0.0003M NaOH solution

Culcairn aggregate corresponds to the lowest Si dissolution in all the cases. Even though the gap seems less significant in Figure 4-2a due to the higher hydroxyl concentrations, it should be noted that there is still a substantial difference in Si concentrations, it should be noted that there is still a substantial difference in Si concentrations in 1M NaOH test setup. Even though Si dissolution of fused silica slightly excelled the ferronickel slag aggregate, both fused silica and ferronickel slag have shown almost similar behaviour at higher NaOH concentrations (1M, 0.03M and 0.003M) as shown in Figure 4-2a, 4-2b and 4-2c. In 0.0003M NaOH solution, Si dissolution of fused silica out passed the other two as illustrated in Figure 4-2d.

As discussed in section 3.2.3.2, Culcairn is a natural aggregate with crystalline bond structure. It basically consists of two phases; andesine and dacite. Even though dacite is known to have well forged crystalline structure, andesine is incorporated with very weak crystalline structure (triclinic structure) which may attribute to the Si providing ability of Culcairn aggregate. In ferronickel slag aggregate, Si providing capability is governed by the availability of amorphous silica formed during its rapid cooling process (water cooling). Fused silica consists of pure amorphous silicates ( $\text{SiO}_2$ ) which is responsible for its Si donating capability (refer section 3.2.3.4). Thus, fused silica has the weakest internal bond structure while ferronickel slag aggregate may rate close to fused silica due to the existence of amorphous silica particles. Even being an ASR reactive aggregate, Culcairn has the strongest internal bond structure among three aggregates used in this study. This consent with the Si dissolution behaviour shown in Figure 4-2 as fused silica shows the highest Si dissolution followed up by ferronickel slag and Culcairn respectively.

In addition, the experimental results suggest that the effect of the internal bond structure of aggregate on the Si dissolution decreases significantly with the alkalinity of the base solution which results in almost similar dissolution behaviours in 1M NaOH

solution. There can be two main reactions taking place when quartz exposed to alkali solutions (Crundwell 2017; Mitsyuk 1984; Schwartzentruber et al. 1987)

1. formation of silicic acid (Eq. 4-1)
2. acid-base reaction (Eq. 4-2)

It should be noted that both these reactions are reversible as shown in Eq. 4-1 and 4-2. Hydroxyl ions can drive the acid-base reaction (Eq. 4-2) forward which enforces the formation of more silicic acid and hence results in higher Si dissolutions in high alkalinity (Eq. 4-1). It is obvious that the degree of enforcement for Si dissolution governed by the concentration of hydroxyl ions in the base solution. With higher enforcements in high alkali solutions, all three aggregates behave almost evenly as shown in Figure 4-2a (1M NaOH solution). However, when the hydroxyl ion content is lower, the enforcement is also lower which results in distinctive Si dissolution behaviours. Due to the stronger bond structure in Culcairn, the distinctive behaviour showed even in 0.03M NaOH solution. Since both ferronickel slag and fused silica have almost similar internal bond stability and reactivity they have shown almost similar dissolution characteristics except in 0.0003M NaOH solution.

#### **4.3.2 Alkalinity of the solution**

Figure 4-3 shows the of Si dissolution behaviour of the three aggregates used with respect to the base solution alkalinity. For simplicity, curves were plotted only at four stages: 1 day, 7days, 50 days and 100 days of exposure. A log scale is used for Si concentration axis in order to have a better view of the behaviour patterns.

In all cases, Si dissolution increases with the base solution alkalinity, and beyond 11.5 pH the trend is approximately linear when plotted in log scale. Furthermore, in all three graphs, lines correspond to 50 days and 100 days seems to overlap each other which indicates that Si dissolution has halted after approximately 50 days.

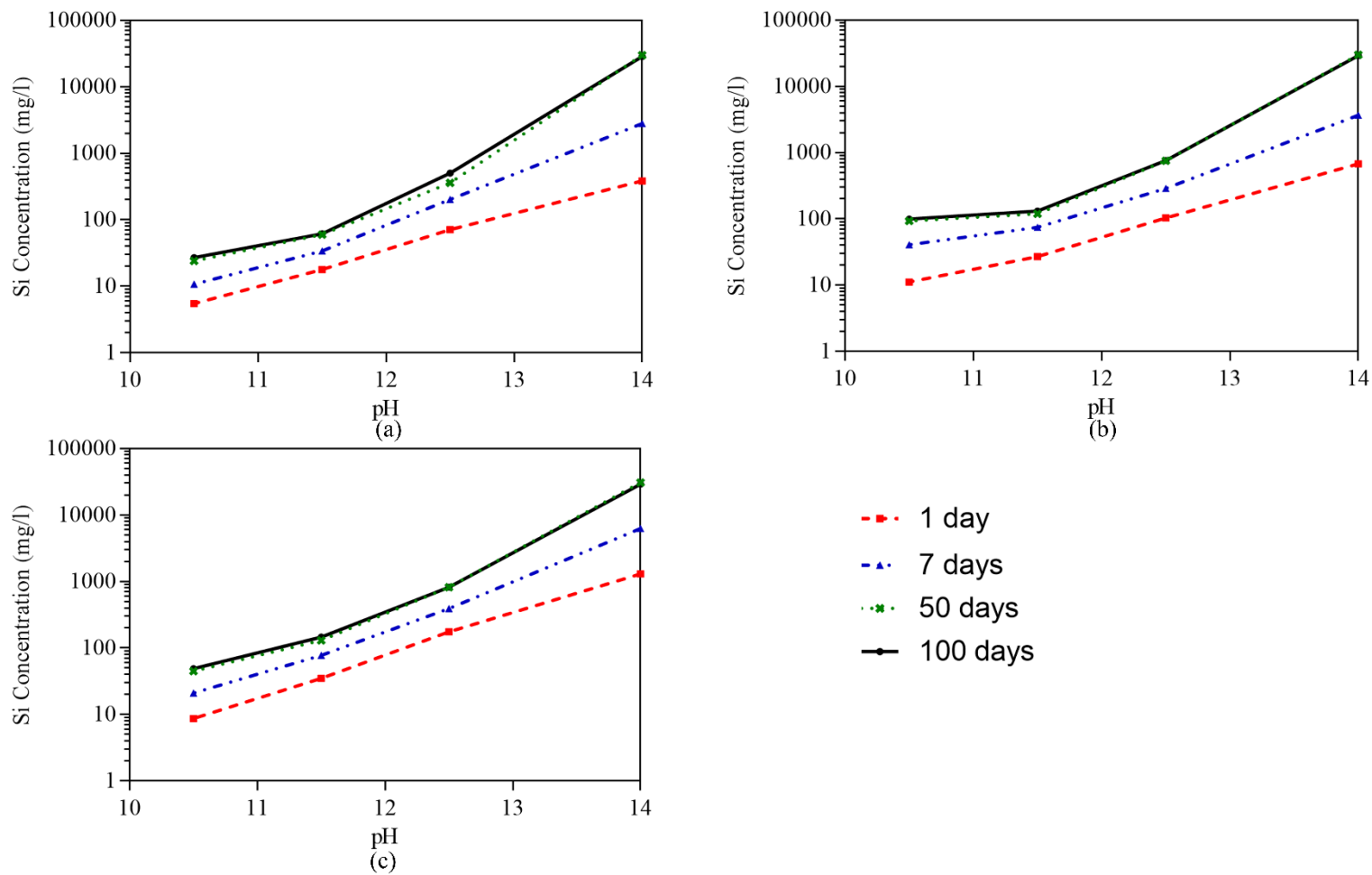


Figure 4-3 : Si dissolution of aggregates with base solution alkalinity (a) Culcairn aggregate (b) Ferronickel slag aggregate (c) Fused silica

### 4.3.3 Particle size

Figure 4-4 shows the variation in Si concentration of the solution over the time for the two different particle sizes: 9.5mm- 8.0mm and 0.6mm-0.3mm. It should be noted that the log scale is used for the Si concentration axis to have a better comparison between two cases.

It is clear that for all base solution concentrations, smaller size fraction (0.6mm-0.3mm) shows a significantly larger Si dissolution compared to its counterpart (9.5mm-8.0mm). This can be explained by the fact that, for a constant weight, the total surface area of the sample increases when the aggregate size is decreasing. Thus, reaction sites per unit weight increase with the reduction of particle size which may result in higher Si dissolution.

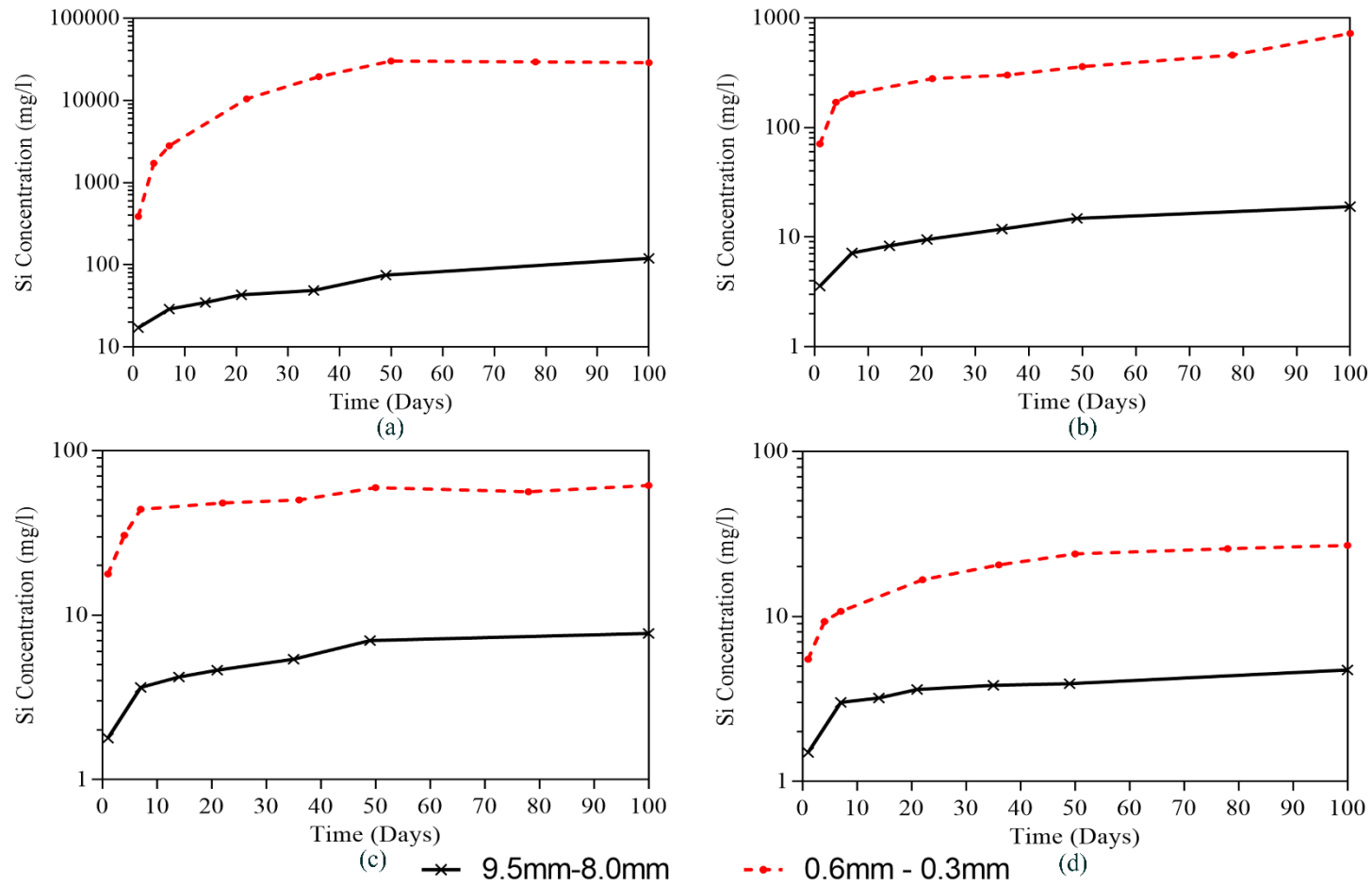


Figure 4-4 : Si dissolution of Culcairn aggregate with time (a) 1M NaOH solution (b) 0.03M NaOH solution (c) 0.003M NaOH solution (d) 0.0003M NaOH solution

#### 4.3.4 Formation of alkali silica products

Formation of white products in the solution was identified in some of the test set up as summarised in Table 4-5.

Table 4-5 : Summary of final outcomes

Aggregate type	Base solution concentration	Final Si Concentration (mg/l)	White substance formation
Culcairn	1M	28709.9	Yes
	0.03M	503.9	No
	0.003M	61.47	No
	0.0003M	26.92	No
Ferronickel slag	1M	29009.9	Yes
	0.03M	764.1	Yes
	0.003M	130.9	No
	0.0003M	99.14	No
Fused silica	1M	29259.9	Yes
	0.03M	822.8	Yes
	0.003M	146.2	No
	0.0003M	48.84	No

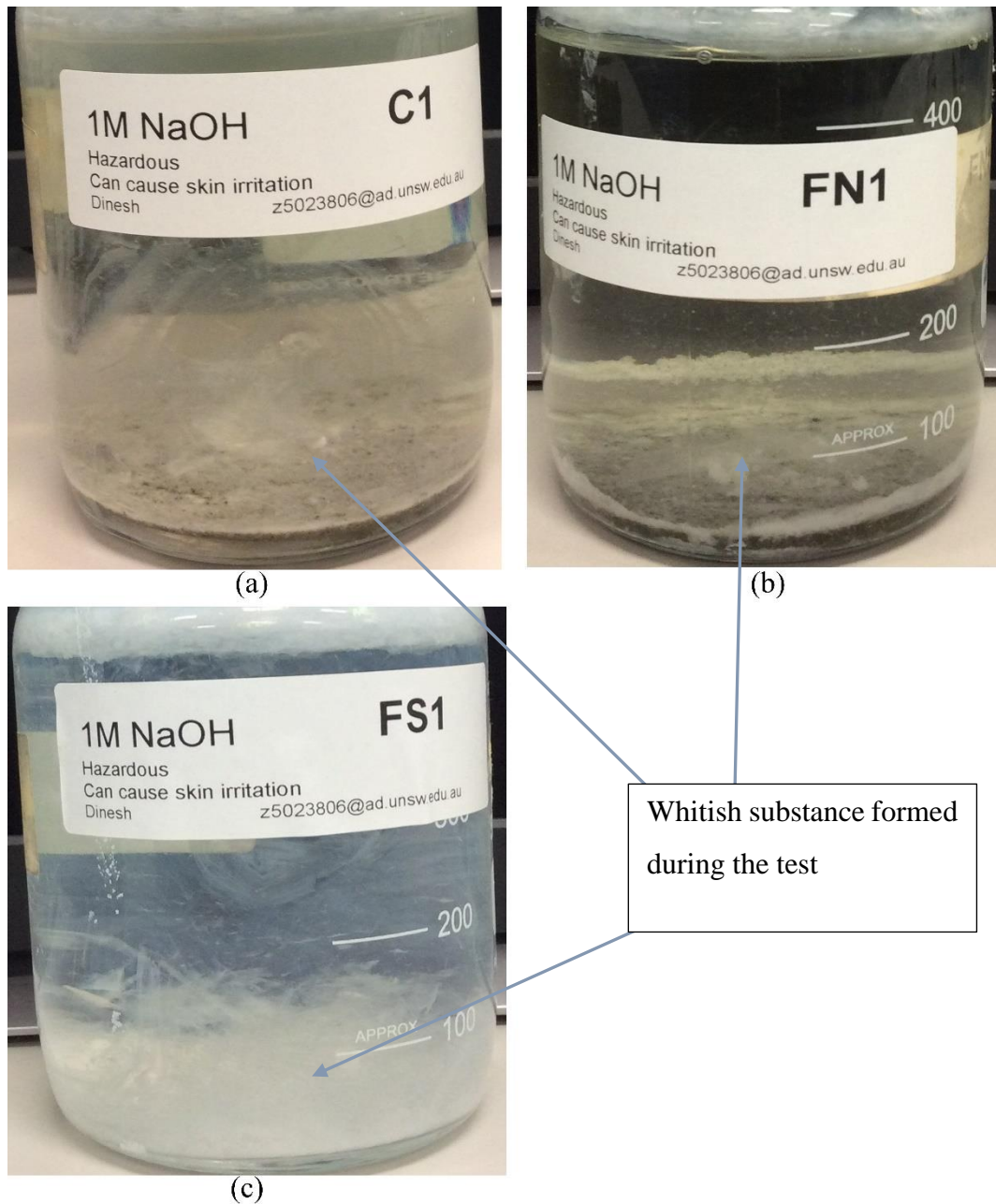


Figure 4-5 : Formation of whitish products in the test set up; (a) Culcairn in 1M NaOH solution (b) Ferronickel slag aggregate in 1M NaOH solution (c) Fused silica in 1M NaOH solution

All three aggregates have shown the formation of the whitish product (closed to opaline) when exposed to 1M NaOH solution (see Figure 4-5). Moreover, fused silica and ferronickel slag have even shown similar formation when exposed to 0.03M NaOH. Since fused silica have very little impurities (based on the XRF analysis), it can be concluded

that the substance formed is a type of alkali silica gel. Formation of this alkali silica substances in high alkali solutions is quite understandable as they have shown very high Si dissolution which might reach the saturation point of alkali silica gel quickly. Furthermore, the formation of this substance doesn't restrict to aggregate surfaces which also consent with the above theory. These findings are in agreement with previous research findings of Kim, Taehwan and Olek, Jan (2014), Leemann et al. (2011), Hou et al. (2004), etc. who stated that ASR gel formations occurred after reaching the saturation point of Si ions in the system.

#### **4.4 Summary**

This chapter describes the dissolution behaviour of aggregate exposed to NaOH solutions. The test was conducted on three different reactive aggregates to assess the effects of chemical and phase composition of aggregate, base solution alkalinity and particle size distribution on the Si supply capability of aggregate.

XRD and XRF analysis revealed that ferronickel slag aggregate and fused silica both consist of amorphous silica phases while Culcairn consists of weak crystalline structure. Both ferronickel slag and fused silica performed similarly in most of the hydroxyl concentrations studied. Even though Culcairn has also supplied an almost similar amount of Si in higher alkaline solution (1M NaOH), Si dissolution capability of Culcairn aggregate has dropped at a higher rate compared to ferronickel slag and fused silica when the base solution alkalinity (NaOH concentration) is decreased. This is because the effect of internal bond structure becomes significant when the hydroxyl ion concentration is reduced.

The alkalinity of the base solution plays a vital role on Si dissolution capability of aggregate. In fact, even for fused silica, Si supply drops by approximately 35 times when the base solution concentration decreases to 0.03M (12.5 pH) from 1M (14.0 pH).

Si dissolution of Culcairn aggregate with two different size fractions over the time revealed that aggregate size also has a major role in Si dissolution rate per unit weight, as the effective surface area increases when the particle size decreases.

Formations of opaline product was observed in all aggregates exposed to 1M NaOH solution while ferronickel slag aggregate and fused silica have shown this product formation even in 0.03M NaOH solution. It should be noted that at 1M NaOH all three aggregates have shown very high and approximately similar Si dissolutions whereas in 0.03M NaOH solution Culcairn has shown significantly lower dissolution compared to other two which showed almost similar Si dissolutions. Thus, it can be concluded that formation of this opaline product depends on the Si dissolution rate of the aggregate. Furthermore, based on the possible chemical reactions occur in fused silica (pure silica source) in high alkali environments, it is highly possible that this substance is a type of alkali silica gel.

# CHAPTER 5 : Alkali aggregate reaction in natural nonreactive aggregate

---

## 5.1 Overview

The theoretical risk of alkali aggregate reaction due to the activator high alkali content is one of the major concerns in geopolymer concrete over the past few decades (Bakharev et al. 2001a). However, the different chemical and internal bond structure of alkali activated materials compared to OPC binders does not allow to compare the performances of two binder systems directly. Thus, the expansion limits stipulated in the standard tests methodologies which were derived based on OPC systems have to be modified for alkali activated binders. Furthermore, Fernández-Jiménez and Puertas (2002) reported that the expansion characteristics of alkali activated mortar bars due to the alkali aggregate reaction consist of a time lag which is not shown in expansion curves of OPC based mortar bars. Thus, it is essential to adopt a controlled test set up to study alkali aggregate reaction in geopolymer mortar.

Basalt is a natural nonreactive aggregate supplied by Boral Australia for structural applications. The XRF and XRD analysis results provided in section 3.2.3.1 are consistent with its good field records. Thus, mortar bar expansion characteristics of basalt aggregate were used to establish the base limits to compare and analyse the expansion behaviours of the three reactive aggregates considered in this study.

Four mixes including three geopolymer mixes with fly ash to slag ratio 9 (Mix 2), 4 (Mix 3) and 1 (Mix 4) and standard OPC mix (Mix 1) as in AS 1141.60.1 have been

used. Section 3.3.1.3 contains all details of the respective mix designs. Mortar test consist of three parts;

1. Expansion readings of mortar bars up to 150 days
2. Cube strength variation up to 28 days
3. SEM/EDS analysis at 21 days and 150 days

## 5.2 Result and analysis

### 5.2.1 Expansion test

Figure 5-1 presents the expansion characteristics of mortar bars cast with basalt aggregate over 150 days. Four mix designs as described in section 3.3.1.3 were used in this study. The data points in the expansion curves were derived by averaging the mortar bar expansions at respective ages. The error bars in Figure 5-1 indicate that the standard deviation of mortar bar expansions of each data point is very low.

0.1% after 21 days is the minimum expansion limit specified in AS 1141.60.1 in order to categorize the aggregate as alkali reactive (AS1141.60.1 2014). Testing time of the AMBT has to be extended in order to encounter the initial time lag in geopolymer mortar mixes.

Table 5-1 : Average expansion of mortar bars with basalt at 10, 21 and 150 days

	Average expansion			
	10 days	21 days	100 days	150 days
Mix 1	0.0107 %	0.0572 %	0.1892%	0.2247 %
Mix 2	0.0102 %	0.0250 %	0.0991%	0.1805 %
Mix 3	0.0012 %	0.0206 %	0.1242%	0.1921 %
Mix 4	-0.0024 %	0.0354 %	0.1483%	0.2009 %

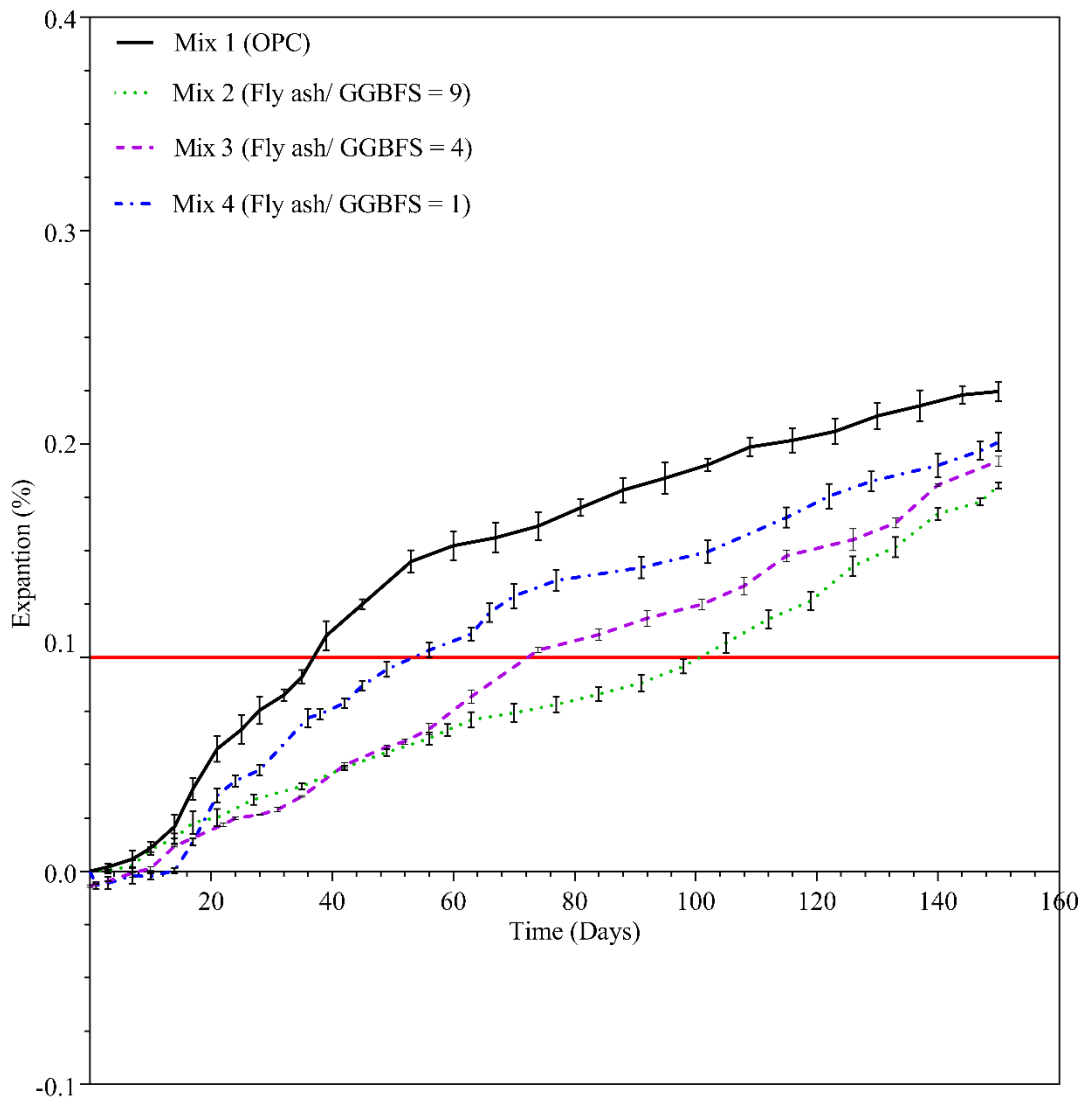


Figure 5-1 : Expansion characteristics of mix 1-4 over 150 days when exposed to accelerated curing conditions. 0.1% (red line) is the minimum expansion limit for reactivity stipulated in AS 1141.60.

Table 5-1 summarises the average mortar bar expansion after 10 days, 21 days 100 days and 150 days of mix 1-4. Mix 1, the standard OPC mix, has shown the highest average expansion throughout the testing period reaching 0.0107% after 10 days and 0.0572% after 21 days. However, the average expansion of Mix 1 did not reach the 0.1% expansion limit stipulated in AS 1141.60.1 with in the period of 21 days and hence basalt aggregate shall be categorised as nonreactive aggregate in OPC concrete (AS1141.60.1

2014). Thus, the accelerated mortar bar test results of basalt aggregate consent with its field records and chemical and mineralogical analysis results based on XRF and XRD analysis (see section 3.2.3.1).

Geopolymer mixes (mix 2-4) also did not show any significant short-term expansions. In fact, mix 3 (FA/GGBFS =4) and mix 4 (FA/GGBFS =1) have shown negative expansion (shrinkage) up to 7 and 10 days respectively before exhibiting positive expansions. Thus, characteristic curves of mortar bars overlapped each other during the initial 21 days of the testing period before settling in their respective positions as shown in Figure 5-1.

Mortar bars of Mix 1 (OPC mix) have shown the highest final average expansion (0.2247%) which indicates that based on AMBT results, OPC system is more vulnerable to alkali aggregate reaction compared to the geopolymer systems used in this study. Among the geopolymer mixes, Mix 4 (FA/GGBFS = 1) has shown the highest final average expansion reaching 0.2009% after 150 days while Mix 3 (FA/GGBFS = 4) and Mix 2 (FA/GGBFS = 9) achieved 0.1921% and 0.1805% final expansions respectively. Thus, it can be concluded that the final average expansions of geopolymer mortar bars increase with the GGBFS content in the system which consent with the works of Bakharev et al. (2001a), Shi, C et al. (2015) and Shi, Z et al. (2015).

Expansion curves typically follow a sigmoidal shape (S-shape) which consist of three phases; initial phase with very low or zero expansion, secondary phase with high expansion and a final phase where expansion has stabilized. However, gradient and the time period of each phase depends on the properties of the mix. It seems that the expansion curves of Figure 5-1 are all following the same characteristic sigmoidal shape.

Mix 1 has 10 days of initial phase followed up by the secondary phase which almost continued throughout the rest of testing time. However, the expansion rate has

clearly slowed down at the end indicating the forthcoming of the final phase. Mix 2-4 ceased their initial phase and entered to the secondary phase after 7 days, 10 days and 14 days respectively as shown in Figure 5-1. This shows that the initial time lag (phase 1) of expansion curves of geopolymer mixes is only marginally increasing with GGBFS content in the mix for non-reactive aggregate. Furthermore, none of the geopolymer mixes has shown a significant decrease in expansion rate during the testing period, though it is expected to stabilize after some time due to the completion of alkali silica reaction.

### 5.2.2 Compressive strength variation

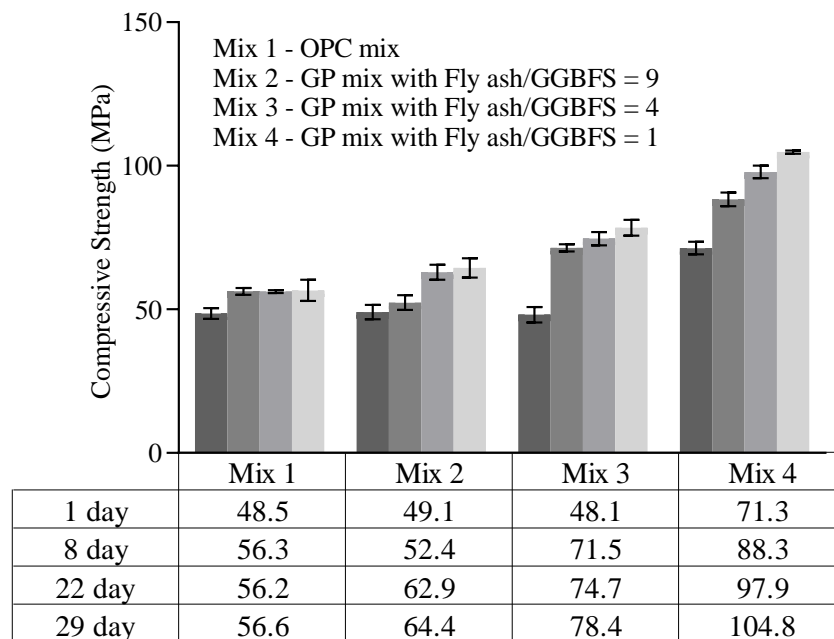


Figure 5-2 : Compressive strength variation of mix 1-4 over 29 days of casting

Figure 5-2 shows the compressive strength development of mixes 1-4 over 29 days based on the 50mm x 50mm x 50mm cube crushing values. Mixes 1, 2 and 3 has shown similar initial strengths (approximately 48 ~ 49 MPa) while mix 4 has achieved the higher initial strength of 71.33 MPa. The strength gain of mix 1-4 during the last 7 days (22-29

days after casting) are 0.71%, 2.28%, 4.76% and 6.61% respectively which indicates that all mixes have almost achieved their maximum strengths by 29 days. The compressive strength of mixes 2 to 4 after 29 days of casting (28 days of testing) suggest that GGBFS content has a positive influence on the compressive strength of geopolymer mortar when all the other parameters of the mix design are maintained identical.

### **5.2.3 Scanning Electron Microscope (SEM) Analysis**

Backscatter SEM/EDS analysis was carried on representative mortar bar samples extracted at 21 days and 150 days to identify the gel formation and its chemical composition.

OPC mortar samples (mix 1) have shown a ASR gel formation at both stages; 21 days and 150 days while ASR gel was identified only at 150 days in geopolymer mortar samples (mix 2-4). Even though ASR gel was identified inside the aggregate as well as at the aggregate binder interface, SEM/EDS analysis targeted only the ASR gel formed inside the aggregate in order to simplify the analysis without interfering with the chemistry of the geopolymer binder. Table 5-2 summarizes the average elemental atomic percentages of ASR gel of Mixes 1 to 4 calculated from the backscatter EDS line profiles. Each gel composition presents in Table 5-2 is an average value of roughly 250 points representing ASR gel formed inside the aggregate. Figure 5-3 to 5-7 are the backscatter EDS line profile graphs which show ASR gel formation in mix 1 at 21 days and mix 1, mix 2, mix 3 and mix 4 at 150 days respectively.

Figure 5-8 is the ternary diagrams plotted from the data in Table 5-2 in order to identify the variations in chemical compositions of ASR gels with respect to the mix and testing time. ASR gels in all mixes mainly consist of Sodium (Na), Calcium (Ca), Silicon (Si) and Aluminium (Al) ions along with Oxygen (O) which is omitted from the EDS line profiles.

Table 5-2 : Summary of SEM /EDS analysis on ASR gel located in mix 1-4

Mix No.		Average atomic percentage (%)						Ratios		
		Na	K	Ca	Mg	Si	Al	$\frac{(Na+K)}{Si}$	$\frac{(Ca+Mg)}{Si}$	$\frac{Al}{Si}$
1	21 days	2.84	0.27	7.41	1.50	20.03	8.06	0.16	0.44	0.40
	150 days	8.92	1.06	5.19	1.68	14.89	7.21	0.67	0.46	0.48
2	21 days	-	-	-	-	-	-	-	-	-
	150 days	7.03	1.85	0.54	0.14	18.80	9.12	0.47	0.04	0.49
3	21 days	-	-	-	-	-	-	-	-	-
	150 days	7.35	2.35	2.31	0.74	18.76	8.16	0.52	0.16	0.43
4	21 days	-	-	-	-	-	-	-	-	-
	150 days	9.65	0.23	3.18	0.07	16.65	8.83	0.59	0.20	0.53

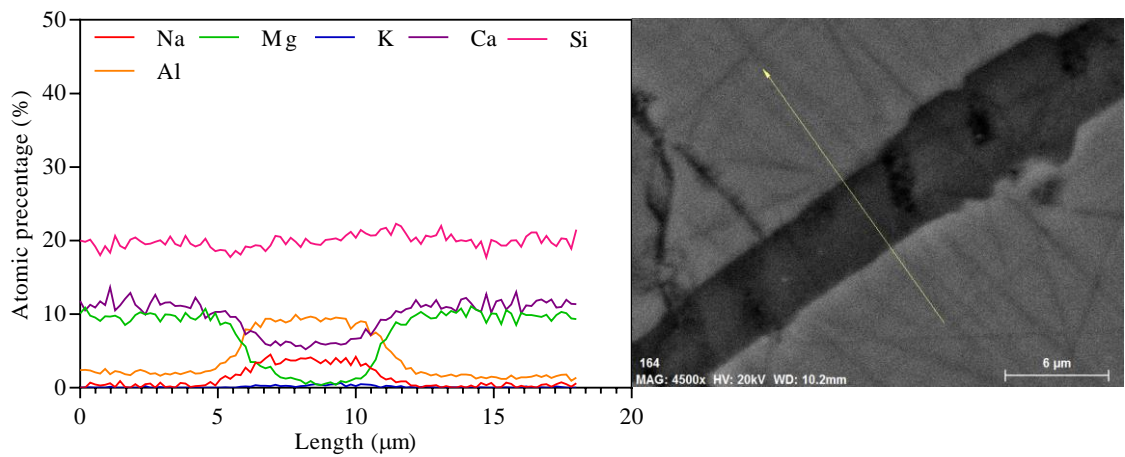


Figure 5-3 : Alkali silica gel identified in the aggregate of mix 1 at 21 days

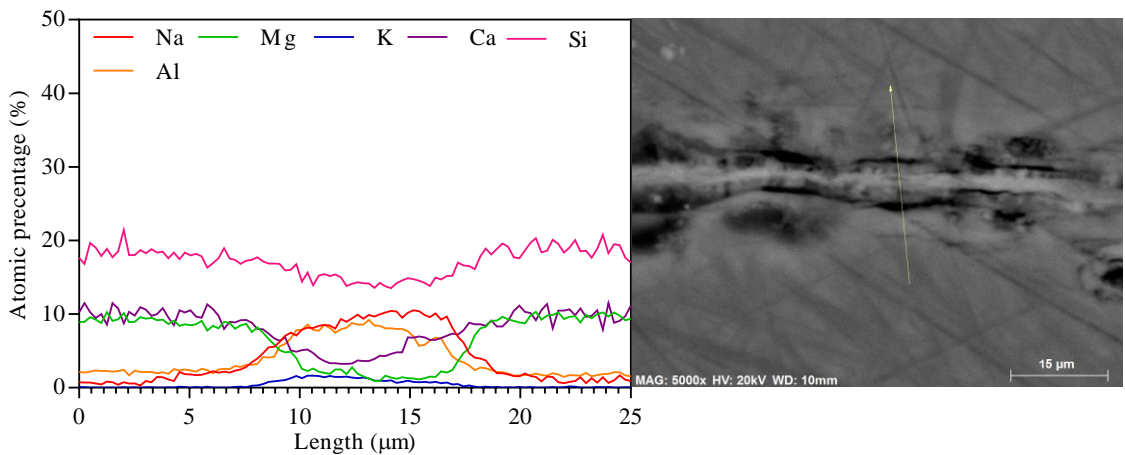


Figure 5-4 : Alkali silica gel identified in the aggregate of mix 1 at 150 days

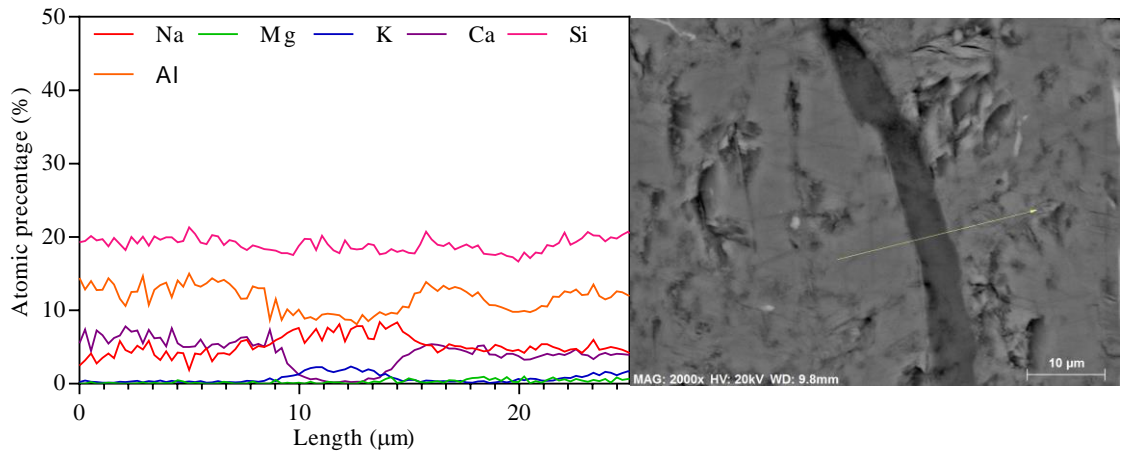


Figure 5-5 : Alkali silica gel identified in the aggregate of mix 2 at 150 days

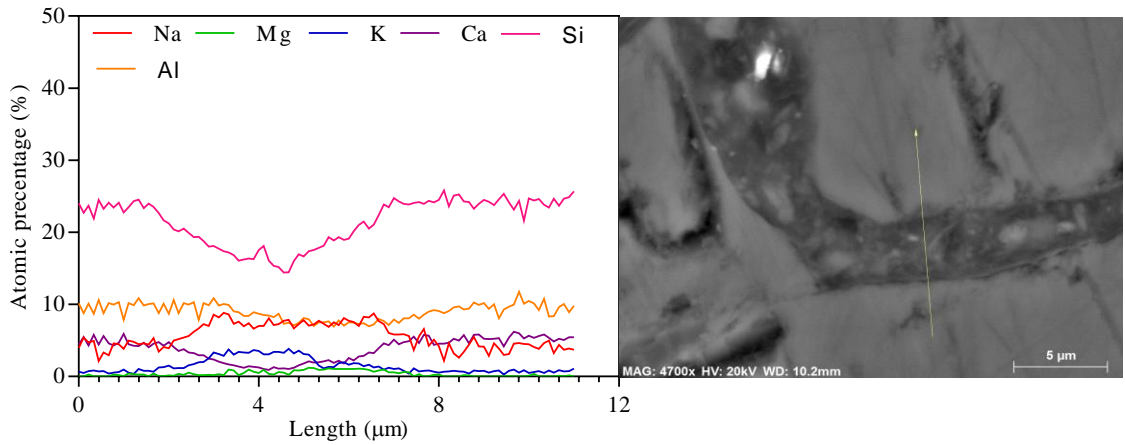


Figure 5-6 : Alkali silica gel identified in the aggregate of mix 3 at 150 days

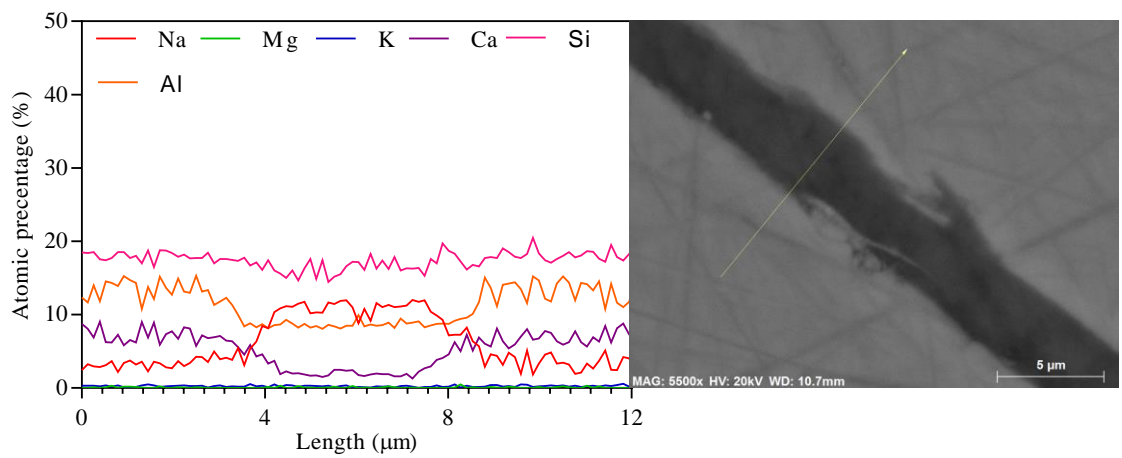


Figure 5-7 : Alkali silica gel identified in the aggregate of mix 4 at 150 days

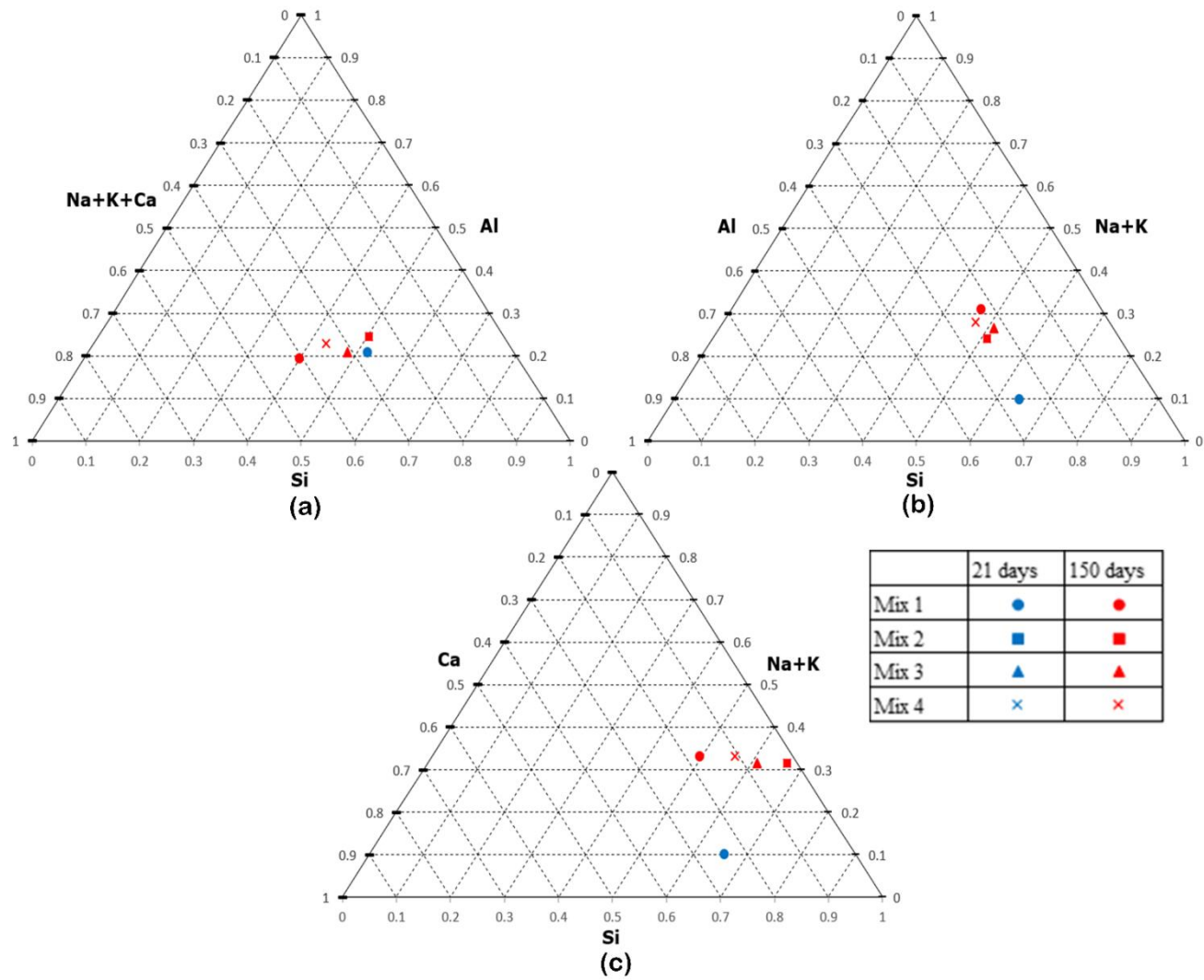


Figure 5-8 : ASR gel composition interpreted in a ternary diagram

Alkali silica gel in Mix 1-4 mainly consists of calcium (Ca), sodium (Na), silicon (Si) and aluminium (Al) with little amount of magnesium (Mg) and potassium (K). Based on the previous studies, (Na+K)/Si ratio and Ca/Si ratio of alkali silica gel typically lies in the range of 0.15~0.3 and 0.10~0.3 respectively (Leemann et al. 2016; Leemann & Lura 2013; Leemann & Merz 2013; Thaulow et al. 1996). EDS analysis results of ASR gel in OPC mortar (Mix 1) presented in Table 5-2 illustrate that (Na+K)/Si and Ca/Si ratios of ASR gel at 21 days are 0.156 and 0.444 whereas at 150 days those ratios become 0.670 and 0.461. It should be noted that all the above values except (Na+K)/Si ratio at 21 days are out of the range defined by various researchers earlier. Furthermore, Figure 5-8 and Table 5-2 clearly indicates that ASR gel formed in OPC system is rich in calcium compared to the ASR gel formed in geopolymer. It is quite understandable given the fact that OPC system contains larger amount of calcium compared to geopolymer systems. But ASR gel formed in Mix 1 also indicates a significant increase in Na over Ca with the time which may be due to the infinite supply of sodium ions provided by 1M NaOH solution (see Figure 5-8b and Table 5-2).

No ASR gel formation identified in geopolymer mixes at 21 days. But all have shown significant gel formation at the end of the test which consent with the expansion results present in Figure 5-1. (Na+K)/Si ratios of Mix 2-4 are 0.47, 0.52 and 0.59 respectively which are out of the above range reported in previous studies. However, Ca/Si ratios of Mix 3 and Mix 4 falls within the range, even though Mix 2 has shown very low Ca content in ASR gel.

Aluminium (Al) has also become a significant element in ASR gel. The Al/Si ratio of the ASR gel found in Mix 1-4 lies in the range of 0.40-0.53. Geopolymer matrix contains significant amount of aluminium endowed from fly ash and GGBFS which typically results in aluminium rich ASR gel in geopolymer mortar. However, since OPC

contains very low aluminium content (see Table 3-1), aluminium rich ASR gel in OPC specimens indicate that aggregate could have also provided significant amount of aluminium to the reaction. This agrees with chemical details of basalt aggregate provided in section 3.2.3.1 and the SEM/EDS analysis results shown in Figure 5-3 to 5-7.

Figure 5-9 is the backscatter SEM images of mix 1-4 at 21 days and 150 days taken at 100 magnifications. It is quite clear that there is an increase in crack propagations over the time which may be due to the stress caused by ASR gel formation. Mix 1 (OPC mix) has shown the lowest crack propagation though it has corresponded to the highest expansion while all geopolymer mixes have shown higher distress compared to OPC mix despite of their lower expansion. Mix 2 has shown the highest microcrack formation followed by Mix 3 and Mix 4 which indicates that microcrack formation is inversely related to the GGBFS content in the mix.

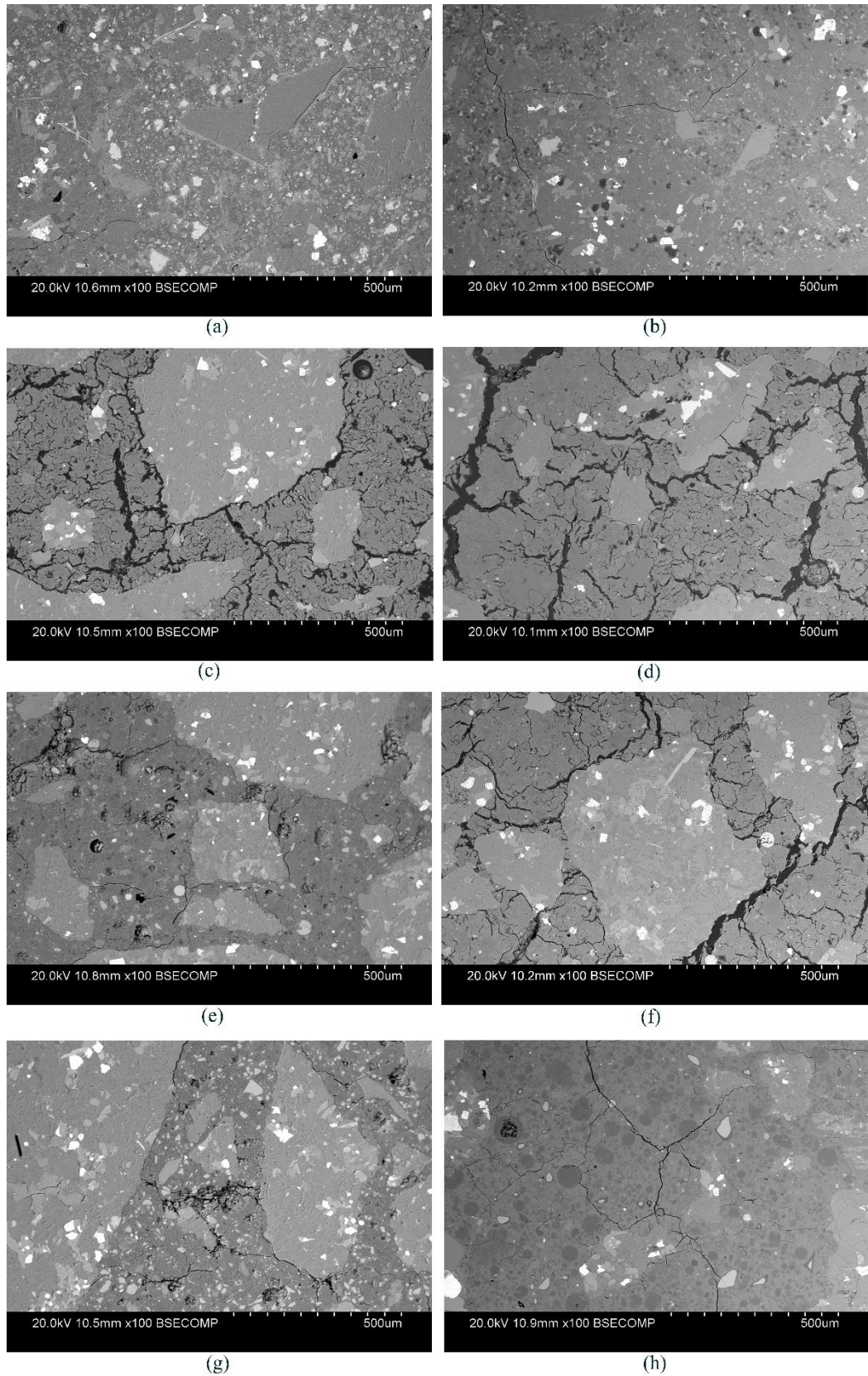


Figure 5-9 : Micro crack propagation in mix 1-4; (a) SEM image of mix 1 at 21 days, (b) SEM image of mix 1 at 150 days, (c) SEM image of mix 2 at 21 days, (d) SEM image of mix 2 at 150 days, (e) SEM image of mix 3 at 21 days, (f) SEM image of mix 3 at 150 days, (g) SEM image of mix 4 at 21 days, (h) SEM image of mix 4 at 150 days,

### 5.2.3.1 Formation of magnesium iron compound

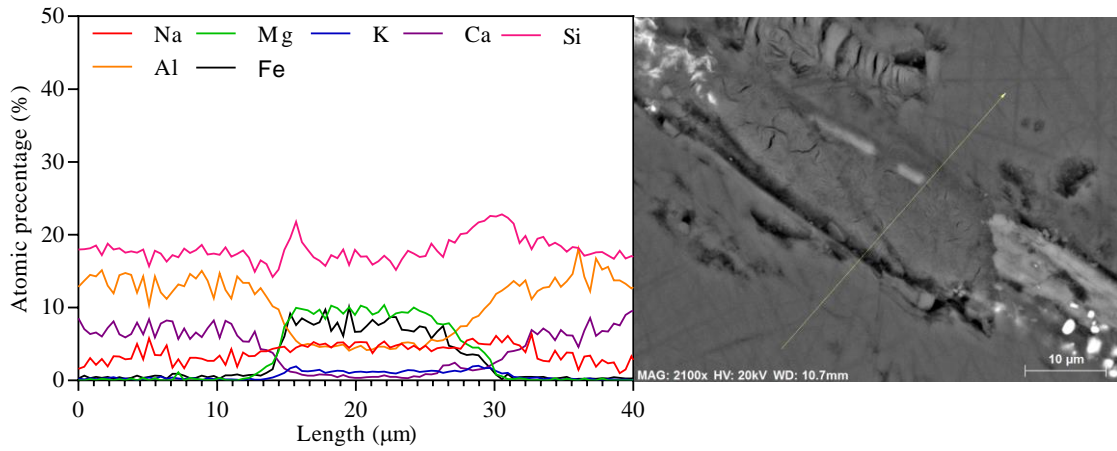


Figure 5-10 : SEM/EDS line profile of new product form inside the cracks of aggregate in mix 4 at 150 days

Table 5-3 : Average chemical composition of the compound

Element	Na	Mg	K	Ca	Si	Al	Fe
Atomic percentage	4.75	8.51	1.28	0.96	17.77	5.52	6.88

Significant amount of cracks filled with a chemical compound as shown in Table 5-3 were identified in all the specimens (mix 1-4). Figure 5-10 is a backscatter EDS line profile of the chemical compound formed inside aggregate crack in mix 4 at 150 days. Apart from the typical ions identified in ASR gel such as sodium, calcium, potassium, silicon and aluminium, significant amount of magnesium and iron were present in these products. Even though aggregate do not show much iron (Fe) and magnesium (Mg) traces it should be noted that both XRD and XRF analysis have indicated significant amount of these two elements in basalt aggregate (refer section 3.2.3.1).

#### 5.2.4 Mortar bar images

Figure 5-12 shows the optical images of mortar bars of mix 1-4 after test completion (150 days). Even though no visible cracks were observed on either mortar specimens, surface of the mortar bars of Mix 2 have shown some surface distortions. The continuous exposure to the 1M NaOH solution might result in surface deterioration which might cause aggregate at the surface to fallout due to weakening in bond structure as seen in Figure 5-12

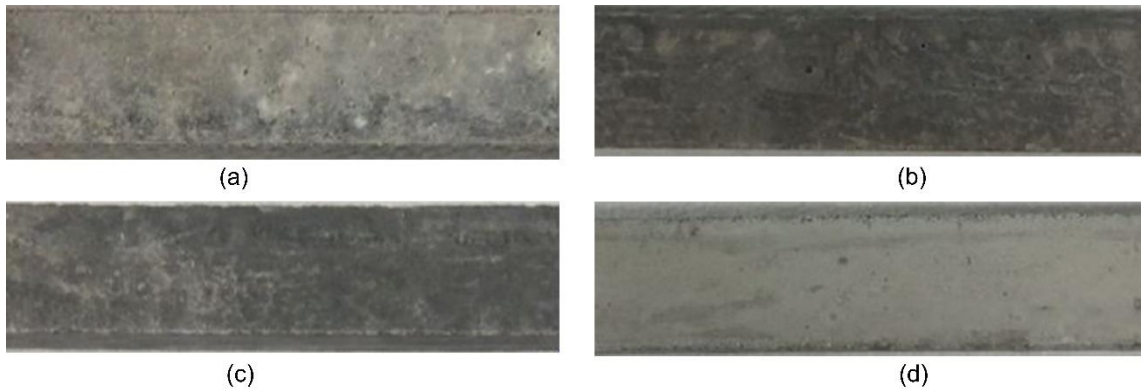


Figure 5-11 : Mortar bar images of mix 1-4 after the test (150 days); (a) Mix 1 at 150 days, (b) Mix 2 at 150 days, (c) Mix 3 at 150 days, (d) Mix 4 at 150 days



Figure 5-12 : surface holes identified in mix 2

### 5.3 Discussion

Based on the field records, the basalt aggregate used is categorized as a non-reactive aggregate in OPC system and has been successfully used in structural applications for a long time. Chemical analysis results (XRF and XRD analysis) as shown in section 3.2.3.1 also showed the non-reactive nature of basalt aggregate. This is further supported by the standard accelerated mortar bar test (AS 1141.60.1) results shown in Figure 5-1 where mortar bars made of standard OPC mix (mix 1) have shown way below expansion values at 10 days (0.0107%) and 21 days (0.0572%) lower than to the minimum expansion limit stipulated in the standards of 0.1% (AS1141.60.1 2014).

Expansion of OPC mortar bars ultimately reached 0.1% after approximately 36 days and reach 0.2247% after 150 days. However, the rate of expansion dropped significantly towards the end (150 days) hinting a possible stabilization phase which is most probably due to a lack of silicon ions for the reaction. Expansion curve of Mix 1 initially showed a time lag of approximately 4 days. This short delay in expansion might be the time required for the ASR gel to form in enough quantity to generate significant pressure on the cement paste to initiate the expansion. No deformations or cracks appeared in the OPC mortar bars (see Figure 5-11a) and only minor micro cracks were observed in SEM images taken at a magnification of 100 (see Figure 5-9a and 5-9b)

For geopolymer mixes (Mix 2-4), the initial time lag was approximately 7, 10 and 14 days respectively. As mentioned before this low expansion period is the initial time that required to generate enough ASR gel to exceed the threshold pressure of the mortar. The duration the initial phase depends on two factors;

1. Amount of ASR gel formation
2. Resistive threshold pressure of mortar reflected by the initial strength development

Mix 1 (OPC) has the highest amount of free Ca in the system (based on Table 3-1 and Table 3-6) and corresponds to the lowest initial compressive strength (see Figure 5-2) which explain the lowest initial time lag in Mix 1 among the four mixes.

Since Ca content in geopolymer mixes is proportional to the GGBFS content, Mix 4 (Fly ash/GGBFS = 1) has the highest Ca content, followed by Mix 3 (Fly ash/GGBFS = 4) and Mix 2 (Fly ash/GGBFS = 9) respectively. Thus, based on the theory presented later in section 6.3.1, The highest ASR gel formation occurs in mix 4 mortar bars, followed by Mix 3 and Mix 2 respectively. However, Figure 5-2 reveals that the compressive strength at a given time is decreasing from Mix 4 to Mix 2. Since the compressive strength is proportional to the resistive threshold pressure of mortar it can be concluded that Mix 4 has the highest resistive pressure followed up by Mix 3 and Mix 2. Mortar with higher resistive pressure requires higher ASR gel formation to show any physical distresses (expansion) which can explain why Mix 4 to have the highest time lag followed up by Mix 3 and Mix 2.

Among geopolymer mixes, Mix 4 has shown the highest final expansion, 0.2009% while Mix 3 and Mix 2 obtained expansions of 0.1921% and 0.1805% respectively. This agrees with the ASR mechanism described later in section 6.3.1 which emphasize that ASR gel formation in geopolymer mortar increases with the increase in calcium (Ca) content in the mix. SEM/EDS analysis results are also in consistent with the expansion results shown in Figure 5-1. In order to assess the long-term expansion in geopolymer mortar, this study has suggested to extend 21 days of testing period stipulated in AMBT to 100 days. Furthermore, minimum expansion limit is also revised to 0.2% to account for the extended testing time. The modified limit categorises basalt as a nonreactive aggregate which consent with its chemical analysis results and field records. However, it

should be noted that more testing is required before adapting these modifications to identify the reactivity of geopolymer mixes.

No ASR gel formation was identified in geopolymer mixes at 21 days which have shown very low expansions. However, OPC mortar has shown a minor gel formation. All the mixes have shown significant gel formation at 150 days. The ASR gel mainly consists of sodium (Na), potassium (K), calcium (Ca), magnesium (Mg), aluminium (Al) and silica (Si). High Al content in ASR gel of Mix 1 (see Table 5-2, Figure 5-3 and Figure 5-4) reveals that aggregate itself has supplied ions other than Si for the reaction. Even though the exact mechanism is unclear many researchers (Chappex & Scrivener 2012; Hüniger 2007; Rajabipour et al. 2015; Shafaatian 2012) have reported the detrimental effect of Al towards ASR which is further explained in section 2.3.4.5. Even though Rajabipour et al. (2015) mentioned a probable reduction in expansiveness of ASR gel due to the incorporation of Al ions, no specific study has been carried out to assess the swelling properties of aluminium rich ASR gel. However, Al ions in ASR gel might lead to formation of crosslinks as in geopolymerization which might reduce the expansiveness of gel first by changing the gel synthesis and then by reducing the water binding capacity (Van Deventer et al. 2007).

Even though there is a clear gel formation identified in all the mixes at 150 days through the SEM/EDS analysis, the composition of the gel seems to be out of the ranges ((Na+K)/Si ratio 0.15~0.3 and Ca/Si ratio 0.1~0.3) reported in previous studies by various researchers (Leemann et al. 2016; Leemann & Lura 2013; Leemann & Merz 2013; Thaulow et al. 1996). In addition, EDS results present in Table 5-3 clearly indicate that the gel formed lacks silica (Si content is less than 20% in all mixes) which may be the reason to have higher composition ratios. Both Rajabipour et al. (2015) and Chappex and Scrivener (2012) described that Al ions in the system might reduce the Si dissolution

of aggregate which results in low Si content in ASR gel. Even though there are no evidence due to lack of specific studies, expansiveness of ASR gel with low Si content might be lower than that of typical ASR gel which explains the expansion results are presented in Figure 5-1.

No visible cracks appeared on any mortar bars as shown in Figure 5-11. However, microcracks propagation with the time was observed in Mix 2-4 as shown in Figure 5-9 which indicates the increase in distresses over the time due to ASR gel formation. Microcrack propagation in Mix 1 was insignificant and hardly reassembled the characteristic crack propagations due to ASR which indicates that the cracks in Figure 5-9(g) and (h) were most probably not ASR related. It should be noted that there can be crack propagations in specimens due to various other reasons which were not related to ASR such as thermal effect, crack propagation during sample preparation, distresses due to other durability issue, excessive drying etc. Geopolymer mortar bars have shown more micro-crack formation despite their low expansion compared to OPC mortar bars. This could be due to the quasi brittle behaviour of zeolitic structure of geopolymer mortar as stated by several researchers based on the stress strain relationship (Fernandez-Jimenez et al. 2006; Noushini et al. 2016; Pan et al. 2011). Among geopolymer mixes, Mix 2 has shown the highest micro crack propagation followed up by Mix 3 and Mix 4. It should be noted that high strength gain increases the elastic limit of the binder which allows it to absorb higher stress without showing any distress. Thus, compressive strength of the mortar is inversely proportional to crack propagation as illustrated by the SEM analysis results presented in Figure 5-9. In addition, cracks help ASR gel pressure to dissipate without causing any further distresses on the mortar. Therefore, high microcrack propagation in Mix 2 might limit the expansion of mortar bars despite of ASR gel formation inside the matrix.

Apart from the Al rich ASR gel which was discussed above, another type of gel was also identified inside the aggregate. This new substance consists of significant amount of iron (Fe) and magnesium (Mg) along with typical ions such as sodium (Na), potassium (K), aluminium (Al) and Silica (Si) as shown in Table 5-3. No current study has assessed the expansiveness of this product. However, formation of this gel inside the cracks of aggregate in several locations suggest the need to assess its expansive properties.

## **5.4 Summary**

This Chapter analyses the probable alkali silica reaction in natural nonreactive aggregate when used in geopolymer under the severe exposure conditions of AMBT. Basalt aggregate, a widely used aggregate in construction purposes with clear history is selected to represent the natural nonreactive category. Standard accelerated mortar bar test (AS 1141.60.1) results and chemical analysis (XRF and XRD) results confirmed the non-reactiveness of basalt aggregate with respect to OPC.

Geopolymer mortar with basalt aggregate haven't shown any excessive expansions. In fact, expansions of geopolymer mixes are lesser than that of OPC mix throughout the testing time. However, all mixes have shown a significant amount of gel formation at 150 days, and OPC mortar specimens have shown a gel formation even at 21 days. EDS analysis revealed considerable amount of aluminium (Al) in the ASR gel in all mixes including OPC mix which might causes the nonreactive behaviour of basalt aggregate.

Despite the low expansions, geopolymer mixes have shown significantly higher microcrack formation compared OPC which fortified the quasi brittle behaviour of the stress strained relationship of geopolymer. Thus, the existing expansion limits shall be modified before adopting respective tests in geopolymer.

In addition, product with sodium, magnesium, aluminium, iron and silica was frequently identified inside the aggregate during the microstructural analysis. Effect of magnesium and iron on the expansiveness of ASR gel should be investigated thoroughly.

## **CHAPTER 6 : Alkali silica reaction in natural reactive aggregate**

---

### **6.1 Overview**

Alkali silica reaction typically takes years to exhibit the initial symptoms, and even if identified, it is virtually impossible to mitigate it under the field circumstances (HB79 2015; Hobbs 1988). In fact, even the laboratory tests take more than a year to draw a definitive conclusion on the alkali silica reaction of a mix. Thus, minimising the risk at the designing stage by manipulating the alkali sources and reactive silica sources are the most common approaches to mitigate the ASR in structures (HB79 2015). Hence assessing the ASR with natural reactive aggregate provides an insight into the behaviour of geopolymer binders in extreme conditions with natural aggregate. In addition, evaluation of abandoned aggregate allows the utilisation of available resources since natural aggregate stocks are diminishing rapidly due to the high consumption.

Natural reactive aggregate for this study were supplied by Boral, Australia from their quarry in Culcairn, NSW and thus labelled as Culcairn during this study. Mineralogical data of the aggregate (XRD and XRF analysis results) revealed the presence of andesine which is classified as a reactive mineral (Diamond 1976). Thus, it is expected to have severe alkali silica reaction with culcairn aggregate.

Apart from the three major geopolymer mixes; Mix 2 (fly ash/GGBFS = 9), Mix 3 (fly ash/GGBFS = 4) and Mix 4 (fly ash/GGBFS = 1), two subsidiary mixes; Mix 2a (fly ash/GGBFS = 9) and Mix 4a (fly ash/GGBFS = 1) were used in this study along with Mix 1 the standard accelerated mortar bar test as in AS 1141.60.1 (refer section 3.3.1.3 for further mix design details). In addition, three curing solutions; 0.003M NaOH, 1M NaOH saturated with  $\text{Ca}(\text{OH})_2$  and water were used along with 1M NaOH solution for

the three major geopolymer mixes. Test setups with 1M NaOH curing solution consist of 6 mortar bars; 5 for continuous expansion measurements and one to be extracted at 21 days while all the other test setups consist of 3 mortar bars for expansion measurements up until 150 days. Periodical compressive strength measurements (at 1 day, 8 days, 22 days and 29 days) were taken for mixes exposed to 1M NaOH solutions and 29-day (28 days after curing) compressive strengths were measured for all the other test setups (refer section 3.3.1.3).

## **6.2 Result and analysis**

### **6.2.1 Effect of GGBFS content**

#### **6.2.1.1 Expansion test**

Figure 6-1 presents the expansion variation of mortar bars exposed to 1M NaOH solution at 80 °C for 150 days. It should be noted that each data point of Figure 6-1 derived by averaging at least 5 expansion measurements. Standard errors of the data points are substantially low as shown in the graph which indicates that the variation of average expansions reassembles the actual expansion variations of the mortar bars. 0.1% is the minimum expansion limit stipulated in AS 1141.60.1 which incorporated with a significant risk of alkali silica reaction. (AS1141.60.1 2014).

Table 6-1 summarises the average mortar bar expansions of Mix 1-4 at 10, 21 and 150 days. Average mortar bar expansion of Mix 1 (standard OPC mix as in AS 1141.60.1) reached 0.1157% by 10 days and 0.3664% by 21 days which categorised the Culcairn aggregate among highly alkali silica reactive aggregates as it exceeded the 0.1% expansion limit within 10 days (AS1141.60.1 2014). This is in agreement with the supplier's recommendations and the preliminary test results (XRD and XRF analysis) as in section 3.2.3.3. The initial expansions (10 days and 21 days) of geopolymer mortar

bars (Mix 2-4) are significantly lower. In fact, none has reached the 0.1% limit during the initial 21 days which implies a substantially lower risk of alkali silica reaction in geopolymer mortar compared to OPC based on AS 1141.60.1 (AS1141.60.1 2014).

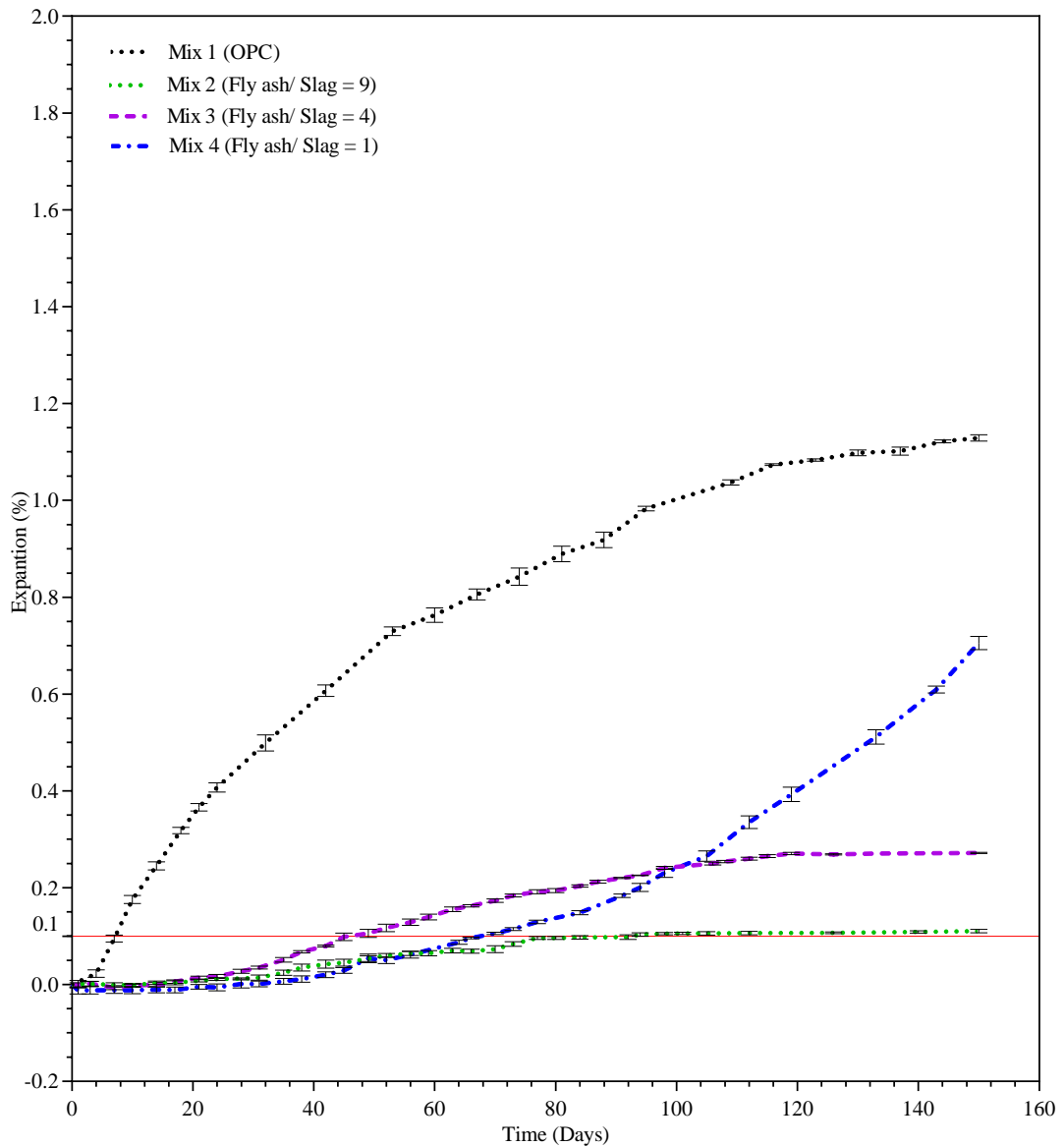


Figure 6-1 : Expansion characteristics of mix 1-4 over 150 days when exposed to accelerated curing conditions. 0.1% (red line) is the minimum expansion limit for reactivity stipulated in AS 1141.60.1.

Table 6-1 : Average expansion of mortar bars at 10, 21 and 150 days

	Average expansion		
	10 days	21 days	150 days
Mix 1	0.1757 %	0.3664 %	1.1287 %
Mix 2	-0.0013 %	0.0077 %	0.1105 %
Mix 3	-0.0016 %	0.0142 %	0.2720 %
Mix 4	-0.0116 %	-0.0048 %	0.7032%

OPC mortar bars (Mix 1) showed the largest final average expansion, 1.1287% which indicates that under the accelerated conditions OPC mortar is more vulnerable to ASR compared to geopolymer mortar. However, despite showing a drop in increment rate, expansions of mortar bars increase throughout the testing time (150 days) signifying the continuation of ASR. In accelerated mortar bar test degree of ASR solely depends on the Si dissolution capability of aggregate since system contains ample amounts of other necessary components; alkali, calcium and water (HB79 2015; Hobbs 1988). Thus, it can be concluded that the system may contain significant Si content for the reaction during the testing period. Meanwhile, none of the geopolymer mixes has managed to reach the 0.1% expansion limit within 21 days and thus can be ranked among the low-risk category. Among the geopolymer mixes, Mix 3 (Fly ash/GGBFS =4) has encountered the highest risk of ASR at 21 days with an expansion of 0.0142% followed up by Mix 2 (Fly ash/GGBFS =9) and Mix 4 (Fly ash/GGBFS =1) with 0.0077% and -0.0048% expansions respectively. However, this early trend changes over the time as Mix 4 out passed other two mixes to reach 0.7032% expansion at 150 days while Mix 2 and Mix 3 were settling to 0.1105% and 0.2720% respectively. The final expansions of geopolymer mixes consent with the existing studies which highlighted the importance of GGBFS content on the ASR

(Bakharev et al. 2001a; Shi, C et al. 2015; Shi, Z et al. 2015). This is further fortified by the research findings of Fernández-Jiménez and Puertas (2002) who stated that short-term testing might not reflect the ASR in alkali-activated materials.

It seems like the expansion curves in Figure 6-1 follow a sigmoidal shape (S shape); initial phase with low expansion, intermediate phase with rapid expansion and final phase with stabilised expansion. However, it should be noted that even though there are three distinct phases visible in the expansion curves, it is hard to separate them as the curve developed smoothly over the testing period. Mix 1 has shown the shortest initial phase (approximately 4 days) followed up with the largest expansion development among all the mixes. Expansion gain of Mix 1 dropped exponentially throughout the intermediate phase hinting of a probable stabilisation at some point. Expansion behaviour of Mix 2 and 3 reassembles the typical S shape curve of ASR. The initial phases of Mix 2 and 3 ceased after approximately 21 and 14 days, and their expansion curves stabilised after 77 and 119 days as shown in Figure 6-1. Expansion curve of Mix 4 only consists of two phases; an initial low expansion period which continued for approximately 28 days followed up with a continuous expansion gain throughout the testing period.

#### **6.2.1.2 Compressive strength variation**

The compressive strength development of mixes 1-4 over 28 days in 1M NaOH solution (29 days of casting) is shown in Figure 6-2. Strength measurements were based on the crushing values of 50mm x 50mm x 50mm mortar cubes exposed to accelerated curing condition (1M NaOH at 80 °C) along with mortar bars. At least 3 cubes were crushed at 1 day, 8 days, 22 days and 29 days after casting to determine the average compressive strength variation over the time. Low standard errors of the data points as shown in Figure 6-2 illustrate that the average variation may represent the actual compressive strength variation of Mix 1-4.

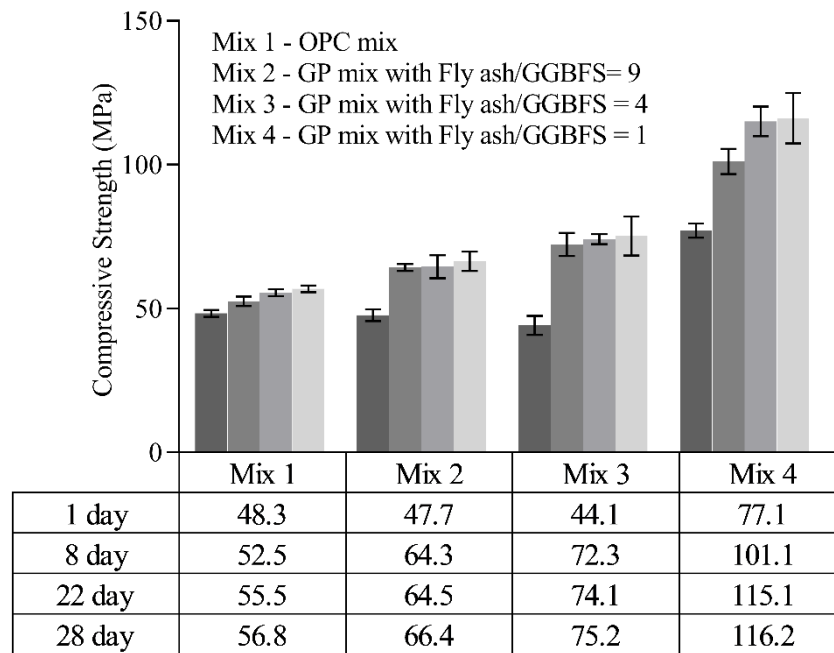


Figure 6-2 : Compressive strength variation of mix 1-4 over 29 days of casting

Mixes 1, 2 and 3 correspond to approximately similar initial strengths which are ranging from 44.1 MPa – 48.3 MPa, while Mix 4 has gained comparatively high initial strength of 77.1 MPa. Mixes 1 to 3 attained more than 92% of their 29-day strengths during the initial 8 days while the compressive strength of Mix 4 increased up to 22 days. Compressive strengths of Mixes 2 to 4 indicated that the increase in GGBFS content of the mix has a positive impact on the compressive strength of geopolymer mortar as suggested by many researchers earlier (Deb et al., 2014, Diaz et al., 2010). It should be noted that the high compressive strength in Mix 4 (116.2 MPa) indicates considerably high elastic modulus and yield stress in Mix 4 compared to other three mixes which might affect to the expansion development of mortar bars as discussed extensively in section 6.3.

### **6.2.1.3 Scanning Electron Microscope (SEM) Analysis**

Mortar specimens extracted during the testing (at 21 days and 150 days) were microscopically analysed with a scanning electron microscope to identify the microcrack formation and ASR gel formation inside the mortar. In addition, Energy-dispersive X-ray spectroscopy (EDS) equipped with a backscatter detector was used to determine the chemical composition ASR gel identified during the SEM analysis.

All the mortar specimens except Mix 2 at 21 days have shown significant ASR gel formation. As illustrated in Figure 6-3, ASR gel was identified inside the aggregate (Figure 6-4 to 6-10), at the aggregate binder interface (Figure 6-11) and inside the binder (Figure 6-12). However, Figure 6-11 and 6-12 clearly showed that both geopolymer binder and ASR gel consist of similar elements but in different proportions which makes it hard to identify the gel boundaries inside geopolymer mortar. Thus, during this study, the microstructural analysis was focused on the ASR gel formed inside the aggregate. In order to make the minor variations more visible, oxygen (O) is omitted from the EDS line profiles (see Figure 6-4 to 6-12) as it is a common element in all products.

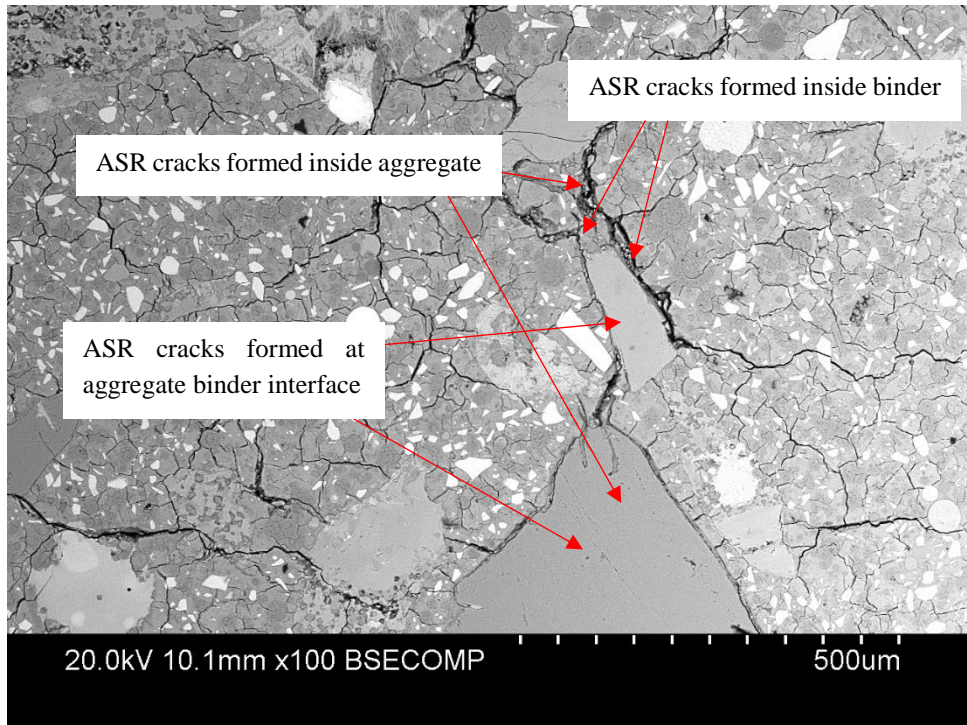


Figure 6-3 : ASR cracks identified in different locations of Mix 4 at 150 days

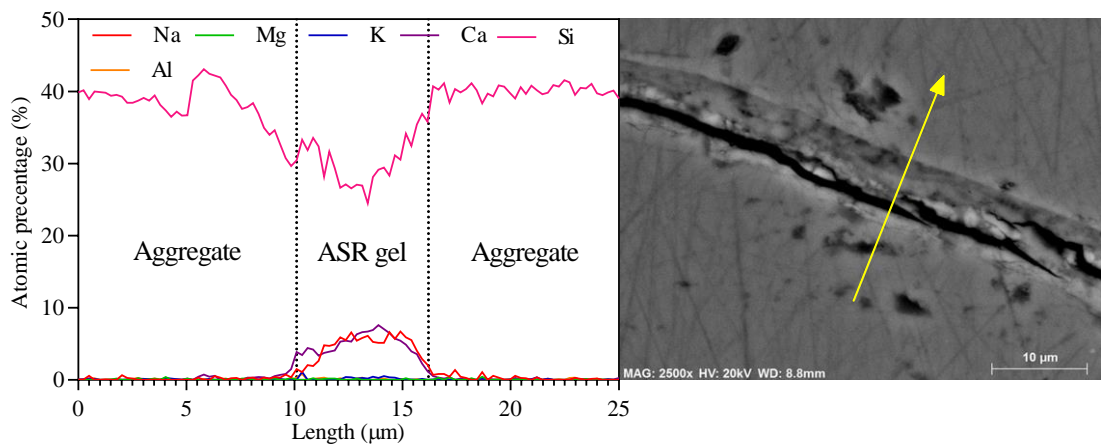


Figure 6-4 : ASR gel identified inside aggregate of Mix 1 at 21 days

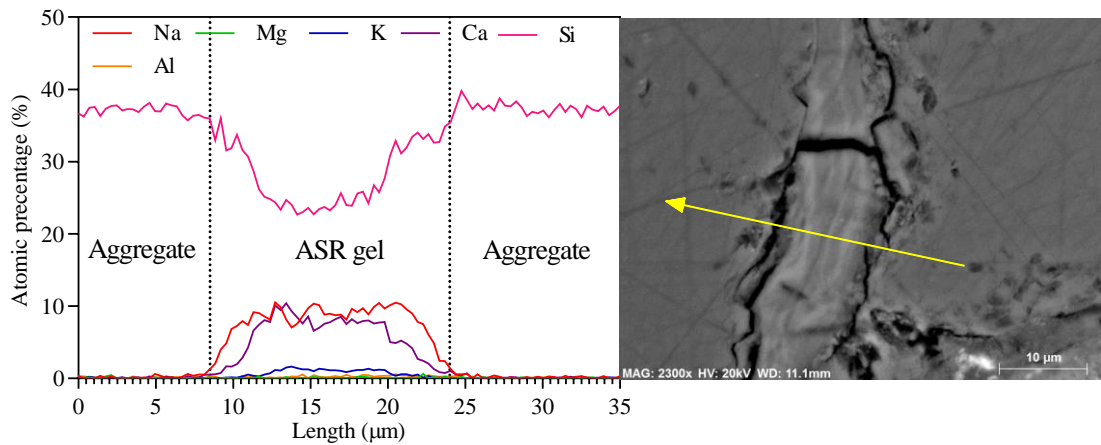


Figure 6-5 : ASR gel identified inside aggregate of Mix 1 at 150 days

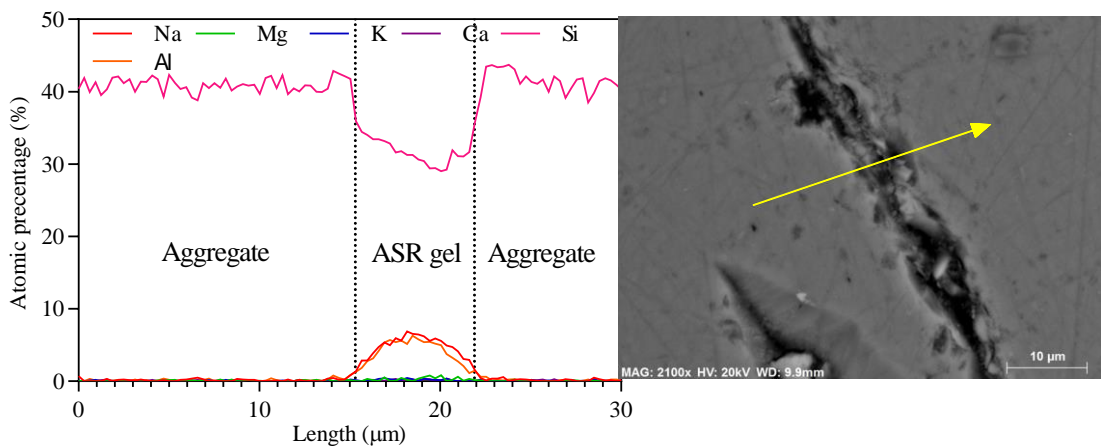


Figure 6-6 : ASR gel identified inside aggregate of Mix 2 at 150 days

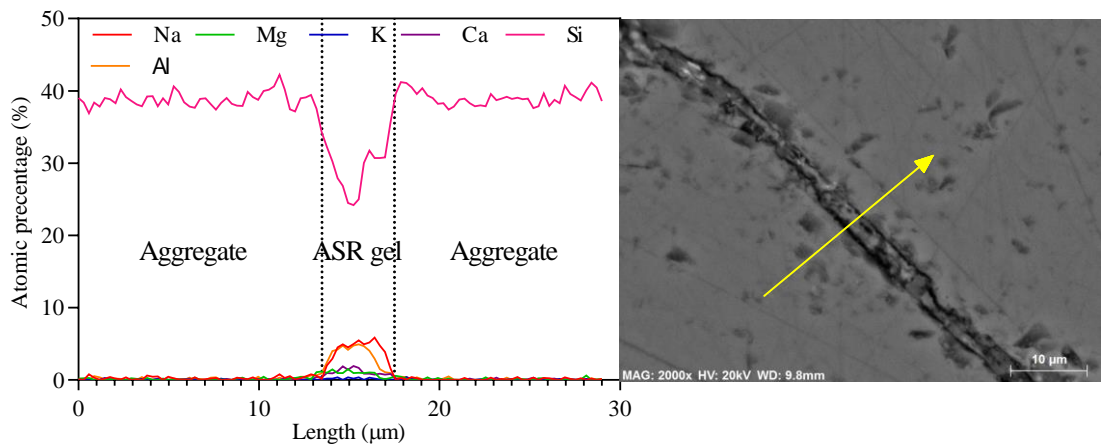


Figure 6-7 : ASR gel identified inside aggregate of Mix 3 at 21 days

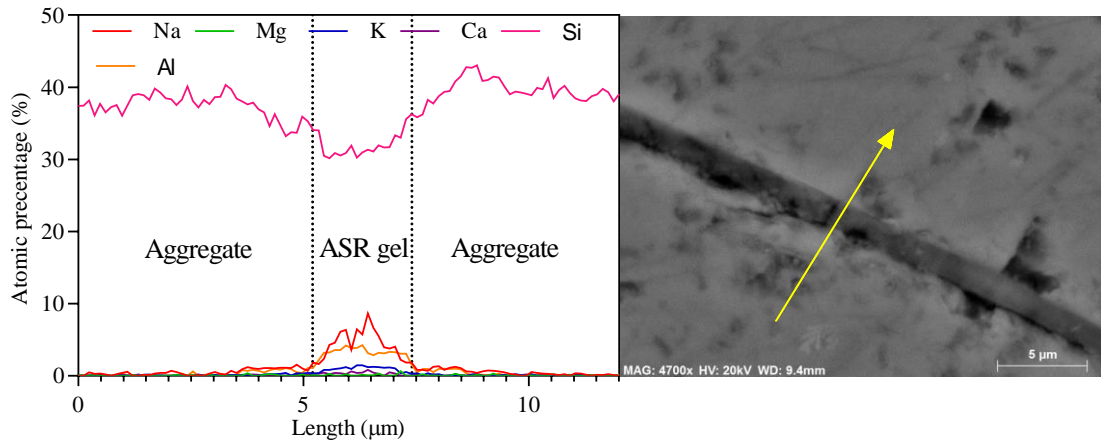


Figure 6-8 : ASR gel identified inside aggregate of Mix 3 at 150 days

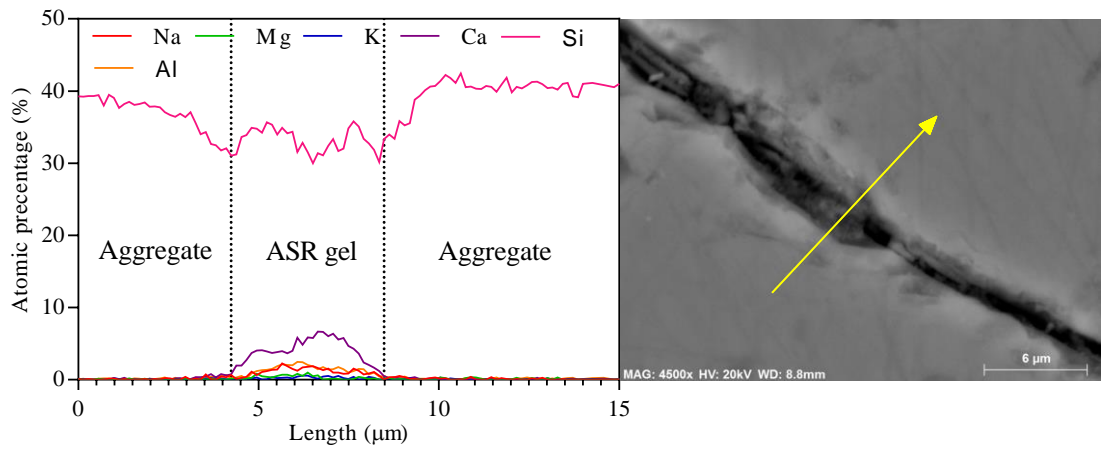


Figure 6-9 : ASR gel identified inside aggregate of Mix 4 at 21 days

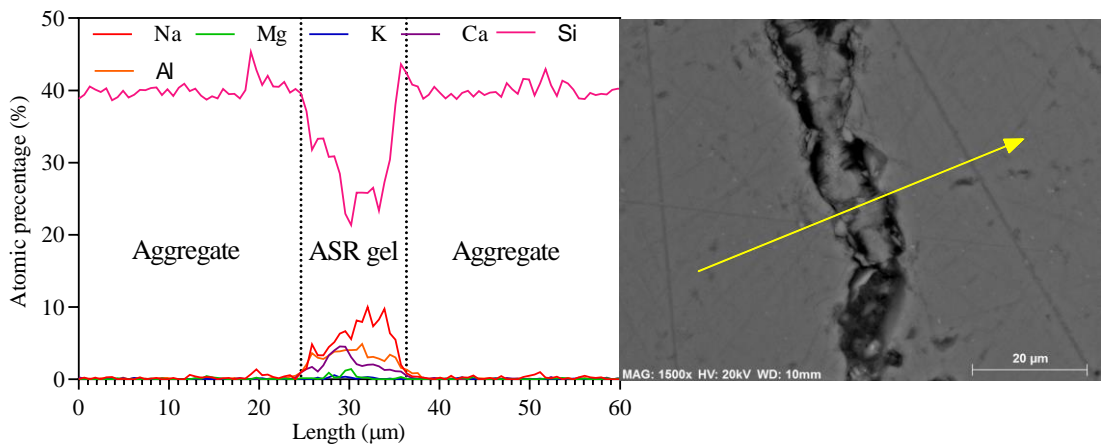


Figure 6-10 : ASR gel identified inside aggregate of Mix 4 at 150 days

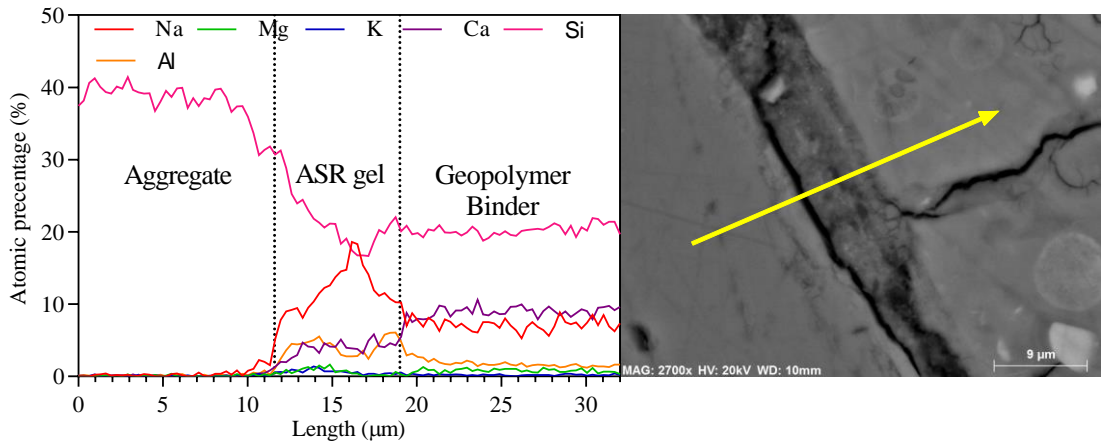


Figure 6-11 : ASR gel identified in the aggregate binder interface of Mix 4 at 150 days

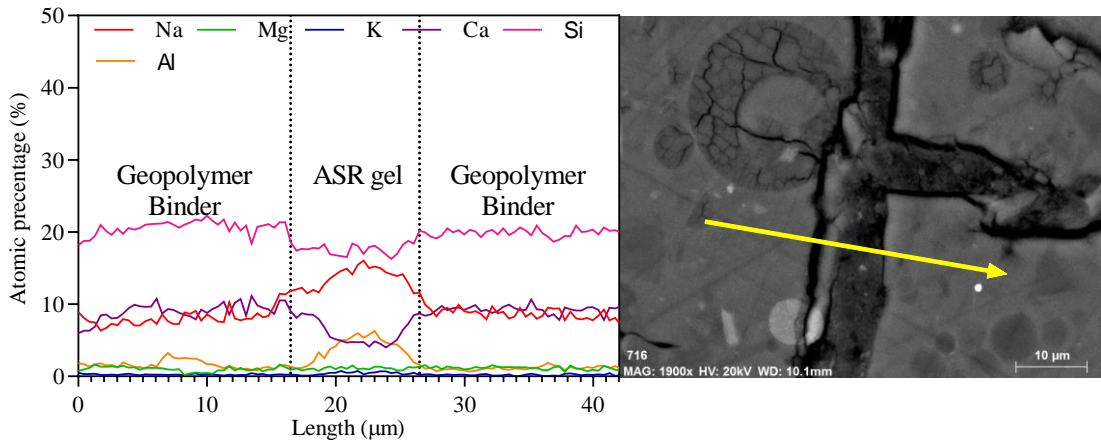


Figure 6-12 : ASR gel identified inside the binder of Mix 4 at 150 days

Elemental atomic percentages of ASR gel formed in Mix 1-4 are summarised in Table 6-2. Except in Mix 3 at 21 days which corresponds to very low ASR gel formation, all the other gel compositions in Table 6-2 are derived by averaging at least 250 data points of ASR gel located inside the aggregate. Elemental data in Table 6-2 is presented in a ternary diagram in Figure 6-13 to identify the correlation among major elements in ASR gel and their variations with respect to the curing time. Variation of Ca/Si ratio with Na+K/Si ratio is plotted in Figure 6-14 to identify the variations in the elemental composition of ASR gel identified in different cases. The shaded area is the ASR gel

compositions suggested by different researchers based on their studies on OPC binder systems (Leemann et al. 2016; Leemann & Lura 2013; Leemann & Merz 2013; Thaulow et al. 1996). Thus, Figure 6-14 allows comparing the experimental data with the published works more effectively.

Table 6-2 : Summary of SEM /EDS analysis on ASR gel located in Mix 1-4

Mix No.		Average atomic percentage (%)						Ratios		
		Na	K	Ca	Mg	Si	Al	$\frac{(Na+K)}{Si}$	$\frac{Ca}{Si}$	$\frac{Al}{Si}$
1	21 days	4.67	0.19	4.81	0.04	30.44	0.13	0.16	0.158	0.004
	150 days	7.40	0.62	5.67	0.11	29.89	0.25	0.27	0.19	0.008
2	21 days	-	-	-	-	-	-	-	-	-
	150 days	4.63	0.19	0.12	0.29	31.80	3.91	0.15	0.004	0.123
3	21 days	4.22	0.26	1.44	0.59	29.20	3.65	0.15	0.049	0.125
	150 days	4.66	0.99	0.36	0.09	32.26	3.43	0.18	0.01	0.106
4	21 days	1.25	0.25	4.05	0.30	33.36	1.73	0.05	0.122	0.052
	150 days	5.68	0.13	2.21	0.30	30.30	3.36	0.19	0.073	0.111

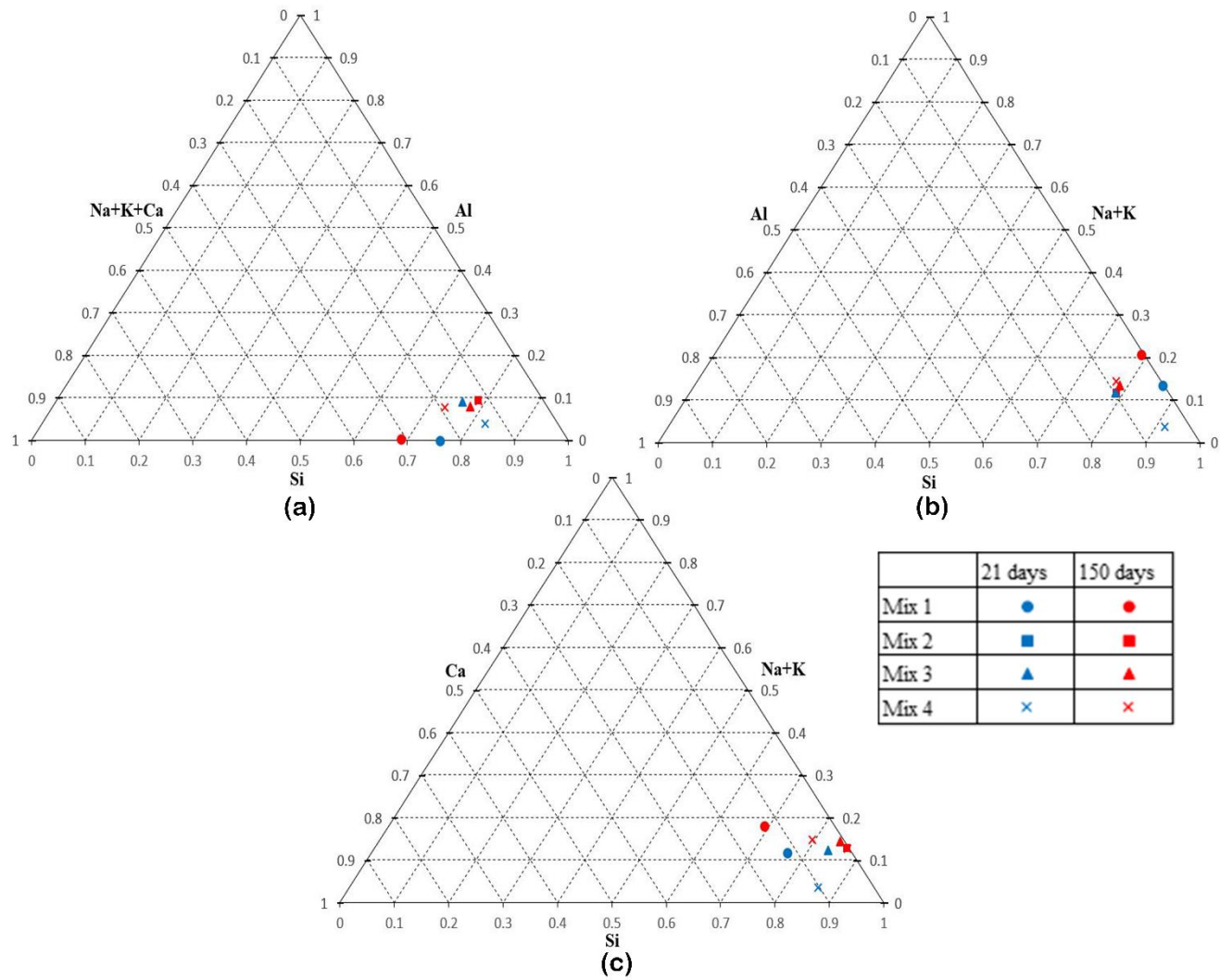


Figure 6-13 : ASR gel composition interpreted in a ternary diagram

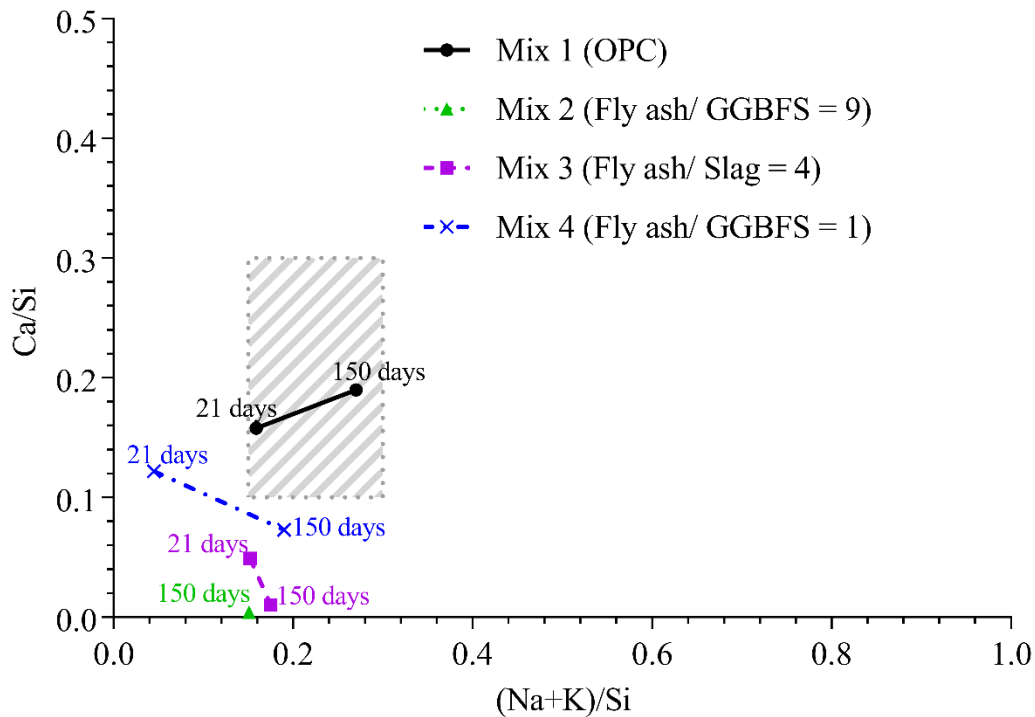


Figure 6-14 : Variation in Na+K/Si vs. Ca/Si (atomic ratio) of ASR gels at 21 days and 150 days from Mix 1-4; shaded area is the alkali silica gel compositions developed base on Thaulow et al. (1996), Leemann et al. (2016), Leemann and Lura (2013) and Leemann and Merz (2013)

ASR gel in OPC typically consists of sodium (Na), potassium (K), calcium (Ca), silicon (Si) and oxygen (O) as illustrated in Figure 6-4, Figure 6-5 and Table 6-2. Based on the previous works by Leemann et al. (2016), Leemann and Lura (2013), Leemann and Merz (2013) and Thaulow et al. (1996) the Na+K/Si and Ca/Si ratios lie in the range of 0.15~0.30 and 0.10~0.30 respectively. Figure 6-14 reveals that the ASR gel compositions of Mix 1 at 21 days and 150 days lie within the above range. In addition, it can be clearly identified that the Na+K/Si and Ca/Si ratios of ASR gel in Mix 1 are increasing with the time. However, given the fact that OPC might contain ample amount of free Ca and 1M NaOH solution act as an infinite source of Na it is expected to have Na and Ca-rich ASR gel in OPC mortar with the

time. It should be noted that the virtually infinite source of Na may contribute to a higher Na increment compared to Ca over the time as seen in Table 6-2.

None of the geopolymer mixes lies inside the reactive region (shaded area in Figure 6-14) which was defined based on the published studies. However, except the ASR gel identified in Mix 4 at 21 days, all the other ASR gels in geopolymer mixes remain in the defined range of Na+K/Si ratio. This seems quite obvious given the fact that all the specimens have virtually infinite sources of Na (1M NaOH solution) and Si (reactive silicious aggregate). Mix 4 has relatively low porosity compared to other mixes due to the high GGBFS content which might result in low ion transportation rate (Luna-Galiano et al. 2016; Provis et al. 2012). Thus, Na ions might take some times to reach the reaction sites and result in Ca-rich gel formation initially as shown in Figure 6-9. Ca/Si ratio of ASR gel increases with the GGBFS content and decreases with the time as shown in Figure 6-14. It is obvious that among geopolymer mixes, Mix 4 may contain the highest free Ca content followed up by Mix 3 and Mix 2 since GGBFS is the main Ca source in geopolymer mixes. ASR gel compositions in geopolymer mixes reflected this as ASR gel in Mix 4 shows the highest Ca content followed up by Mix 3 and Mix 2. However, over the time, free Ca content wear off result in the formation of Na rich ASR gel as exhibited in Figure 6-14.

Table 6-2 and EDS line profiles of ASR gel in Mix 2-4 (Figure 6-6 to 6-12) emphasise that aluminium (Al) also become a significant element in ASR gel formed in geopolymer mortar. In fact, the Al/Si ratio of ASR gel in geopolymer varied from 0.05 to 0.125 while OPC mixes have shown much lower ratios; 0.004 and 0.008 as shown in Table 6-2. Mix 4 initially (at 21 days) showed relatively low Al content ( $Al/Si = 0.052$ ) compared to other geopolymer cases ( $0.1 < Al/Si < 0.125$ ) which might be due to its low ion transportation capability as described above. It should be noted that ASR gel in contact with geopolymer binder may

consist of higher Al/Si ratios (0.184 and 0.211 based on Figure 6-11 and 6-12) compared to the ASR gel located inside aggregate (0.110 based on Figure 6-10).

In Figure 6-15, backscatter SEM images taken at a fixed magnification (100) is used to optically analyse the distress development in Mix 1-4 over the time. All mixes have shown clear stress development over the time which might be due to the ASR gel formation.

Mix 1 has shown a significant crack formation even at 21 days which evolved with time as exhibits in Figure 6-15b. However, despite showing severe crack propagation inside the aggregate, OPC binder hasn't displayed any noticeable crack formation as illustrated in Figure 6-15a and 6-15b. None of the geopolymer mixes (Mix 2-4) has shown a significant crack formation at 21 days. It should be noted that deformities present in Figure 6-15c are the resultants of partially formed geopolymer binders which seems to rectify with the time due to the continuation of the geopolymerization process. In geopolymer mixes, it is clear that microcracks were not restricted to the aggregate as observed in OPC. In fact, Figure 6-15 shows that geopolymer binders exhibited severe crack propagation compared to the aggregate. These observations along with the higher distress visible in Mix 4 compared to Mix 1 can be explained as the effect of the quasi-brittle behaviour of geopolymer binders (Fernandez-Jimenez et al. 2006; Noushini et al. 2016; Pan et al. 2011). In addition, cracks in binder facilitate the ASR gel dispersion without generating intensive internal stresses inside mortar which might result in low expansion development as observed in Figure 6-1. The higher distresses visible in Mix 4 is due to the combined effect of Ca and the intrinsic properties of the binder which will further discuss in Section 6.3.

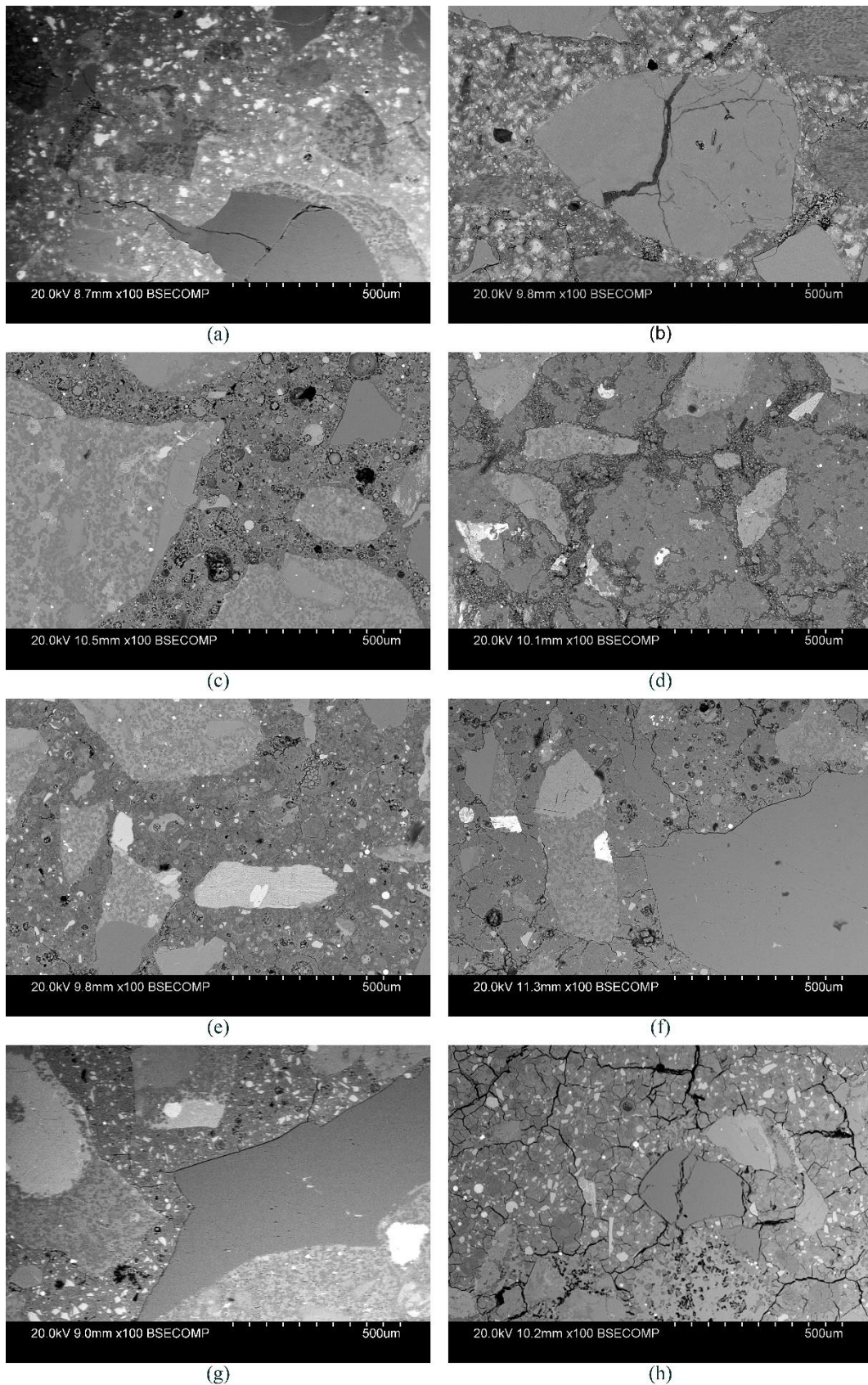


Figure 6-15 : Micro crack propagation in mix 1-4; (a) SEM image of mix 1 at 21 days, (b) SEM image of mix 1 at 150 days (c) SEM image of mix 2 at 21 days, (d) SEM image of mix 2 at 150 days, (e) SEM image of mix 3 at 21 days, (f) SEM image of mix 3 at 150 days, (g) SEM image of mix 4 at 21 days, (h) SEM image of mix 4 at 150 days,

#### 6.2.1.4 Mortar bar images

Mortar bar images of Mix 1-4 after 150 days are shown in Figure 6-16. All the mixes except Mix 2 have displayed visible cracks on the surface. Mix 4 has shown the severest crack formation followed up by Mix 1 and Mix 2 respectively. Despite showing higher mortar bar expansions, Mix 1 attributed to milder crack formation compared to Mix 4 might be due to the distinctive intrinsic mechanical properties of Mix 1 and Mix 4 (Fernandez-Jimenez et al. 2006; Noushini et al. 2016; Pan et al. 2011). It should be noted that cracks formed in mortar bars are identified similar to the characteristic map cracking in ASR affected structures which fortified the occurrence of ASR inside the mortar bars (HB79 2015).



Figure 6-16 : Mortar bar images of mix 1-4 after the test (150 days); (a) Mix 1 at 150 days, (b) Mix 2 at 150 days, (c) Mix 3 at 150 days, (d) Mix 4 at 150 days

#### 6.2.2 Effect of mix design

Effect of mechanical properties of the geopolymer mixes on the ASR is evaluated by comparing the behaviour of main mixes with subsidiary mixes design to achieve lower compressive strengths since compressive strength is commonly used as a representative parameter of mechanical properties of mortar. In fact, it is well established that the elastic modulus, yield stress and flexural strength have shown positive correlations to the compressive strength in undamaged concrete specimens (Gunasekara 2016; Phoo-ngernkham et al. 2013;

Ryno 2014). Mix designs of Mix 2 and Mix 4 were modified to achieve lower final strengths while maintaining the probable risk of ASR equal or lower than their originals. Table 3-6 illustrates the comprehensive mix design details of the main mixes (Mix 2 and Mix 4) and subsidiary mixes (Mix 2a and Mix 4a) used in this study. It should be noted that subsidiary mixes contain a lower amount of fly ash, GGBFS, NaOH, Na<sub>2</sub>SiO<sub>3</sub> and higher amount of aggregate and water compared to the main mixes which might reduce their alkali silica reactivity. Higher aggregate contents in subsidiary mixes may not interfere to the final outcome as even main mixes contain an adequate amount of reactive silica for the continuation of ASR for 150 days.

#### **6.2.2.1 Expansion test**

Figure 6-17a is the average expansion variation of mortar bars of Mix 2 and Mix 2a, and Figure 6-17b is the average expansion variation of mortar bars of Mix 4 and Mix 4a. Substantially low standard errors at data points exhibited in Figure 6-17 reveal that average expansion variation shall represent the individual expansion behaviours of mortar bars. 0.1% minimum expansion limit stipulated in AS 1141.60.1 is shown in the graphs in a red horizontal line for the comparison purposes.

Average mortar bar expansions at 10, 21 and 150 days are summarised in Table 6-3. None of the mixes exceeded the 0.1% minimum expansion limit during the initial 21 days. Furthermore, it should be noted that subsidiary mixes (Mix 2a and Mix 4a) showed much higher initial expansions (10 days and 21 days) compared to their counterparts. However, despite showing negative expansion at 21 days, Mix 4 displays the highest final expansion while Mix 4a only managed to achieve approximately 50% of it as shown in Table 6-3. Mix 2 and Mix 2a showed approximately similar final expansions, even though Mix 2 managed approximately 11.6% of the 21-day expansion of Mix 2a.

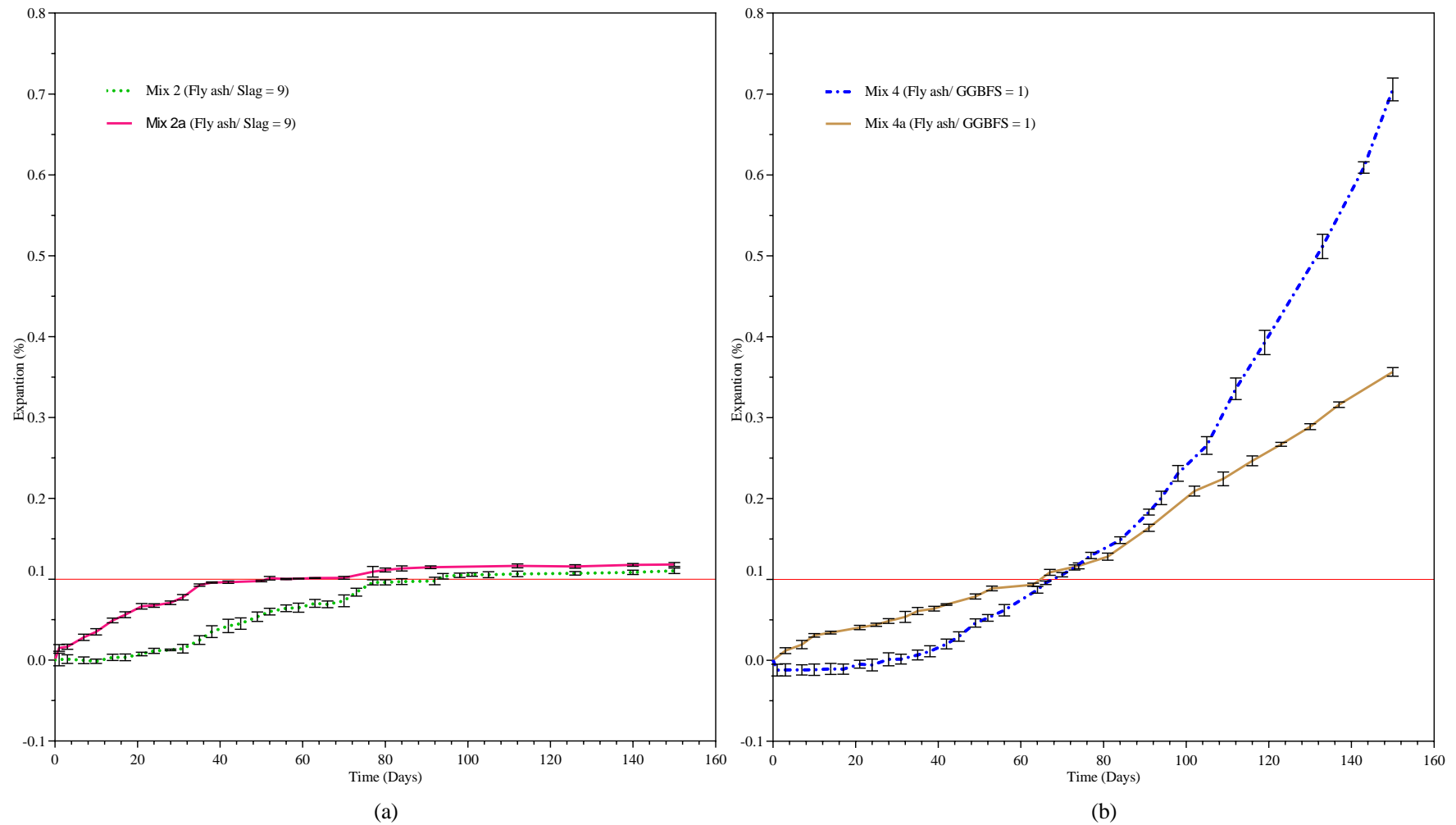


Figure 6-17 : Expansion behaviour of main mixes and subsidiary mixes when exposed to accelerated curing conditions. 0.1% (red line) is the minimum expansion limit for reactivity stipulated in AS 1141.60.1.

Table 6-3 : Average expansion of mortar bars at 10, 21 and 150 days

	Average expansion		
	10 days	21 days	150 days
Mix 2	-0.0013 %	0.0077 %	0.1105 %
Mix 2a	0.0351 %	0.0665 %	0.1182 %
Mix 4	-0.0116 %	-0.0048 %	0.7032 %
Mix 4a	0.0310 %	0.0406 %	0.3565 %

Mix 2 has gone through a negative expansion period for 21 days before starting to increase as illustrated in Figure 6-17a. The expansion increment drastically dropped at around 77 days after attaining 87% of its final expansion (0.0962), subsequently results in a relatively flattened curve during the rest of the testing period. Meanwhile, Mix 2a has initialised the expansion development straight away and reach a relatively stabilised point after achieving 81% of its final expansion at around 40 days. However, it should be noted that even though Mix 2 and Mix 2a behave differently, both managed to achieve almost similar final expansions; 0.1105% and 0.1182%.

Expansion curve of Mix 4 also displays an initial time lag of approximately 28 days before starting to increase exponentially and reach 0.7032% after 150 days. In the meantime, mortar bars of Mix 4a start to show almost linear expansion development from the beginning without going through low expansion period and reach 0.3565% by 150 days. Even though Mix 4 commences from the behind due the time lag, the rapid expansion gain allows it to achieve almost twice expansion compared to Mix 4a at the end of testing. Thus, it can be concluded that although the mechanical properties of the Mix affect the expansion behaviour,

both Mix 2 and Mix 4 displayed their ASR potential over the time. This also highlighted the importance of prolonged testing time in identifying ASR of geopolymer mixes.

### 6.2.2.2 Compressive strength variation

Compressive strength variation of main mixes (Mix 2 and Mix 4) and subsidiary mixes (Mix 2a and Mix 4a) over 29 days are shown in Figure 6-18. Compressive strengths were calculated based on the crushing values of 50mm x 50mm x 50mm mortar cubes casted along with the mortar bars and exposed to similar curing conditions (1M NaOH at 80 °C). At least three cubes were crushed for single strength measurement, and standard errors of the data as shown in Figure 6-18 reveal that averaged values may represent the actual compressive strengths. It should be noted that compressive strength shall depict the mechanical properties of undamaged mortar such as elastic modulus, yield stress, flexural strength, etc. (Gunasekara 2016; Phoo-ngernkham et al. 2013; Ryno 2014).

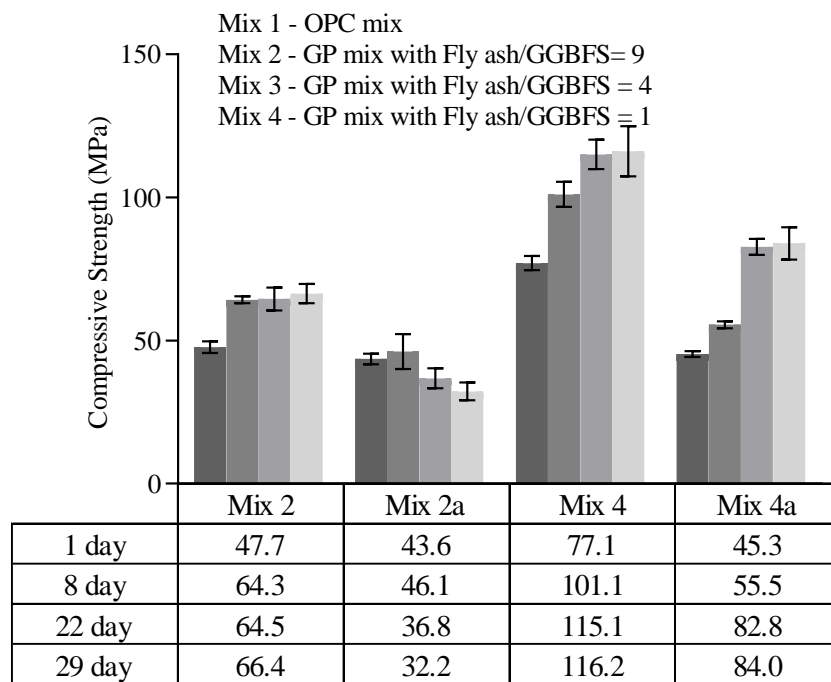


Figure 6-18 : Compressive strength variation of mixes over 29 days after casting

Mix 2, Mix 2a and Mix 4a have shown almost similar initial strengths 47.7 MPa, 43.6 MPa and 45.3 MPa respectively while Mix 4 displayed 77.1 MPa. Compressive strengths of all mixes increased during the initial 29 days of casting except in Mix 2a which displays strength loss after 8 days most probably due to the internal crack development caused by ASR. It seems like Mix 2, Mix 4 and Mix 4a almost achieved the peak strengths by 29 days as their strength gains become substantially lower with the time as illustrated in Figure 6-18. Many researchers demonstrated that the stress-strain behaviour of undamaged geopolymer mortar has a positive relationship with the compressive strength (Chitrana et al. 2018; Gunasekara 2016). Thus, higher compressive strengths of main mixes (Mix 2 and Mix 4) compared to subsidiary mixes (Mix 2a and Mix 4a) may result in higher yield stresses and elastic modules which indicates superior mechanical resistance in mortar towards ASR gel pressure development in main mixes with respect to their subsidiary mixes in the early stages.

### **6.2.2.3 Scanning Electron Microscope (SEM) Analysis**

Scanning electron microscope analysis was performed on the representative mortar bar samples extracted at 21 days and 150 days to identify the stress development in specimens and reinforce the involvement of ASR on the distresses in mortar bars. In addition, backscatter EDS analysis was performed to identify the chemical composition of ASR gel.

ASR gel formation was identified in all geopolymer mortar specimens except in Mix 2 at 21 days. Even though the microstructural analysis was targeted on the ASR gel formed inside the aggregate due to the ease of identification, it should be noted that ASR gel can also be found at the aggregate binder interface and inside binder as presented in Figure 6-3. Figure 6-6 (Mix 2 at 150 days), Figure 6-9 (Mix 4 at 21 days) and Figure 6-10 (Mix 4 at 150 days) are the EDS line profiles of ASR gel identified in main mixes and Figure 6-19 to 6-22 are the EDS line profiles correspond to subsidiary mixes. In order to make the variations of minor elements

more visible oxygen (O) was omitted as it is a common element in all substances of the present in the targeted profile.

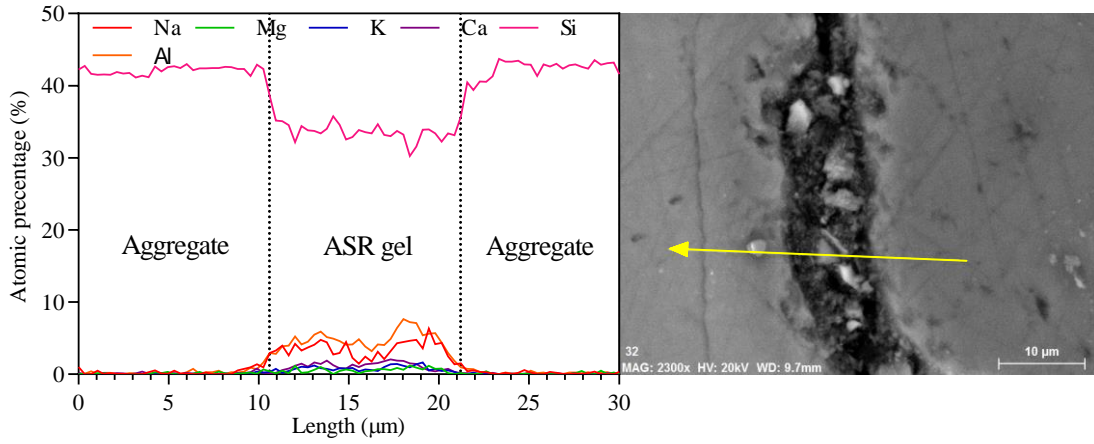


Figure 6-19 : ASR gel identified inside aggregate of mix 2a at 21 days

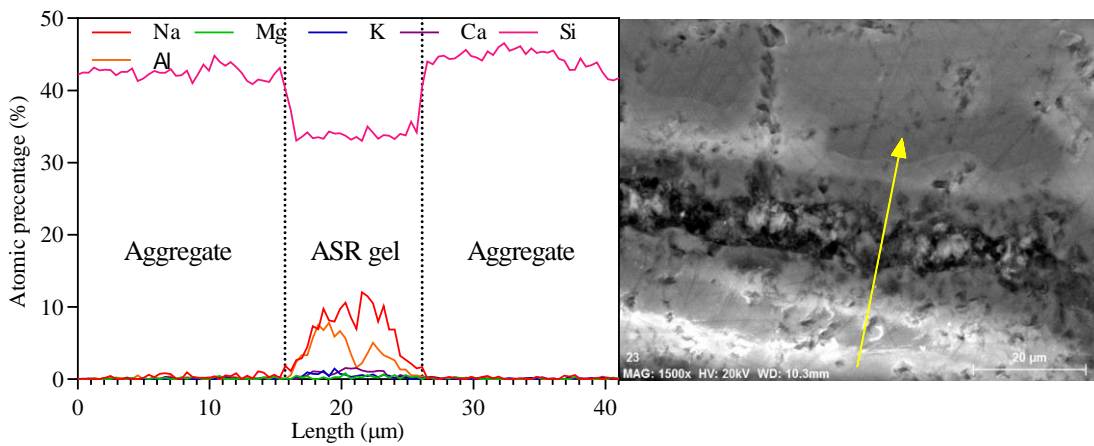


Figure 6-20 : ASR gel identified inside aggregate of mix 2a at 150 days

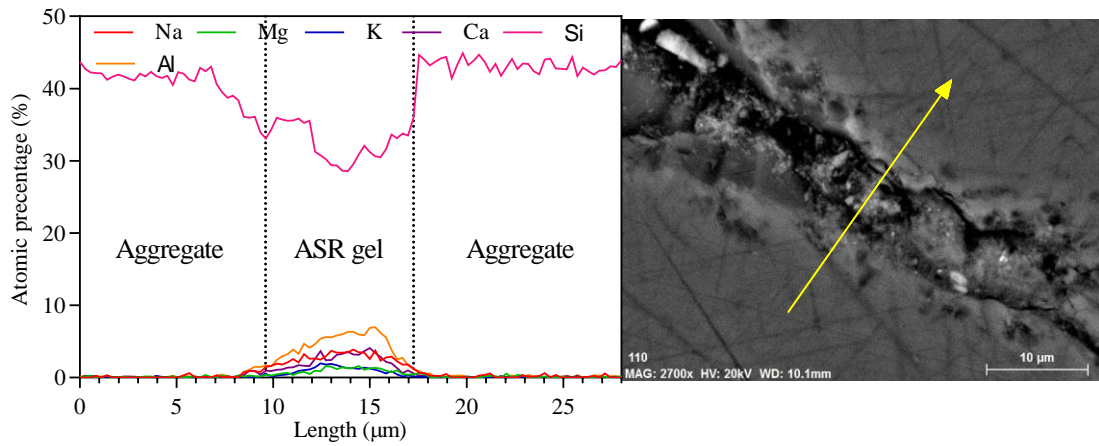


Figure 6-21 : ASR gel identified inside aggregate of mix 4a at 21 days

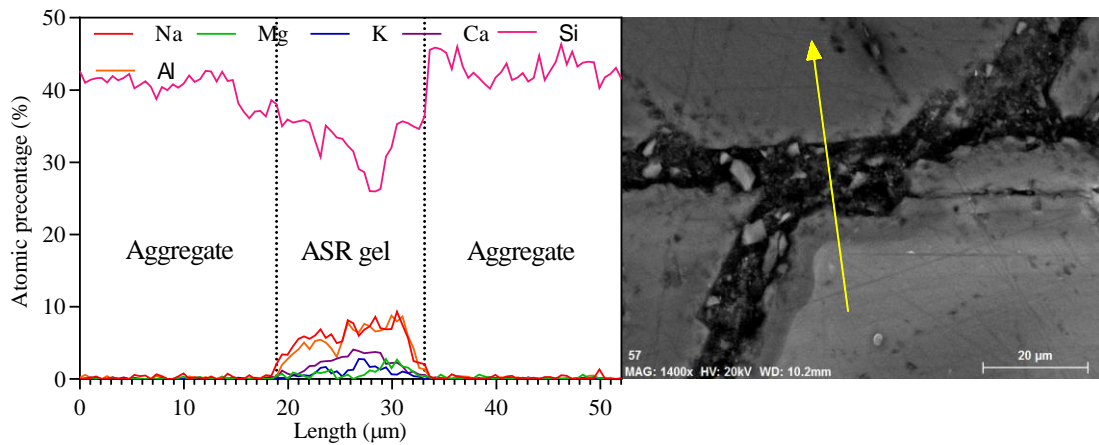


Figure 6-22 : ASR gel identified inside aggregate of mix 4a at 150 days

Elemental atomic percentages of ASR gel located in geopolymer mixes (Mix 2, Mix 2a, Mix 4 and Mix 4a) were summarised in Table 6-4. It should be noted that at least 250 data points were considered when calculating the average values. Na+K/Si ratio, Ca/Si ratio and the Al/Si ratio was calculated to identify any trends in ASR gel compositions. Figure 6-23 contains the tertiary diagrams plotted based on the data in Table 6-4 which graphically illustrates the ASR gel compositions of corresponding mixes.

Table 6-4 : Summary of SEM /EDS analysis on ASR gel in geopolymer mixes

Mix No.		Average atomic percentage (%)						Ratios		
		Na	K	Ca	Mg	Si	Al	$\frac{(Na+K)}{Si}$	$\frac{Ca}{Si}$	$\frac{Al}{Si}$
2	21 days	-	-	-	-	-	-	-	-	-
	150 days	4.63	0.19	0.12	0.29	31.80	3.91	0.15	0.004	0.123
2a	21 days	3.41	0.78	1.04	0.54	33.76	4.60	0.12	0.031	0.137
	150 days	6.40	0.47	0.42	0.29	34.58	3.54	0.19	0.018	0.104
4	21 days	1.25	0.25	4.05	0.30	33.36	1.73	0.05	0.122	0.052
	150 days	5.68	0.13	2.21	0.30	30.30	3.36	0.19	0.073	0.111
4a	21 days	2.85	0.95	3.15	0.90	31.25	4.41	0.12	0.101	0.141
	150 days	5.73	0.96	2.02	0.89	33.26	5.02	0.20	0.061	0.151

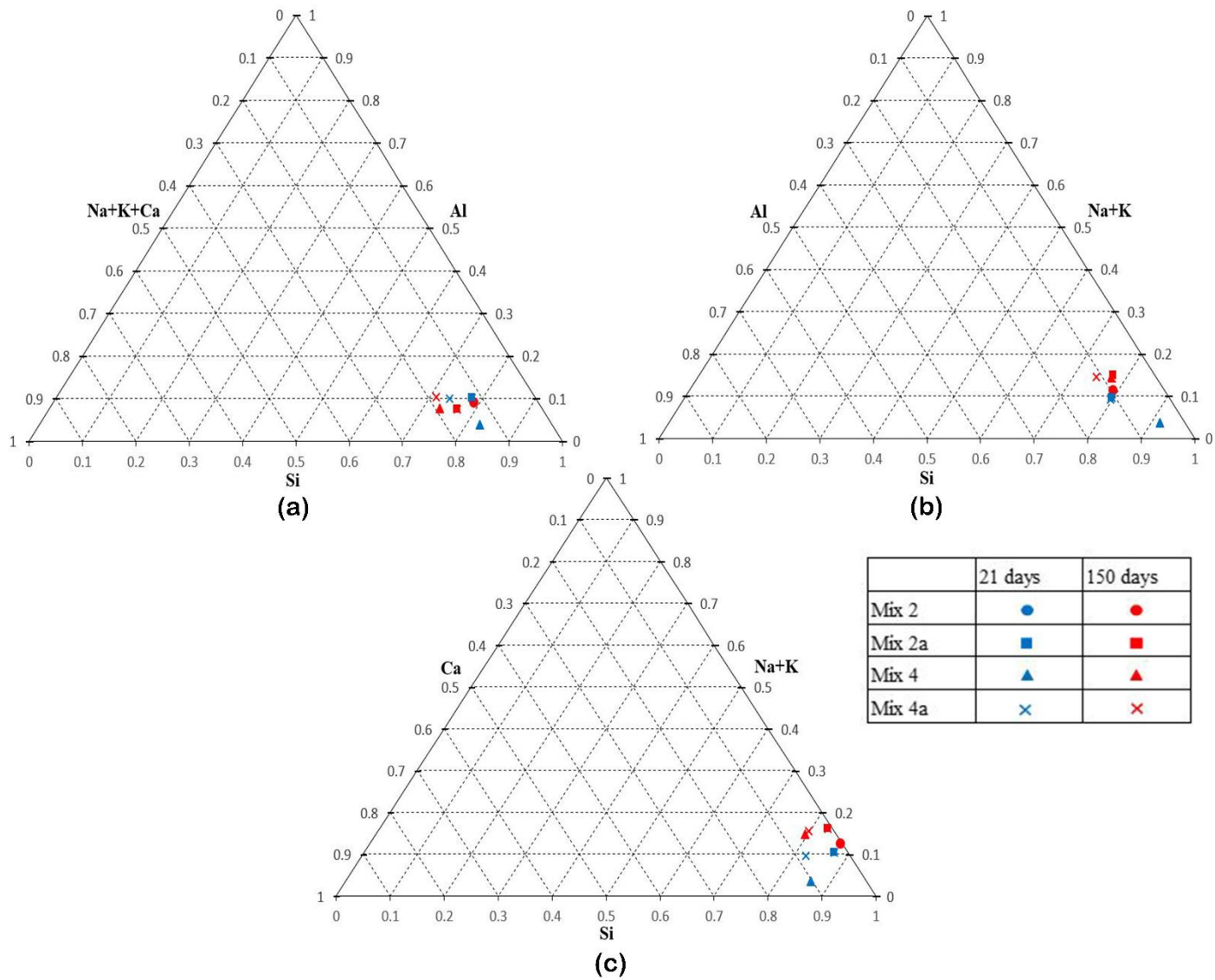


Figure 6-23 : ASR gel composition interpreted in a ternary diagram

ASR gel located in all the specimens contains a significant amount of aluminium (Al) in addition to the typical gel elements; alkalis (Na and K), calcium (Ca), silicon (Si) and oxygen (O) as shown in Table 6-4 and Figure 6-23 which consent with the ASR gel compositions identified throughout this study (Leemann et al. 2016; Leemann & Lura 2013; Leemann & Merz 2013; Thaulow et al. 1996). ASR gel in all mixes have initially shown lower alkali content with their (Na+K)/Si ratio lied below the 0.15; the lower limit of the range for ASR gel defined based on existing studies. However, the alkali to silica ratio of ASR gel located in 150 days old samples lies perfectly inside the defined region for ASR;  $0.15 < (\text{Na}+\text{K})/\text{Si} < 0.3$  as shown in Table 6-4 (Leemann et al. 2016; Leemann & Lura 2013; Leemann & Merz 2013; Thaulow et al. 1996). The increment of Na content in ASR gel is quite obvious given the fact that mortar specimens were exposed to virtually infinite alkali source (1M NaOH) throughout the testing time.

Mixes with high GGBFS content (Mix 4 and Mix 4a) exhibited Ca rich ASR gel formation compared to the other two mixes (Mix 2 and Mix 2a). In fact, both Mix 4 and Mix 4a have shown high Ca contents at 21 days ( Ca/Si ratio is greater than 0.1) and settled at more or less similar compositions at the end as presented in Table 6-4. It should be noted that ASR gel located in Mix 4 at 21 days have shown high Ca content accompanied by substantially low Na content which might indicate the formation of CSH before ASR gel due to its low saturation energy as illustrated by many researchers (Hou et al. 2004; Kim, Taehwan & Olek, Jan 2014; Kim, Taehwan & Olek, Jan 2014).

Figure 6-24 contains the backscatter SEM images of main mixes (Mix 2 and Mix 4) and their subsidiary mixes (Mix 2a and Mix 4a) at 21 days and 150 days. The magnifications of the SEM images were fixed at 100 to simplify the distress analysis.

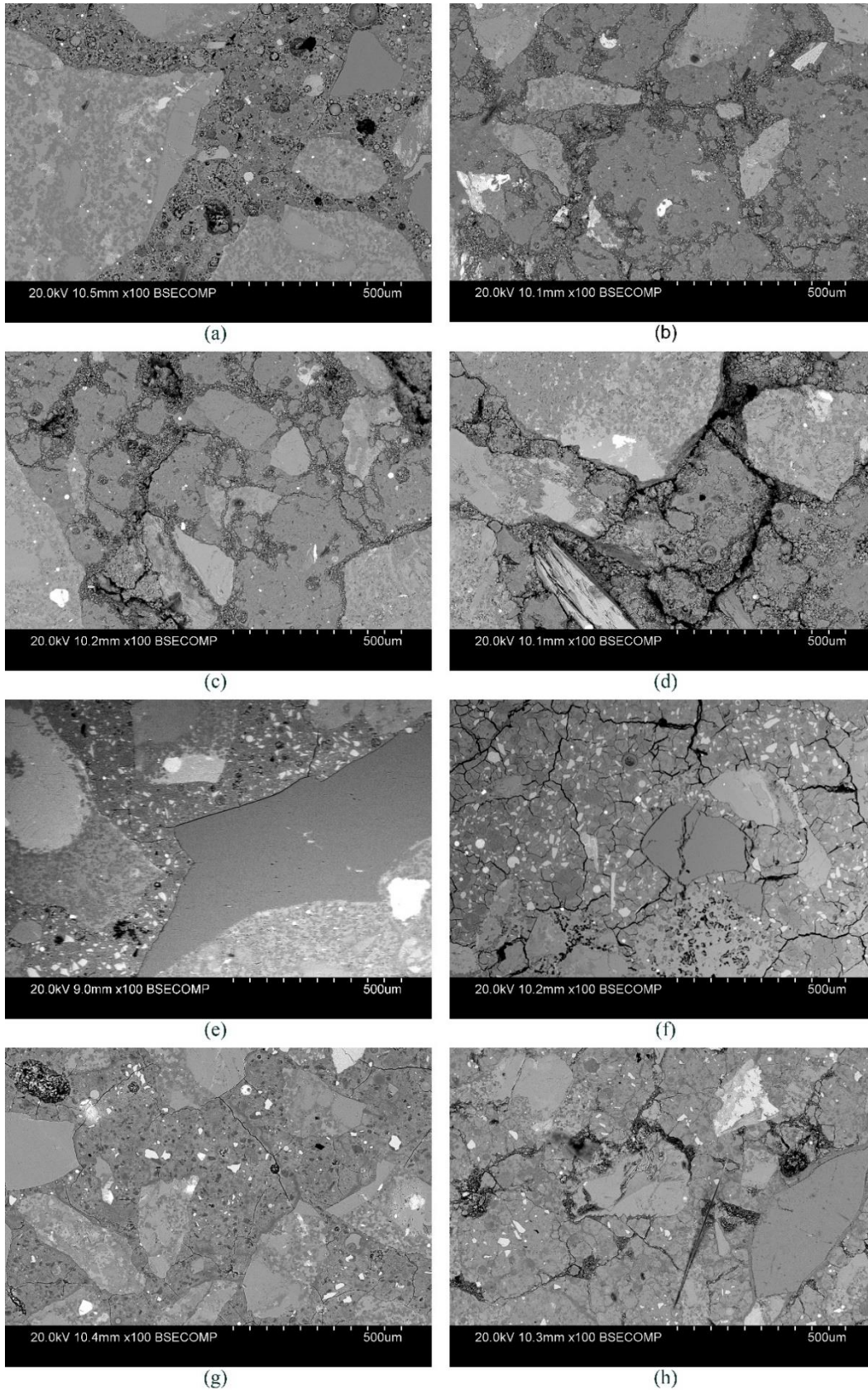


Figure 6-24 : Micro crack propagation of mixes over the time; (a) SEM image of mix 2 at 21 days, (b) SEM image of mix 2 at 150 days (c) SEM image of mix 2a at 21 days, (d) SEM image of mix 2a at 150 days, (e) SEM image of mix 4 at 21 days, (f) SEM image of mix 4 at 150 days, (g) SEM image of mix 4a at 21 days, (h) SEM image of mix 4a at 150 days.

Subsidiary mixes (Mix 2a and Mix 4a) have shown considerably higher crack formation at 21 days compared to the main mixes (Mix 2 and Mix 4). It should be noted that the deformities present in Mix 2 at 21 days (Figure 6-24a) are unreacted or partially reacted sites in the binder and it seems like they were healing over the time most probably due to the continuous geopolymerization process. Mix 2a has clearly displayed severe distresses at 21 days compared to Mix 4a which might be due to its lower mechanical properties as discussed in section 6.2.2.2.

All the mixes have shown an increase in distresses with the time. In fact, ASR induced cracks can be identified inside the binder, at aggregate binder interface and inside the aggregate in all mixes at the end of the test (150 days). However even though all mixes have shown significantly higher cracks inside the binder, SEM images at 150 days clearly indicate substantially lower distress inside aggregate in Mix 2 and Mix 2a compared to Mix 4 and Mix 4a. Furthermore, despite having almost no cracks at 21 days, Mix 4 managed to exhibit the severest crack propagation at the end of the testing period (150 days) as seen in Figure 6-24f.

#### **6.2.2.4 Mortar bar images**

Figure 6-25 exhibits the surface conditions of the mortar bars of Mix 2, Mix 2a, Mix 4 and Mix 4a after the test. No crack formation was observed in Mix 2 while a minor crack formation was identified in Mix 2a as shown in Figure 6-25a and 6-25b. Mix 4 and Mix 4a displayed the characteristic map cracking of ASR (HB79 2015). In fact, Mix 4 has shown the severest crack formation followed up by Mix 4a and Mix 2a respectively which aligns with the expansion results in section 6.2.2.1.

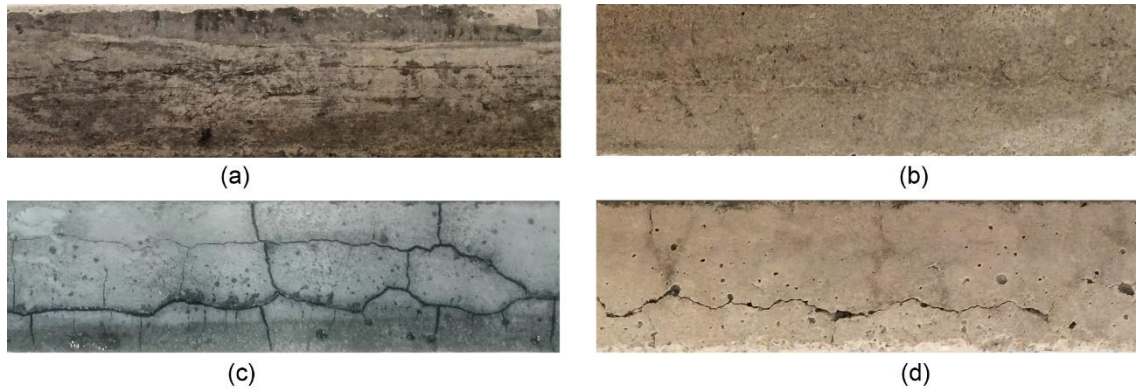


Figure 6-25 : Mortar bar images of main mixes and their subsidiary mixes; (a) Mix 2 at 150 days, (b) Mix 2a at 150 days, (c) Mix 4 at 150 days, (d) Mix 4a at 150 days

### 6.2.3 Effect of curing solution

#### 6.2.3.1 Expansion test

Figure 6-26 presents the average expansion variation of geopolymer mortar bar (Mix 2-4) exposed to four different curing conditions; I 1M NaOH solution; II 0.003M NaOH solution; III 1M NaOH solution saturated with  $\text{Ca}(\text{OH})_2$ ; IV water. At least three mortar bars expansion measurements were used during the study. Substantially low standard errors in Figure 6-26 suggested that the average variation may represent the individual expansion development of mortar bars. All mortar specimens were exposed to an elevated temperature to further accelerate the reaction and prolonged testing time (150 days) was adapted to identify any late booms in the expansion behaviours. Table 6-5 summarises the average expansions at 10, 21 and 150 days of each mix.

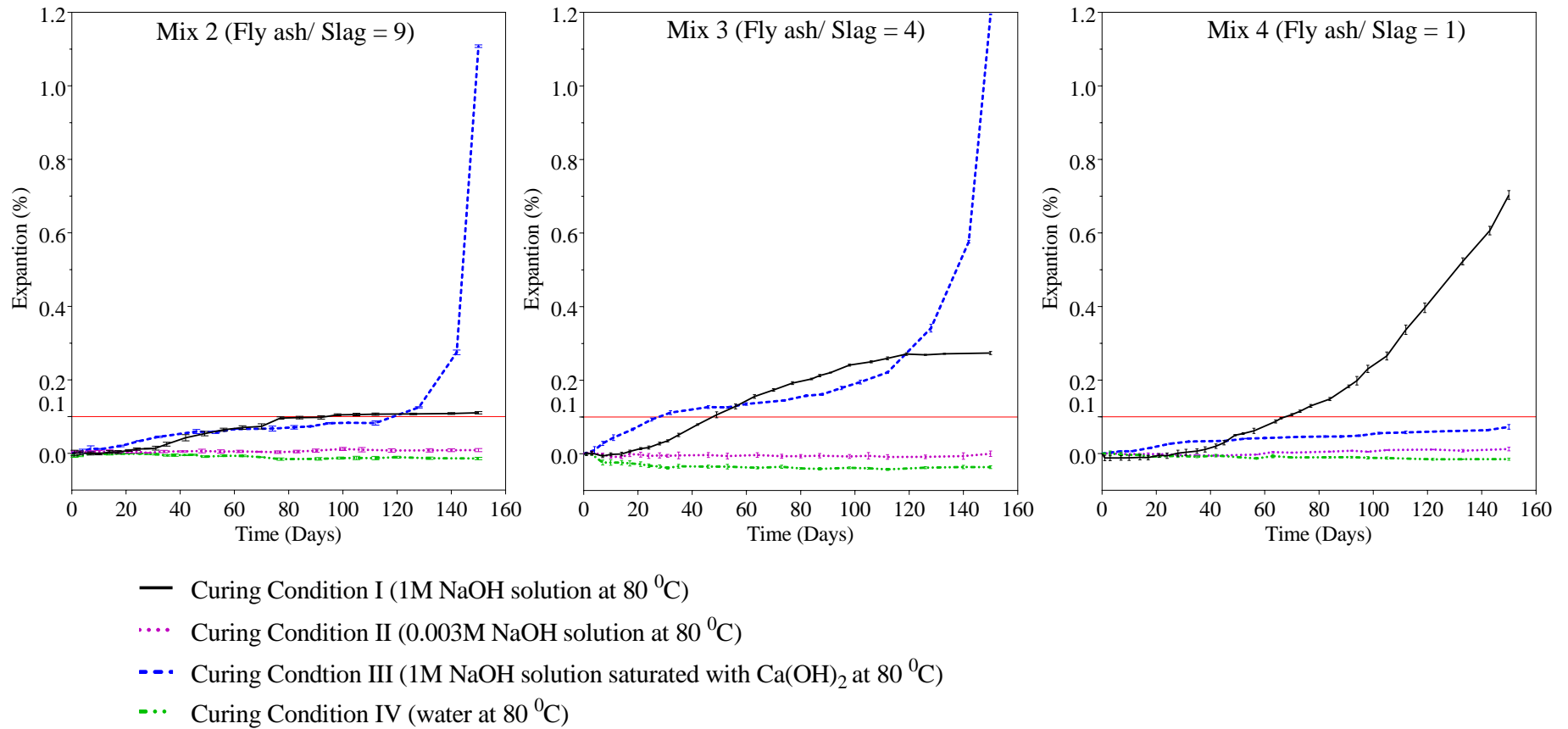


Figure 6-26 : Expansion characteristics of Mix 2-4 over 150 days when exposed to different curing conditions. 0.1% (red line) is the minimum expansion limit for reactivity stipulated in AS 1141.60.1.

Table 6-5 : Average expansion of mortar bars at 10, 21, 29 and 150 days

	Curing Condition	Average Expansion (%)			
		10 days	21 days	29 days	150 days
Mix 2	I	-0.0013	0.0077	0.0128	0.1105
	II	-0.0025	-0.0002	0.0015	0.0070
	III	0.0118	0.0258	0.0384	1.1080
	IV	-0.0012	-0.0015	-0.0018	-0.0139
Mix 3	I	-0.0016	0.0142	0.0276	0.2737
	II	-0.0077	-0.0022	-0.0046	0.0078
	III	0.0420	0.0778	0.1011	1.1944
	IV	-0.0422	-0.0483	-0.0347	-0.0311
Mix 4	I	-0.0116	-0.0048	0.0013	0.7032
	II	-0.0014	-0.0013	-0.0062	0.0123
	III	0.0064	0.0205	0.0292	0.0725
	IV	-0.0034	-0.0078	-0.0042	-0.0152

Curing condition IV corresponds to the lowest expansions in all three mixes. In fact, all the mixes have shown a negative expansion throughout the test. None of the mixes exhibited an expansion gain which indicates no significant ASR gel formation inside the mortar. It should be noted that alkali leaching in the geopolymer specimens might reduce the free alkali content in the system and thus, curtail the reaction (L. Ly 2007).

Curing condition II showed the second lowest expansion development among all. Expansion curves of mortar bars exposed to curing condition II (0.003M NaOH) started with negative expansions but managed to achieve positive expansion by the end of the test. 0.003M NaOH solution has approximately similar alkali content compared to geopolymer which controlled alkali transportation in either direction. Thus, the ASR expansion occurred in the mortar bars are most probably due to the free alkalis available in the mortar itself. Table 6-5 reveals that the Mix 2-4 only managed to achieve 7%, 7.8% and 12.3% of the minimum expansion limit for deleterious ASR stipulated in AS 1141.60.1 (0.1%), even after 150 days

which signifies that risk of deleterious ASR in geopolymer mixes without external alkalis is negligible.

Expansion behaviour of mortar bars exposed to curing condition I is analysed extensively in section 6.2.3.1. In general, Mix 4 has shown the highest final expansion followed up by Mix 3 and Mix 2 respectively. All mortar bars have shown an initial time lag, and then expansion gain continuously increased in Mix 4 while the other two mixes have stabilised after some time.

In curing condition III,  $\text{Ca}^{2+}$  was also supplied by the solution along with  $\text{Na}^+$  ions. Thus, all the mixes have an ample amount of Ca for the reaction. Figure 6-26 illustrated that geopolymer mortar bars exposed to curing condition III do not show any time lags as in mortar bars exposed to curing condition I. Expansion curves of both Mix 2 and Mix 3 have shown a similar behaviour; initial increment followed up by a stabilizing phase and then an exponential increment at the end to reach; 1.1080% and 1.1944% respectively. In Mix 2 and Mix 3, expansions correspond to the curing condition III are the highest except in the middle region (approximately 60 days) where expansions of mortar bars of curing condition I have taken the lead as shown in Figure 6-26. Mix 4 has shown a slightly different behaviour since it doesn't show a stabilisation period in the middle of exponential growth towards the end like other geopolymer mixes. In Mix 4, mortar bars of curing condition III have shown an expansion development straightaway as in other two mixes. However, despite having a time lag of approximately 28 days, curing condition I have managed to out pass curing condition III approximately within 45 days as seen in Figure 6-26.

### 6.2.3.2 Compressive strength variation

Figure 6-27 displays the compressive strengths of Mix 2-4 at 29 days of casting (28 days in curing). At least three mortar cubes were crushed and averaged to obtain the 29-day compressive strength. Comparatively low standard errors in Figure 6-27 suggest that average compressive strengths may represent the actual values.

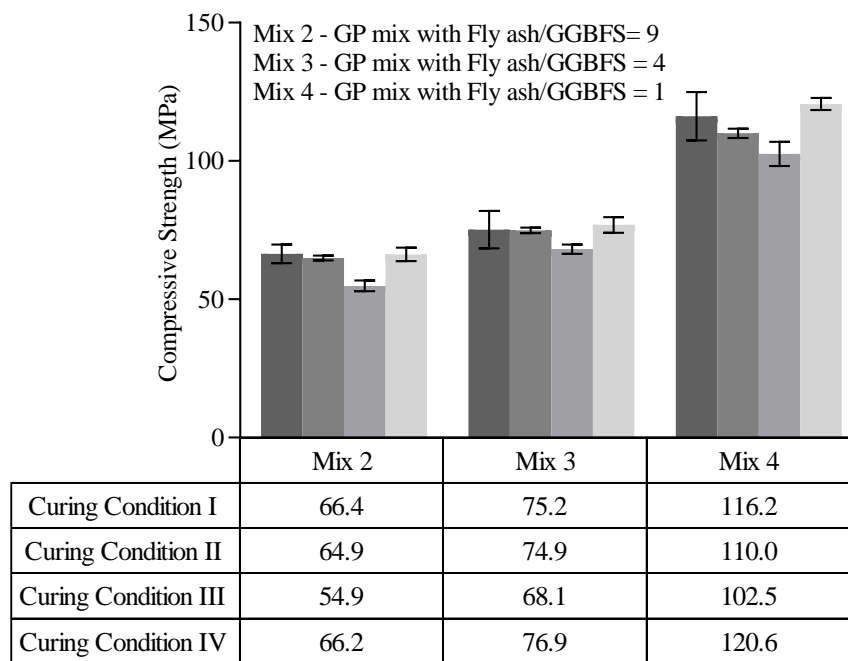


Figure 6-27 : the 29-day compressive strength of Mix 2-4 exposed to different curing conditions

Despite the curing condition, Mix 4 has shown the highest compressive strengths followed up by Mix 3 and Mix 2. However, there is a noticeable deviation with the type of curing condition which most probably due to ASR crack formation in a mortar. Curing condition III (1M NaOH saturated with  $\text{Ca}(\text{OH})_2$ ) corresponds to the lowest strength followed up by curing condition I (1M NaOH), II (0.003M NaOH) and IV (water) which consent with the expansion results in Figure 6-26.

### 6.2.3.3 Scanning Electron Microscope (SEM) Analysis

Microstructural analysis was performed at the end of the test to identify the ASR gel formation and microcrack propagations in mortar bars exposed to different curing conditions. In addition, backscattered EDS analysis was used to identify the chemical compositions of ASR gel identified during the SEM analysis.

Curing condition II and IV haven't shown a noticeable gel formation during the microstructural analysis which consent with their almost zero expansion developments. All the geopolymer mixes (Mix 2-4) exposed to curing condition I have shown a significant gel formation at 150 days (see Figure 6-6, Figure 6-8 and Figure 6-10) and extensively analysed in section 6.2.1.3 and thus not be repeated in this section. Figure 6-28 to 6-32 are the EDS line profiles of ASR gel located in mortar specimens exposed to curing condition III. Mix 2 and Mix 3 have shown gel formations in all regions; inside aggregate, at aggregate binder interface and inside the geopolymer binders while Mix 4 have shown a distinctive gel formation only inside the aggregate. Figure 6-28, 6-30 and 6-32 are the gels located inside aggregate and Figure 6-29, and 6-31 are the gels located at the aggregate binder interface of Mix 2-4 respectively.

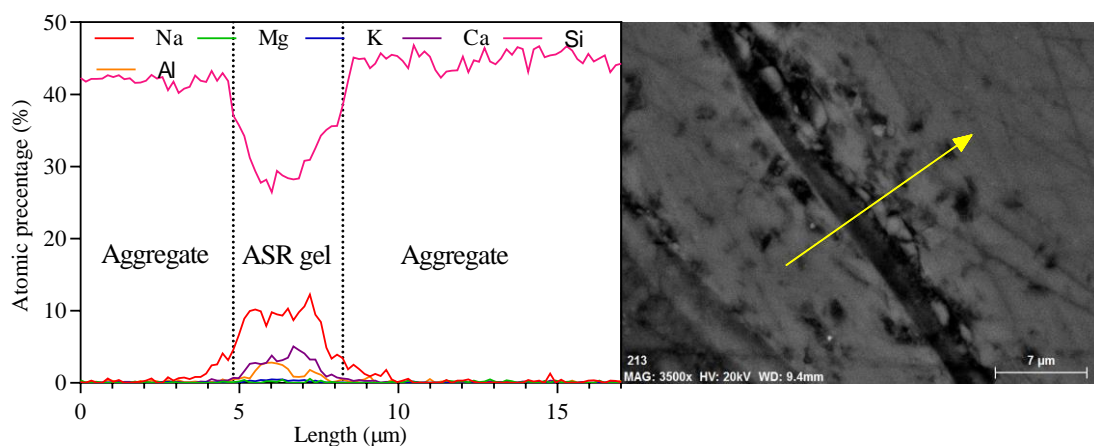


Figure 6-28 : ASR gel identified inside aggregate of Mix 2 exposed to curing condition III for 150 days

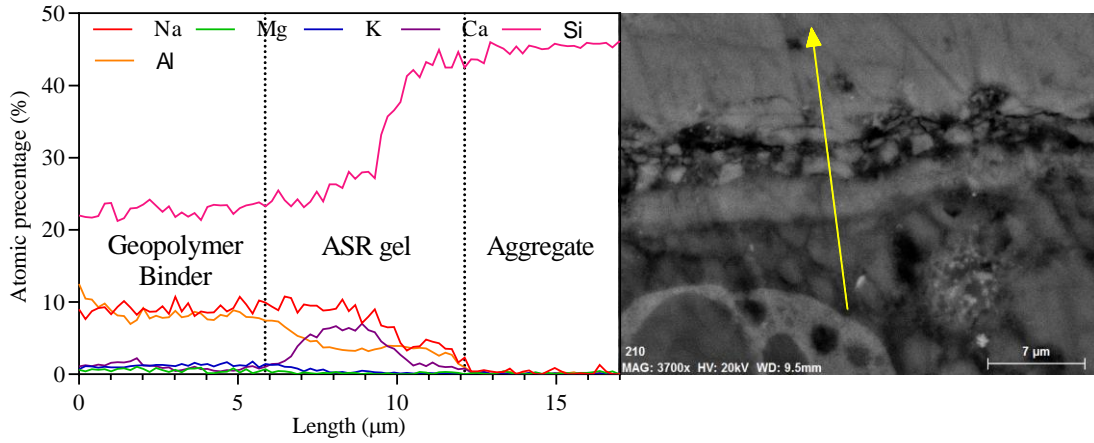


Figure 6-29 : ASR gel identified at aggregate binder interface of Mix 2 exposed to curing condition III for 150 days

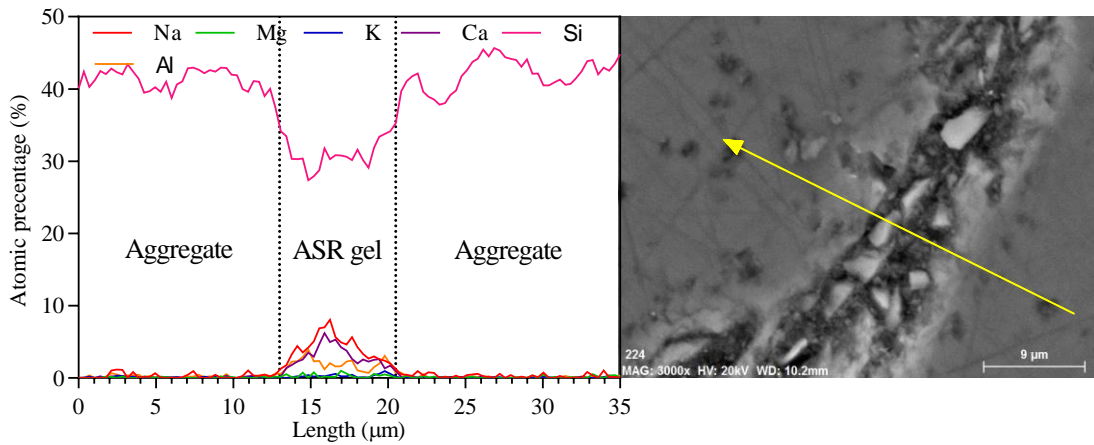


Figure 6-30 : ASR gel identified inside aggregate of Mix 3 exposed to curing condition III for 150 days

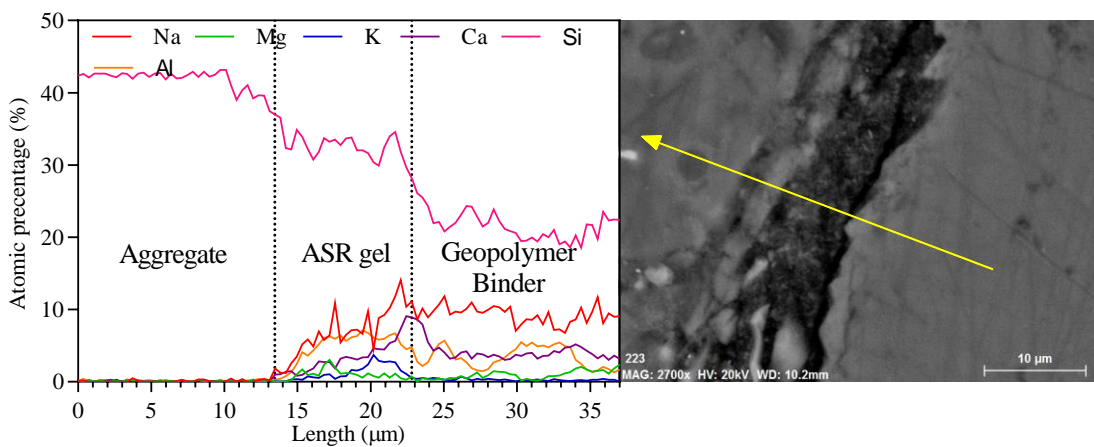


Figure 6-31 : ASR gel identified at aggregate binder interface of Mix 3 exposed to curing condition III for 150 days

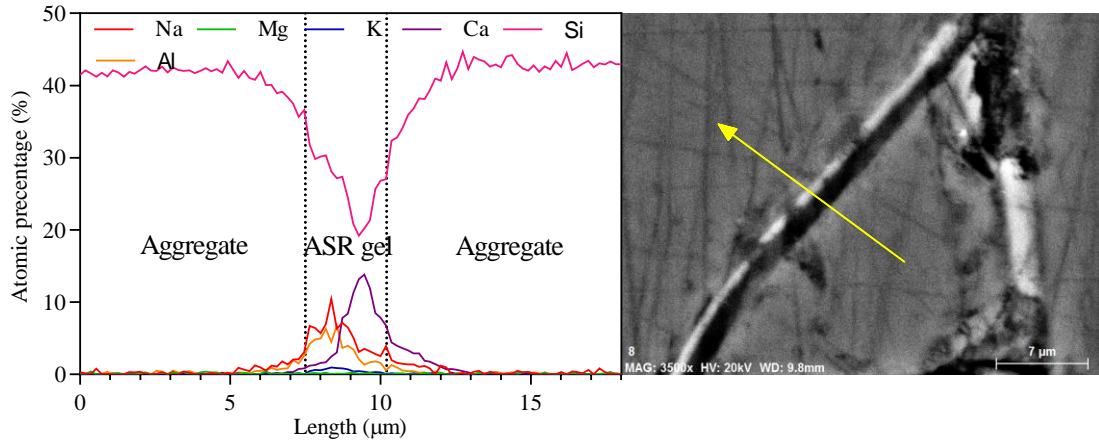


Figure 6-32 : ASR gel identified at aggregate binder interface of Mix 4 exposed to curing condition III for 150 days

Table 6-6 summarises the elemental atomic percentages of ASR gel identified on mortar bars exposed curing condition III. At least 250 data points of ASR gel identified during the SEM/EDS analysis were averaged to obtain the elemental compositions in Table 6-6.

Table 6-6 : Summary of SEM /EDS analysis on ASR gel located in mix 2-4 exposed to curing condition III for 150 days

Mix No.	Location	Average atomic percentage (%)						Ratios		
		Na	K	Ca	Mg	Si	Al	$\frac{(Na+K)}{Si}$	$\frac{Ca}{Si}$	$\frac{Al}{Si}$
2	Inside aggregate	8.19	0.24	2.50	0.14	31.73	1.32	0.27	0.079	0.042
	At boundary	7.06	0.42	3.47	0.18	32.13	4.01	0.23	0.108	0.125
3	Inside aggregate	4.28	0.67	2.84	0.30	31.12	1.86	0.16	0.087	0.057
	At boundary	6.89	1.24	3.50	0.97	32.61	4.69	0.25	0.107	0.144
4	Inside aggregate	5.21	0.49	6.35	0.10	26.68	3.39	0.21	0.238	0.127
	At boundary	-	-	-	-	-	-	-	-	-

Alkali silica gel in geopolymer mortar exposed to curing condition III typically consists of sodium (Na), potassium (K), calcium (Ca), aluminium (Al) and silicon (Si) as illustrated in EDS line profiles (Figure 6-28 to 6-32) and Table 6-6. Even though it seems like ASR gels correspond to curing condition I and III have almost similar elemental compositions, there is a distinctive rise in Ca content of ASR gels in curing condition III which might be due to the availability of external Ca via curing solution. ASR gels in Mix 2 and Mix 3 exposed to curing condition III have almost similar Ca contents as shown in Table 6-6. Gels located inside aggregate have slightly lesser Ca content ( $\text{Ca/Si} < 0.1$ ) compared to the gels at the boundary ( $\text{Ca/Si} > 0.1$ ) which most probably due to the limited amount of Ca inside aggregate. Alkalis (Na+K) to silica ratios of gels correspond to curing condition III lies inside the 0.15~0.3 range and Ca/Si ratios fluctuate at the lower boundary of the 0.10~0.3 range defined based on the literature in Mix 2 and Mix 3 while mix 4 have shown a fairly high Ca content ( $\text{Ca/Si} = 0.234$ ) even inside aggregate (Leemann et al. 2016; Leemann & Lura 2013; Leemann & Merz 2013; Thaulow et al. 1996). EDS line profiles at aggregate boundaries (Figure 6-29 and 6-31) have shown a Ca accumulation at the binder gel interface which aligns with the ASR mechanism described in section 6.3.1. High Ca content in gels of Mix 4 might explain the low expansions of respective mortar bars since the Ca reduces the swelling properties of the ASR gel despite playing a major role in expansion development as discussed in section 6.3.1. Gels correspond to curing condition III have shown approximately similar Al compositions to curing condition I. It should be noted that gels inside aggregate consist of lower Al contents compared to gels at the boundary.

Backscatter SEM images of mortar specimens exposed to curing condition I, II, III and IV are displayed in Figure 6-33 and 6-34. All images were taken at 100 magnification to simplify the distress analysis.

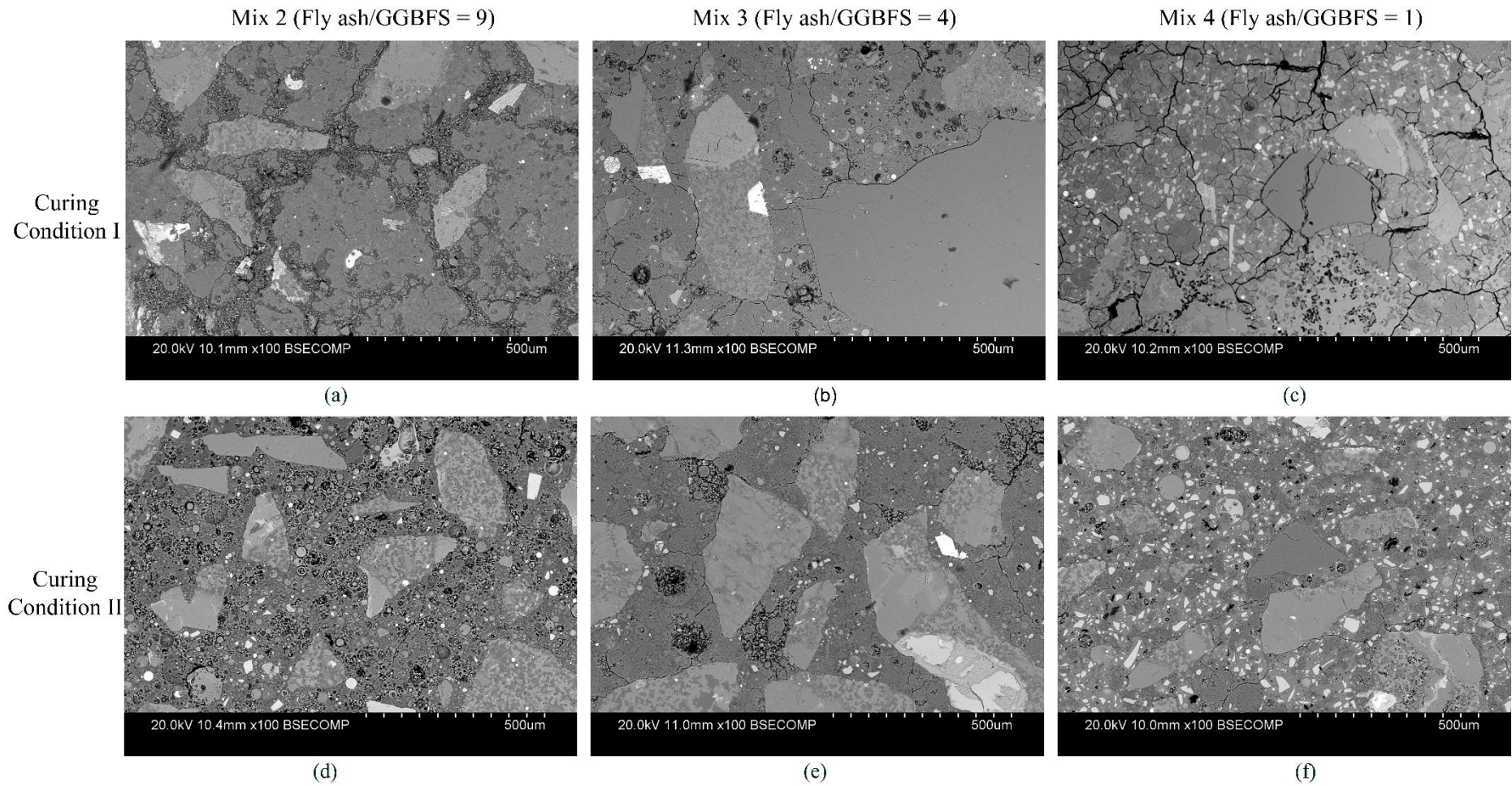


Figure 6-33 : Micro crack propagation of Mix 2-4 at 150 days exposed to Curing condition I (1M NaOH at 80 °C) and Curing condition II (0.003M NaOH at 80 °C)

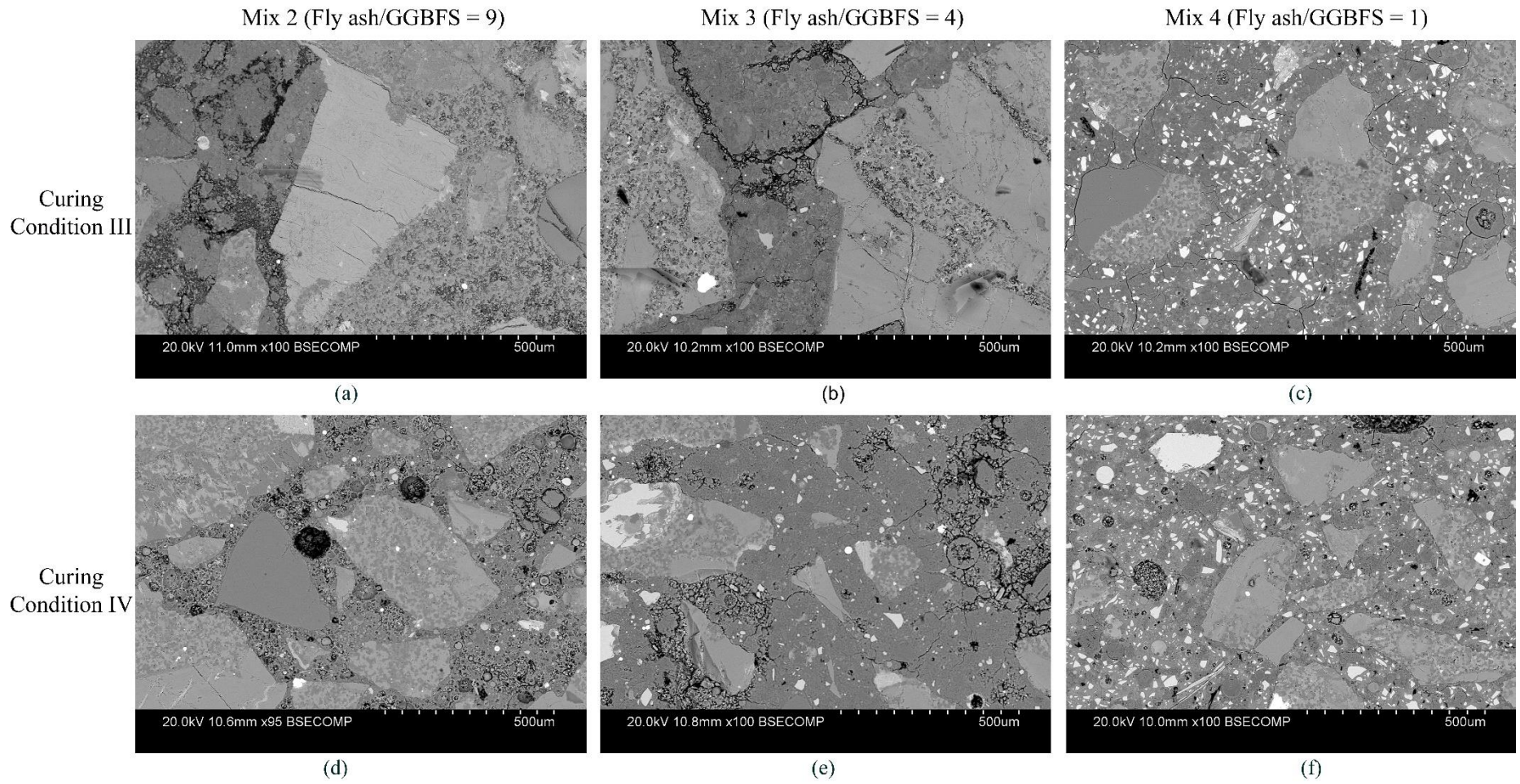


Figure 6-34 : Micro crack propagation of Mix 2-4 at 150 days exposed to Curing condition III (1M NaOH saturated with  $\text{Ca}(\text{OH})_2$  at  $80\text{ }^\circ\text{C}$ ) and Curing condition IV (Water at  $80\text{ }^\circ\text{C}$ )

Curing condition II and IV haven't shown a significant microcrack formation due to ASR in any of the geopolymer mixes even though there are few cracks inside the binder which most probably developed during the sample preparation process. It is clear that mortar specimens exposed to curing condition II and IV consist of fairly high unreacted areas compared to curing condition I and III which indicates the continuation of the geopolymerization process when the external alkalis are available.

Despite showing lower expansions compared to Mix 2 and Mix 3 exposed to curing condition III, Mix 4 with curing condition IV has shown the severest microcrack formation which might fall largely due to the quasi-brittle nature of geopolymer with high GGBFS contents (Gunasekara 2016; Noushini et al. 2016). Mortar bars exposed to curing condition III corresponds to the highest distresses in Mix 2 and Mix 3 which consent with the expansion results. However, it should be noted that in geopolymers, binders are more susceptible to crack formations compared to aggregate in all the mixes.

#### **6.2.3.4 Mortar bar images**

Surface images of mortar bars exposed to different curing conditions are shown in Figure 7-17. In curing condition I, the clear crack formation can be identified in Mix 3 and Mix 4 while in curing condition III, Mix 2 and Mix 3 have shown the crack formations. It should be noted that all cracks are similar to the characteristic map cracks identified in ASR affected structures (HB79 2015). Mix 4 has shown the severest surface crack formation which consent with the SEM images present in Figure 6-33.

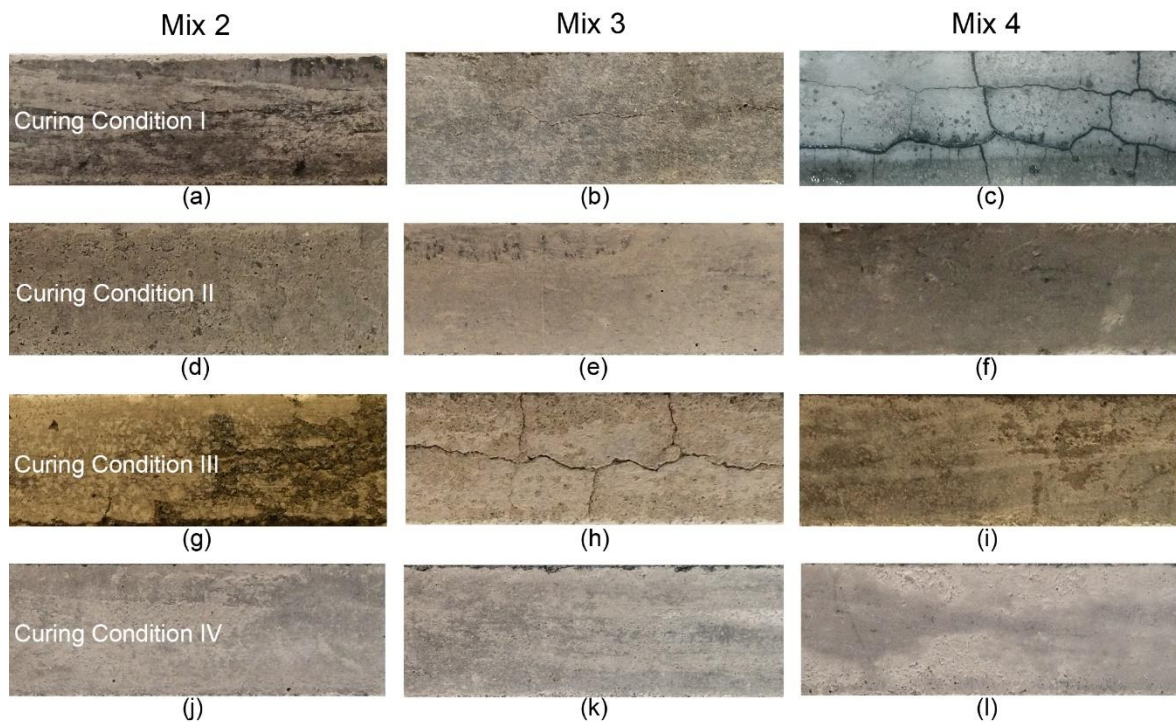


Figure 6-35 : Mortar bar images of mix 1-4 after the test (150 days); (a) Mix 1 at 150 days, (b) Mix 2 at 150 days, (c) Mix 3 at 150 days, (d) Mix 4 at 150 days

## 6.3 Discussion

### 6.3.1 Alkali silica reaction mechanism in geopolymers mortar

Despite being identified in the 1940s, the exact reaction mechanism of ASR is not yet established. However, there are many theories developed to explain the expansion behaviour of ASR in OPC systems. Thus, based on the existing literature, the ASR mechanism is developed for the geopolymer mortar that can explain the experimental results obtained during this study. Figure 6-36 is a schematic diagram of the proposed ASR mechanism in geopolymer mortar.

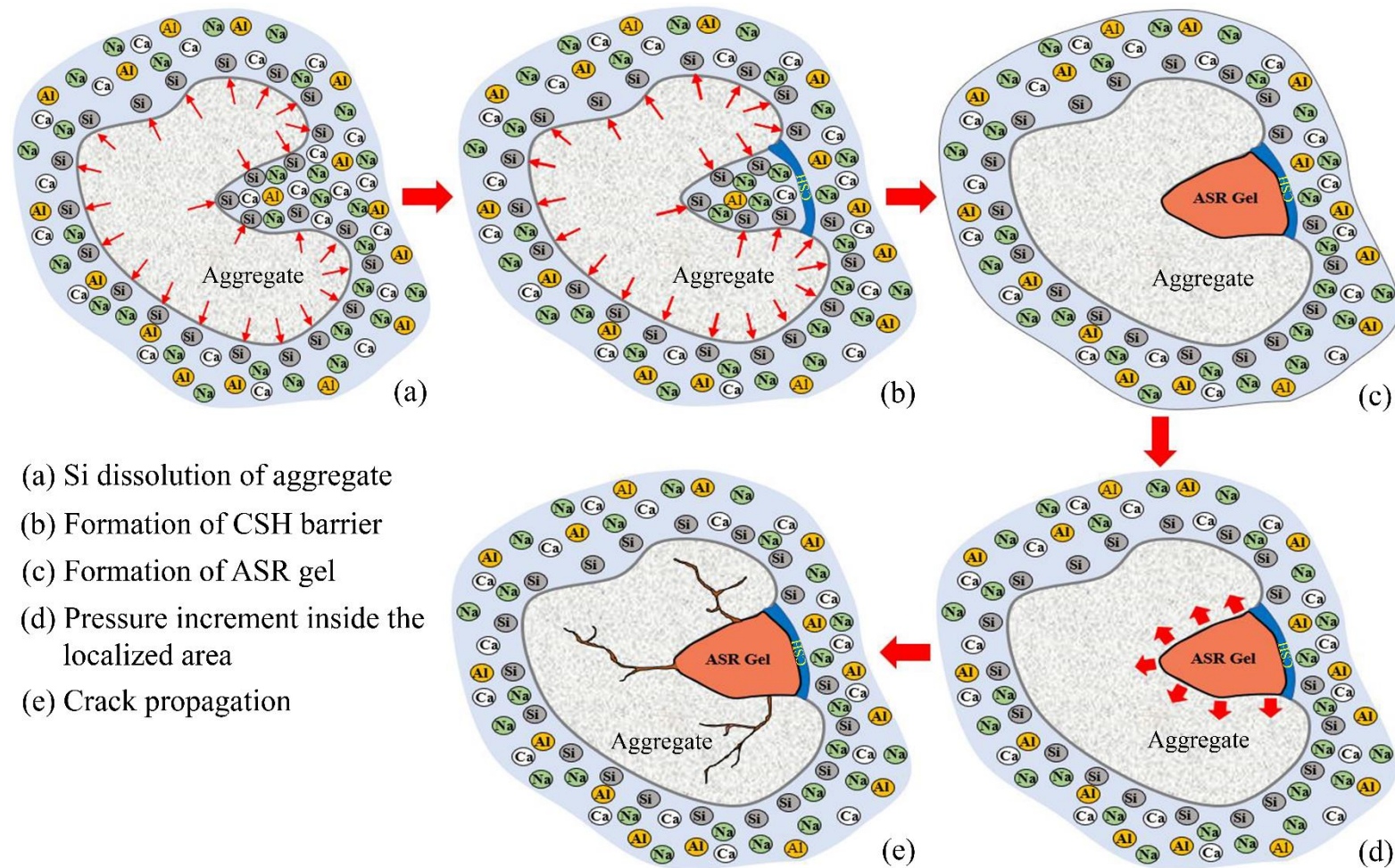


Figure 6-36 : Alkali silica reaction mechanism in geopolymer mortar (developed based on Hou et al. (2004), Kim and Olek (2014) and Ichikawa and Miura (2007))

ASR initiates with the Si dissolution where  $\text{SiO}_2$  in aggregate reacts with the hydroxyl ions ( $\text{OH}^-$ ) in the solution which results in aqueous siliceous products (Kim, Taehwan & Olek, Jan 2014). The continuous Si dissolution from the aggregate leads to rise in Si ion concentration in the proximity of aggregate. Since calcium silica hydrates (CSH) have low saturation point compared to ASR gel as depicted by numerous researchers, CSH formed at the vicinity of the aggregate before ASR gel (Hou et al. 2005; Hou et al. 2004; Kim, Taehwan & Olek, Jan 2014; Kim, Taehwan & Olek, Jan 2014; Leemann et al. 2011). Then, CSH act as a barrier to entrap ions inside the localised areas of aggregate as shown in Figure 6-36. This results in a rapid increase in Si concentrations and thus formation of ASR gel rapidly compared to other locations. In addition, CSH barriers would restrict the ASR gel diffusion into the binder and thus amplify the gel pressure development inside mortar causing severe distress developments. However, it should be noted that, in highly alkaline systems, there can be an ASR gel formation and stress development eventually even without CSH formations due to the availability of enough Si ions and alkalis for the continuous reaction.

### **6.3.2 Effect GGBFS content**

ASR expansion in mortar bars may be influenced by various factors including; i) characteristics of reactive silica phases, ii) distribution of reactive silica phases in the aggregate, iii) alkali concentration, iv) silica ion concentration, v) calcium ion concentration, vi) moisture content, vii) exposure condition, viii) physical and mechanical properties of mortar bars (Fournier & Bérubé 2000; Hobbs 1988). Since all mortar bars had same reactive aggregate and exposed to an identical testing condition (1M NaOH solution at  $80^\circ\text{C}$ ), the effect of factors; i), ii), iii), vi), and vii) on ASR expansion in mortar bars would be identical in all four mixes. In addition, the dissolution rates of silica seem to be more or less similar in all mixes since immersion in 1M NaOH solution might result in high but approximately constant pore solution

alkalinity ( $\text{pH} \approx 14$ ) in Mix 1-4. It is, therefore, reasonable to assume that the difference in expansion observed in Figure 6-1 would be mainly due to the combination of calcium concentration and the physical and mechanical properties of mortar bars.

Expansion curve of Mix 1 (OPC mortar) in Figure 6-1 follows the typical S-shape expansion behaviour of OPC mortar bars with highly reactive aggregates (Fournier & Bérubé 2000; Hobbs 1988). The initial low expansion period is most probably due to the mechanical resistance of the binder since ASR gel formed almost instantly in Mix 1 as it contains high free Ca content. In addition, Figure 6-14 reveals that both Na and Ca contents of ASR gel in Mix 1 increases with the time which indicates the availability of sufficient sodium and calcium contents for the ASR up until the end. Thus, the decrease in expansion rate seems to be caused by the lack of reactive silica phases.

As described by many researchers (Gaboriaud et al. 1999; Ichikawa & Miura 2007; Leemann et al. 2011; Struble & Diamond 1981; Wang & Gillott 1991), expansion induced by sodium base ASR gel is significantly lower than that of sodium-calcium base gel. ASR gels in geopolymer mixes consistently showed a lower Ca content compared to the OPC mix though alkali contents in ASR gels were more or less identical. This might explain the lower expansion exhibited by geopolymer mixes compared to OPC mix even after 150 days of reaction.

In geopolymer mortars, calcium mainly comes from GGBFS which implies that Mix 4 has the highest Ca content followed up by Mix 3 and Mix 2 respectively. The low calcium contents in Mix 2 and Mix 3 might not be enough to form CSH in sufficient quantities to create the barriers required to achieve the Si concentration necessary to trigger ASR gel formation as described in section 6.3.1. Thus, much longer time is required for Si concentration to reach the saturation point of ASR gels (Hou et al. 2004; Kim, Taehwan & Olek, Jan 2014; Kim, Taehwan & Olek, Jan 2014). SEM analysis also agrees with the above conclusions since no ASR gels were located in Mix 2 and comparatively fewer gel sites were located in Mix 3 at 21 days. In

addition, low Ca/Si ratios in ASR gels located in Mix 2 and Mix 3 support the insufficient Ca content in these geopolymer mixes (see Table 6-2 and Figure 6-14). Meanwhile, among geopolymer mixes, it is expected to have the highest degree of ASR in Mix 4 which might lead to immediate expansion development based on the above mechanism due to its high Ca content. Even though Mix 4 attributed to the highest final expansion, a substantial initial delay was observed in the characteristic expansion curve as shown in Figure 6-1. However, SEM/EDS analysis of Mix 4 at 21 days identified a significant amount of gel formation (see Table 6-2 and Figure 6-9) despite showing no expansion. The initial time lag in expansion curves depend on several factors; the rate of ASR pressure generation, resistive threshold pressure of mortar, and the magnitude of shrinkage. Even though the rate of ASR pressure generation is higher in Mix 4 due to the high Ca content, it also has a higher resistive pressure as indicated by the high compressive strengths (see Figure 6-2) which might result in a time lag in expansion curve (Gunasekara 2016).

All mortar bars have shown significant distress at 150 days while Mix 1 has shown a noticeable crack formation even at 21 days. However, it can be identified that the amount of cracks formed inside mortar is greater than that of aggregate in geopolymer mixes while OPC hasn't shown a noticeable crack formation inside the binder despite showing severe cracks in aggregate (see Figure 6-15). In fact, even in geopolymers, the amount of cracks formed inside the aggregate lowered with the initial Ca content which further reinforce the crack formation mechanism in section 6.3.1. In addition, the formation of cracks inside binder creates a dispersion path for low viscous ASR gel (Na based gel) which eventually reduces the internal pressure development and thus the expansions as in Mix 2 and Mix 3.

### **6.3.3 Effect of mix design**

Two subsidiary mixes; Mix 2a and Mix 4a were designed to achieve lower mechanical properties compared to the main mixes; Mix 2 and Mix 4. Subsidiary mixes have managed only 72.3% and 69.4% of the maximum strengths of their respective main mixes which indicates noticeably lower mechanical properties in Mix 2a and Mix 4a (Gunasekara 2016). Even though based on section 6.3.1, it is expected to have larger initial time lags in Mix 2a and Mix 4a due to their low Ca contents compared to the respective main mixes, the lower mechanical properties have endorsed almost zero-time lag in expansion curves of both subsidiary mixes. However, the effect of low Ca content showed up in Mix 4a as it only managed to achieve 50% of the final expansion of Mix 4. Mix 2 and Mix 2a have shown almost similar final expansions as both have substantially low Ca contents. This is further reinforced by the SEM/EDS analysis results as ASR gels located in Mix 4 have shown higher Ca contents compared to ASR gels in Mix 4a. Mix 2 and Mix 2a have shown much lower Ca contents as expected. Mix 4 has shown the severest distress followed up by Mix 4a, Mix 2a and Mix 2 which consent with the expansion results. Mix 2 and Mix 2a have severe crack formations inside the binder despite showing no substantial distresses in aggregate which might be due to the low Ca content as described in section 6.3.1. Mix 4a also shows comparatively higher crack formation inside the binder as expected due to its lower Ca contents.

### **6.3.4 Effect of curing conditions**

Curing condition clearly has a significant influence on the ASR in geopolymer mortar. Despite having a high initial alkali content, it is clear that geopolymer may not possess any greater threat of ASR compared to OPC since geopolymer mixes exposed to both water and 0.003M NaOH haven't shown any compelling expansions even after 150 days. In fact, geopolymer has shown comparatively lower expansions even when exposed to 1M NaOH solution indicating a lower risk of ASR compared to OPC.

Mortar bars exposed to curing condition III (1M NaOH saturated with  $\text{Ca(OH)}_2$ ) have exhibited significantly higher expansions in Mix 2 and Mix 3 which reveals that the low expansions observed in Mix 2 and Mix 3 exposed to curing condition I is due to the lack of Ca for the reaction which consent with the mechanism present in section 6.3.1. SEM/EDS analysis results of ASR gels at the aggregate binder interface (see Figure 6-29 and Figure 6-31) further justify the above ASR mechanism as clear Ca accumulations can be spotted at the ASR gel boundaries. Furthermore, SEM images have shown higher distresses in aggregate of Mix 2 and Mix 3 exposed to curing condition III compared to curing condition I as predicted by the proposed mechanism.

In addition, higher expansions observed in Mix 2 and Mix 3 when exposed to curing condition III reveals that the external Ca supply might able to trigger a deleterious alkali silica reaction in geopolymer binders. Thus, aggregates with Ca possess a significantly high ASR risk when used with geopolymer binders as they might supply Ca to the system.

### **6.3.5 Role of Aluminium**

As described by several researchers, earlier aluminium may have several indirect influences on the ASR; reducing the Si dissolution, reduce free Ca content by the formation of CASH, reduce permeability etc. (Rajabipour et al. 2015). In addition, throughout this study, Al has become a consistent constituent of ASR gel which indicates Al might reduce the swelling properties of ASR gel. As in geopolymerization process, Al has the ability to form crosslinks which might reduce the swelling properties of the gel; first by restricting the swelling behaviour with more bonds and then by restricting the attachment of water ions. However, the role of aluminium needs to be analysed extensively before concluding its effects on the ASR in geopolymer mortar.

### **6.3.6 Validation of standard expansion test methods**

Expansion results in Figure 6-1 indicate that geopolymer binder requires a significantly larger period of time for expansion to start compared to OPC system. Thus, accelerated test results obtained according to existing standard can probably lead to erroneous conclusions on the ASR susceptibility of geopolymer binders as their specified testing period may not be sufficient to detect any substantial expansion.

The mortar bar images of Mix 4 (fly ash/GGBFS = 1) and Mix 1 (OPC mix) suggest that the crack widths are lower in Mix 1 despite showing a higher expansion. This could be due to the quasi-brittle behaviour of the zeolitic structure of geopolymer mortar compared to OPC mortar, which was reported by several researchers (Fernandez-Jimenez et al. 2006; Noushini et al. 2016; Pan et al. 2011). Thus, geopolymer mortar tends to show severe distresses compared to OPC mortar once the internal stresses exceed the threshold limit of mortar which means that the expansion limits stipulated in existing standard test might have to be revised for geopolymer mixes

## **6.4 Summary**

This Chapter focused on the probable alkali silica reaction in geopolymer mortar with natural reactive aggregate. Analysis on ASR is primarily based on the accelerated mortar bar test results and the SEM/EDS analysis results of representative samples. Aggregate quarried from Culcairn, Australia were used in this study to represent the natural reactive aggregate category. Standard accelerated mortar bar test (AS 1141.60.1) results and chemical analysis (XRF and XRD) results confirmed the alkali silica reactivity of Culcairn aggregate with OPC.

Expansion results suggest that Geopolymer mixes have lower ASR potential compared to the standard OPC mix (Mix 1). Furthermore, test results clearly demonstrated that the risk of ASR in geopolymer mixes increase with the GGBFS content (Ca content) in the mix. In fact,

providing the very harsh conditions in AMBT, it can be safely assumed that the risk of ASR in geopolymer mortar with GGBFS content less than  $61.5 \text{ kg/m}^3$  is very low. However, it should be noted that, even with significantly higher ASR expansions observed in other two geopolymer mixes (Mix 3 and Mix 4), it is still inappropriate to draw conclusions on their reactivity because of the severe curing conditions in AMBT.

SEM/EDS analysis on the representative samples at 150 days further confirmed the occurrence of ASR in mixes. Geopolymer mixes showed low Ca and high Al ASR gel formations compared to OPC that aggravate with time which might explain the lower expansions (as describe in Section 6.3.1 and 6.3.5) observed in geopolymer specimens. In addition, the pattern of gel formation identified at 21 days (no gel formation in Mix 2, minor formation in Mix 3 and significantly high formation in Mix 1 and Mix 4) aligned with the ASR mechanism described in Section 6.3.1. In fact, excessive expansions in Mix 2 and Mix 3 when exposed to curing condition III and the Ca rich ASR gel ring formed at the aggregate binder interface closed to binder fortified the vital role in Ca in ASR.

Geopolymer mixes have shown an initial time lag in expansion development which is due to the combined effect of high mechanical properties (depicted by high strength gain), and low Ca content in the mix. The effect of mechanical properties on the expansion curve is analysed further in Section 6.3.3. and effect of Ca is discussed in Section 6.3.4. In addition, test results of curing condition II revealed that the internal alkalis alone won't cause any severe ASR in geopolymer mortar. Therefore, aggregates classified as nonreactive with OPC can be used with geopolymer without having any additional risk. Furthermore, the test results suggest that geopolymer mortar exhibits quasi- brittle behaviour in stress-strain relationship which clearly indicated the need of modification in expansion limits of any expansion tests before adopting them in the geopolymer mortar.

# CHAPTER 7 : Alkali aggregate reaction in manufactured reactive aggregate

---

## 7.1 Overview

Aggregate is the most quarrying product in the world based on the statistical data published by the National Institute for Occupational Safety and Health (CDC). The numbers are expected to grow exponentially due to the increasing demand for concrete which is the primary consumer of aggregate (Neves 2016; Saha & Sarker 2017). It is well established that excessive aggregate mining has led to many socio-economic and environmental issues which urge researchers to develop alternatives to natural aggregate (Langer & Arbogast 2002).

Being a by-product of nickel refining process, ferronickel slag is a potential substitute for natural aggregate in concrete (Katsiotis et al. 2015; Saha & Sarker 2016). In addition, the disposal crisis due to the expanding industrial waste generation has also braced the utilisation of industrial by-products effectively (Katsiotis et al. 2015). However, even though air-cooled ferronickel slag aggregate performed satisfactorily against alkali silica reaction, experimental studies show that water cooled (rapidly cooled) ferronickel slag aggregate have shown excessive expansion when used in OPC mixes (Choi & Choi 2015; Saha & Sarker 2016). It is believed that the amorphous silica particles formed during the rapid cooling process may provide significant amount of Si into the system which results in excessive distress due to ASR gel formations (Choi & Choi 2015; Saha & Sarker 2016).

Societe Le Nickel (SLN) has supplied rapidly cooled ferronickel slag aggregate for this study which was manufactured at their nickel refining plant in New Caledonia. XRF

analysis (refer Table 3-4) reveals that aggregate mainly consists of silicon (Si), magnesium (Mg) and iron (Fe). XRD analysis (see Figure 3-11) indicates the formation of magnesium iron silicates (forsterite) which is the most stable phase among two common chemical phases in ferronickel slag aggregate: forsterite and enstatite (Choi & Choi 2015). Even though there is a lot of Mg in the system, the formation of brucite ( $\text{Mg}(\text{OH})_2$ ) is restrained by the forsterite phases (Choi & Choi 2015). Si dissolution test results for ferronickel slag consent with the availability of amorphous silica in the system as both ferronickel slag and fused silica (pure amorphous silica) have shown almost similar Si dissolutions (see Figure 4-2). The SEM images also confirm the availability of spherical shape amorphous silica among aggregate as shown in Figure 3-12. Thus, it is expected to have deleterious alkali silica reaction in mortar specimens cast with ferronickel slag aggregate.

Four mortar mixes, one OPC mix (based on AS 1141.60.1) and three geopolymer mixes with fly ash to GGBFS ratio 9, 4 and 1 (see 3.3.1.3 for mix design details) were used to identify the alkali aggregate reaction in mortar with ferronickel slag aggregate. For each mix design, at least six mortar bar specimens were casted, 5 for continuous expansion measurements up to 150 days and one to be extracted at 21 days to perform microstructural analysis. 12 mortar cubes were cast for compressive strength measurement at different times up to 29 days. All the mortar specimens were exposed to similar testing conditions as described in section 3.3.1.

## 7.2 Result and analysis

### 7.2.1 Expansion test

The average expansions of mortar bars with ferronickel slag aggregate over 150 days is presented in Figure 7-1. Error bars at each data points shows the standard deviation from the mean value. It should be noted that all standard deviations presented in Figure 7-1 are very low. The red horizontal line at 0.1% represents the minimum expansion limit specified in AS 1441.60.1 to be categorized as alkali silica reactive. Prolonged testing period (150 days) was adopted for the expansion testings to identify any late booms in the expansion curves which was often observed in geopolymer systems (Fernández-Jiménez & Puertas 2002).

Table 7-1 showcases the average mortar bar expansions of mix 1-4 at 10, 21 and 150 days. Mix 1, the standard OPC mix has shown the highest average final expansion of 1.2256% followed by Mix 3, Mix 2 and Mix 4 respectively. The average mortar bar expansion of Mix 1 exceed the 0.1% limit within 10 days reaching 0.3128% and the 0.3% limit within 21 days reaching 0.8204% which categorised the ferronickel slag aggregate among highly reactive aggregates based on AS 1141.60.1 (AS1141.60.1 2014). This is in agreement with the literature (Choi & Choi 2015; Saha & Sarker 2016), preliminary test results (XRD and XRF analysis) shown in section 3.2.3.3 and Si dissolution test results present in section 4.3.1 which endorse the presence of amorphous silica in water-cooled ferronickel slag aggregate. Geopolymer mortar bars (Mix 2-4) have shown significantly lower expansions compared to Mix 1. In fact, none has reached the 0.1% limit even at 21 days which suggests a significantly lower risk of alkali silica reaction in geopolymer mortar compared to OPC mortar.

Table 7-1 : Average expansion of mortar bars at 10, 21 and 150 days

	Average expansion		
	10 days	21 days	150 days
Mix 1	0.3128 %	0.8204 %	1.2256 %
Mix 2	0.0101 %	0.0312 %	0.2021 %
Mix 3	0.0265 %	0.0712 %	0.2555 %
Mix 4	-0.0176 %	-0.0024 %	0.1594 %

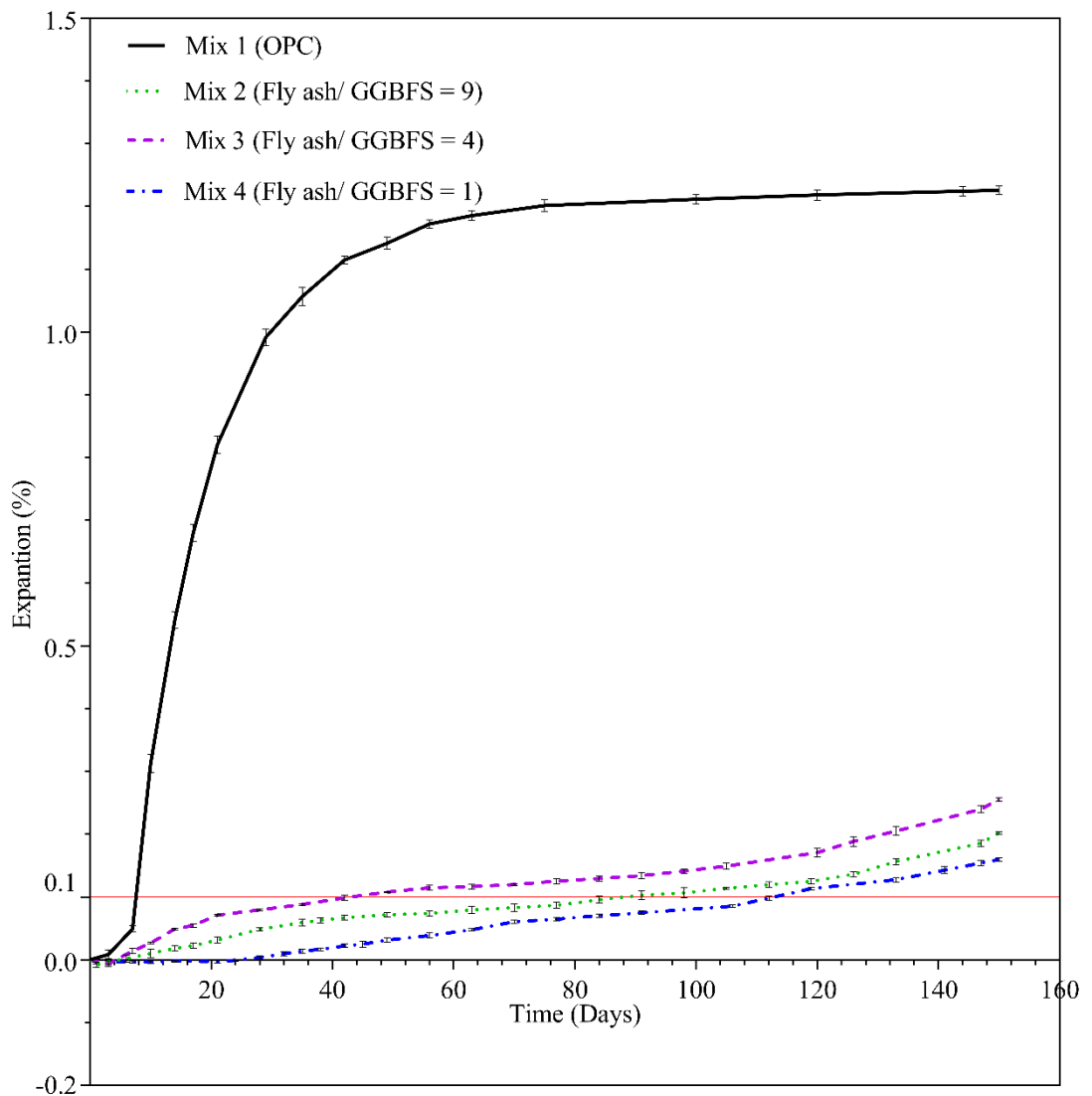


Figure 7-1 : Expansion characteristics of mix 1-4 over 150 days when exposed to accelerated curing conditions. 0.1% (red line) is the minimum expansion limit for reactivity stipulated in AS 1141.60.1.

Expansion curve of Mix 1 follows a sigmoidal shape (S shape); initial phase with low expansion, intermediate phase with rapid expansion and final phase with stabilised expansion. It should be noted that even though there are three distinct phases visible in the expansion curve of Mix 1, it is difficult to separate them as the curve developed smoothly over the testing period. Mortar bars of Mix 1 have achieved more than 98% of the final expansion during the first half (75 days) of the testing period and then entered to an almost stabilised final phase.

Geopolymer mixes (Mix 2-4) have shown significantly lower expansion compared to the OPC mix as Mix 2-4 have only reached 16.5%, 20.8% and 13.0% of the final expansion of Mix 1 respectively. Both Mix 2 and Mix 3 initially went through a similar negative expansion period ( about 5 days) before exhibiting a positive expansion. Meanwhile, expansion curve of Mix 4 displays a prolonged negative expansion period (approximately 25 days) compared to other two mixes. Mix 3 displayed a slightly higher initial expansion compared to the Mix 2 but the expansion curves of Mix 2 and Mix 3 became almost similar approximately after 20 days. Mix 4 has also shown a similar expansion increment to Mix 2 and 3 after the initial time lag which illustrates that expansion of Mix 4 always lags behind the other mixes. However, none of the geopolymer mixes (Mix 2-4) has shown a decrease in expansion rate which indicates that all components for ASR are still available in the systems even though expansion gain is very low.

### **7.2.2 Compressive strength variation**

Figure 7-2 displays the compressive strength variation of mixes 1-4 over 29 days after casting (28 days in NaOH solution). 50mm x 50mm x 50mm mortar cubes were cast along with the mortar bars and exposed to a similar curing conditions (1M NaOH at 80 °C) before testing them at 1 day, 8 days, 22 days and 29 days to determine the

corresponding compressive strengths. At least three mortar cubes were crushed and the averaged to deduce each compressive strengths. Standard error calculated for each data point based on the standard deviation is also present in Figure 7-2. It should be noted that the standard errors shown in Figure 7-2 are very low compared to the corresponding compressive strengths.

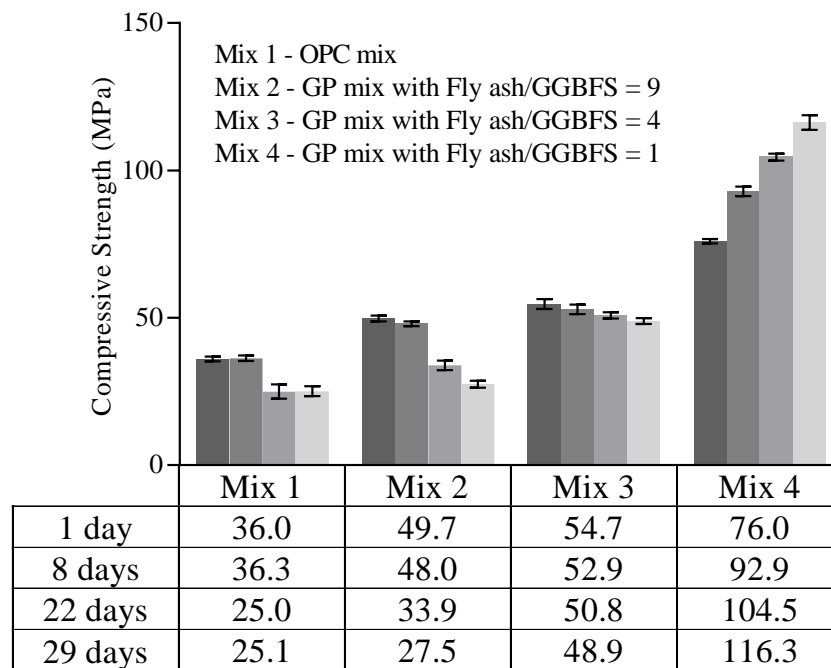


Figure 7-2 : Compressive strength variation of mix 1-4 over 29 days after casting

Mix 1, the OPC mix has shown the lowest initial compressive strength among four mixes while Mix 4 exhibits the highest initial strength followed by Mix 3 and Mix 2 respectively as illustrated in Figure 7-2. The initial strength of the geopolymer mortar mixes increases with the GGBFS content in the mix design as suggested by many researchers earlier (Deb et al., 2014, Diaz et al., 2010). All the mixes except Mix 4 have shown a reduction in compressive strengths over the time. However, the magnitude of strength reduction varies from one mix to another. Mix 2 has shown the highest reduction

of 44.7% followed by Mix 1 with 30.3% and Mix 3 with 10.6% strength losses over 28 days. Strength reductions observed in Mix 1-3 might be the result of crack formations due to ASR (see Figure 7-16). The compressive strength of Mix 4 increases with time to reach 116 MPa after 29 days of casting which allows it to have considerably high elastic modulus and yield stress compared to other three mixes (Gunasekara 2016; Phoo-ngernkham et al. 2013). It should be noted that the compressive strength may depict the mechanical performance of mortar specimens at early stage before the formation of cracks.

### **7.2.3 Scanning Electron Microscope (SEM) Analysis**

Microstructural analysis with scanning electron microscope was performed to identify microcracks and ASR gel formation inside the mortar specimens extracted at 21 days and 150 days. Furthermore, Energy-dispersive X-ray spectroscopy (EDS) with backscatter detector was used to determine the chemical composition of ASR gel identified during the SEM analysis.

All mixes (Mix 1-4) have shown significant ASR gel formation at both 21 days and 150 days. ASR gel was identified inside the aggregate, at the aggregate binder interface and inside the binder as shown in Figure 7-3. However, during the microstructural analysis, priority was given to the ASR gel formed inside the aggregate to avoid any interference between geopolymer binder and ASR gel as clearly visible in Figure 7-12 and 7-13. Figure 7-4 to 7-11 are backscatter EDS line profiles of ASR gel identified inside the aggregate of Mix 1-4 respectively. Figure 7-12 and Figure 7-13 are backscatter EDS line profiles of ASR gel located at the aggregate binder interface and inside binder respectively of Mix 3 at 150 days. Being a common element in all products, oxygen (O) is omitted from the EDS line profiles (see Figure 7-4 to 7-13).

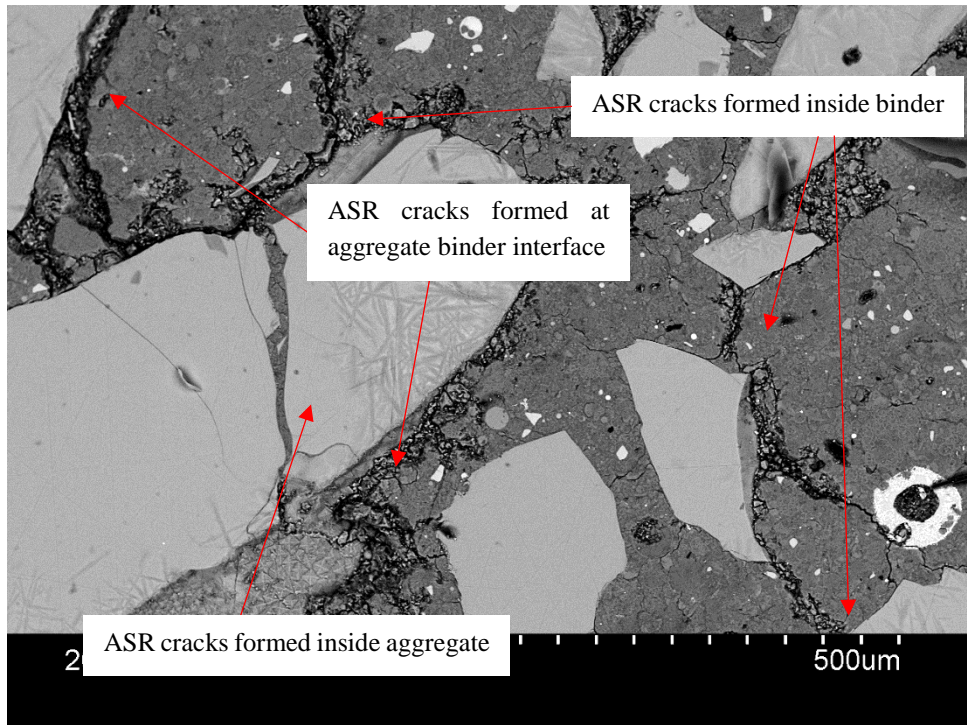


Figure 7-3 : ASR cracks identified in different locations of Mix 3 at 150 days

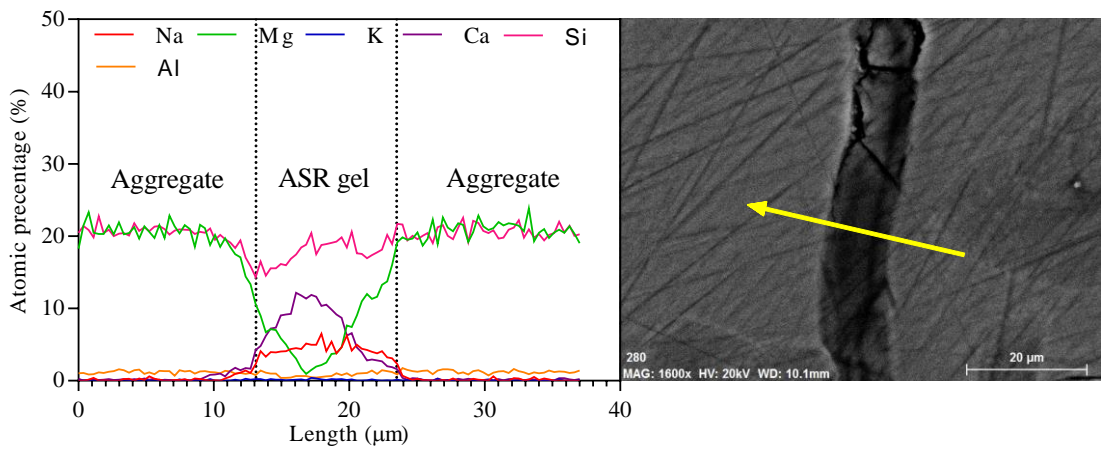


Figure 7-4 : ASR gel identified inside aggregate of mix 1 at 21 days

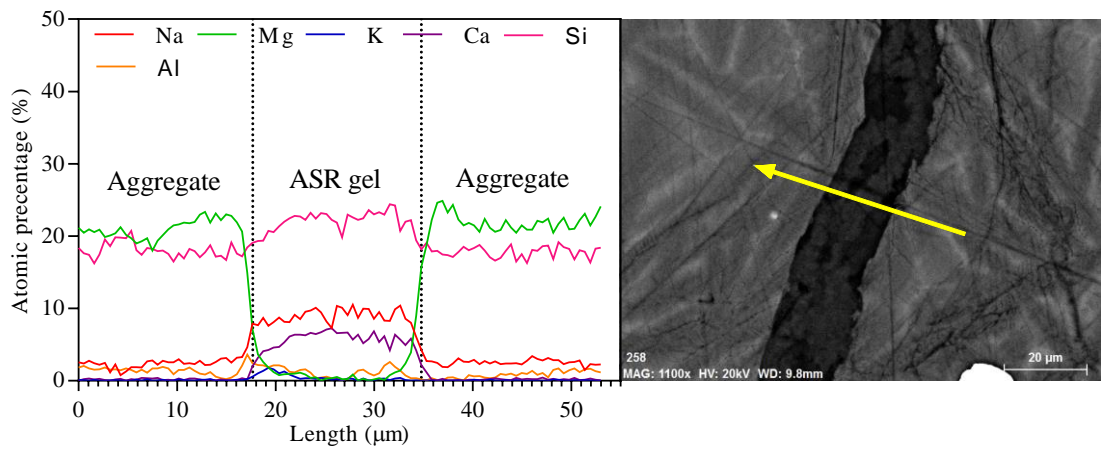


Figure 7-5 : ASR gel identified inside aggregate of mix 1 at 150 days

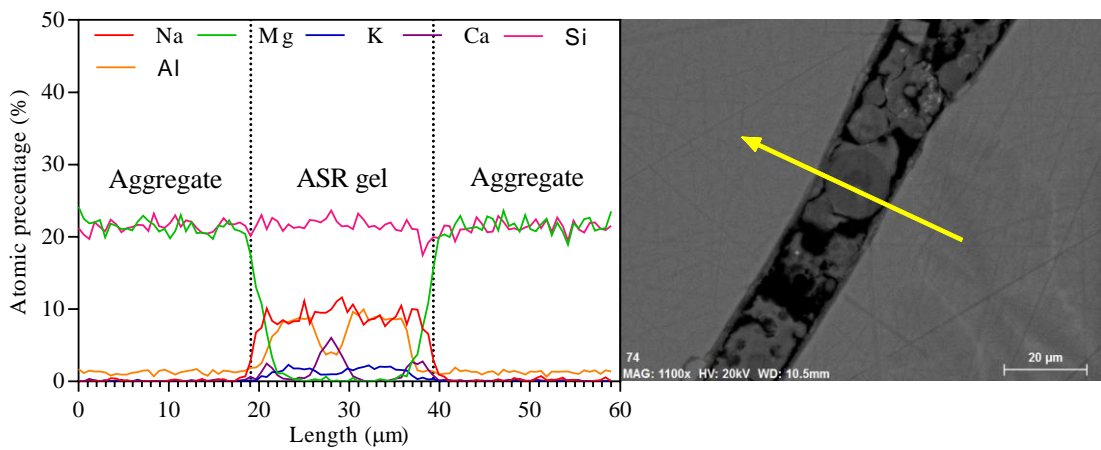


Figure 7-6 : ASR gel identified inside aggregate of mix 2 at 21 days

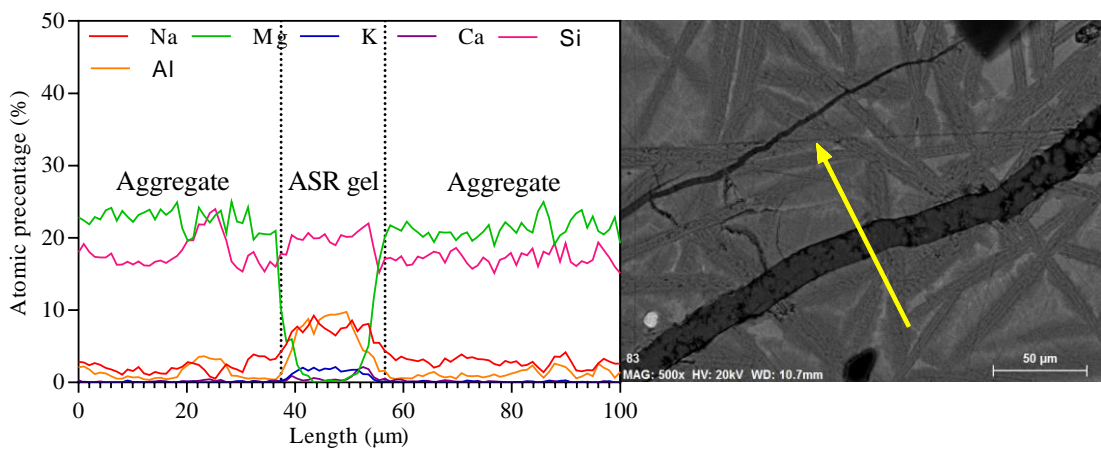


Figure 7-7 : ASR gel identified inside aggregate of mix 2 at 150 days

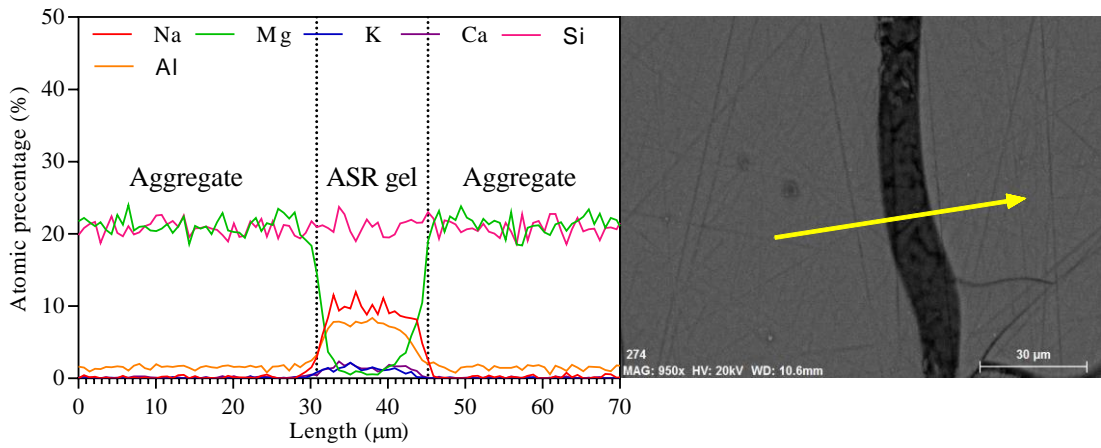


Figure 7-8 : ASR gel identified inside aggregate of mix 3 at 21 days

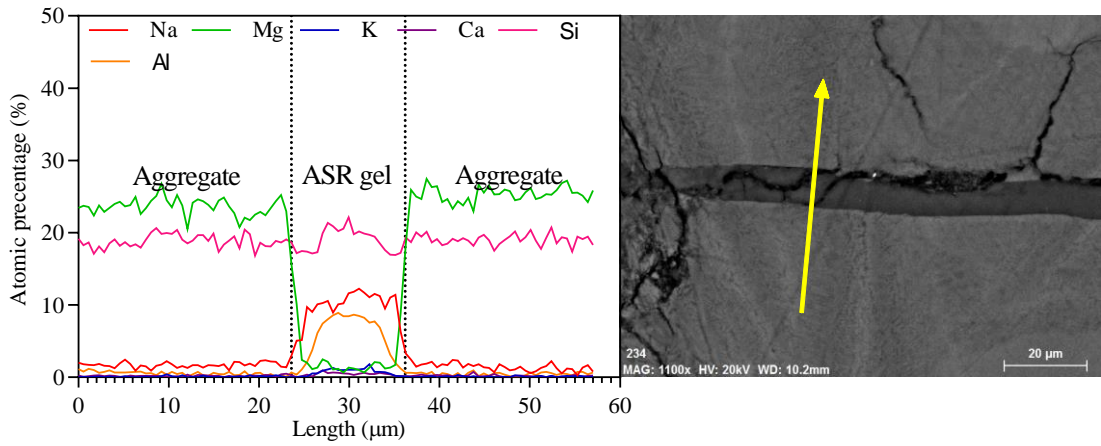


Figure 7-9 : ASR gel identified inside aggregate of mix 3 at 150 days

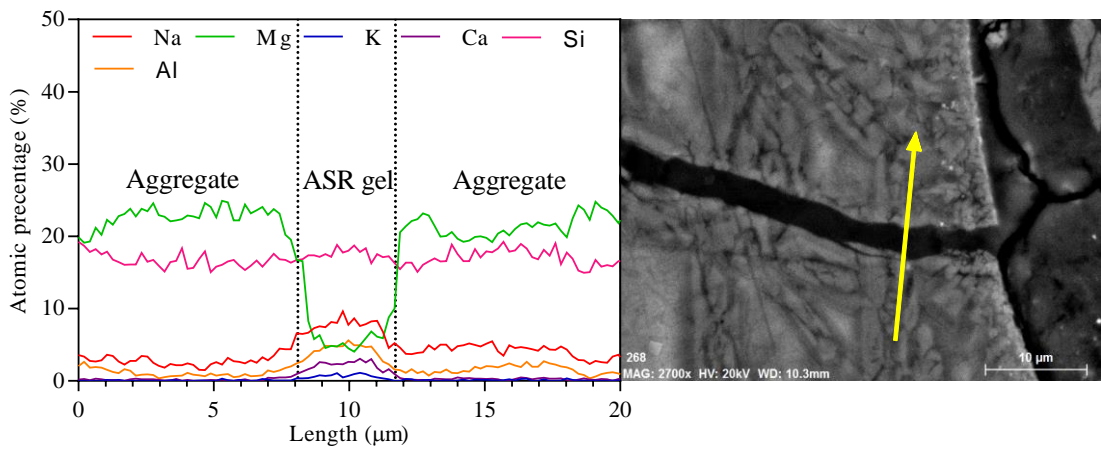


Figure 7-10 : ASR gel identified inside aggregate of mix 4 at 21 days

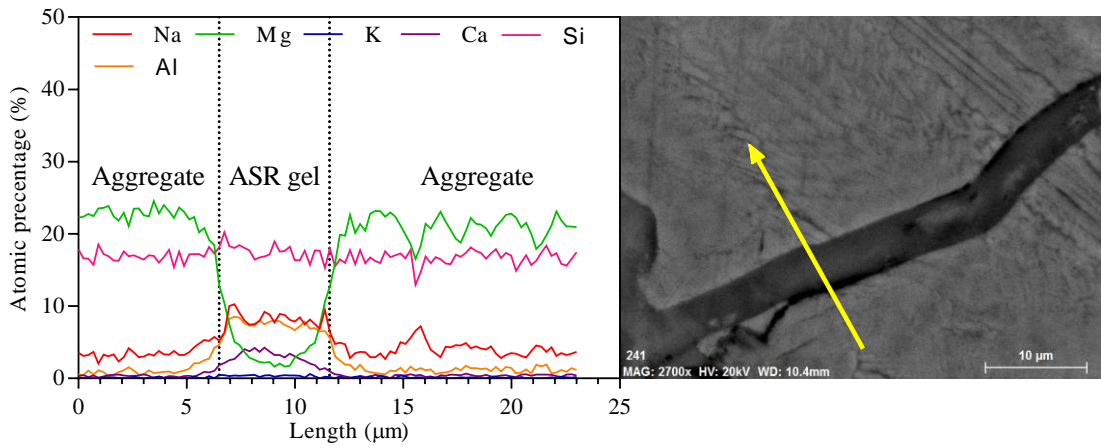


Figure 7-11 : ASR gel identified inside aggregate of mix 4 at 150 days

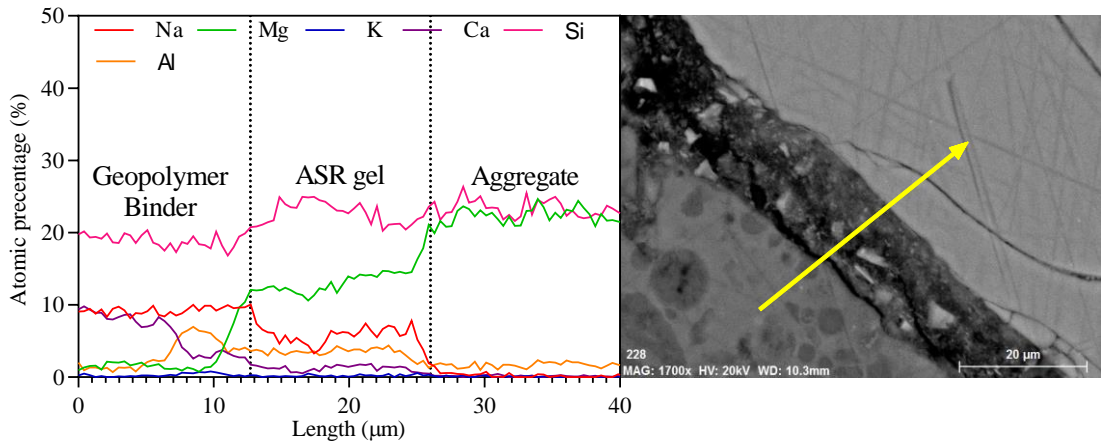


Figure 7-12 : ASR gel identified in aggregate binder interface of Mix 3 at 150 days

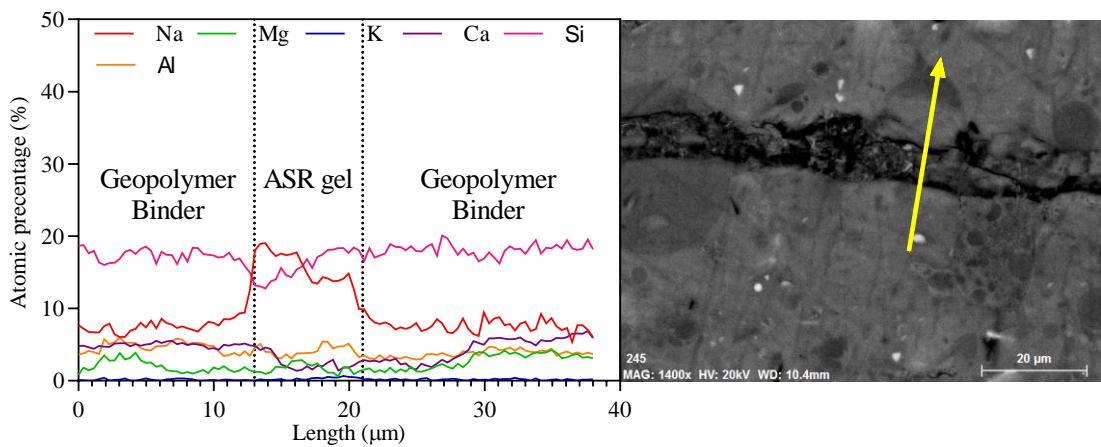


Figure 7-13 : ASR gel identified inside the binder of Mix 3 at 150 days

Table 7-2 summarises the elemental atomic percentages of ASR gel identified in Mix 1-4. Approximately 250 data points of ASR gel formed inside aggregate were averaged to obtain the elemental compositions shown below in Table 7-2. Figure 7-14 contains the ternary diagrams plotted from the data in Table 7-2 in order to identify the correlation between elements in ASR gel and their variation with respect to the mix and exposure time. Figure 7-15 shows the variation of Ca/Si ratio with Na+K/Si ratio over the time in Mix 1-4. This graphical representation of the atomic composition of ASR gels allow an easy comparison with published works. Indeed, the shaded area shown in Figure 7-15 corresponds to the ASR compositions published in the literature (Leemann et al. 2016; Leemann & Lura 2013; Leemann & Merz 2013; Thaulow et al. 1996).

Table 7-2 : Summary of SEM /EDS analysis on ASR gel located in mix 1-4

Mix No.		Average atomic percentage (%)						Ratios		
		Na	K	Ca	Mg	Si	Al	$\frac{(Na+K)}{Si}$	$\frac{Ca}{Si}$	$\frac{Al}{Si}$
1	21 days	4.24	0.14	6.99	7.36	17.90	0.87	0.25	0.39	0.048
	150 days	8.71	0.45	5.52	1.84	21.90	1.21	0.42	0.25	0.055
2	21 days	8.60	1.31	1.50	2.85	21.48	6.18	0.46	0.07	0.288
	150 days	6.97	1.32	0.68	4.35	19.53	6.20	0.42	0.03	0.317
3	21 days	8.48	1.10	1.35	4.29	21.15	6.32	0.45	0.06	0.299
	150 days	9.24	0.68	0.42	3.53	18.96	5.36	0.52	0.02	0.283
4	21 days	7.38	0.61	2.07	9.35	17.46	3.97	0.46	0.12	0.227
	150 days	8.07	0.35	2.81	4.93	17.64	5.77	0.48	0.16	0.327

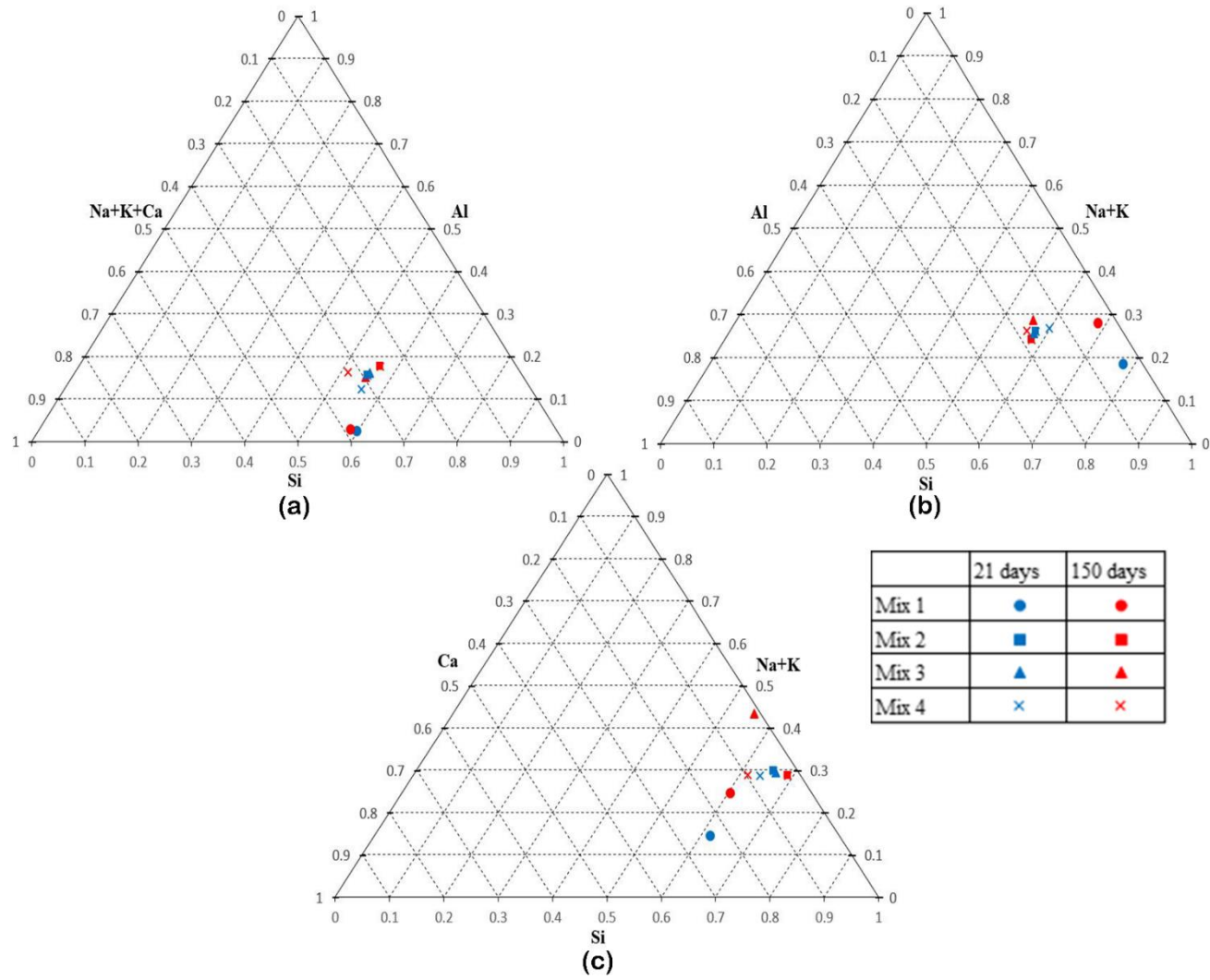


Figure 7-14 : ASR gel composition interpreted in a ternary diagram

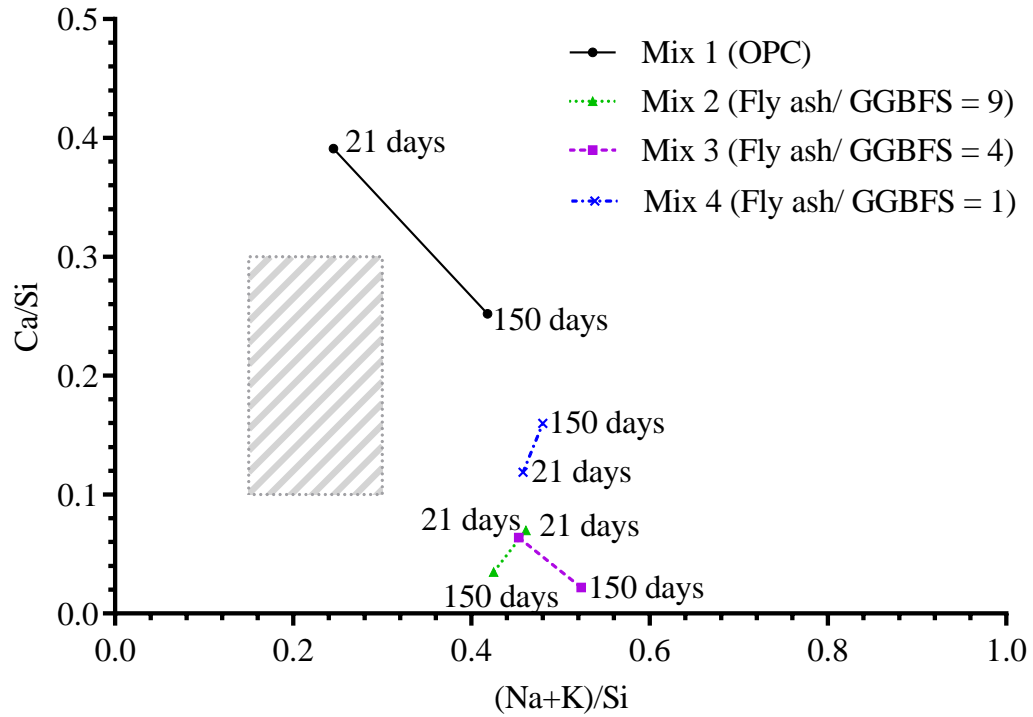


Figure 7-15 : Variation in Na+K/Si vs. Ca/Si (atomic ratio) of ASR gels at 21 days and 150 days from Mix 1-4; shaded area is the alkali silica gel compositions developed base on Thaulow et al. (1996), Leemann et al. (2016), Leemann and Lura (2013) and Leemann and Merz (2013)

Alkali silica gel in OPC typically consists of calcium (Ca), sodium (Na), Potassium (K) and silicon (Si) with (Na+K)/Si and Ca/Si ratios in the range of 0.15~0.3 and 0.10~0.3 respectively (Leemann et al. 2016; Leemann & Lura 2013; Leemann & Merz 2013; Thaulow et al. 1996). However, in geopolymer binders, aluminium (Al) also becomes a significant element as observed throughout this study. Table 7-2 indicates a high magnesium (Mg) content in ASR gel located inside the ferronickel slag aggregate. But EDS line profiles (Figure 7-4 to 7-11) reveals that Mg accumulates only at the gel boundaries which might be due to the high Mg content in ferronickel slag aggregate. This was further reinforced by the EDS line profile of ASR gel inside the binder (Figure 7-13)

which indicates a substantially low Mg content compared to Na and Si. Thus, Mg is not considered in the composition analysis in Figure 7-14 and 7-15.

Based on Figure 7-15 it is clear that none of the mixes has shown ASR gel composition within the above range reported by various researchers. ASR gel in Mix 1 consist of high Ca content despite having (Na+K)/Si ratio within the defined region. Over the time, the Na content of ASR gel in Mix 1 increases to exceed the upper limit while Ca/Si ratio falls into the expected range. This is quite understandable given the fact that OPC mortar specimens have an infinite supply of Na and high but still a limited amount of free Ca compared to free Na. All geopolymer mixes have shown very high (Na+K)/Si ratios (ranging from 0.42~0.52) which might also be due to the infinite supply of Na offered by the 1M NaOH solution. Mix 2 and 3 have shown very low Ca/Si ratios due to substantially low GGBFS contents while Ca/Si ratios of ASR gel in Mix 4 at 21 days and 150 days lie in the above defined range ( $>0.1$ ) since Mix 4 has considerably high Ca content compared to other two geopolymer mixes. Tertiary diagrams in Figure 7-14 also indicates a similar outcome.

Aluminium (Al) becomes a significant element in ASR gel formed in geopolymer mortar with Al/Si ratio ranging from 0.227 to 0.327. ASR gel in OPC specimens showed considerably lower Al/Si ratios (0.048~0.055) compared to the above range. This might be due to the availability of substantial amount of free Al in geopolymer systems compared to OPC since both fly ash, and GGBFS may provide Al to the system.

Backscatter SEM images of mortar specimens correspond to Mix 1-4 at 21 days and 150 days are shown in Figure 7-16. The magnification of the SEM images was fixed at 100 to simplify the distress analysis.

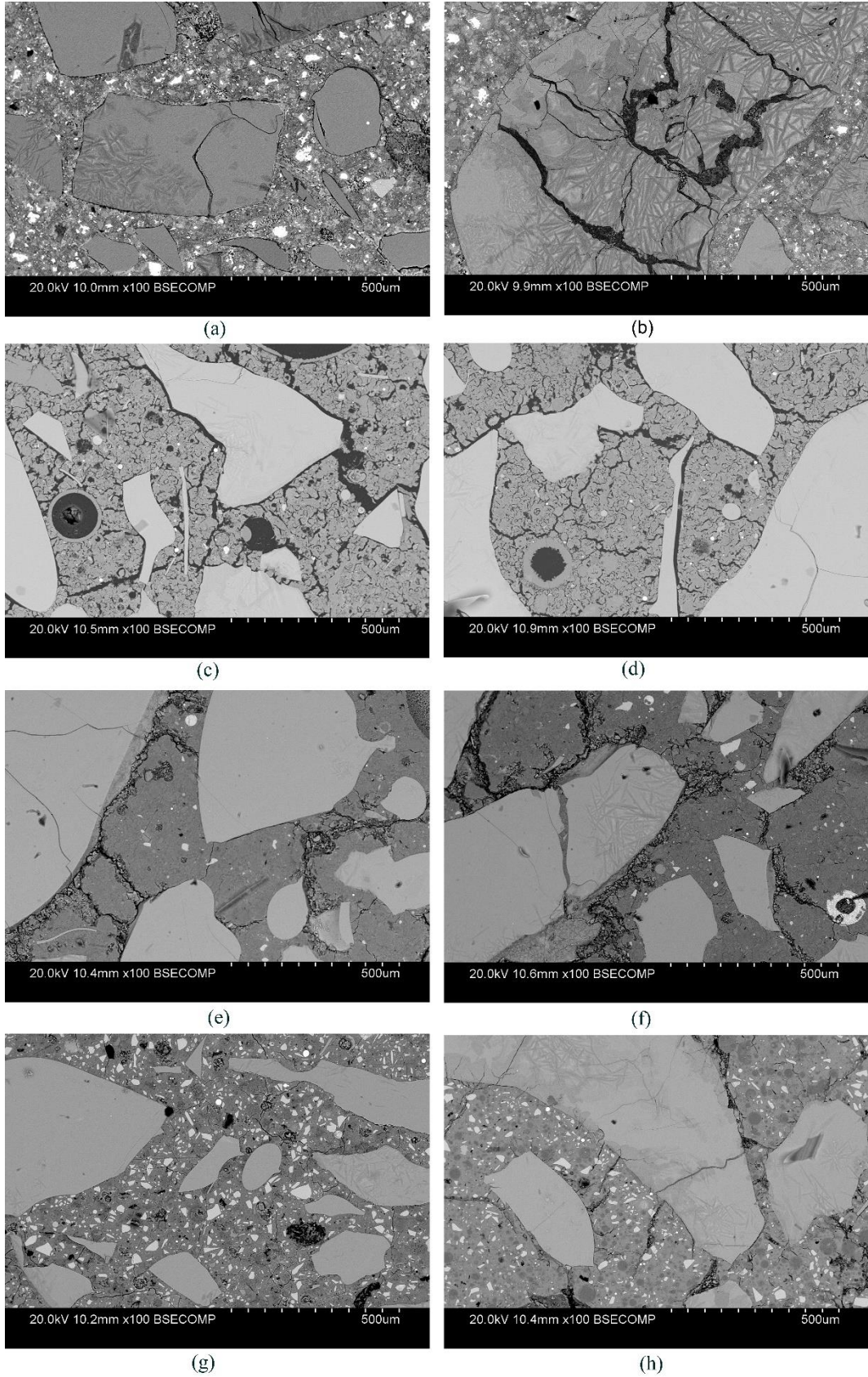


Figure 7-16 : Micro crack propagation in mix 1-4; (a) SEM image of mix 1 at 21 days, (b) SEM image of mix 1 at 150 days (c) SEM image of mix 2 at 21 days, (d) SEM image of mix 2 at 150 days, (e) SEM image of mix 3 at 21 days, (f) SEM image of mix

3 at 150 days, (g) SEM image of mix 4 at 21 days, (h) SEM image of mix 4 at 150 days,

All specimens except Mix 4 at 21 days have shown distresses particularly in the aggregate. Furthermore, all mixes have shown clear microcrack development over the time which might be due to the formation of ASR gel. Mix 1 (OPC mix) has shown the highest distress among all. However, microcrack propagations in OPC specimens were limited to aggregate. Mix 3 has shown the highest microcrack formation inside aggregate among geopolymer mixes which consent with the expansion results. Even though Mix 2 has shown lots of microcracks in the binder, there were not many crack formations inside the aggregate. Mix 4 has demonstrated clear stress development in the mortar as well as inside the aggregate at 150 days despite having no significant crack developments at 21days. It should be noted that all mixes except Mix 4 have shown significant crack formation even at 21 days which explains the early strength losses observed in Mix 1-3 (see Figure 7-2).

#### **7.2.4 Mortar bar images**

Mortar bar images of Mix 1-4 after the test are shown in Figure 7-17. Mix 1 and Mix 3 has displayed the characteristic map cracking identified in ASR affected structures (HB79 2015). Mix 1 shows the severest crack formation followed by Mix 3 which consent with the expansion results. No crack formation was identified in mortar bars of Mix 2 and Mix 4 even though mortar bar surfaces of Mix 2 is clearly deteriorated due to surface scaling.



Figure 7-17 : Mortar bar images of mix 1-4 after the test (150 days); (a) Mix 1 at 150 days, (b) Mix 2 at 150 days, (c) Mix 3 at 150 days, (d) Mix 4 at 150 days

### 7.3 Discussion

Ferronickel slag aggregate used in this study was identified as highly alkali silica reactive due to the availability of amorphous silica particles in the system. The chemical analysis results in section 4.3.1 confirmed the high Si dissolution capability of ferronickel slag aggregate since it offers almost similar amount of Si ions to the system as fused silica which is considered as a pure amorphous silica source. Spherical shaped amorphous silica particles in ferronickel slag aggregate was identified during the SEM analysis on the aggregate (see Figure 3-13).

Expansion test results of Mix 1 which followed the standard accelerated mortar bar test specified in AS 1141.60.1, fortified the high alkali silica reactivity of ferronickel slag aggregate as the average mortar bar expansion of Mix 1 exceeded 0.1% reaching 0.3128% within the initial 10 days (AS1141.60.1 2014). Expansion curve of Mix 1 in Figure 7-1 reassembles the characteristic sigmoidal curve (S shape) of ASR with three distinctive phases; Initial phase with low expansions, intermediate phase with rapid expansion gain and stabilising phase. Initial phase typically depends on two factors:

1. ASR gel pressure development
2. Yield stress of the binder

In accelerated mortar bar test, ASR gel formation mostly depends on Si dissolution rate of aggregate as the system contains ample amount of all the other requisitions. Therefore, due to the high Si dissolution capability of ferronickel aggregate, ASR gel formed almost instantly in Mix 1. In addition, due to the high Ca content in the system, Ca rich ASR gel may also form which acts as a rigid layer facilitating ASR gel accumulation in localized areas and thus, amplifying the stresses inside the mortar (Ichikawa & Miura 2007). SEM/EDS analysis results presented in Figure 7-17a and Figure 7-17b confirmed this pressure development mechanism since severe crack propagation could be identified in aggregate while no distresses were visible inside the OPC binder. Yield stress is an intrinsic property of the binder which controls the expansion development in mortar bars. Based on the stress-strain relationship of mortar, the expansion development is low until the internal stress exceeds the yield stress. But once the yield stress is exceeded, the expansion increases exponentially with the stress gain which characterises the intermediate phase. The expansion gain dropped substantially towards the end indicating a stabilisation phase most probably due to the lack of Si for the reaction.

All geopolymer mixes have shown significantly low expansions compared to the OPC mix as shown in Figure 7-1. In fact, none of the geopolymer mixes has reached the 0.1% expansion limit during the initial 21 days and thus categorized ferronickel slag aggregate as non-reactive based on AS1141.60.1 (AS1141.60.1 2014). Mix 3 (Fly ash/GGBFS = 4) has shown the highest final expansion; 0.2555% followed up by Mix 2 (Fly ash/GGBFS = 9) and Mix 4 (Fly ash/GGBFS = 1) with 0.2021% and 0.1594% expansion respectively. Expansion curves of Mix 2 and Mix 3 consist of approximately similar negative expansion periods; 5 days whereas Mix 4 associated with a prolonged negative expansion period of 25 days. Despite having slightly higher initial expansion

development in Mix 3, expansion curves of all three mixes seems to increase at approximately similar rate without having any exponential expansion increments. Therefore it is possible to deduce that none of the geopolymer mixes has entered the intermediate phase as observed in OPC mix.

The initial negative expansion period in geopolymer expansion curves depend on several factors; resistive threshold pressure of mortar, the rate of ASR pressure generation and magnitude of autogeneous shrinkage. Threshold resistive pressure is governed by the compressive strength of mortar which indicates that Mix 4 may have the highest resistive pressure followed up by Mix 3 and Mix 2. It should be noted that the resistive threshold pressure of Mix 3 and Mix 2 might be similar as depicted by their similar compressive strengths. ASR pressure development depends on the Ca content in the system based on the theory presented in section 6.3.1. However, due to the high Si dissolution rate of ferronickel slag aggregate, gel pressure development might be more or less similar in all three mixes. Zheng (2009) stated that the autogeneous shrinkage of geopolymer mortar increases with the GGBFS content in the mix design. Thus, despite generating higher gel pressure due to higher Ca content, high resistive threshold pressure combined with high shrinkage enforced Mix 4 to have a prolonged negative expansion period (see Figure 7-1). Mix 2 and Mix 3 have shown a high early expansion gain before settling down with more or less similar expansion increment. Mix 3 has shown the higher expansion increment among the two mixes which might be due to the higher Ca content in the system since Ca amplify the ASR gel pressure by constraining them as discussed further in section 6.3.1. However limited amount of Ca in the system holds the mechanism prematurely which might result in a drop in expansion rate. Having significantly higher Ca content in the system due to the high GGBFS content, Mix 4 is expected to show much higher expansion increment compare to other two mixes after its initial time lag.

However, Mix 4 also compromise with high initial elastic modulus (uncracked) due to high GGBFS content in the mix design (Phoo-ngernkham et al. 2013; Ryno 2014). This is further justified by the significantly higher initial compressive strength development shown in Figure 7-2 (Gunasekara, 2016, Phoo-ngernkham et al., 2013). Thus, based on the stress-strain relationship, Mix 4 tends to display lower initial expansion increment even with higher stress development due to ASR.

The chemical composition of ASR gel in geopolymer mortar mainly consists of alkalis (Na and K), silicon (Si), calcium (Ca) and aluminium (Al). It should be noted that despite having a significant amount of magnesium (Mg), Mg is omitted in the analysis as EDS line profiles clearly show that Mg only present at the gel boundaries which might be due to the high Mg content in aggregate. In fact, ASR gel formed inside the binder shows considerably low Mg content compared to the gel formed inside aggregate (see Figures 7-6 to 7-13).

Figure 7-15 indicates that none of the ASR gels analysed lies within the usual ASR gel composition range in OPC system:  $0.15 < (Na+K)/Si < 0.3$  and  $0.1 < Ca/Si < 0.3$  derived based on past works (Leemann et al. 2016; Leemann & Lura 2013; Leemann & Merz 2013; Thaulow et al. 1996). In fact, 7 out of 8 (Na+K)/Si ratios of ASR gel (except Mix 1 at 21 days) have shown much higher values ranging of from 0.42 to 0.52 as illustrated in Table 7-1. Furthermore, despite having ample amount of Na in the system (Na+K)/Si ratio of ASR gel has not shown a significant increment from 21 days to 150 days. Even though it is not clear with geopolymer mixes due to their low overall expansions, OPC mix has shown that the increase in (Na+K)/Si ratio might result in lower expansion as the expansion increment dropped drastically from 21 days to 150 days while (Na+K)/Si ratio increased from 0.25 to 0.42. Low expansion development with high (Na+K)/Si ratio of ASR gel might be due to either or both of below reasons since (Na+K)/Si ratio deemed

nondetrimental on the free swelling capacity of ASR gel (Gholizadeh-Vayghan & Rajabipour 2017; Struble & Diamond 1981);

1. Formation of low viscous gel (Struble & Diamond 1981)
2. Termination of ASR due to lack of free Si

ASR gel composition in geopolymer is almost similar to that of the geopolymer binder apart from the high sodium (Na) content in ASR gel as visible in Figure 7-12 and 7-13. In fact, Van Deventer et al. (2007) explained that early age geopolymer gels; aluminosilicate oligomers and aluminosilicate amorphous gel later transformed into the zeolitic nanocrystalline phases of geopolymer which might allow ASR gel to blend with existing geopolymer binder limiting the stress development inside the mortar. Furthermore, the formation of a low viscous gel with high (Na+K)/Si ratios as observed in this study enables more efficient gel dispersion into the mortar. GGBFS content has a significant impact on the degree of gel dispersion in geopolymer binders;

1. Reduces the porosity of binder (Luna-Galiano et al. 2016; Provis et al. 2012)
2. Facilitate the CSH formation by supplying Ca to the system which acts as a rigid layer confining the low viscous ASR gel as described in section 6.3.1

Thus, based on above mechanism, it is expected to develop higher stresses in Mix 4 (Fly ash/GGBFS = 1) followed by Mix 3 (Fly ash/GGBFS = 4) and Mix 2 (Fly ash/GGBFS = 9). However, higher elastic modulus of Mix 4 due to higher GGBFS content might explain the lower expansion development compared to other two mixes (Phoo-ngernkham et al. 2013; Ryno 2014). Incorporation of Al in ASR gel might result in a cross-linked network with a dense bond structure as in geopolymer binders which substantially reduces the water binding capacity of ASR gel which is one of the governing factors in the swelling mechanism of ASR gel (Bernal & Provis 2014; HB79 2015). It should be noted that ASR gel in Mix 4 corresponds to the highest Al content with a final Al/Si ratio of 0.327

followed by Mix 2, Mix 3 and Mix 1 with 0.317, 0.283 and 0.055 respectively, which correlates well with the reduction in final expansion of the mortar bars. Therefore, it can be deduced that Al ions reduce the expansiveness of ASR gel which may cause low expansions in Geopolymer mortars.

Mortar bars of Mix 1 and 3 have exhibited the characteristic map cracking of ASR on the surface as shown in Figure 7-17 (HB79 2015). Even though Mix 2 and Mix 4 have not shown any crack formation, surface of the Mix 2 seems deteriorated with scaling of mortar. Aggregate in Mix 1 exhibit severe microcracks formation which might explain the decrease in strength of mortar as illustrated in Figure 7-2. However, binder of the Mix 1 has not shown any noticeable distress despite showing significant expansion increment compared to other mixes which consent with the crack formation mechanism described in section 6.3.1. Mix 2 clearly indicates severe microcracks propagation even at 21 days which led to a significant initial strength drop (31.8% within 21 days) as reflected by the compressive strength reduction over the time. Mix 3 has shown severe distress in both aggregate and binder which is consisting with the expansion and strength results. In spite of having the lowest expansion development, Mix 4 has shown distresses inside both binder and aggregate as shown in Figure 7-16.

Ferronickel slag aggregate is a manufactured aggregate which consist of amorphous silica due to their rapid cooling process. Being true to its expected reactive nature, ferronickel slag has displayed excessive expansions with OPC mortar. However, ferronickel slag aggregate has performed satisfactorily with geopolymer binders even with severe curing conditions in AMBT. But since accelerated mortar bar test is not a conclusive test, the performance of ferronickel slag aggregate in geopolymer concrete must be further tested with concrete prism test before adopting it in construction purposes.

## 7.4 Summary

Use of industrial waste in a productive manner is one of the prime goals in modern world. By product of Nickel refining process, ferronickel slag aggregate is classified as alkali silica reactive with OPC (depicted by standard AMBT results, microstructural analysis with SEM and chemical analysis) and thus cannot be used in construction works. This Chapter analyses the feasibility of ferronickel slag aggregate in geopolymer with respect to ASR.

Geopolymer mixes have shown considerably lower expansion development compared to OPC. Even though all three mixes managed to exceed the 0.1% limit eventually, due to the severe exposure conditions adopted in tests, none of the geopolymer mixes can be classified as ASR susceptible because of the progressions in their expansion curves. However, despite showing lower expansion developments, ASR gel formations were identified in all geopolymer mixes at both 21 and 150 days indicating the occurrence of ASR from the beginning. EDS analysis identified low Ca and high Al contents in ASR gel located in geopolymer mixes compared to the OPC mix which might affect the stress development due to gel formation. Based on the earlier studies, it is believed that Ca has a positive impact on expansion development whereas Al has detrimental influences on the swelling capacity of ASR gel.

On the other hand, all mixes except Mix 4 have shown compressive strength reduction during the initial 29 days which most probably due to the microcrack formation inside mortar. SEM analysis exhibited significantly high microcrack development in geopolymer which might be due its characteristic quasi-brittle behaviour. ASR gel might disperse into these cracks causing low internal stresses and thus low expansion developments. However, it should be noted that the formation of Ca rich ASR gel in OPC

(CSH) might be able to control this gel dispersion based on the reaction rim theory which caused the high expansion development in Mix 1.

## **CHAPTER 8 : Alkali aggregate reaction in fused silica**

---

### **8.1 Overview**

Si dissolution rate of aggregate is one of the governing factors of alkali aggregate reaction in any binder system (Fournier & Bérubé 2000). In fact, based on the mechanisms described in section 2.3.3.1, Si dissolution is the initiation process of alkali silica reaction. Si ion releasing capability of aggregate depends on many parameters including; chemical composition and internal bond structure of aggregate, surface area of aggregate, alkalinity of pore solution, presence of certain ions such as aluminium, temperature and pressure etc (Fournier & Bérubé 2000; Hobbs 1988; Rajabipour et al. 2015). Among all, chemical composition and internal bond structure are the main parameters for aggregate reactivity classification since they only depend on the origin of aggregate. It is obvious that aggregates with higher Si content and weaker bond structure may lead to higher Si dissolution which would lead to higher alkali silica reaction. Internal bond structure of aggregate varies from well-ordered three-dimensional crystalline lattices such as quartz to amorphous phases with no particular order (Hobbs 1988). Fused silica is a glassy material made of amorphous silicon dioxide (refer section 3.2.3.4). Hence, Si dissolution of fused silica shall be higher than that of natural aggregates under similar conditions which was confirmed by the dissolution tests in section 4.3.1. Therefore, using fused silica allows assessing the performance of geopolymer mortar against ASR with highly reactive aggregates which would be the worst-case scenario of alkali silica reaction in geopolymer mortar. Furthermore, the use of fused silica as

aggregate allows assessing the role of the binder on ASR gel formation as fused silica only provides Si ions for the reaction.

Fused silica is a manufactured translucent material supplied by Sila Australia. XRD and XRF analysis confirmed that fused silica is made of amorphous silicon dioxide with more than 98% of purity (refer section 3.2.3.4). Si dissolution test in section 4.3.1 consents with the high Si dissolution capability of fused silica over natural aggregates. Therefore, it is expected to observe significantly higher alkali silica reaction in geopolymer mortar cast with fused silica.

Four mortar mixes were considered: OPC mix as in AS 1141.60.1 (Mix 1) along with three geopolymer mixes with fly ash to slag ratio of 9 (Mix 2), 4 (Mix 3) and 1 (Mix 4). Section 3.3.1.3 contains all details of the respective mix designs. At least five mortar bars were cast from each mix for the expansion measurements along with another mortar bar for SEM/EDS analysis which is carried out at 21 days. 12 mortar cubes were cast and exposed to similar conditions along with the mortar bars to determine the compressive strength variation up to 29 days after casting (28 days of exposure).

## **8.2 Result and analysis**

### **8.2.1 Expansion test**

Figure 8-1 shows the expansions of mortar mixes 1-4 cast with fused silica over 150 days. Expansion curves were developed by averaging at least five expansion values at each data point. Error bars in Figure 8-1 illustrates that the standard deviations of mortar bar expansions at each data point is insignificant. 0.1% is the minimum expansion limit specified in AS 1141.60.1 in order to categorize the aggregate as alkali reactive (AS1141.60.1 2014). Testing time of the standard AMBT is extended to identify any delay in the expansion due to alkai silica reaction.

Table 8-1 summarizes the average mortar bar expansions of mix 1-4 after 10 days, 21 days 100 days and 150 days. The standard OPC mix (Mix 1) has shown the highest average expansions, reaching 1.2924% after 10 days and 1.8072% after 21 days which categorizes fused silica among highly reactive aggregates (AS1141.60.1 2014). In fact, expansions of Mix 1 mortar bars were beyond the measurable limit of the comparator after 21 days which enforces the test to be terminated. This is consistent with the expected expansion behaviour of fused silica based on its chemical composition and internal bond structure (refer section 3.2.3.4). Geopolymer mortar bars (Mix 2-4) have shown significantly lower expansions at 10 days and 21 days. In fact, only Mix 3 exceeded the 0.1% lower limit, but still categorized among slowly reactive aggregates since it hasn't reached 0.3% by 21 days (AS1141.60.1 2014). Thus, even fused silica is categorised as non-reactive when used in geopolymer based on the standard accelerated mortar bar test which further implies that there may not be any risk of ASR in geopolymer binders.

Table 8-1 : Average expansion of mortar bars at 10, 21, 100 and 150 days

	Average expansion			
	10 days	21 days	100 days	150 days
Mix 1	1.2924 %	1.8072 %	-	-
Mix 2	0.0474 %	0.0806 %	0.2395%	0.2910 %
Mix 3	0.0987 %	0.1445 %	0.2614%	0.3432 %
Mix 4	0.0294 %	0.0546 %	0.1775%	1.4023 %

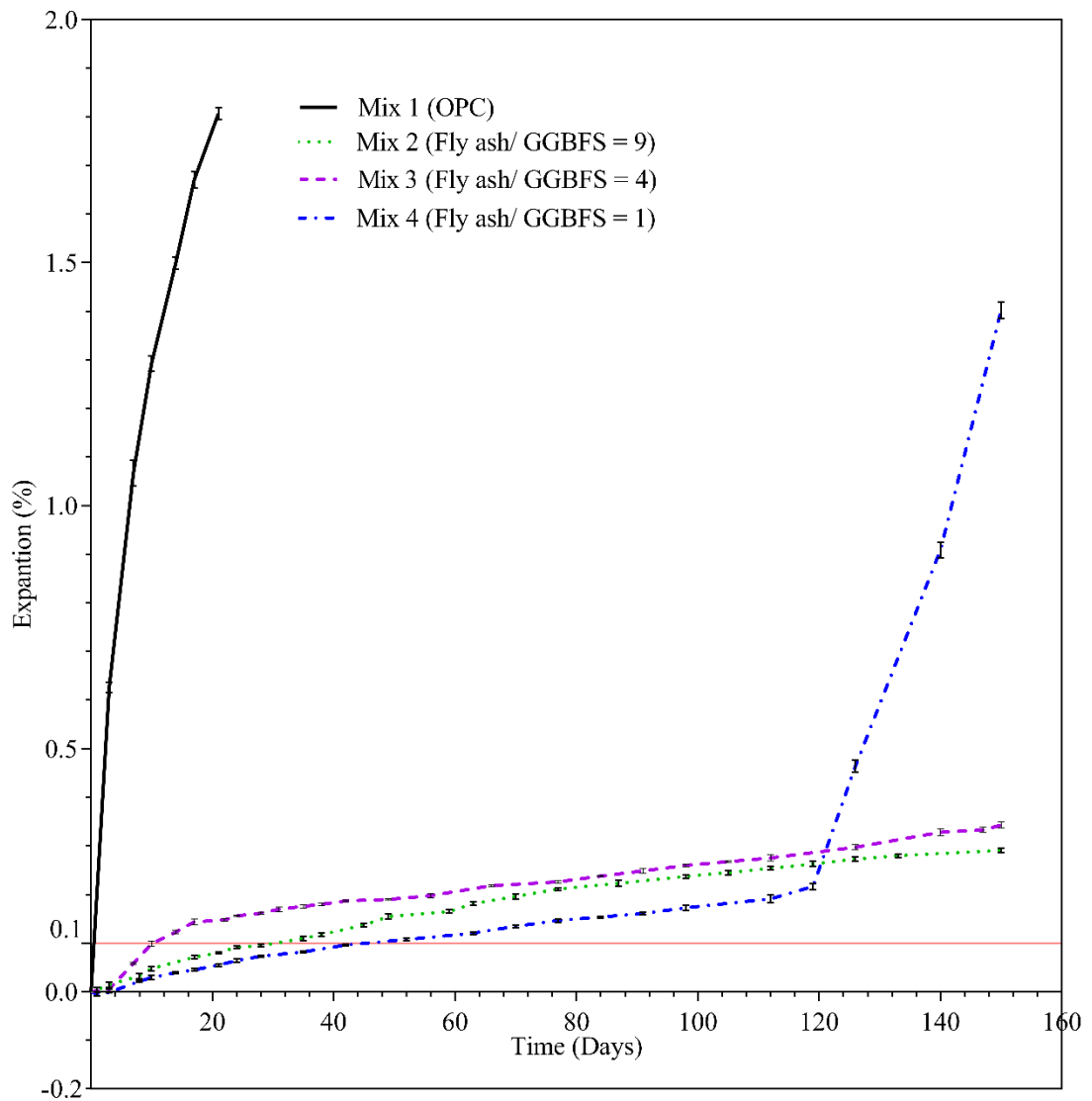


Figure 8-1 : Expansion characteristics of mix 1-4 over 150 days when exposed to accelerated curing conditions. 0.1% (red line) is the minimum expansion limit for reactivity stipulated in AS 1141.60.1.

Mortar bars of Mix 1 has shown the highest final expansion; 1.8072% even though the test ended after 21 days as the expansions exceeded the measurable limit. In geopolymer mixes (Mix 2-4), Mix 4 (FA/GGBFS =1) has shown the highest final expansion; 1.4023% primarily due to a delayed strong expansion that started approximately at 120 days.

Expansion curve of Mix 1 shows a rapid increment to reach 1.8072% by 21 days without showing any initial time lag. However, the slope of the curve seems decreased towards the end hinting of a stabilization phase at some point.

Geopolymer mixes (mix 2-4) also haven't shown any time lag which was experienced with natural aggregates in Chapter 5 and 6. Mix 3 has shown the highest expansion followed up by Mix 2 and Mix 4 up until approximately 120 days. At 120 days, only the expansion curve of Mix 4 shows an exponential growth out passing the other two geopolymer mixes

Expansion curve of Mix 2 develops smoothly to reach 0.2910% expansion by 150 days. However, it can be noticed that the growth slightly decelerated over the time hinting a probable stabilization phase. Expansion curve of Mix 3 clearly shows two distinguish segments. Initial phase with comparatively high growth rate ends approximately after 17 days achieving about 20% of the total expansion (0.0711%). The second phase which is linear and smoother continued up until the end (150 days) to reach 0.3432% expansion. Expansion curve of Mix 4 showed a similar characteristic to Mix 2 but with a lower magnitude to reach 0.2165% after approximately 120 days, the lowest among all mixes at that stage. However, the exponential expansion development after 120 days led to 1.4023% at 150 days which is second only to Mix 1 (OPC mix). Nevertheless, final expansion results (at 150 days) of geopolymer mortar bars follow a similar trend as observed in other aggregates during this study; expansion due to alkali silica reaction increases with the GGBFS content in the initial mix.

### 8.2.2 Compressive strength variation

Figure 8-2 shows the compressive strength variation of mixes 1-4 over 29 days after casting (28 days of exposure). 50mm x 50mm x 50mm cubes were cast and exposed to same conditions along with mortar bars before crushing them at specific intervals (1 day, 8 days, 22 days and 29 days after casting) to determine the initial compressive strength variation.

Mixes 1 and 2 have shown approximately a similar strength after one day: 37.7 MPa and 36.8 MPa respectively. Mix 4 has achieved the highest initial strength of 62.5 MPa followed by Mix 3 with 44.5 MPa. Compressive strengths of geopolymer mixes after one day increase with the increase in GGBFS content which has been reported by many researchers earlier (Deb et al. 2014; Diaz et al. 2010). Figure 8-2 clearly indicates that the compressive strength of all four mixes dropped over the time. Mix 3 has shown the largest strength reduction (76.6%) after 29 days compared to the 67.4% and 65.9% strength reductions for the other two geopolymer mixes: Mix 2 and Mix 3. It should be noted that Mix 3 have shown significantly higher expansion compared to the other two geopolymer mixes. Thus, the strength reduction observed in Mix 1-4 might be due to the formation of alkali silica gel inside the matrix and degradation of the Interfacial Transition Zone (ITZ) and the loss of bonding between the aggregate and the binder due to the excessive dissolution of the aggregate.

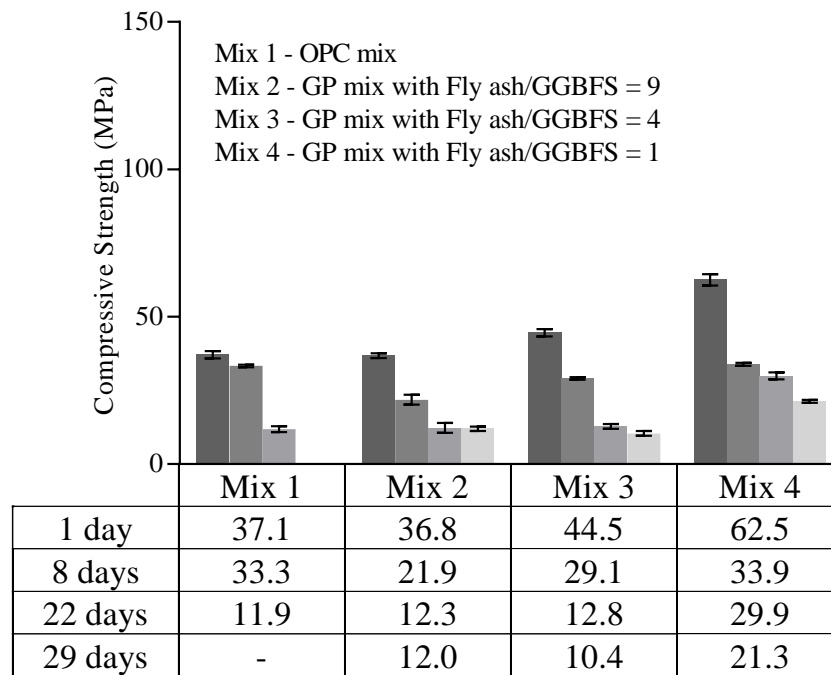


Figure 8-2 : Compressive strength variation of mix 1-4 over 29 days after casting

### 8.2.3 Scanning Electron Microscope (SEM) Analysis

Representative mortar samples extracted at 21 days and 150 days were studied microscopically with SEM analysis to identify any microcracks and ASR gel formation. Furthermore, backscattered EDS analysis was implemented to determine the chemical composition of ASR gel in each sample.

All mixes except Mix 1 have shown ASR gel formation at both stages; 21 days and 150 days. for Mix 1 (OPC mix), SEM/EDS analysis was carried out only at 21 days as testing was ceased after 21 days because the expansion exceeded the measurable limits. ASR gel was identified inside the aggregate, at the aggregate binder interface and inside the binder as shown in Figure 8-3 for Mix 3 after 150 days. Figure 8-4 to Figure 8-10 are the backscatter EDS line profiles of ASR gel identified inside the aggregate of Mix 1-4. Figure 8-11 and Figure 8-12 are backscatter EDS line profiles of ASR gel identified at the aggregate binder interface and inside the binder respectively for Mix 3 at 150 days. It

is clear that ASR gel and geopolymer both consist of similar elements; sodium (Na), calcium (Ca), aluminium (Al) and silicon (Si) along with oxygen (O) which is omitted from line profile graphs. Thus, it is more accurate to analyse the ASR gel formed inside aggregate compared to the other two locations (Figure 8-4 to Figure 8-10).

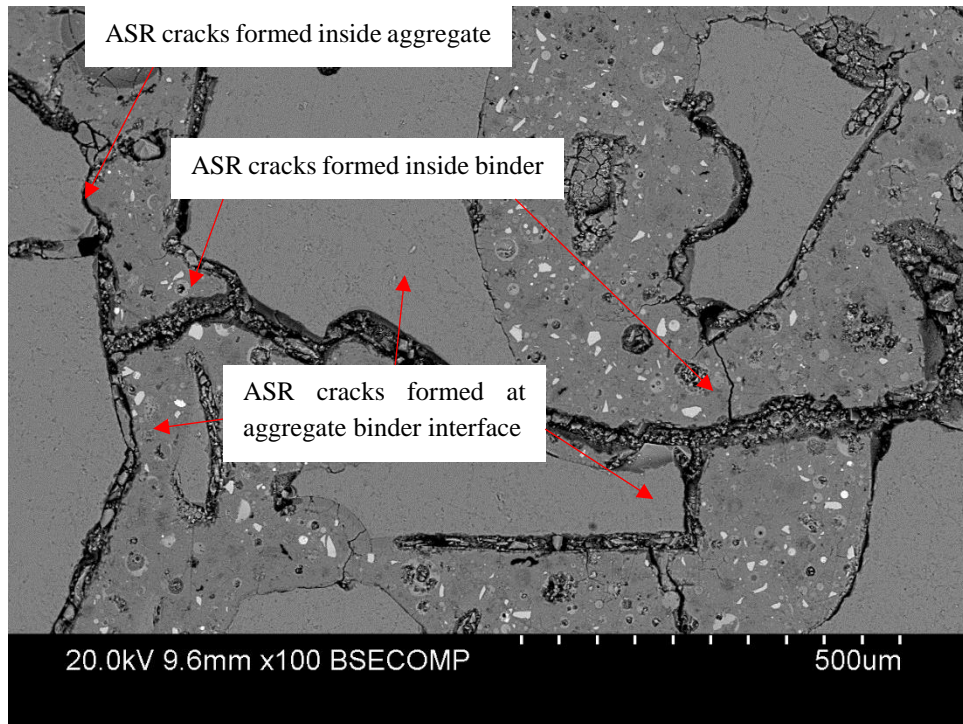


Figure 8-3 : ASR cracks identified at different locations of Mix 3 at 150 days

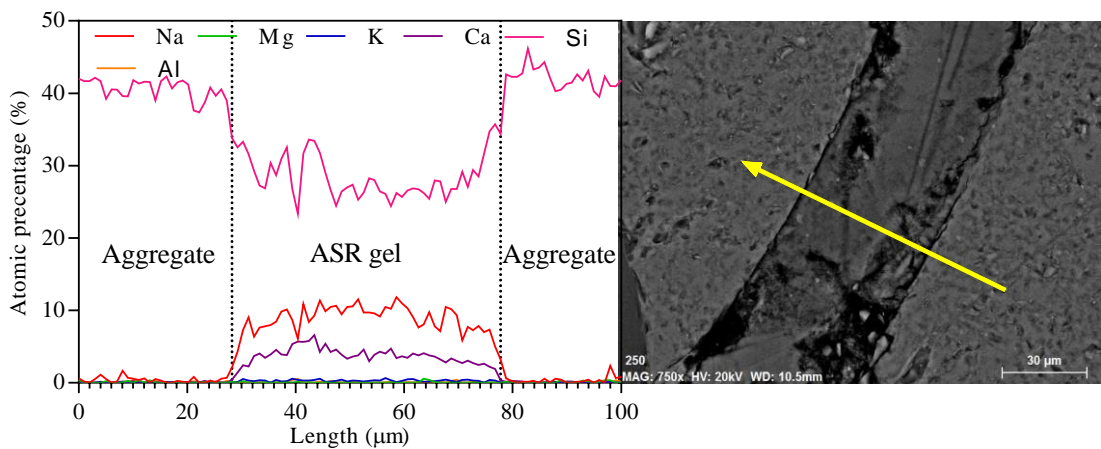


Figure 8-4 : ASR gel identified inside aggregate of mix 1 at 21 days

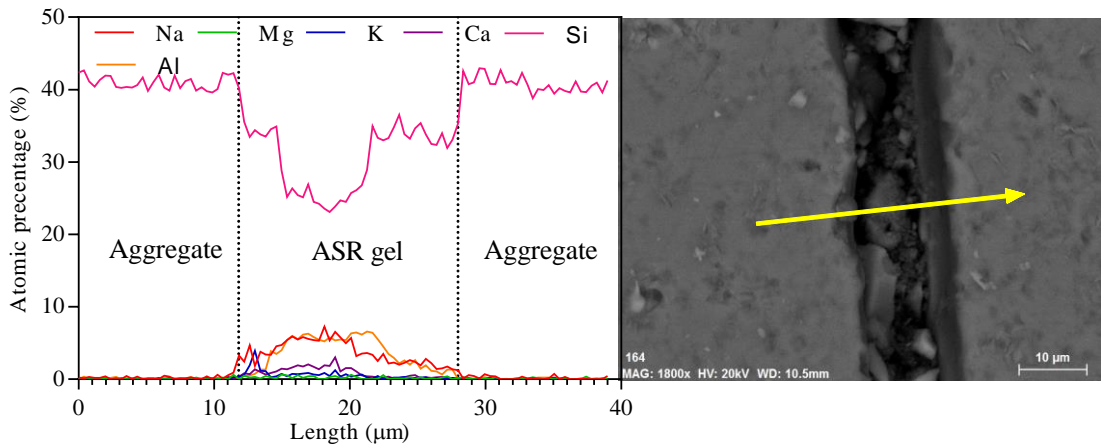


Figure 8-5 : ASR gel identified inside aggregate of mix 2 at 21 days

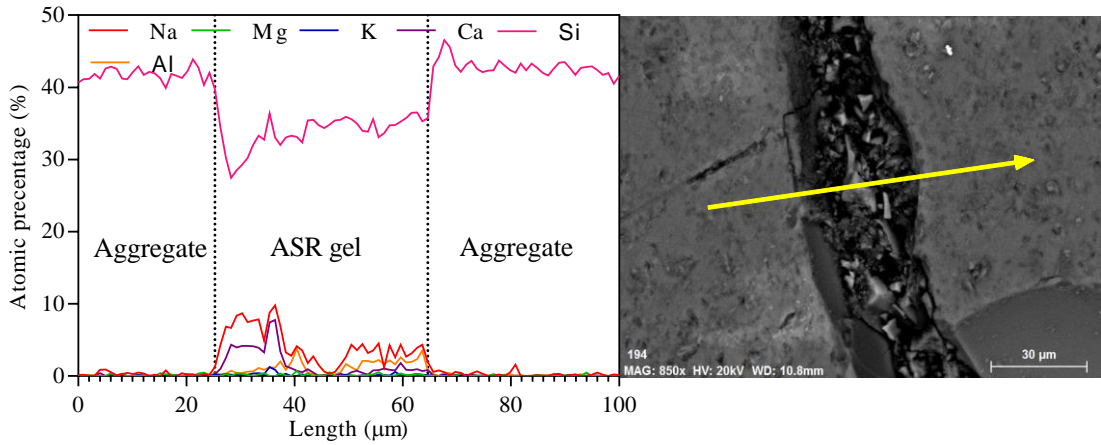


Figure 8-6 : ASR gel identified inside aggregate of mix 2 at 150 days

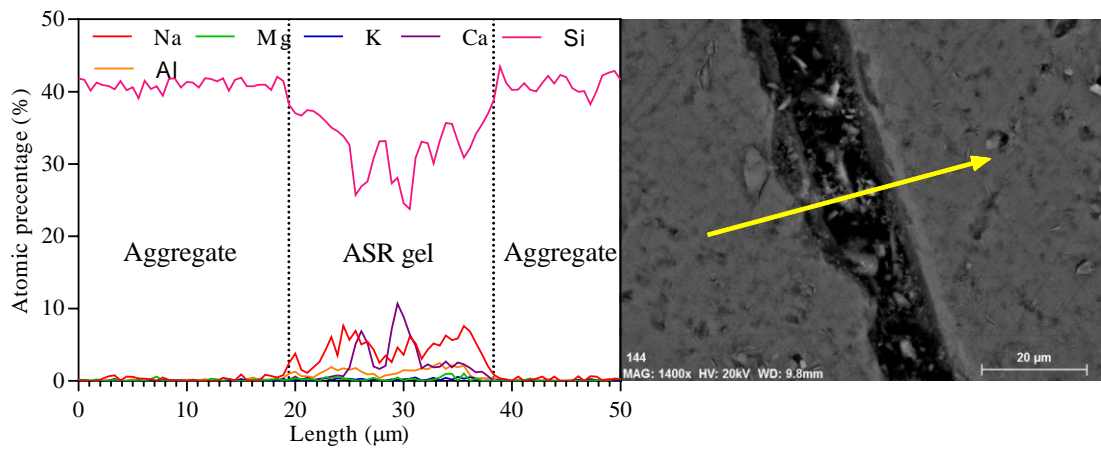


Figure 8-7 : ASR gel identified inside aggregate of mix 3 at 21 days

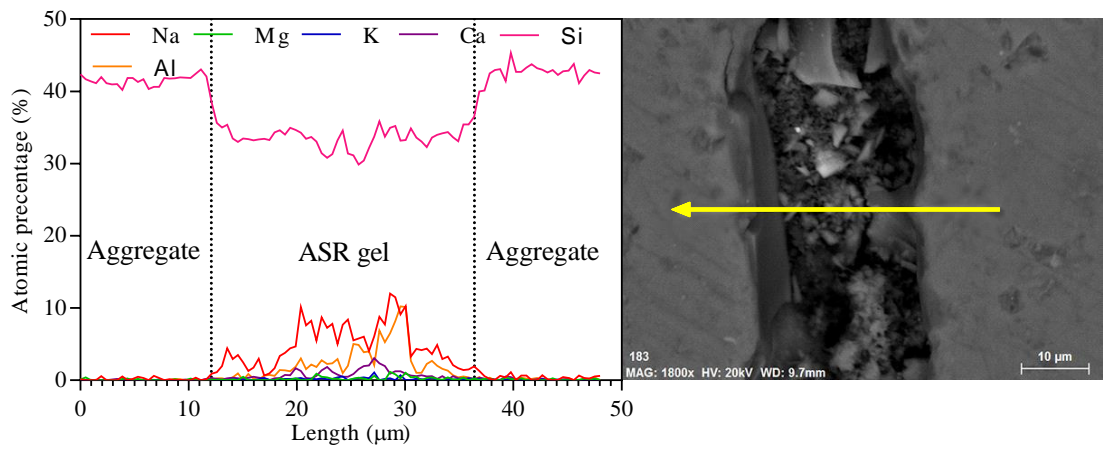


Figure 8-8 : ASR gel identified inside aggregate of mix 3 at 150 days

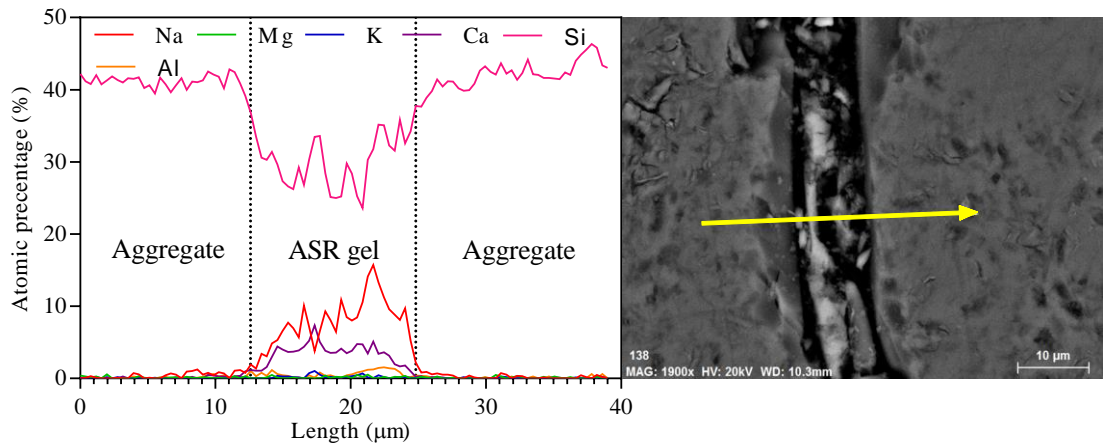


Figure 8-9 : ASR gel identified inside aggregate of mix 4 at 21 days

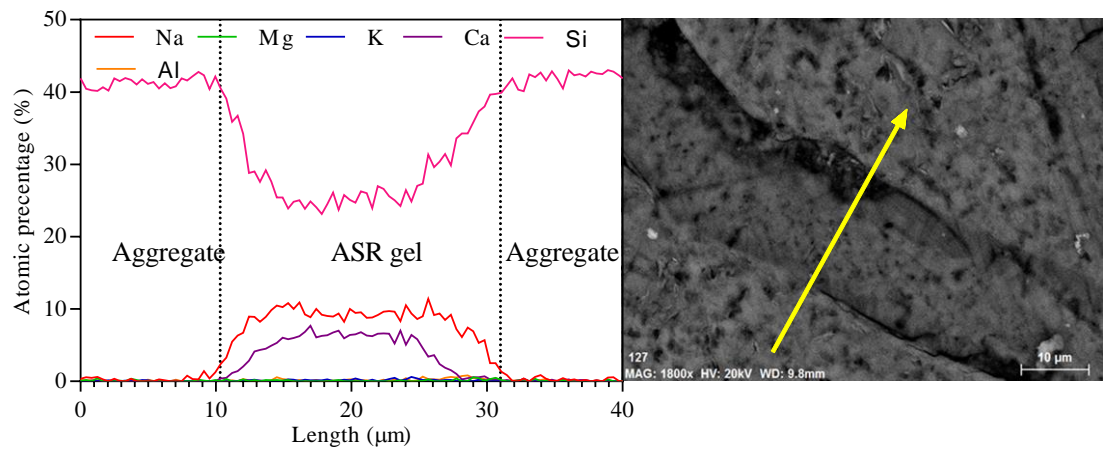


Figure 8-10 : ASR gel identified inside aggregate of mix 4 at 150 days

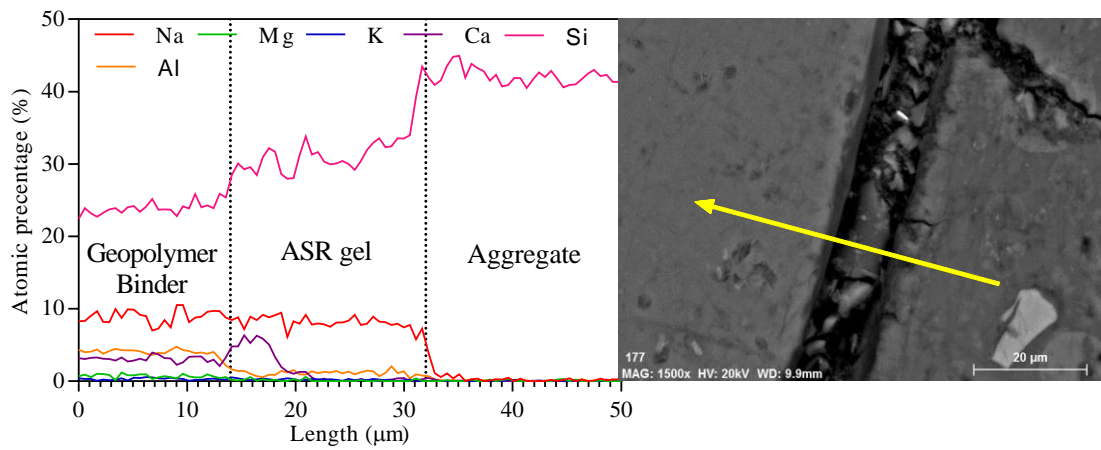


Figure 8-11 : ASR gel identified in aggregate mortar interface of Mix 3 at 150 days

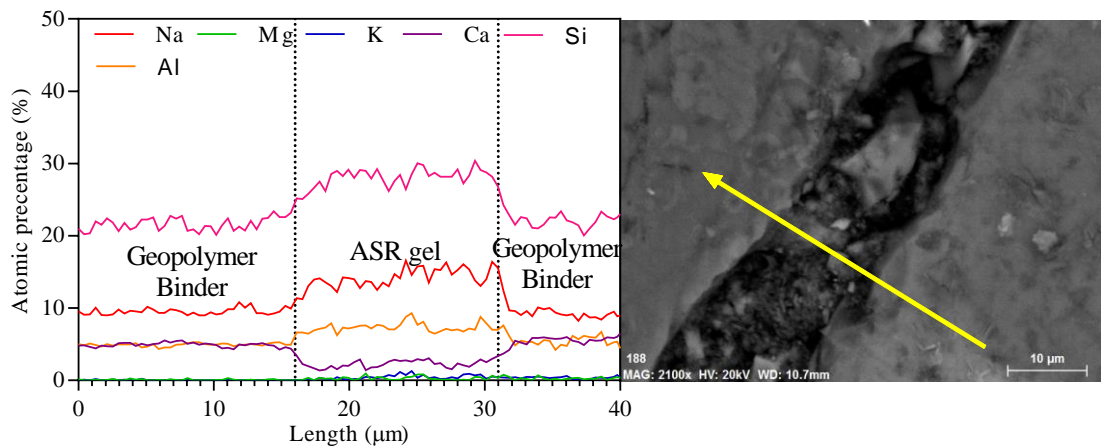


Figure 8-12 : ASR gel identified inside mortar of Mix 3 at 150 days

Average elemental atomic percentages of ASR gel identified in Mixes 1 to 4 are summarized in Table 8-2. Elemental compositions were calculated by averaging approximately 250 data points of ASR gel formed inside the aggregate. Figure 8-13 is the variation of Ca/Si ratio versus Na+K/Si ratio over the time in Mix 1-4. Figure 8-14 contains the ternary diagrams plotted from the data in Table 5-2 in order to identify the correlation between elements identified in ASR gel and their variation with respect to the mix and exposure time.

Table 8-2 : Summary of SEM /EDS analysis of ASR gel located inside aggregate of mix

1-4

Mix No.		Average atomic percentage (%)						Ratios		
		Na	K	Ca	Mg	Si	Al	$\frac{(Na+K)}{Si}$	$\frac{(Ca+Mg)}{Si}$	$\frac{Al}{Si}$
1	21 days	8.63	0.30	3.62	0.04	28.64	0.09	0.31	0.13	0.003
	150 days	-	-	-	-	-	-	-	-	-
2	21 days	3.67	0.55	1.89	0.23	30.71	3.59	0.14	0.04	0.117
	150 days	4.18	0.18	1.71	0.15	33.95	1.27	0.13	0.05	0.037
3	21 days	4.35	0.22	2.56	0.27	32.84	1.26	0.14	0.09	0.038
	150 days	4.81	0.18	0.76	0.23	33.68	2.29	0.15	0.03	0.068
4	21 days	7.55	0.23	3.36	0.15	30.45	0.63	0.26	0.12	0.021
	150 days	8.19	0.16	4.16	0.10	29.31	0.53	0.28	0.15	0.018

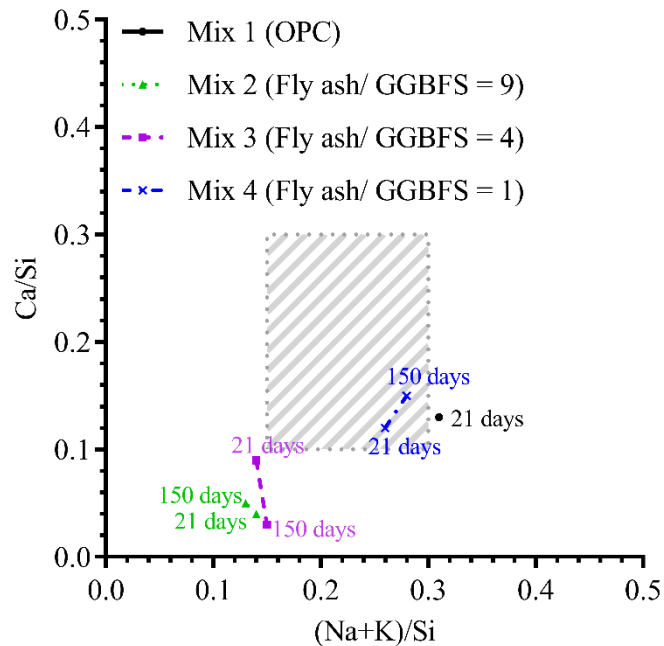


Figure 8-13 : Variation in Na+K/Si vs. Ca/Si (atomic ratio) of ASR gels at 21 days and 150 days from Mix 1-4; shaded area is the alkali silica gel compositions developed base on Thaulow et al. (1996), Leemann et al. (2016), Leemann and Lura (2013) and Leemann and Merz (2013)

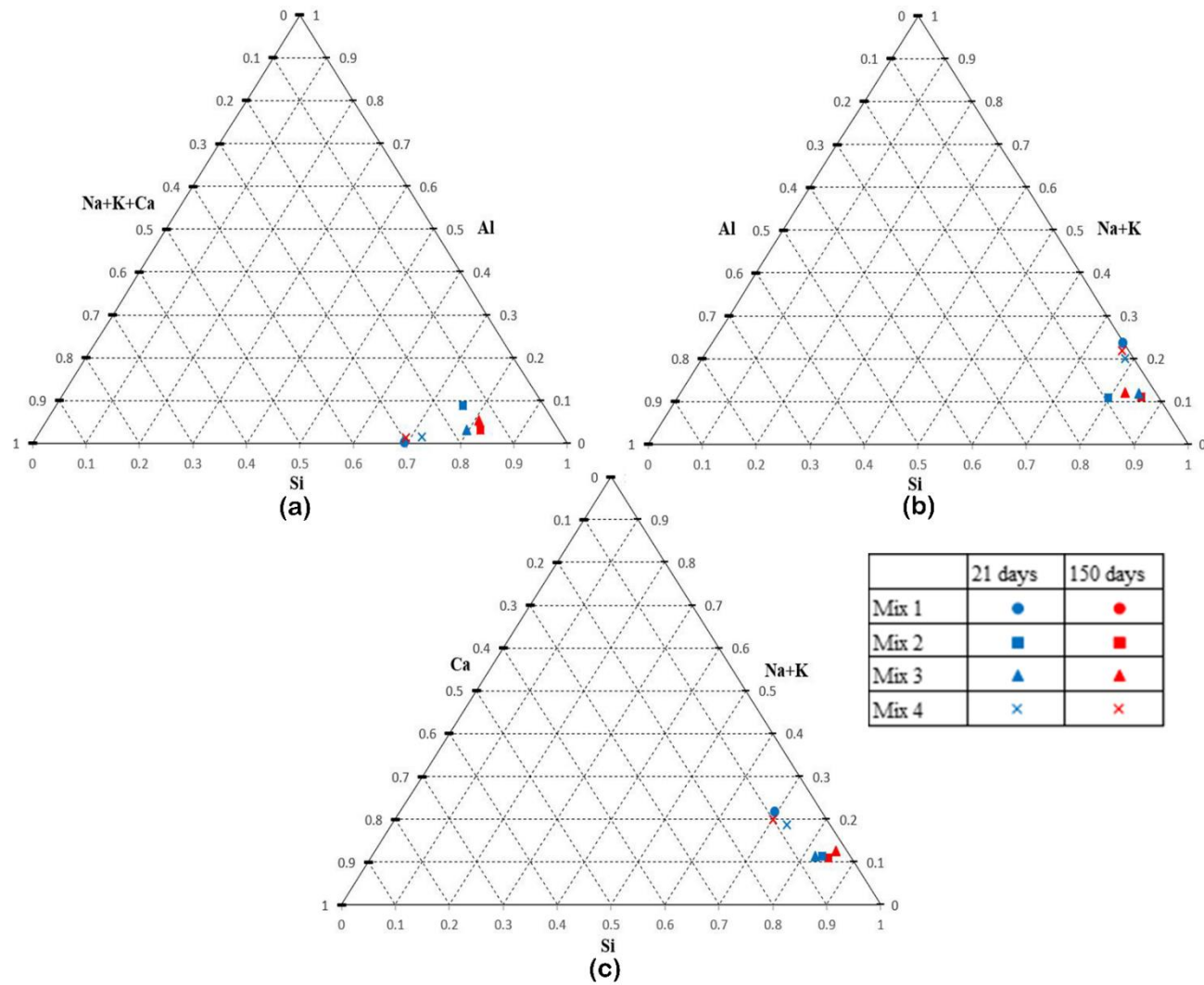


Figure 8-14 : ASR gel composition interpreted in a ternary diagram

Table 8-2 shows that alkali silica gel in mortar bars cast with fused silica mainly consists of calcium (Ca), sodium (Na), silicon (Si) and aluminium (Al) ions. Researchers who worked on ASR in OPC binders reported that (Na+K)/Si ratio and Ca/Si ratio of alkali silica gel typically lies in the range of 0.15~0.3 and 0.10~0.3 respectively (Leemann et al. 2016; Leemann & Lura 2013; Leemann & Merz 2013; Thaulow et al. 1996). Na+K/Si ratio of Mix 1 at 21 days is 0.31 which is slightly higher than the upper limit of the range defined above. However, Ca/Si ratio of ASR gel in Mix 1 lies inside the above range because OPC mortar contains a considerable amount of free Ca. (Na+K)/Si ratios of ASR gel in Mix 2 and 3 is below the lower limit of the above range except for Mix 3 at 150 days which shows exactly 0.15. Table 8-2 clearly shows that the Si content is much higher in Mix 2 and Mix 3 compared to Mix 1 which might explain the low ratios. Furthermore, their Ca+Mg/Si ratios are also below the lower limit which might be due to the limited amount of free Ca available in the system. Mix 4 has shown the perfect ratios as both lies within the range irrespective of the exposure time.

Figure 8-13 shows that the Na+K/Si ratio and Ca/Si ratio of Mix 2 do not change much over time which indicates that ample amounts of Si and Na are available in the system even at 150 days along with very low free Ca content. In Mix 3, Ca content clearly dropped over the time which suggest the formation of sodium silica gel instead of sodium calcium silica gel due to low free Ca content. Due to a higher GGBFS content, Mix 4 has higher Ca content in the system compared to the other two geopolymer mixes which results in the formation of Ca rich ASR gel. thus, it is clear that the Ca content in ASR gel is related to the initial GGBFS content in the mortar mix.

Aluminium (Al) has also become a significant element in ASR gel formed in geopolymer mortar. The Al/Si ratio of the ASR gel in geopolymer lies in the range of

0.117-0.18 compared to 0.003 in ASR gel found in OPC mix. It should be noted that ASR gel in Mix 4 corresponds to the lowest Al/Si ratio among geopolymer mixes as shown in Table 8-2.

Figure 8-15 contains the backscatter SEM images of Mix 1-4 at 21 days and 150 days. The magnification of the SEM images kept at 100 to compare the distresses in specimens. OPC mix (Mix 1) only consist of SEM image at 21 days as the was test terminated after that. Cracks filled with ASR gel can be clearly identified in all the specimens. However, none of the SEM images shows significant microcrack propagation inside the binder. Thus, it can be concluded that even though there is a clear evidence of alkali silica reaction in all the specimens, the gel pressure has been dissipated without inserting any stresses in geopolymer mixes. Furthermore, circular shaped carves filled with binder were observed in aggregate as shown in Figure 8-15. These are most likely to be voids generated while due to the dissolution of fused silica aggregate were then filled with ASR gel.

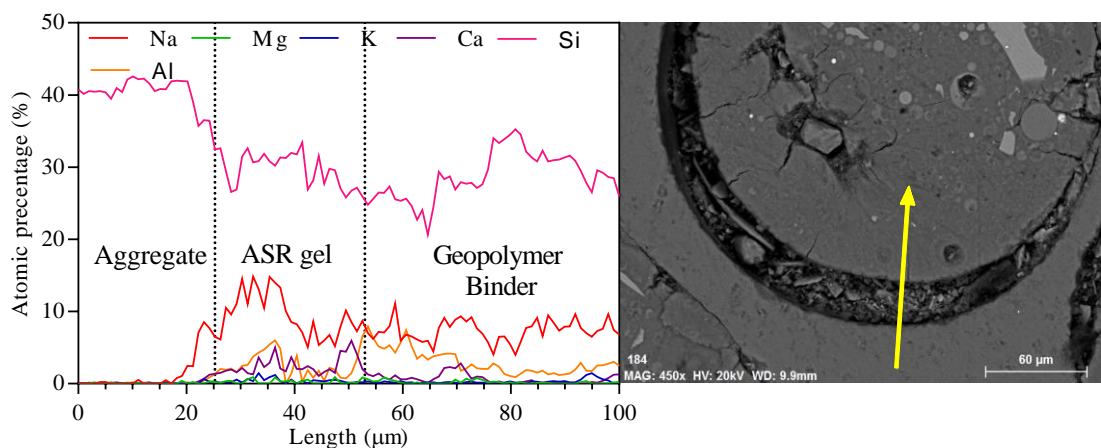
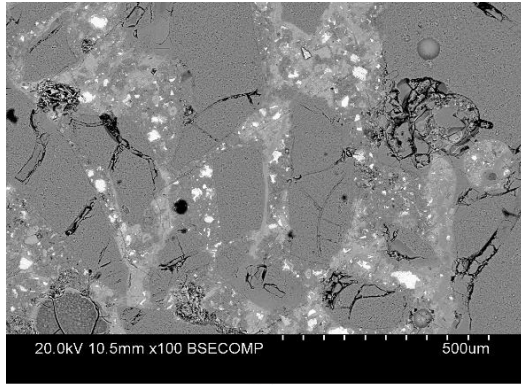
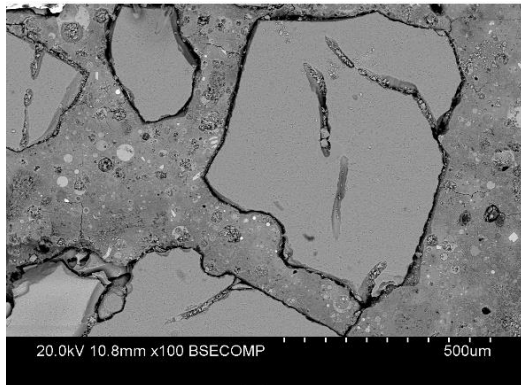


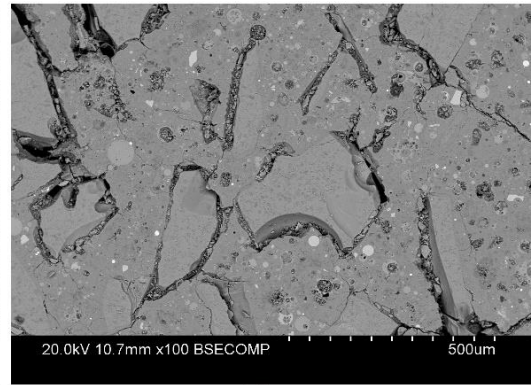
Figure 8-15 : Circular carves identified in Mix 3 at 150 days



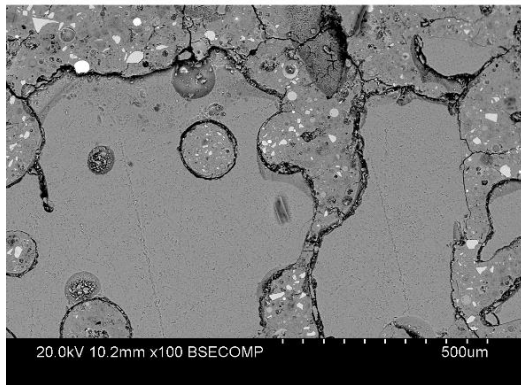
(a)



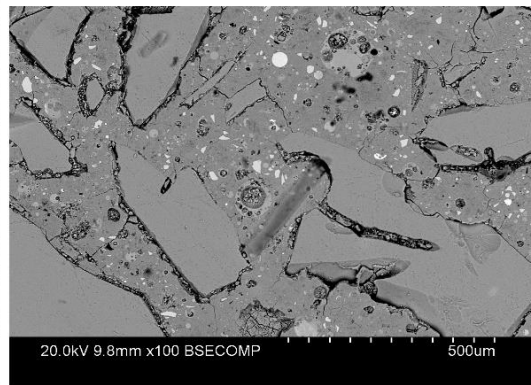
(c)



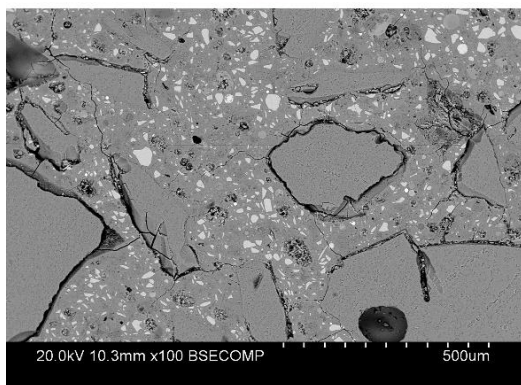
(d)



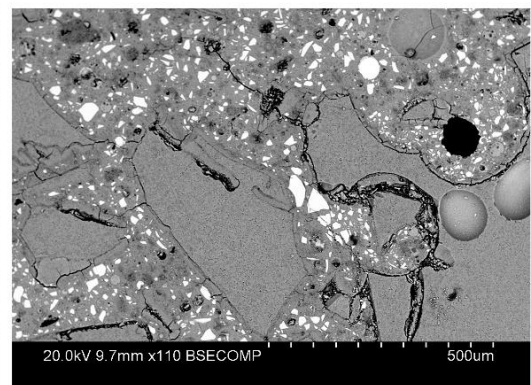
(e)



(f)



(g)



(h)

Figure 8-16 : Micro crack propagation in mix 1-4; (a) SEM image of mix 1 at 21 days, (c) SEM image of mix 2 at 21 days, (d) SEM image of mix 2 at 150 days, (e) SEM image of mix 3 at 21 days, (f) SEM image of mix 3 at 150 days, (g) SEM image of mix 4 at 21 days, (h) SEM image of mix 4 at 150 days,

#### 8.2.4 Mortar bar images

The images of mortar bars of Mix 1-4 after the test completion are shown in Figure 8-17. Mix 1, Mix 3 and Mix 4 have shown the characteristic map cracking of the ASR on the surface. The surface of Mix 2 is clearly deteriorated even though it did not show any crack formation on the surface. This might be due to the removal of aggregate at the surface as a result of continuous exposure to the 1M NaOH solution. It should be noted that high Si dissolution from the aggregate might weaken the bond between aggregate and mortar which may result in aggregate fall outs. However, the stronger and densified bond structure of the other two geopolymer mixes due to their higher Ca contents allowed to hold the aggregate despite the ASR gel formation.



Figure 8-17 : Mortar bar images of mix 1-4 after the test completion; (a) Mix 1 at 21 days, (b) Mix 2 at 150 days, (c) Mix 3 at 150 days, (d) Mix 4 at 150 days

### 8.3 Discussion

Fused silica is categorized as highly reactive aggregate due to its high Si dissolution capability which was confirmed by the chemical test results presented in section 4.3.1. This is clearly reflected as well by the expansion test results of Mix 1 (OPC mortar) shown in Figure 8-1. Indeed, the average expansion of OPC mortar bars reached 1.2924% after only 10 days and 1.8072% after 21 days exceeding by far the 0.1% and 0.3% limits stipulated in the Australian standard; AS1141.60.1 (Australia, 2014). Even though the rate of expansion slightly reduced after about 10 days, the test had to be terminated after 21 days because the expansion of the mortar bars exceeded the measurable limit of the comparator.

For accelerated mortar bar test using OPC based mortar, Si dissolution rate of aggregate governs the degree of ASR as the system contains a substantial amount of all other required components: alkalis, moisture and calcium ions. Based on the chemical test results in section 4.3.1, it is clear that fused silica supplies significantly higher Si content to the system than natural aggregates which can explain the higher ASR related expansion observed in Figure 8-1 compared to that observed using natural aggregates (see chapter 6). In addition, OPC paste provide a dense and rigid barrier around aggregate entrapping ASR gel which eventually amplifies the internal stresses generated on aggregate and paste by facilitating the gel pressure accumulation (Ichikawa and Miura, 2007). After some time, cracks developed into the fused silica aggregate dissipating ASR gel pressure developed inside the reaction rim, explaining the decrease in expansion rate observed after about 10 days. The above mechanism is further confirmed by the microstructural analysis. Indeed, SEM/EDS analysis allowed observing some microcracks in the aggregate which were then filled with Ca rich ASR gel (see Figure 8-4) while no microcracks were observed in the paste (see Figure 8-16a). Moreover, the

ASR gel formed in the vicinity of aggregate might act as a barrier for hydroxyl ions reducing the Si dissolution from fused silica which might contribute the reduction in expansion rate as well (see Figure 8-1). As observed using natural aggregate (chapter 6), Mix 1 mortar bars with fused silica also has not shown any time lag in expansion. This is due to the rapid formation ASR gel in the system as discussed above which eventually results in an immediate increment in expansion as seen in Figure 8-1.

Geopolymer mixes (Mixes 2 to 4) have shown significantly lower expansion than OPC mix (see Figure 8-1). In fact, despite using highly reactive aggregate in the system, none of the geopolymer mixes has reached the 0.1% expansion limit within 10 days, and only Mix 3 exceeded this limit after 21 days (0.1445%) which classified fused silica in Mix 3 mortar as only slowly reactive based on the AS 1141.60.1 (Australia, 2014). Even though ASR gel formed at a very high rate, there are significant number of voids formed due to dissolution of aggregate which allows ASR gel to disperse without exerting any internal stresses. Indeed, in geopolymer, ASR gel rich with Al might also able to blend with existing paste which further reduces the stress development and thus the expansions. SEM images with circular shaped voids filled with geopolymer binder (Figure 8-15 and 8-16) further proves this mechanism. Though Mix 1 also contains these voids, OPC binder itself might act as a rigid barrier which facilitate the ASR gel accumulation and thus, high internal stress development.

A noticeable difference between the geopolymer AMBT results obtained on natural aggregate and fused silica is that mortar bar expansions of fused silica does not show any time lag as observed in natural aggregate (Culcairn). The high Si dissolution rate of fused silica seems to make the Si concentration reaching the saturation point of ASR almost instantly leading to an immediate expansion. This seems to confirm that the delay in expansion observed in geopolymer mortar using natural aggregate is mainly due to the

lack of calcium content preventing CSH to form in suitable quantity to create a barrier around aggregate. This barrier is required to achieve the Si concentration necessary to trigger ASR gel formation in a short period of time when the Si supply rate is slow (with natural aggregate).

Except the time lag effect discussed above, the expansion curves observed using natural aggregate and fused silica are overall very similar: Mix 3 (Fly ash/GGBFS = 4) shows the highest expansion initially, followed by Mix 2 (Fly ash/GGBFS = 9) and Mix 4 (Fly ash/GGBFS = 1) until Mix 4 shows a sudden huge expansion after about 120 days with an expansion rate similar to that of OPC Mix 1, reaching 1.4023% after 150 days. Even though formation of CSH is not necessary to reach the saturation point of ASR, Ca still plays a significant role in second part of the mechanism described in section 6.3.1 by facilitating the ASR gel accumulation in localized areas which eventually results in internal stress development and thus expansion. Mix 2 corresponds to the lowest GGBFS content among geopolymer mixes. Therefore, it is expected to have the lowest expansions in Mix 2 based on the mechanism described in section 6.3.1 which consent with the final expansions shown in Figure 8-1 and Table 8-1. SEM/EDS analysis further confirms the formation of low Ca ASR gel with high Al content at both stages, 21 days and 150 days (see Figure 8-5 and 8-6). However, Mix 4 which is expected to show the highest expansions among geopolymer mixes has shown the lowest expansions up until 120 days before incorporating a sudden expansion growth to out pass both Mix 2 and Mix 3. Figure 8-13 reveals that ASR gel compositions of Mix 4 at 21 days and 150 days are almost similar and lies inside the reactive region defined by previous studies (Leemann et al. 2016; Leemann & Lura 2013; Leemann & Merz 2013; Thaulow et al. 1996). Therefore, it can be deduced that the sudden expansion increment observed is more likely to be due to the variation mechanical characteristic of mortar. It should be noted that high GGBFS

content also results in high elasticity modulus in the paste (Gunasekara 2016; Phoo-ngernkham et al. 2013; Ryno 2014). Thus, despite having higher internal stresses generated due to ASR, Mix 4 exhibited low expansions because of its high modulus of elasticity. However, once the internal stresses exceed the yield stress, the expansion gain becomes exponential as observed for Mix 4 in Figure 8-1. Mix 3 has shown a substantial expansion gain initially but dropped its expansion at about 17 days probably due to lack of free Ca in the system before continuing at a constant rate to reach 0.3432% after 150 days. SEM/EDS analysis confirms the absence of calcium for the ASR gel formation as Ca/Si ratio of ASR gel clearly dropped from 0.09 to 0.03 during the testing period as illustrated in Figure 8-13.

Mortar images of Figure 8-17 have shown characteristic map cracking in the surface of all mixes except Mix 2 which was severely deteriorated due to surface pop outs (HB79 2015). However, even though Figure 8-16 has not shown any distresses in the binder, some large cracks filled with ASR gel was identified in geopolymer mixes during the SEM/EDS analysis as shown in Figure 8-12. These cracks along with cracks in aggregate might form failure paths inside mortar which substantially lowered the strength as illustrated in Figure 8-2. Even though OPC mix has only shown cracks inside aggregate, low strength of the binder combined with severe crack formations inside aggregate shown in Figure 8-4 might drop the compressive strength substantially during the initial 21 days. However, loss of bonding between the aggregate and binder and the degradation of the ITZ due to the excessive Si dissolution of the aggregates may significantly affect the overall strengths of mortar (Singh et al., 2015). This was confirmed by the microstructural analysis since void between aggregate and binder were clearly visible (see Figure 8-3, 8-15 and 8-16).

SEM/EDS analysis clearly shows that aluminium (Al) has also become a significant constituent in ASR gel formed in geopolymer mortar (see Table 8-2). Incorporation of Al might encourage ASR to form crosslinks and form aluminosilicate oligomers and aluminosilicate amorphous gel which were later transformed into the zeolitic nanocrystalline phases of geopolymer as described by Van Deventer et al. (2007). The Formation of cross links might result in low water binding capacity which reduces the swelling properties of ASR gel (Bernal & Provis 2014). It should be noted that ASR gel formed in Mix 2 composed of the highest amount of Al followed up by Mix 3, Mix 4 and Mix 1 respectively which is the descending order of final expansions as shown in Figure 8-1. Therefore, since the experimental results align with the above hypothesis on the role of aluminium, it can be concluded that Al might reduce the expansiveness of ASR gel.

#### **8.4 Summary**

Study of geopolymer mortar with highly reactive aggregate would illustrate the ASR in geopolymer under extreme cases. Chemically, amorphous silica source is the highest reactive aggregate that can be used to assess the ASR in geopolymer. XRF and XRD analysis proved that fused silica is almost pure (<98%) amorphous silica source which was fortified by the chemical dissolution test results and standard accelerated mortar bar test results.

Even though geopolymer mixes have shown considerable expansion developments, the magnitude is substantially lesser compared to the OPC mortar which indicates low ASR potential in geopolymer mortar. However, despite showing lower expansions, all mixes have significantly high ASR gel formations at both 21 and 150 days. Hence, it can be concluded that the effective stress development inside geopolymer mortars due to the ASR is significantly lower compared to OPC. Low effective internal stresses in geopolymer might be due to the dispersion of ASR gel into the voids and formation of

ASR gel with low swelling capacity. SEM analysis confirmed the availability of voids around the aggregate due to the high decaying of aggregate which might facilitate the gel dispersion. EDS analysis revealed the formation of low Ca and high Al ASR gel in geopolymer compared to OPC which might reduce the swelling capacity of gel considerably. It should be noted that due to the high initial alkalinity in geopolymer, high Si dissolution might occur in aggregate causing the void formation as observed. However, these Si most probably contributed to the geopolymerization reaction without causing any ASR gel formations. Thus, amorphous Si sources such as fused silica is not suitable to assess the ASR in geopolymer mortar.

## **CHAPTER 9 : Conclusions and Recommendations**

---

### **9.1 General**

OPC has been one of the highest consumable material in the world. However, the increase in environmental and socioeconomic issues due to high OPC consumption have urged the need for more sustainable and ecofriendly alternative. Geopolymer concrete is considered as the most reliable substitute to the OPC based concrete. This study assesses one of the grey areas in geopolymer binders, the alkali silica reaction in geopolymer mortar based on the accelerated mortar bar test results and SEM/EDS analysis results. In addition, recommendations for future works related to this study are briefly discussed at the end of this chapter.

### **9.2 Chemical performance of reactive aggregate exposed to an alkali solution**

- ♦ Si dissolution of aggregate depends on the alkalinity of the base solution. Significantly higher Si dissolution is observed in higher hydroxyl ion concentrations. In addition, the Si dissolution of aggregate is more sensitive to the variation in hydroxyl ion concentration at higher alkalinities compared to the lower alkalinities. Since the pore solution alkalinity of geopolymer is generally considered lesser than that of OPC, Si ion dissolution shall be lesser in geopolymer compared to OPC and thus, the degree of ASR.
- ♦ Si dissolution capability of aggregate depends on the internal bond structure of the aggregate. Aggregates with stronger internal bonds tend to supply lesser Si

ions when exposed to similar conditions. Thus, amorphous silica shall have the highest Si dissolution, and Si dissolution may drop with the degree of crystallinity.

- ◆ Effect of crystallinity on the Si dissolution capability reduces drastically with the alkalinity of the base solution. It should be noted that all three aggregates have shown almost similar Si dissolution when exposed to 1M NaOH solutions. Thus, alkalinity of the exposure solution would reduce the reliability of the test results which might result in false identification of ASR in certain aggregates.
- ◆ All three aggregates have shown almost similar dissolution behaviours with base solution pH but in different magnitudes. Aggregates have displayed an approximately linear development when the pH is higher than 11.5. Furthermore, Si concentration in the base solution is stabilised approximately after 50 days which indicates Si ion saturation within 50 days of exposure
- ◆ Higher surface area per unit weight in smaller size fractions might result in substantially higher number of reaction locations in aggregate and thus higher Si dissolution rate compared to larger aggregates. Therefore, degree of ASR increases when the aggregate size is decreased.
- ◆ Formation of spiky opaline products were observed in all three aggregates at higher alkalinities. Based on the formations in fused silica, it can be concluded that this product is sodium silica hydrates (a form of ASR gel). In addition, magnitude of this product formation depends on the Si dissolution rate of aggregate.

### **9.3 Alkali silica reaction in geopolymer**

- ◆ All four aggregates have shown expansions induced by ASR over the time but in different magnitudes which indicates the occurrence of alkali silica reaction at

different rates. As expected, fused silica corresponds to the highest expansion followed up by Ferronickel slag aggregate, Culcairn aggregate and Basalt. Since Basalt is categorised as non-reactive based on the service records and preliminary testings, expansion results of basalt aggregate illustrated the overestimation of reactivity with accelerated mortar bar test which is highlighted by many researchers.

### 9.3.1 Reaction Mechanism

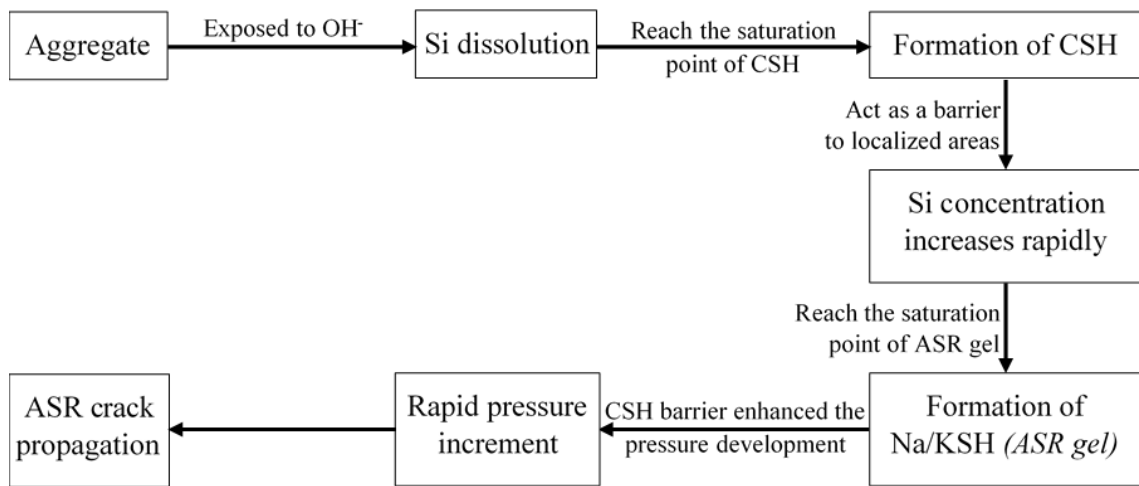


Figure 9-1: Alkali silica reaction mechanism in geopolymer mortar

- ♦ ASR in geopolymer mixes increase with the Ca content in the mix (see Figure 9-1). Since GGBFS is the main Ca source in geopolymer, it can be concluded that GGBFS content controls the ASR in geopolymer.
- ♦ Geopolymer mortar with fly ash/GGBFS = 9 (GGBFS content 61.5 kg/m<sup>3</sup>) demonstrated ASR resistiveness irrespective of the aggregate. Significantly low expansions observed in extremely reactive aggregates such as fused silica would indicate the low risk of ASR in geopolymer mortar with fly ash/GGBFS = 9 (GGBFS content 61.5 kg/m<sup>3</sup>). It should be noted that the severe exposure

conditions in AMBT might induce certain amount of expansion as observed in Mix 2 and Basalt aggregate. However, even though the other two geopolymer mixes (Mix 3 and Mix 4) have exceeded the 0.1% expansion limit eventually, it is still inappropriate to draw conclusions because of the severe curing conditions in AMBT.

- ◆ All the geopolymer mixes have shown an initial time lag in expansion development which is most probably due to the combined effect of high mechanical properties (depicted by high strength gain), and low Ca content in the mix. Thus, the existing short-term expansion tests might not be able to identify the probable ASR in geopolymer mixes.
- ◆ Test results of subsidiary mixes (Mix 2a and Mix 4a) suggest that the influence of mechanical properties (depicted by strength development) on the expansion gains. It can be clearly identified that the characteristic time lag in expansion curves of geopolymer decreases with the characteristic strength of mortar.
- ◆ Geopolymer shows no significant ASR expansion over the time when exposed to 0.03 M NaOH solution which has approximately similar alkalinity to geopolymer pore solution. It should be noted that similar alkalinity in immersed solution and inside geopolymer would maintain the pore solution alkalinity approximately constant throughout the test. Thus, the Si dissolution during the test would be approximately similar to the Si dissolution inside geopolymer under normal conditions while other acceleration modes incorporated in AMBT would increase the reaction. Experimental results of test set up exposed to 0.03M NaOH (both expansion results and SEM/EDS analysis) suggest that the high initial alkali content in geopolymer doesn't increase its ASR potential and hence, aggregates

classified as nonreactive with OPC can be used with geopolymer without having any additional risk.

- ◆ Mortar bars exposed to Curing Condition III exhibited clear boost in ASR compared to mortar bars exposed to Curing Condition I. It should be noted that the introduction of Calcium increases the final expansions and decreases (almost eliminate) the characteristic time lag in the expansion curves of geopolymer. This strongly suggested the vital role of Ca in ASR mechanism in geopolymer. SEM/EDS analysis in mortar specimens exposed to Curing Condition III further endorses the above reaction mechanism as significant traces of Ca can be identified at the boundary of ASR gel.
- ◆ Since externally supplied calcium (Ca) can induce ASR in geopolymer mortar, there is a serious ASR risk associated with aggregates that can supply Ca (limestone) to the system. Thus, all aggregates with significant Ca traces have to be reviewed before using with geopolymer. In fact, as encountered by few others earlier, alkali carbonate reaction (ACR) might be a more serious issue in geopolymer systems. In addition, activators contain calcium can also increase the risk of ASR in geopolymer systems.
- ◆ Cracks filled with ASR gel were identified in all mixes at the end of the test (150 days) which confirm the occurrence of ASR in mortar mixes. Mix 1 (OPC) and Mix 4 have shown a clear Ca rich gel formation when used with reactive aggregate even at 21 days which aligns with the above mechanism. Mix 2 haven't shown any gel formation and Mix 3 have shown significantly lower gel formation with naturally reactive aggregate (Culcairn). However, all mixes have shown significant ASR gel formation with Ferronickel slag aggregate and fused silica at 21 days which is expected due to the presence of amorphous silica in aggregates.

It should be noted that amorphous silica rapidly increases the Si concentration in the system even at low alkalinity conditions as demonstrated in Chapter 4 and thus, do not need CSH in the system to reach the saturation point of ASR.

- ◆ ASR gel identified in geopolymer contained high aluminium content which might have a detrimental effect on its expansiveness as Al might propel the formation of crosslinks inside ASR gel as in geopolymerization reaction. This significantly reduces the water binding capacity and the swelling capacity of ASR gel which suggest that the distresses caused by the ASR gel in geopolymer is lower than that of OPC.
- ◆ Despite showing lower final expansion compared to Mix 1 (OPC), geopolymer mortar specimens have shown severe distresses (micro crack formation) in SEM analysis. In fact, Mix 4 have shown severe crack formation compared to Mix 1 (OPC) when used with natural reactive aggregate (Culcairn). This is most probably due to the quasi-brittle behaviour of geopolymer mortar. Thus, the existing expansion limits in the AMBT have to be modified before adopting to the geopolymer mortar.
- ◆ Pure amorphous silica sources (fused silica) are not suitable to assess the alkali silica reactivity of geopolymer because amorphous silica act as a silica source in geopolymerization reaction which forms cavities at the binder aggregate interface. So even though ASR gel formed at an alarming rate due to the high Si dissolution, most of them were dissipated into these cavities, minimizing the effective stress development inside geopolymer mortar as depicted by the respective expansion curves.

#### **9.4 Recommendation for a modified accelerated mortar bar test**

1. Conventional initial curing with water (before zero reading) in accelerated mortar bar test might result in excessive alkali leaching which might affect adversely in final outcomes. However, keeping mortar bars at 80 °C without water led to excessive drying and crack formation. Therefore, keeping bars at 80 °C in humidify environment is recommended and incorporated in this study. In addition, mortar bars can be wrapped and sealed before exposed to 80 °C in order to reduce the water evaporation further.
2. 21 days of testing period is not enough to identify the ASR in geopolymer since expansion curves of geopolymer has an initial time lag. Therefore, based on the experimental results of this study it is recommended to continue the test for at least 150 days. However, amount of data in this study is not enough to draw a conclusive recommendation on the test duration.
3. Geopolymer mortar clearly showed a quasi-brittle behaviour compared to OPC which consent with the earlier studies. Therefore, the existing expansion limits have to modified before assessing the reactivity of geopolymer mortar. However, the test data of this study is not enough to define the new limits and required more focused analysis on expansion development and crack formation in geopolymer mortar due to ASR.

#### **9.5 Recommendations for future study**

1. Accelerated mortar bar test is not a definitive test due to the severe curing conditions and often displayed excessive expansions even in normal aggregates which were proven innocuous based on the field records. Thus, it is best to

confirm the ASR in geopolymer with a more accurate test with milder testing conditions such as concrete prism test.

2. Effect of aluminium in the expansiveness of ASR gel shall be analysed further in a more controlled environment. Al rich ASR gel synthesis can be formed at the laboratory to compare the swelling properties with basic ASR gel.
3. This study uses only four aggregates representing each aggregate category. Thus, this study shall be extended further with more reactive and nonreactive aggregates to further confirm the above conclusions.
4. GGBFS is an important component in the practical adaptation of geopolymer as it allows the ambient curing of concrete. Thus, optimum GGBFS content in geopolymer concrete should be experimentally derived based on more experimental data with different GGBFS contents. In fact, it is possible to suggest different GGBFS limits based on the reactivity of aggregate.
5. Effect of external Ca on ASR in geopolymer should be thoroughly analysed to identify the optimum Ca content in a geopolymer mix. It is ideal to identify the limits based on all possible Ca source; aluminosilicate source, activator, aggregate, water, etc.
6. Effect of using Ca rich aggregates (specially limestones) should be further analysed as externally supplied Ca can clearly trigger the ASR in geopolymer systems. In fact, finding the minimum Ca content in aggregate to cause deleterious ASR in geopolymer mortar is important before industrial adaptation of geopolymer.
7. Expansion limits have to be modified before adopting existing testing protocols (designed for OPC) to assess geopolymer systems. It is important to provide

more safety margin in geopolymer due to its quasi-brittle behaviour compared to OPC binders.

## References

- Abdullah, M, Hussin, K, Bnhussain, M, Ismail, K & Ibrahim, W 2011, 'Mechanism and chemical reaction of fly ash geopolymer cement-a review', *Int. J. Pure Appl. Sci. Technol*, vol. 6, no. 1, pp. 35-44.
- Ahmed, W. & Vander Voort, G. 2000. Petrographic examination methods. *Buehler, Ltd. Tech-Notes*, 3.
- Al-Otaibi, S 2008, 'Durability of concrete incorporating GGBS activated by water-glass', *Construction and building materials*, vol. 22, no. 10, pp. 2059-67.
- Al Bakri, AM, Abdulkareem, OA, Rafiza, A, Zarina, Y, Norazian, M & Kamarudin, H 2013, 'Review on Processing of low calcium fly ash geopolymer concrete', *Australian Journal of Basic and Applied Sciences*, vol. 7, no. 5, pp. 342-9.
- Aldred, J & Day, J 2012, 'Is geopolymer concrete a suitable alternative to traditional concrete', in *37th Conference on our world in concrete & structures, Singapore*, pp. 29-31.
- Álvarez-Ayuso, E, Querol, X, Plana, F, Alastuey, A, Moreno, N, Izquierdo, M, Font, O, Moreno, T, Diez, S & Vázquez, E 2008, 'Environmental, physical and structural characterisation of geopolymer matrixes synthesised from coal (co-) combustion fly ashes', *Journal of Hazardous Materials*, vol. 154, no. 1, pp. 175-83.
- Antonić, T, Čižmek, A & Subotić, B 1994, 'Dissolution of amorphous aluminosilicate zeolite precursors in alkaline solutions. Part 2.—Mechanism of the dissolution', *Journal of the Chemical Society, Faraday Transactions*, vol. 90, no. 13, pp. 1973-7.

- Aquino, W, Lange, D & Olek, J 2001, 'The influence of metakaolin and silica fume on the chemistry of alkali-silica reaction products', *Cement and Concrete Composites*, vol. 23, no. 6, pp. 485-93.
- AS1141.60.1 2014, *Methods for sampling and testing aggregates Method 60.1: Potential alkali-silica reactivity-Accelerated mortar bar method*, AS 1141.60.1-2014, Standards Australia, Sydney.
- AS1141.60.2 2014, *Methods for sampling and testing aggregates Method 60.2: Potential alkali-silica reactivity-Concrete prism method*, AS 1141.60.2-2014, Standards Australia, Sydney.
- ASTM-C289-07 2007, *Standard Test Method for Potential Alkali-Silica Reactivity of Aggregates (Chemical Method)* ASTM International, West Conshohocken.
- ASTM-C618-17 2017, *Standard Specification for Coal Fly Ash and Raw or Calcined Natural Pozzolan for Use in Concrete*, ASTM International, West Conshohocken.
- AS 1141.60.1 2014, *Methods for sampling and testing aggregates Method 60.1: Potential alkali-silica reactivity-Accelerated mortar bar method*, Standards Australia, Sydney.
- HB79 2015, *Alkali Aggregate reaction - Guidelines on Minimising the Risk of Damage to Concrete Structures in Australia*, Standards Australia, Sydney.
- AS 3582.1 2016a, *Supplementary cementitious materials Part 1: Fly ash*, Standards Australia, Sydney.
- AS 3582.2 2016b, *Supplementary cementitious materials Part 2: Slag-Ground granulated blast-furnance*, Standards Australia, Sydney.
- Badar, MS, Kupwade-Patil, K, Bernal, SA, Provis, JL & Allouche, EN 2014, 'Corrosion of steel bars induced by accelerated carbonation in low and high calcium fly ash geopolymer concretes', *Construction and building materials*, vol. 61, pp. 79-89.

- Bakharev, T 2005, 'Resistance of geopolymer materials to acid attack', *Cement and Concrete Research*, vol. 35, no. 4, pp. 658-70.
- Bakharev, T, Sanjayan, J & Cheng, YB 2001a, 'Resistance of alkali-activated slag concrete to alkali-aggregate reaction', *Cement and Concrete Research*, vol. 31, no. 2, pp. 331-4.
- Bakharev, T, Sanjayan, J & Cheng, YB 2001b, 'Resistance of alkali-activated slag concrete to carbonation', *Cement and Concrete Research*, vol. 31, no. 9, pp. 1277-83.
- Bakharev, T, Sanjayan, J & Cheng, YB 2002, 'Sulfate attack on alkali-activated slag concrete', *Cement and Concrete Research*, vol. 32, no. 2, pp. 211-6.
- Bernal, SA & Provis, JL 2014, 'Durability of alkali- activated materials: progress and perspectives', *Journal of the American Ceramic Society*, vol. 97, no. 4, pp. 997-1008.
- Bernal, SA, Provis, JL, Brice, DG, Kilcullen, A, Duxson, P & van Deventer, JS 2012, 'Accelerated carbonation testing of alkali-activated binders significantly underestimates service life: the role of pore solution chemistry', *Cement and Concrete Research*, vol. 42, no. 10, pp. 1317-26.
- Bickmore, BR, Nagy, KL, Gray, AK & Brinkerhoff, AR 2006, 'The effect of  $Al(OH)_4^-$  on the dissolution rate of quartz', *Geochimica et Cosmochimica Acta*, vol. 70, no. 2, pp. 290-305.
- Castel, A & Foster, SJ 2015, 'Bond strength between blended slag and Class F fly ash geopolymer concrete with steel reinforcement', *Cement and Concrete Research*, vol. 72, pp. 48-53.

- CDC *Aggregate quarrying*, Centers for Disease Control and Prevention, viewed 18.01 2018, <<https://www.cdc.gov/niosh/mining/works/statistics/factsheets/miningfacts2014.html>>.
- CEMBUREAU 2016, *ACTIVITY REPORT*, The European Cement Association.
- Chan, S 1989, 'A review on solubility and polymerization of silica', *Geothermics*, vol. 18, no. 1-2, pp. 49-56.
- Chappex, T & Scrivener, KL 2012, 'The influence of aluminium on the dissolution of amorphous silica and its relation to alkali silica reaction', *Cement and Concrete Research*, vol. 42, no. 12, pp. 1645-9.
- Chatterji, S, Jensen, AD, Thaulow, N & Christensen, P 1986, 'Studies of alkali-silica reaction. Part 3. Mechanisms by which NaCl and Ca(OH)<sub>2</sub> affect the reaction', *Cement and Concrete Research*, vol. 16, no. 2, pp. 246-54.
- Chatterji, S. & Christensen, P. 1990. Studies of alkali-silica reaction. Part 7. Modelling of expansion. *Cement and Concrete Research*, 20, 285-290.
- Chindaprasirt, P, Chareerat, T & Sirivivatnanon, V 2007, 'Workability and strength of coarse high calcium fly ash geopolymer', *Cement and Concrete Composites*, vol. 29, no. 3, pp. 224-9.
- Chitralla, S, Jadaprolu, GJ & Chundupalli, S 2018, 'Study and predicting the stress-strain characteristics of geopolymer concrete under compression', *Case studies in construction materials*, vol. 8, pp. 172-92.
- Choi, YC & Choi, S 2015, 'Alkali-silica reactivity of cementitious materials using ferro-nickel slag fine aggregates produced in different cooling conditions', *Construction and building materials*, vol. 99, pp. 279-87.
- Christy, CF & Tensing, D 2011, 'Greener building material with fly ash', *Asian Journal of Civil Engineering*, vol. 12, no. 1, pp. 87-105.

- Comi, C., Kirchmayr, B. & Pignatelli, R. 2012. Two-phase damage modeling of concrete affected by alkali–silica reaction under variable temperature and humidity conditions. *International Journal of Solids and Structures*, 49, 3367-3380.
- Crundwell, FK 2017, ‘On the mechanism of the dissolution of quartz and silica in aqueous solutions’, *ACS Omega*, vol. 2, no. 3, pp. 1116-27.
- Curtis, D. D. A review and analysis of AAR-effects in arch dams. The 11th International Conference on Alkali–Aggregate reaction (ICAAR), Quebec, Canada, 2000. 1273-1282.
- Dang, J, Shen, X, Castel, A & Aldred, J 2016, ‘Monitoring Apparent pH Value in Geopolymer Concrete Using Glass Electrode’, in *ISARC. Proceedings of the International Symposium on Automation and Robotics in Construction*, vol. 33, p. 1.
- Davidovits, J 1991, ‘Geopolymers: inorganic polymeric new materials’, *Journal of Thermal Analysis and calorimetry*, vol. 37, no. 8, pp. 1633-56.
- Davidovits, J 1994, ‘Properties of geopolymer cements’, in *First international conference on alkaline cements and concretes*, vol. 1, pp. 131-49.
- Davidovits, J 2002, ‘years of successes and failures in geopolymer applications. Market trends and potential breakthroughs’, in *Geopolymer 2002 Conference*, vol. 28, p. 29.
- Davidovits, J 2008, *Geopolymer chemistry and applications*, 1<sup>st</sup> edn, Geopolymer Institute.
- Davidovits, J 2011, *Geopolymer chemistry and applications*, 3<sup>rd</sup> edn, Geopolymer Institute.
- Deb, PS, Nath, P & Sarker, PK 2014, ‘The effects of ground granulated blast-furnace slag blending with fly ash and activator content on the workability and strength

- properties of geopolymer concrete cured at ambient temperature', *Materials & Design (1980-2015)*, vol. 62, pp. 32-9.
- Diamond, S 1976, 'A review of alkali-silica reaction and expansion mechanisms 2. Reactive aggregates', *Cement and Concrete Research*, vol. 6, no. 4, pp. 549-60.
- Diaz, E & Allouche, E 2010, 'Recycling of fly ash into geopolymer concrete: creation of a database', in *Green Technologies Conference, 2010 IEEE*, pp. 1-7.
- Diaz, E, Allouche, E & Eklund, S 2010, 'Factors affecting the suitability of fly ash as source material for geopolymers', *Fuel*, vol. 89, no. 5, pp. 992-6.
- Douglas, E, Bilodeau, A & Malhotra, V 1992, 'Properties and durability of alkali-activated slag concrete', *Materials Journal*, vol. 89, no. 5, pp. 509-16.
- Dung, NT, Chang, T-P & Chen, CT 2014, 'Engineering and sulfate resistance properties of slag-CFBC fly ash paste and mortar', *Construction and building materials*, vol. 63, pp. 40-8.
- Duxson, P, Fernández-Jiménez, A, Provis, JL, Lukey, GC, Palomo, A & Van Deventer, J 2007, 'Geopolymer technology: the current state of the art', *Journal of Materials Science*, vol. 42, no. 9, pp. 2917-33.
- Duxson, P & Provis, JL 2008, 'Designing precursors for geopolymer cements', *Journal of the American Ceramic Society*, vol. 91, no. 12, pp. 3864-9.
- Fadhil Nuruddin, M & Razak, SNA 2014, 'Effects of Geopolymer Concrete Fly Ash Based on Alkali Silica Reaction (ASR)', *Applied Mechanics & Materials*, no. 567.
- Fang, Y & Kayali, O 2013, 'The fate of water in fly ash-based geopolymers', *Construction and building materials*, vol. 39, pp. 89-94.
- Farny, JA & Kosmatka, SH 1997, *Diagnosis and control of alkali-aggregate reactions in concrete*, Portland Cement Association.

- Fernandes, I & Broekmans, MA 2013, 'Alkali-silica reactions: an overview. Part I', *Metallography, Microstructure, and Analysis*, vol. 2, no. 4, pp. 257-67.
- Fernández-Jiménez, A & Palomo, A 2003, 'Characterisation of fly ashes. Potential reactivity as alkaline cements☆', *Fuel*, vol. 82, no. 18, pp. 2259-65.
- Fernández-Jiménez, A & Puertas, F 2002, 'The alkali-silica reaction in alkali-activated granulated slag mortars with reactive aggregate', *Cement and Concrete Research*, vol. 32, no. 7, pp. 1019-24.
- Fernandez-Jimenez, AM, Palomo, A & Lopez-Hombrados, C 2006, 'Engineering properties of alkali-activated fly ash concrete', *ACI Materials Journal*, vol. 103, no. 2, pp. 106-12.
- Fifinatasha, S, Kamarudin, H, Zarina, Y, Rafiza, AR & Liyana, J 2013, 'Reviews on the different sources materials to the geopolymer performance'.
- Fournier, B & Bérubé, M-A 2000, 'Alkali-aggregate reaction in concrete: a review of basic concepts and engineering implications', *Canadian Journal of Civil Engineering*, vol. 27, no. 2, pp. 167-91.
- Gaboriaud, F, Nonat, A, Chaumont, D & Craievich, A 1999, 'Aggregation and Gel Formation in Basic Silico- Calco- Alkaline Solutions Studied: A SAXS, SANS, and ELS Study', *The Journal of Physical Chemistry B*, vol. 103, no. 28, pp. 5775-81.
- Ganesan, N, Abraham, R & Raj, SD 2015, 'Durability characteristics of steel fibre reinforced geopolymer concrete', *Construction and building materials*, vol. 93, pp. 471-6.
- Garcia-Diaz, E, Riche, J, Bulteel, D & Vernet, C 2006, 'Mechanism of damage for the alkali-silica reaction', *Cement and Concrete Research*, vol. 36, no. 2, pp. 395-400.

- García-Lodeiro, I, Palomo, A & Fernández-Jiménez, A 2007, 'Alkali–aggregate reaction in activated fly ash systems', *Cement and Concrete Research*, vol. 37, no. 2, pp. 175-83.
- Gholizadeh-Vayghan, A & Rajabipour, F 2017, 'The influence of alkali–silica reaction (ASR) gel composition on its hydrophilic properties and free swelling in contact with water vapor', *Cement and Concrete Research*, vol. 94, pp. 49-58.
- Gifford, P & Gillott, J 1996, 'Alkali-silica reaction (ASR) and alkali-carbonate reaction (ACR) in activated blast furnace slag cement (ABFSC) concrete', *Cement and Concrete Research*, vol. 26, no. 1, pp. 21-6.
- Gijbels, K, Pontikes, Y, Iacobescu, RI, Schreurs, S, Schroevers, W & Kuppens, T 2017, 'Techno-economic and environmental analysis of alkali-activated materials containing phosphogypsum and blast furnace slag'.
- Giorla, A. B. 2013, Modelling of alkali-silica reaction under multi-axial load. Doctor of Philosophy (PhD), École polytechnique fédérale de Lausanne.
- Glasser, LD 1979, 'Osmotic pressure and the swelling of gels', *Cement and Concrete Research*, vol. 9, no. 4, pp. 515-7.
- Glasser, L. D. & KATAOKA, N. 1981. The chemistry of 'alkali-aggregate' reaction. *Cement and concrete research*, 11, 1-9.
- Gourley, J 2003, 'Geopolymers; opportunities for environmentally friendly construction materials', in *Materials 2003 Conference: Adaptive Materials for a Modern Society*, Sydney, Institute of Materials Engineering Australia.
- Grattan-Bellew, P 1992, '8 Alkali-silica reaction—Canadian experience', *The Alkali-Silica Reaction in Concrete*, pp. 223-48.

- Gunasekara, C 2016, 'Influence of properties of fly ash from different sources on the mix design and performance of geopolymer concrete', Doctor of Philosophy (PhD) thesis, RMIT University.
- Hardjito, D 2005, 'Studies of fly ash-based geopolymer concrete', PhD thesis, Curtin University, accessed 27 August 2018 from escape - Curtin's institutional repository.
- Hardjito, D & Rangan, BV 2005, 'Development and properties of low-calcium fly ash-based geopolymer concrete', escape - Curtin's institutional repository.
- Hardjito, D, Wallah, S, Sumajouw, D & Rangan, B 2004, 'Brief review of development of geopolymer concrete', in *8th CANMET/ACI International Conference on fly ash, silica fume, slag and natural pozzolans in concrete. Las Vegas (USA)*.
- Hardjito, D, Wallah, SE, Sumajouw, DM & Rangan, BV 2004, 'On the development of fly ash-based geopolymer concrete', *ACI Materials Journal-American Concrete Institute*, vol. 101, no. 6, pp. 467-72.
- Hasanbeigi, A, Price, L & Lin, E 2012, 'Emerging energy-efficiency and CO<sub>2</sub> emission-reduction technologies for cement and concrete production: A technical review', *Renewable and Sustainable Energy Reviews*, vol. 16, no. 8, pp. 6220-38.
- HB79 2015, *Alkali Aggregate reaction - Guidelines on Minimising the Risk of Damage to Concrete Structures in Australia*, SA HB79-2015, Standards Australia, Sydney.
- Hobbs, DW 1988, *Alkali-silica reaction in concrete*, Thomas Telford Publishing.
- Hong, S-Y & Glasser, F 2002, 'Alkali sorption by CSH and CASH gels: Part II. Role of alumina', *Cement and Concrete Research*, vol. 32, no. 7, pp. 1101-11.
- Hou, X, Kirkpatrick, RJ, Struble, LJ & Monteiro, PJ 2005, 'Structural investigations of alkali silicate gels', *Journal of the American Ceramic Society*, vol. 88, no. 4, pp. 943-9.

- Hou, X, Struble, LJ & Kirkpatrick, RJ 2004, 'Formation of ASR gel and the roles of CSH and portlandite', *Cement and Concrete Research*, vol. 34, no. 9, pp. 1683-96.
- <http://www.sandatlas.org> TAS diagram, Sandatlas, viewed 18.01.2018, <<http://www.sandatlas.org/tas-diagram/>>.
- Hünger, K-J 2007, 'The contribution of quartz and the role of aluminum for understanding the AAR with greywacke', *Cement and Concrete Research*, vol. 37, no. 8, pp. 1193-205.
- Ichikawa, T 2009, 'Alkali-silica reaction, pessimum effects and pozzolanic effect', *Cement and Concrete Research*, vol. 39, no. 8, pp. 716-26.
- Ichikawa, T & Miura, M 2007, 'Modified model of alkali-silica reaction', *Cement and Concrete research*, vol. 37, no. 9, pp. 1291-7.
- Islam, M. S. & Ghafouri, N. 2016. Experimental study and empirical modeling of lithium nitrate for alkali-silica reactivity. *Construction and Building Materials*, 121, 717-726.
- Ismail, I, Bernal, SA, Provis, JL, Hamdan, S & van Deventer, JS 2013, 'Microstructural changes in alkali activated fly ash/slag geopolymers with sulfate exposure', *Materials and Structures*, vol. 46, no. 3, pp. 361-73.
- Jensen, A. D., Chatterji, S., Christensen, P. & Thaulow, N. 1984. Studies of alkali-silica reaction—part II effect of air-entrainment on expansion. *Cement and Concrete Research*, 14, 311-314.
- Jones, A. & Clark, L. 1996. The effects of restraint on ASR expansion of reinforced concrete. *Magazine of Concrete Research*, 48, 1-13.
- Katsiotis, N, Tsakiridis, P, Velissariou, D, Katsiotis, M, Alhassan, S & Beazi, M 2015, 'Utilization of ferronickel slag as additive in Portland cement: a hydration leaching study', *Waste and Biomass Valorization*, vol. 6, no. 2, pp. 177-89.

- Kawamura, M. & Fuwa, H. 2003. Effects of lithium salts on ASR gel composition and expansion of mortars. *Cement and Concrete Research*, 33, 913-919.
- Kim, T & Olek, J 2014, 'Chemical Sequence and Kinetics of Alkali- Silica Reaction Part I. Experiments', *Journal of the American Ceramic Society*, vol. 97, no. 7, pp. 2195-203.
- Kim, T & Olek, J 2014, 'Chemical Sequence and Kinetics of Alkali–Silica Reaction Part II. A Thermodynamic Model', *Journal of the American Ceramic Society*, vol. 97, no. 7, pp. 2204-12.
- Kriven, W, Gordon, M, Ervin, B & Reis, H 2007, 'Corrosion protection assessment of concrete reinforcing bars with a geopolymer coating', in *Ceram. Eng. Sci. Proc*, vol. 28, pp. 373-81.
- Krivenko, P, Drochytka, R, Gelevera, A & Kavalerova, E 2014, 'Mechanism of preventing the alkali–aggregate reaction in alkali activated cement concretes', *Cement and Concrete Composites*, vol. 45, pp. 157-65.
- Kuehl, H 1908, *Slag cement and process of making the same*, Google Patents, <https://www.google.com.au/patents/US900939>.
- Kukko, H & Mannonen, R 1982, 'Chemical and mechanical properties of alkali-activated blast furnace slag (F-concrete)', *Nordic Concrete Research*, no. 1.
- Kumar, S, Kumar, R & Mehrotra, S 2010, 'Influence of granulated blast furnace slag on the reaction, structure and properties of fly ash based geopolymer', *Journal of Materials Science*, vol. 45, no. 3, pp. 607-15.
- Kupwade-Patil, K & Allouche, E 2011, 'Effect of alkali silica reaction (ASR) in geopolymer concrete', in *World of Coal Ash (WOCA) conference*, pp. 9-12.

- Kupwade-Patil, K & Allouche, EN 2012, 'Impact of alkali silica reaction on fly ash-based geopolymer concrete', *Journal of materials in Civil Engineering*, vol. 25, no. 1, pp. 131-9.
- Ly, L, Vance ER, Perera, DS, Aly, Z and Olufson, K 2007, 'Leaching of Geopolymers in Deionised Water', *Azo Journal of Materials Online*.
- Langer, WH & Arbogast, BF 2002, 'Environmental impacts of mining natural aggregate', in *Deposit and geoenvironmental models for resource exploitation and environmental security*, Springer, pp. 151-69.
- Law, DW, Adam, AA, Molyneaux, TK, Patnaikuni, I & Wardhono, A 2015, 'Long term durability properties of class F fly ash geopolymer concrete', *Materials and Structures*, vol. 48, no. 3, pp. 721-31.
- Le Maitre, RW, Streckeisen, A, Zanettin, B, Le Bas, M, Bonin, B & Bateman, P 2005, *Igneous rocks: a classification and glossary of terms: recommendations of the International Union of Geological Sciences Subcommission on the Systematics of Igneous Rocks*, Cambridge University Press.
- Lee, W & Van Deventer, J 2007, 'Chemical interactions between siliceous aggregates and low-Ca alkali-activated cements', *Cement and Concrete Research*, vol. 37, no. 6, pp. 844-55.
- Leemann, A, Katayama, T, Fernandes, I & Broekmans, MA 2016, 'Types of alkali-aggregate reactions and the products formed', *Proceedings of the Institution of Civil Engineers-Construction Materials*, vol. 169, no. 3, pp. 128-35.
- Leemann, A, Le Saout, G, Winnefeld, F, Rentsch, D & Lothenbach, B 2011, 'Alkali-silica reaction: the influence of calcium on silica dissolution and the formation of reaction products', *Journal of the American Ceramic Society*, vol. 94, no. 4, pp. 1243-9.

- Leemann, A & Lura, P 2013, 'E-modulus of the alkali-silica-reaction product determined by micro-indentation', *Construction and building materials*, vol. 44, pp. 221-7.
- Leemann, A & Merz, C 2013, 'An attempt to validate the ultra-accelerated microbar and the concrete performance test with the degree of AAR-induced damage observed in concrete structures', *Cement and Concrete Research*, vol. 49, pp. 29-37.
- Li, C, Sun, H & Li, L 2010, 'A review: The comparison between alkali-activated slag (Si+ Ca) and metakaolin (Si+ Al) cements', *Cement and Concrete Research*, vol. 40, no. 9, pp. 1341-9.
- Li, Z, Ding, Z & Zhang, Y 2004, 'Development of sustainable cementitious materials', in *Proceedings of international workshop on sustainable development and concrete technology, Beijing, China*, pp. 55-76.
- Lloyd, N & Rangan, V 2010, 'Geopolymer concrete with fly ash', in *Proceedings of the Second International Conference on Sustainable Construction Materials and Technologies*, pp. 1493-504.
- Lloyd, RR, Provis, JL & Van Deventer, JS 2010, 'Pore solution composition and alkali diffusion in inorganic polymer cement', *Cement and Concrete Research*, vol. 40, no. 9, pp. 1386-92.
- Lu, D, Liu, Y, Zheng, Y, Xu, Z & Shen, X 2013, 'Alkali-aggregate reactivity of typical siliceous glass and carbonate rocks in alkali-activated fly ash based geopolymers', in *Fourth International Conference on Smart Materials and Nanotechnology in Engineering, International Society for Optics and Photonics*, vol. 8793, p. 879313.
- Luna-Galiano, Y, Fernández-Pereira, C & Izquierdo, M 2016, 'Contributions to the study of porosity in fly ash-based geopolymers. Relationship between degree of

- reaction, porosity and compressive strength', *Materiales de Construcción*, vol. 66, no. 324, p. 098.
- Ma, Q, Nanukuttan, SV, Basheer, PM, Bai, Y & Yang, C 2016, 'Chloride transport and the resulting corrosion of steel bars in alkali activated slag concretes', *Materials and Structures*, vol. 49, no. 9, pp. 3663-77.
- Malhotra, V 2002, 'Introduction: sustainable development and concrete technology', *Concrete International*, vol. 24, no. 7.
- McCormick, Av & Bell, A 1989, 'The solution chemistry of zeolite precursors', *Catalysis Reviews—Science and Engineering*, vol. 31, no. 1-2, pp. 97-127.
- McCoy, W & Caldwell, A 1951, 'New approach to inhibiting alkali-aggregate expansion', in *Journal Proceedings*, vol. 47, pp. 693-706.
- Mikulčić, H, Klemeš, JJ, Vujanović, M, Urbaniec, K & Duić, N 2016, 'Reducing greenhouse gasses emissions by fostering the deployment of alternative raw materials and energy sources in the cleaner cement manufacturing process', *Journal of Cleaner Production*, vol. 136, pp. 119-32.
- Miranda, J, Fernández-Jiménez, A, González, J & Palomo, A 2005, 'Corrosion resistance in activated fly ash mortars', *Cement and Concrete Research*, vol. 35, no. 6, pp. 1210-7.
- Mitsyuk, B 1984, 'Mechanism of silica dissolution and state of silicic acid in hydrothermal solutions', *Theoretical and Experimental Chemistry*, vol. 19, no. 5, pp. 554-9.
- Monticelli, C, Natali, M, Balbo, A, Chiavari, C, Zanotto, F, Manzi, S & Bignozzi, M 2016, 'Corrosion behavior of steel in alkali-activated fly ash mortars in the light of their microstructural, mechanical and chemical characterization', *Cement and Concrete Research*, vol. 80, pp. 60-8.

- Multon, S. & Toutlemonde, F. 2006. Effect of applied stresses on alkali–silica reaction-induced expansions. *Cement and Concrete Research*, 36, 912-920.
- Multon, S, Cyr, M, Sellier, A, Leklou, N & Petit, L 2008, ‘Coupled effects of aggregate size and alkali content on ASR expansion’, *Cement and Concrete Research*, vol. 38, no. 3, pp. 350-9.
- Multon, S & Toutlemonde, F 2010, ‘Effect of moisture conditions and transfers on alkali silica reaction damaged structures’, *Cement and Concrete Research*, vol. 40, no. 6, pp. 924-34.
- Nath, P 2014, ‘Study of fly ash based geopolymer concrete cured in ambient condition’, PhD thesis, Curtin University, accessed 27 August 2018 from escape - Curtin’s institutional repository.
- Neto, AAM, Cincotto, MA & Repette, W 2008, ‘Drying and autogenous shrinkage of pastes and mortars with activated slag cement’, *Cement and Concrete Research*, vol. 38, no. 4, pp. 565-74.
- Neves, JM 2016, ‘The Alkali-Silica Reaction in Alkali-Activated Fly Ash Concrete’, MSc thesis, The Pennsylvania State University, accessed 27 August 2018 from Pennstate.
- Neville, A 1995, ‘Chloride attack of reinforced concrete: an overview’, *Materials and Structures*, vol. 28, no. 2, p. 63.
- Neville, AM 2011, *Properties of concrete by A.M. Neville*, Harlow : Prentice Hall, 2011, 5th ed.
- Niibori, Y, Kunita, M, Tochiyama, O & Chida, T 2000, ‘Dissolution rates of amorphous silica in highly alkaline solution’, *Journal of nuclear science and technology*, vol. 37, no. 4, pp. 349-57.

- Noushini, A, Aslani, F, Castel, A, Gilbert, RI, Uy, B & Foster, S 2016, 'Compressive stress-strain model for low-calcium fly ash-based geopolymer and heat-cured Portland cement concrete', *Cement and Concrete Composites*, vol. 73, pp. 136-46.
- Palomo, A, Grutzeck, M & Blanco, M 1999, 'Alkali-activated fly ashes: a cement for the future', *Cement and Concrete Research*, vol. 29, no. 8, pp. 1323-9.
- Palomo, A, Krivenko, P, Garcia-Lodeiro, I, Kavalerova, E, Maltseva, O & Fernández-Jiménez, A 2014, 'A review on alkaline activation: new analytical perspectives', *Materiales de Construcción*, vol. 64, no. 315, p. 022.
- Pan, J, Feng, Y, Wang, J, Sun, Q, Zhang, C & Owen, D 2012, 'Modeling of alkali-silica reaction in concrete: a review', *Frontiers of Structural and Civil Engineering*, vol. 6, no. 1, pp. 1-18.
- Pan, Z, Sanjayan, JG & Rangan, BV 2011, 'Fracture properties of geopolymer paste and concrete', *Magazine of concrete research*, vol. 63, no. 10, pp. 763-71.
- Panias, D, Giannopoulou, IP & Perraki, T 2007, 'Effect of synthesis parameters on the mechanical properties of fly ash-based geopolymers', *Colloids and Surfaces A: Physicochemical and Engineering Aspects*, vol. 301, no. 1, pp. 246-54.
- Patankar, SV, Ghugal, YM & Jamkar, SS 2014, 'Effect of concentration of sodium hydroxide and degree of heat curing on fly ash-based geopolymer mortar', *Indian Journal of Materials Science*, vol. 2014.
- Penttala, V 1997, 'Concrete and sustainable development', *ACI Materials Journal*, vol. 94, no. 5, pp. 409-16.
- Phoo-ngernkham, T, Chindaprasirt, P, Sata, V, Pangdaeng, S & Sinsiri, T 2013, 'Properties of high calcium fly ash geopolymer pastes with Portland cement as an

- additive’, *International Journal of Minerals, Metallurgy, and Materials*, vol. 20, no. 2, pp. 214-20.
- Pokrovsky, OS & Schott, J 2000, ‘Kinetics and mechanism of forsterite dissolution at 25 C and pH from 1 to 12’, *Geochimica et Cosmochimica Acta*, vol. 64, no. 19, pp. 3313-25.
- Pouhet, R & Cyr, M 2015, ‘Alkali–silica reaction in metakaolin-based geopolymer mortar’, *Materials and Structures*, vol. 48, no. 3, pp. 571-83.
- Poyet, S, Sellier, A, Capra, B, Foray, G, Torrenti, JM, Cognon, H & Bourdarot, E 2007, ‘Chemical modelling of alkali silica reaction: influence of the reactive aggregate size distribution’, *Materials and Structures*, vol. 40, no. 2, p. 229.
- Prezzi, M, Monteiro, PJ & Sposito, G 1997, ‘The alkali–silica reaction: Part I. Use of the double-layer theory to explain the behavior of reaction-product gels’, *ACI Materials Journal*, vol. 94, no. 1, pp. 10-7.
- Provis, JL 2014, ‘Geopolymers and other alkali activated materials: why, how, and what?’, *Materials and Structures*, vol. 47, no. 1-2, pp. 11-25.
- Provis, JL, Fernández-Jiménez, A, Kamseu, E, Leonelli, C & Palomo, A 2014, ‘Binder Chemistry–Low-Calcium Alkali-Activated Materials’, in *Alkali Activated Materials*, Springer, pp. 93-123.
- Provis, JL, Myers, RJ, White, CE, Rose, V & van Deventer, JS 2012, ‘X-ray microtomography shows pore structure and tortuosity in alkali-activated binders’, *Cement and Concrete Research*, vol. 42, no. 6, pp. 855-64.
- Puertas, F, Martínez-Ramírez, S, Alonso, S & Vazquez, T 2000, ‘Alkali-activated fly ash/slag cements: strength behaviour and hydration products’, *Cement and Concrete Research*, vol. 30, no. 10, pp. 1625-32.

- Puertas, F, Palacios, M, Gil-Maroto, A & Vázquez, T 2009, 'Alkali-aggregate behaviour of alkali-activated slag mortars: Effect of aggregate type', *Cement and Concrete Composites*, vol. 31, no. 5, pp. 277-84.
- Puertas, F, Palacios, M & Provis, JL 2014, 'Admixtures', in JL Provis & JSJ van Deventer (eds), *Alkali Activated Materials: State-of-the-Art Report, RILEM TC 224-AAM*, Springer Netherlands, Dordrecht, pp. 145-56.
- Rajabipour, F, Giannini, E, Dunant, C, Ideker, JH & Thomas, MD 2015, 'Alkali-silica reaction: current understanding of the reaction mechanisms and the knowledge gaps', *Cement and Concrete Research*, vol. 76, pp. 130-46.
- Reddy, DV, Edouard, J-B & Sobhan, K 2012, 'Durability of fly ash-based geopolymer structural concrete in the marine environment', *Journal of materials in Civil Engineering*, vol. 25, no. 6, pp. 781-7.
- Rivard, P., Fournier, B. & Ballivy, G. 2002. The Damage Rating Index Method for ASR Affected Concrete—A Critical Review of Petrographic Features of Deterioration and Evaluation Criteria. *Cement, Concrete, and Aggregates*, 1.
- Ryno, B 2014, 'Mechanical properties of fly ash/slag based geopolymer concrete with the addition of macro fibres', MSc thesis, Stellenbosch University, accessed 27 August 2018 from SUNScholar Research Repository.
- Ryu, GS, Lee, YB, Koh, KT & Chung, YS 2013, 'The mechanical properties of fly ash-based geopolymer concrete with alkaline activators', *Construction and building materials*, vol. 47, pp. 409-18.
- Saha, AK & Sarker, PK 2016, 'Expansion due to alkali-silica reaction of ferronickel slag fine aggregate in OPC and blended cement mortars', *Construction and building materials*, vol. 123, pp. 135-42.

- Saha, AK & Sarker, PK 2017, 'Sustainable use of ferronickel slag fine aggregate and fly ash in structural concrete: Mechanical properties and leaching study', *Journal of Cleaner Production*.
- Šahinagić-Isović, APM, Šahinagić-Isović, M, Markovski, G & Čećez, M 2012, 'Shrinkage strain of concrete-causes and types', *Građevinar*, vol. 64, no. 09, pp. 727-34.
- Sanchez, L., Fournier, B., Jolin, M., Bedoya, M., Bastien, J. & Duchesne, J. 2016. Use of Damage Rating Index to Quantify Alkali-Silica Reaction Damage in Concrete: Fine versus Coarse Aggregate. *ACI Materials Journal*, 113.
- Sang, JC, Jakubik, RF, Barkatt, A & Saad, EE 1994, 'The interaction of solutes with silicate glass and its effect on dissolution rates', *Journal of non-crystalline solids*, vol. 167, no. 1-2, pp. 158-71.
- Sarker, PK 2011, 'Bond strength of reinforcing steel embedded in fly ash-based geopolymer concrete', *Materials and Structures*, vol. 44, no. 5, pp. 1021-30.
- Schwartzentruber, J, Fürst, W & Renon, H 1987, 'Dissolution of quartz into dilute alkaline solutions at 90 C: a kinetic study', *Geochimica et Cosmochimica Acta*, vol. 51, no. 7, pp. 1867-74.
- Schwing, K 2010, 'Use of Fly Ash in the Mitigation of Alkali-Silica Reaction in Concrete', MSc thesis, Oregon State University.
- Shafaatian, S 2012, 'Innovative methods to mitigate alkali-silica reaction in concrete materials containing recycled glass aggregates', PhD thesis, The Pennsylvania State University, accessed 27 August 2018 from PennState
- Shi, C, Roy, D & Krivenko, P 2006, *Alkali-activated cements and concretes*, CRC press.

- Shi, C, Shi, Z, Hu, X, Zhao, R & Chong, L 2015, 'A review on alkali-aggregate reactions in alkali-activated mortars/concretes made with alkali-reactive aggregates', *Materials and Structures*, vol. 48, no. 3, pp. 621-8.
- Shi, Z, Shi, C, Wan, S & Ou, Z 2017, 'Effect of alkali dosage on alkali-silica reaction in sodium hydroxide activated slag mortars', *Construction and building materials*, vol. 143, pp. 16-23.
- Shi, Z, Shi, C, Zhao, R & Wan, S 2015, 'Comparison of alkali-silica reactions in alkali-activated slag and Portland cement mortars', *Materials and Structures*, vol. 48, no. 3, pp. 743-51.
- Shon, CS, Zollinger, DG & Sarkar, SL 2002, 'Evaluation of modified ASTM C 1260 accelerated mortar bar test for alkali-silica reactivity', *Cement and Concrete Research*, vol. 32, no. 12, pp. 1981-7.
- Sindhunata, Van Deventer, J, Lukey, G & Xu, H 2006, 'Effect of curing temperature and silicate concentration on fly-ash-based geopolymerization', *Industrial & engineering chemistry research*, vol. 45, no. 10, pp. 3559-68.
- Singh, B, Ishwarya, G, Gupta, M & Bhattacharyya, S 2015, 'Geopolymer concrete: a review of some recent developments', *Construction and building materials*, vol. 85, pp. 78-90.
- Sofi, M, Van Deventer, J, Mendis, P & Lukey, G 2007a, 'Bond performance of reinforcing bars in inorganic polymer concrete (IPC)', *Journal of Materials Science*, vol. 42, no. 9, pp. 3107-16.
- Sofi, M, Van Deventer, J, Mendis, P & Lukey, G 2007b, 'Engineering properties of inorganic polymer concretes (IPCs)', *Cement and Concrete Research*, vol. 37, no. 2, pp. 251-7.

- Soh, WM, Tan, J, Heng, JY & Cheeseman, C 2017, 'Production of cenospheres from coal fly ash through vertical thermal flame (VTF) process'.
- Song, X 2007, 'Development and performance of class F fly ash based geopolymer concretes against sulphuric acid attack', PhD thesis, University of New South Wales, Sydney, Australia, accessed 27 August 2018 from National Library of Australia (Trove),
- Standon, T 1940, 'Expansion of Concrete Through Reaction Between Cement and Aggregate [C]', in *Proc. ASCE*, vol. 6, p. 1.
- Stark, D 1991, 'The moisture condition of field concrete exhibiting alkali-silica reactivity', *Special Publication*, vol. 126, pp. 973-88.
- Stokes, J 2011, 'An Analysis of the Design and Assembly of the AAR Tri-axial Machine', PhD thesis, Polytechnic University of Catalonia, accessed 27 August 2018
- Struble, LJ & Diamond, S 1981, 'Swelling properties of synthetic alkali silica gels', *Journal of the American Ceramic Society*, vol. 64, no. 11, pp. 652-5.
- Summerbell, DL, Barlow, CY & Cullen, JM 2016, 'Potential reduction of carbon emissions by performance improvement: A cement industry case study', *Journal of Cleaner Production*, vol. 135, pp. 1327-39.
- Swamy, RN 2002, *The alkali-silica reaction in concrete*, CRC Press.
- Tänzer, R, Jin, Y & Stephan, D 2017, 'Effect of the inherent alkalis of alkali activated slag on the risk of alkali silica reaction', *Cement and Concrete Research*, vol. 98, pp. 82-90.
- Temuujin, J, Rickard, W & Van Riessen, A 2013, 'Characterization of various fly ashes for preparation of geopolymers with advanced applications', *Advanced Powder Technology*, vol. 24, no. 2, pp. 495-8.

- Tennakoon, CK 2016, 'Assessment of properties of ambient cured geopolymer concrete for construction applications', PhD thesis, Swinburne University of Technology, accessed 27 August 2018 from Swinburne Research Bank.
- Thaulow, N, Jakobsen, UH & Clark, B 1996, 'Composition of alkali silica gel and ettringite in concrete railroad ties: SEM-EDX and X-ray diffraction analyses', *Cement and Concrete Research*, vol. 26, no. 2, pp. 309-18.
- Thomas, M 1998, 'The role of calcium in alkali-silica reaction', in *Materials Science of Concrete—The Sidney Diamond Symposium Westerville, OH: American Ceramic Society Bulletin*, pp. 325-37.
- Thomas, M, Fournier, B, Folliard, K & Resendez, Y 2011, *Alkali-Silica Reactivity Field Identification Handbook*, Federal Highway Administration, United States of America.
- Tiecher, F, Gomes, ME, Dal Molin, DC, Hasparyk, NP & Monteiro, PJ 2017, 'Relationship between Degree of Deformation in Quartz and Silica Dissolution for the Development of Alkali-Silica Reaction in Concrete', *Materials*, vol. 10, no. 9, p. 1022.
- Van Deventer, J, Provis, J, Duxson, P & Lukey, G 2007, 'Reaction mechanisms in the geopolymeric conversion of inorganic waste to useful products', *Journal of Hazardous Materials*, vol. 139, no. 3, pp. 506-13.
- van Deventer, JS, Provis, JL, Duxson, P & Brice, DG 2010, 'Chemical research and climate change as drivers in the commercial adoption of alkali activated materials', *Waste and Biomass Valorization*, vol. 1, no. 1, pp. 145-55.
- van Jaarsveld, J & Van Deventer, J 1999, 'Effect of the alkali metal activator on the properties of fly ash-based geopolymers', *Industrial & engineering chemistry research*, vol. 38, no. 10, pp. 3932-41.

- Van Jaarsveld, J, Van Deventer, J & Lukey, G 2002, 'The effect of composition and temperature on the properties of fly ash-and kaolinite-based geopolymers', *Chemical Engineering Journal*, vol. 89, no. 1, pp. 63-73.
- Van Jaarsveld, J, Van Deventer, J & Lukey, G 2003, 'The characterisation of source materials in fly ash-based geopolymers', *Materials Letters*, vol. 57, no. 7, pp. 1272-80.
- Wallah, S, Hardjito, D, Sumajouw, D & Rangan, B 2005, 'Performance of Geopolymer Concrete Under Sulfate Exposure', *ACI SPECIAL PUBLICATIONS*, vol. 225, p. 27. Wallah, S & Rangan, BV 2006, 'Low-calcium fly ash-based geopolymer concrete: long-term properties'.
- Wang, H & Gillott, J 1991, 'Mechanism of alkali-silica reaction and the significance of calcium hydroxide', *Cement and Concrete Research*, vol. 21, no. 4, pp. 647-54.
- Warner, SJ 2012, 'The role of alumina in the mitigation of alkali-silica reaction', MSc thesis, Oregon State University, accessed 27 August 2018 from ScholarsArchive@OSU.
- Williamson, T & Juenger, MC 2016, 'The role of activating solution concentration on alkali-silica reaction in alkali-activated fly ash concrete', *Cement and Concrete Research*, vol. 83, pp. 124-30.
- www.mindat.org *Basalt*, viewed 18.01.2018, <<https://www.mindat.org/min-48492.html>>.
- www.mindat.org *Rhyodacite*, viewed 18.01.2018, <<https://www.mindat.org/min-48448.html>>.
- Xu, H & Van Deventer, JS 2002, 'Geopolymerisation of multiple minerals', *Minerals Engineering*, vol. 15, no. 12, pp. 1131-9.

- Yip, CK, Lukey, GC, Provis, JL & van Deventer, JS 2008, 'Effect of calcium silicate sources on geopolymerisation', *Cement and Concrete Research*, vol. 38, no. 4, pp. 554-64.
- You-zhi, C, Xin-cheng, P, Chang-hui, Y & Qing-jun, D 2002, 'Alkali aggregate reaction in alkali slag cement mortars', *Journal of Wuhan University of Technology--Materials Science Edition*, vol. 17, no. 3, pp. 60-2.
- Zapala-Slaweta, J. & Owaiak, Z. 2016. The role of lithium compounds in mitigating alkali-gravel aggregate reaction. *Construction and Building Materials*, 299-303.
- Zheng, YC 2009, *Shrinkage behaviour of geopolymer*, MSc thesis, University of Melbourne, accessed 27 August 2018 from Minerva Access.
- Zuhua, Z, Xiao, Y, Huajun, Z & Yue, C 2009, 'Role of water in the synthesis of calcined kaolin-based geopolymer', *Applied Clay Science*, vol. 43, no. 2, pp. 218-23.